ON CONSTITUTIVE MODELLING OF FIBRE-REINFORCED COMPOSITE MATERIALS

By

REZA VAZIRI

B.Sc. (Eng.), University of London, U.K., 1982

M.A.Sc., University of British Columbia, 1985

A THESIS SUBMITTED IN PARTIAL FULFILLMENT OF

THE REQUIREMENTS FOR THE DEGREE OF

DOCTOR OF PHILOSOPHY

in

THE FACULTY OF GRADUATE STUDIES

Department of Civil Engineering

We accept this thesis as conforming

to the required standard

THE UNIVERSITY OF BRITISH COLUMBIA

September 1989

In presenting this thesis in partial fulfilment of the requirements for an advanced degree at the University of British Columbia, I agree that the Library shall make it freely available for reference and study. I further agree that permission for extensive copying of this thesis for scholarly purposes may be granted by the head of my department or by his or her representatives. It is understood that copying or publication of this thesis for financial gain shall not be allowed without my written permission.

Department of _Civil Engineering_

The University of British Columbia
Vancouver, Canada

Date _6th Oct 1989_

ABSTRACT

A relatively simple but comprehensive constitutive model is presented herein for predicting the nonlinear behaviour of laminated composite structures comprising layers of unidirectional and/or bidirectional (e.g. woven) fibre-reinforced materials (FRMs). The FRM layer is treated as an orthotropic but homogeneous continuum undergoing isothermal infinitesimal deformation.

The proposed constitutive model for single layers of FRM is built within the framework of rate-independent theory of orthotropic elastoplasticity. The constitutive equations so developed, are then superimposed using the classical lamination theory, to arrive at the governing response relations for multilayer laminates. The model invokes a 3-parameter quadratic yield surface and the associated flow rule of plasticity. During plastic flow the evolution of the yield surface in the stress space is described by a non-proportional change in the parameters of the initial yield function. A 3-parameter quadratic failure surface similar in form to that of the initial yield surface is defined to mark the upper limit of plastic flow. Once failure is reached, it is identified as fibre or matrix mode of failure depending on the relative magnitude of various stress ratio terms appearing in the failure criterion. In the post-failure modelling, both brittle and ductile type of behaviour are considered in the direction of the offending stress. Unidirectional and bidirectional FRM layers are treated within the same general framework with the exception that yielding (and failure) in these layers are assumed to be governed by different criteria, namely, Hill's and Puppo-Evensen's yield (and failure) criteria, respectively.

To completely quantify the proposed elastic-plastic-failure model three pieces of experimental stress-strain curves are required, namely, the uniaxial stress-strain curves along the two principal axes of orthotropy, and the in-plane shear stress-strain curve. Once established, these stress-strain curves are represented by bilinear approximations thus clearly defining the key parameters under the various loading programs. No provisions are made for the difference between tensile and compressive responses.

Based on the proposed model, constitutive equations are properly formulated. A nonlinear finite element code is developed to incorporate the derived constitutive equations. The program is based on the conventional displacement method finite element procedure using two dimensional 8-node isoparametric elements. The nonlinearities in the equilibrium equations are handled by a mixed incremental and Newton-Raphson iterative procedure. Analysis restart and cyclic loading capabilities are also included to expand the program's usefulness.

The performance of the program and the effectiveness of the model are verified for a number of in-plane loading paths applied to a wide variety of laminated FRMs with and without geometric discontinuities. The favourable comparisons of the model to experimental results available in the literature support the validity of the model.

TABLE OF CONTENTS

TABLE OF CONTENTS (Continued)

LIST OF FIGURES

LIST OF FIGURES (Continued)

LIST OF TABLES

LIST OF SYMBOLS

A list of important symbols is compiled here. All symbols are defined in the text when they first appear.

A_{ij}; $[A]$	anisotropic strength parameters written in tensorial notation and matrix format, respectively
A^e	elemental area
a	inner radius of the isotropic thick-walled cylinder
a_i; $\{a\}$	plastic flow vector defined by Eq. (3.26)
$[B]$	strain-displacement matrix
b	outer radius of the isotropic thick-walled cylinder
b_i	defined by Eq. (B.12)
C^e_{ij}; C^p_{ij}; C^{ep}_{ij}	generalized elastic; plastic; and elasto-plastic material stiffness tensor
c_i	defined by Eq. (B.12)
E_i; E_{T_i}; E_{P_i}	elastic, tangent and plastic moduli referring to a generic σ_i-ϵ_i curve
e_{ij}	strain tensor
$\{F\}$	external force vector
f_0; f; f_u	initial yield; subsequent yield; and failure function
G; G_T; G_p	elastic; tangent; and plastic moduli referring to an in-plane shear stress-strain curve
g	plastic potential
$[H]^e_k$	matrix defined by Eq. (4.14)
H; H'	defined by Eqs. (3.22) and (3.33)
$[J]$	Jacobian matrix
$[K_T]$	tangent stiffness matrix
k_0; k; k_u	effective initial yield; subsequent yield; and failure stress
L	half-length of a sheet with a central hole
L_i	tensor defined by Eq. (A.3)
M	total number of subincrements into which the strain increment is divided
$\{N\}$	vector of in-plane stress resultants
n	total number of layers through the laminate thickness

Q^e_{ij}; Q^p_{ij}; Q^{ep}_{ij}; Q^f_{ij}	plane stress elastic; plastic; elastoplastic; and post-failure material stiffness tensors
q	order of Gaussian integration
$\{R\}$	released force vector defined by Eq. (4.51)
R	radius of the hole defined in Figs. (5.8) and (5.33)
r_i	defined by Eq. (B.11)
S_0; S; S_u	initial yield; subsequent yield; failure stress in pure shear
s_i	defined by Eq. (B.11)
$[T]$	transformation matrix defined by Eq. (3.63)
t	total laminate thickness
t_k	thickness of the kth layer
U_0; U	initial and subsequent yield stress of a 45° off-axis specimen
u	displacement along the x-axis
u_r	radial displacement
V^e	elemental volume
v	displacement along the y-axis
v_B	longitudinal displacement at point B in Fig. (5.33)
W_i	weighting factor for Gauss integration
W^p	plastic work per unit volume
w	width defined in Figs. (5.8) and (5.33)
X_0; X; X_u	initial yield; subsequent yield; and failure stress along the principal material direction, x_1
x_1, x_2, x_3	principal axes of orthotrpoy for a single layer
x, y, z	laminate coordinate system
Y_0; Y; Y_u	initial yield; subsequent yield and failure stress along the principal material direction, x_2
α_i	tensor describing the origin of the yield surface
β	defined by Eq. (4.30)
Γ_{0i}; Γ_i; Γ_{u_i}	initial yield; subsequent yield; and failure stress tensor
γ_{xy}	shear strain in plane of the laminate
Δ	incremental quantities
$\{\delta\}$	displacement vector

$\bar{\epsilon}^p$	effective plastic strain
ϵ_i	strain tensor defined in Table 3.1
$\epsilon_x ; \epsilon_y$	x and y components of overall laminate strains
$d\epsilon_i^e ; d\epsilon_i^p$	elastic and plastic strain increment tensors
ζ_1, ζ_2	defined by Eq. (5.5)
η	natural coordinate of an isoparametric element
θ	Angle between the layer and laminate coordinate axes defined in Fig. (3.5)
κ	hardening parameter defined by Eqs. (3.21a,b)
Λ	interaction factor in the Puppo-Evensen criterion defined by Eq. (3.54c)
$d\lambda$	hardening parameter defining the length of the plastic strain increment vector $d\epsilon_i^p$
μ	defined by Eq. (3.55)
$\nu_{12} ; \nu_{21}$	major and minor Poisson's ratio
ξ	natural coordinate of an isoparametric element
$\rho_1 ; \rho_2$	defined by Eq. (5.6)
$\bar{\sigma}$	effective stress defined by Eq. (3.17)
σ_∞	remote stress applied to perforated plates
σ_θ	circumferential stress
$\{\sigma^c\}$	stress vector at contact with the initial yield lsurface defined in Fig. (4.3)
σ_i	stress tensor defined in Table 3.1
$\sigma_x ; \sigma_y$	x and y components of overall laminate stresses
$\{\Delta\sigma^p\}$	plastic stress increment vector define by Eq. (4.31)
τ_{xy}	shear stress in the overall laminate coordinate system
Φ	strain-energy density function defined by Eq. (3.4)
ϕ_i	shape functions for an 8-node isoparametric element
χ	defined by Eq. (A.3)
$\{\psi\}$	vector of the unblanaced forces defined by Eq. (4.17)
ω	angle defined by Eq. (4.47)

LIST OF SYMBOLS (Cont'd)

Suffix

o	initial yield value
u	failure value
e	elastic or elemental quantities depending on the context used
p	plastic
ep	elastoplastic
r	quantities related to the rth iteration
k	quantities related to the kth layer of a laminate
m	quantities related to the mth strain subincrement
()'	quantities transformed from ply to laminate coordinates
{}	vector quantities
[]	matrix quantities

ACKNOWLEDGEMENT

CHAPTER 1

INTRODUCTION

1.1 Introduction

The possibility of manufacturing materials with desirable mechanical properties by reinforcing a matrix material with strong fibres having high elastic extensional modulus has recently received a great deal of attention, both experimental and theoretical. Recent activity has largely been stimulated by the development of new types of high strength fibres, but the idea is a very old one. Artificial materials such as fibreglass and reinforced concrete which are of this type have been available for some time, and many natural materials, for example wood and bone, are essentially of this character.

Composite materials involving fibre reinforcement are continuing to replace traditional materials at a rapid rate. The driving force for this replacement is due to their outstanding specific properties (i.e. high strength and stiffness-to-weight ratios). These superior properties of composite materials over the monolithic metals makes these materials very attractive for weight and stiffness sensitive structures. The applications range from sports equipment, automotive parts, aircraft and aerospace structures to high performance military structures (e.g. ground, underwater and space vehicles).

The rapid growth rate of this field entails a good understanding of the mechanics of composites so that they may be efficiently utilized in engineering applications. With the present state of development of finite-element computer programs, the problem of modelling the mechanical behaviour of composites remains one of the most difficult challenges in the field of

composite structural engineering. Materials behaviour refers to multi-dimensional stress-strain[†] relations which adequately describe the basic characteristics of the material subjected to monotonic and cyclic loading.

The emphasis in this thesis is placed upon the constitutive modelling in analytical and numerical analysis of composite structures. We shall be concerned primarily with continuum theories and "macroscopic" models of material behaviour. However, the properties of the composite materials we consider derive ultimately from the properties and geometrical arrangements of their constituents. Thus in formulating the macroscopic mechanical properties of the composite it is impossible to disregard entirely the properties of its constituents. Therefore for background and motivation we begin in this introductory chapter with a brief discussion of some of the properties of composite materials, and the way in which these depend on the properties of their constituents. We do not, however, attempt to give in any way a comprehensive account of the great volume of work which has been done in studying the interactions between constituents of composites, or determining the properties of composites in terms of their constituents. Although these problems are of great importance, they are outside the scope of this thesis.

1.2 Types of Composites and Basic Terminology

A composite material is defined to be any material consisting of two or more distinct constituents (or phases). For the sake of convenience, one of the phases will be referred to as the "matrix", while the others as the

---

[†]The stress-strain relations are also referred to as constitutive relations as they describe the mechanical constitution of the material.

"reinforcement". Even though reinforcement implies strengthening of the material, the term is used to denote any phase that is imbedded in the matrix. Thus cracks and voids are included within this term. The main types of reinforcement are particles, chopped (or discontinuous), continuous fibres and flakes. Although flakes and particles have become important constituents in many composite systems, fibre reinforcement dominates the field and are by far the most extensively analysed. For the remainder of this thesis, emphasis will be placed on fibre-reinforced materials (FRM). It is useful at this stage to examine the constituents of these materials.

Fibre-reinforced materials are usually divided into three broad groups according to the matrix materials: plastic (e.g. epoxies); metal (e.g. aluminum and magnesium); and ceramic. The role of the matrix material is to bind the reinforcing fibres together into a solid mass and therefore enable the transfer of load to the fibres. The matrix also permits ease of fabrication into a desired configuration. In many structural applications the fibre properties are the most important and the matrix may be chosen based on cost and minimum weight. There are, however, a significant number of applications in aircraft, spacecraft, etc. where the matrix must possess particular properties. In these cases the material is subjected to high temperatures, where plastic matrix composites are unusable, so that either metal or in the case of extreme temperatures, ceramic matrix composites must be considered. Commonly used fibres are glass, boron, kevlar, and carbon (graphite). The fibres may be continuous, in which case each fibre extends through a body from one boundary to another, or discontinuous in the form of chopped fibres. Continuous FRM can be made either by aligning all the fibres in one direction (unidirectional), or weaving a cloth (bidirectional). The chopped fibre composites are statistically isotropic and their analytical

treatment does not pose a great difficulty. With that in mind much of what will be discussed in this thesis implies composites made from continuous fibres.

Unidirectional FRMs have exceptional strength and stiffness properties in the direction of fibres, however, their properties in any other direction are rather poor. The overall properties are normally improved by laminating single plies[†] with different reinforcing directions. This leads to what is called "laminated composites" or "laminates". The laminate is tailored to just meet specific requirements. By appropriate consideration of the loads and their directions, a laminate can be constructed of individual plies in such a manner as to just resist those loads and no more. In this respect isotropic materials are usually inefficient because excess strength and stiffness is inevitably available in some direction.

Bidirectional woven fabrics have inferior mechanical properties (in the fibre direction) to their unidirectional counterparts. This is due in part to the weaving process which may cause fibre damage. Layers of woven fabric are therefore often used as filler layers where strength and stiffness are not critical. The main reasons for the use of these materials are ease of handling (with consequent reduction in labour costs), and the ability of fabric to conform to complex shapes. They are extensively used in boat construction and ship superstructures. Woven composites are also known to result in better containment of impact damage and improved residual proper-ties after impact compared with nonwoven materials (Smith, C.S., 1986).

[†]Some authors use the term "lamina" to denote a single layer or ply. However, this terminology is not used here, since it is easily confused with the term "laminate", which means all of the layers bonded together.

1.3 General Remarks on the Mechanical Properties of Fibre Composites

The aim of this section is to convey in a qualitative manner a general understanding of the mechanical behaviour of composites.

The behaviour of composite materials can be studied theoretically from three levels of magnification. They are

i) Micromechanics - which considers the problems of local interactions at the interfaces between the fibre and the matrix phase. For the study of interface problems attention is given to a single fibre and its surrounding matrix material. For purposes of analysis the usual procedure is to regard the composite as an assemblage of circular cylindrical fibres surrounded by concentric hollow cylinders of matrix material. Examples of the use of this approach can be found in the survey articles by Hashin (1983), Francis and Bert (1975), and Chamis and Sendeckyj (1968). Apart from using them for comparison purposes, the micromechanical analyses will not be pursued in this thesis.

ii) Minimechanics - which relates the properties of the composite to the individual properties of the fibre and the matrix. A mathematical model of a composite is constructed by applying any of the rheological proper- ties (e.g. elastic, viscoelastic, plastic, etc.) to the fibre and any one to the matrix. Geometry of the phases are not taken into account here. In this approach the fibre and matrix are usually separated and rearranged in series or in parallel as may be appropriate.

iii) Macromechanics - which describes the behaviour of the composite by continuum models without direct reference to the properties of the individual constituents. In other words the FRM is treated as a homo- geneous anisotropic continuum with some average properties known from experiments. Such an approach which is followed in this thesis is

appealing to the engineer or designer who requires reasonably simple (yet realistic) methods of stress and strain analysis of composite materials. This appears to be at variance with the approach of the metallurgist who wishes to give an accurate description of the mechanisms which take place.

It can be seen that the macroscopic behaviour is a consequence of the behaviour on the miniscale. In turn the behaviour on the miniscale depends upon the behaviour on the microscale and so on down (Drucker, 1975). Under sufficiently simple conditions, we can proceed with confidence one step up or down in scale. Most often it is not possible to give more than a qualitative prediction of the influence of one level on the next. For example it is likely to be difficult to predict quantitatively the mechanical properties of a FRM in terms of the properties of the constituents. However, it is helpful to have at least a qualitative appreciation of material behaviour at the micro and miniscales in order to formulate the macroscopic theory which will be developed in later chapters. With this in mind we give a brief discussion on the general properties of FRMs.

The introduction of a family of fibres in a definite orientation in the matrix immediately introduces a preferred direction in the material. Thus even if the constituents of a fibre reinforced composite are isotropic, the composite itself will be macroscopically anisotropic. Indeed if there are large differences between the mechanical properties of the fibre and matrix then the properties along and perpendicular to fibre would be quite different. This gives rise to a "strongly anisotropic" material[*] (such as

---

[*]Fibre-reinforced composite layers, whether unidirectional or bidirectional, are almost invariably orthotropic possessing three planes of material symmetry. Moreover, since the fibres are generally at random locations the unidirectional FRM is macroscopically transversely isotropic.

uni-directional composites). By the same token a matrix reinforced by two families of fibres (such as woven-cloth reinforced composites) are considered as "weakly anisotropic" on the macroscopic level.

In a real composite, the matrix material has a low stiffness and strength compared to the fibre. Fibres generally exhibit linear elastic behaviour. Metal matrix materials exhibit elastic-plastic behaviour and polymeric matrices usually are viscoelastic if not viscoplastic. Consider a unidirectional FRM. Along the fibre direction the properties of the composite is predominantely that of the fibre resulting in fibre fracture (or multiple matrix cracking if the ultimate strain of the matrix is lower than that of the fibre). In the direction transverse* to the fibres, the inherent mismatch of stiffnesses between fibre and the matrix results in the development of high local strain concentrations in the matrix. To accommodate these high local strains without inducing local failures, matrix materials are normally selected which have high strains to failure. This permits local plastic flow to occur in regions of high strain concentration causing a redistribution of stresses (stress relief). Thus, even if the average applied transverse stress on the composite is relatively low, local stresses and strains within the composite material may have exceeded the elastic limit. At this point the matrix flows or fractures (according to the degree of ductility of the matrix material). The strain to failure of the composite in such cases is very small compared to that of the matrix.

Shear response in the material principal directions exhibits considerable nonlinearity indicating the dominance of the (soft) matrix material

---

*Here the term "transverse" is reserved for the in-plane direction which is perpendicular to the longitudinal direction. Out of plane direction will be referred to as "thickness" (as opposed to transverse) direction.

under such loadings. It is readily apparent that these shear stress components are present even when the composite layer is subjected to normal stresses at an angle to the principal material axes. The nonlinear shear response is therefore a major, perhaps the major, source of nonlinearities in the response of composite laminates. Any analysis which hopes to provide realistic assessments of the stresses and strains in various plies of the laminated composites must account for the nonlinear shear response.

There are many ways in which a FRM layer may fail. These may be in the form of matrix cracks, fibre fracture, interface separation (i.e. fibre pull out) and local plastification in the matrix. Some of these failure mechanisms resemble brittle fracture of the composite, with low energy absorption, while others produce a ductile type of fracture with the absorption of a large quantity of energy. Experimental evidence shows that for laminates consisting of polymeric matrix fibre composites, under static or cyclic load, there are two major types of cracks: (a) intralaminar (or intraply) cracks within certain plies; and (b) interlaminar (or interply) cracks which develop on planes between plies. Metal matrix composites usually deform plastically and do not exhibit extensive matrix cracking under monotonic loads, but are quite susceptible to matrix fatigue cracking when subjected to cyclic loading (Dvorak and Johnson, 1980). Intralaminar cracks are either short cracks (perpendicular to the fibres) that rupture the fibres and debond fibre matrix interfaces, or, long cracks (parallel to the fibres) that traverse from edge to edge and are essentially normal to the plane of the ply.

Interlaminar cracks which debond the ply interfaces either originate at laminate edges due to the presence of high values of interlaminar normal and shear stress, or, at regions of high transverse shear in laminated plates under bending.

From the above brief discussion it is clear that the consideration of nonlinear behaviour is important even for composite materials subjected to applied stresses which are intended to remain below the apparent elastic limit of the composite. For laminated structures designed to an ultimate strength criterion, the need for consideration of nonlinear behaviour, in particular inelastic effects including failure, is even more apparent.

1.4 Purpose and Scope of the Present Study

The basic objective in this thesis is to develop a relatively comprehensive plasticity-based macroscopic constitutive model for the individual layer of unidirectional and bidirectional FRMs. This model is to be used in the nonlinear analysis of laminates having an arbitrary number of such layers with various fibre orientations. Finite element analyses will be developed for the case of symmetric laminates subjected to membrane loading. It will be shown that plasticity theory, when not interpreted too narrowly, is a very flexible model - one that can be used to describe a wide variety of behaviour including cracking of polymeric composites.

Chapter 2 aims at reviewing some of the immense existing body of the literature on constitutive modelling of fibre-reinforced composites.

Chapter 3 outlines the theoretical formulation of the proposed constitutive model.

Chapter 4 describes the implementation of the constitutive model in a two dimensional finite element program used to perform progressive failure analysis of composite laminates. The numerical analysis developed is then applied to a series of problems and the results are compared with a wide range of experimental and other numerical results in Chapter 5.

Chapter 6 outlines the conclusions that can be drawn from the results of the proposed theory. The applicability of the constitutive model is discussed and further areas of research are suggested.

CHAPTER 2

REVIEW OF THE LITERATURE

2.1 Introduction

Although large-scale finite element software packages now have a wide range of application in stress analysis of composites (Griffin, 1982), inadequate material models are often one of the major obstacles for a rigorous analysis. Errors associated with material properties are usually far greater than errors inherent in the numerical methods of solving the field equations. A large variety of models have been proposed to characterize the stress-strain and failure behaviour of fibre reinforced materials (FRMs) under multidimensional stress states. All these models have certain inherent advantages and disadvantages which depend to a large degree on their particular application. The objective of this section is to present a summary of various proposed material models of FRM and to determine the range of their applicability, relative merits and limitations. No survey or list of references can even approach complete coverage of such a wide field and the references cited here afford only a glimpse of the extensive literature available and are by no means exhaustive.

2.2 Background

In constructing a constitutive model for laminated composites the underlying point of view is that the laminate response must be understood in terms of the behaviour at the ply level. In other words the mechanical behaviour of a single layer forms the basic building block in the analysis of laminated structures (consisting of several individual layers). The gross behaviour of perfectly elastic laminated plates under bending and stretching deformations can be exactly analyzed in terms of the ply properties and their stacking

arrangement. These analyses are based on the classical lamination theory (CLT) which is well known in the composites literature. The basic assumption in CLT is that there is a perfect bonding at the ply interfaces and that each ply, which is considered to be homogeneous and anisotropic, is under a state of plane stress. Once the strain field is prescribed (such as uniform strain in case of membrane loading, and linear distribution according to the Kirchhoff-Love hypothesis in the case of bending), the stress field is directly determined by the stress-strain relations of each ply. However, in inelastic laminates such a direct determination of the stress field from the strain distribution is not possible due to the path dependent nature of the stress-strain relations. This does not pose an insurmountable problem in view of the power of modern numerical computation. The conclusion is that analysis of "undamaged" laminates, even for rather complicated cases of material behaviour (of individual plies) can be carried out. The problems emerge when one considers "damage" and "failure". Composite laminates under static or cyclic loading experience failure in one or more layers early during the loading process, which in most cases does not lead to the failure of the entire laminate. Such a failure implies damage in terms of crack distribution within the failed ply (or plies). To determine subsequent failures it is necessary to perform stress analysis of the "damaged" laminate. Thus the laminate must be subjected to a progressive failure analysis until its load carrying capacity is exhausted. Such analytical determination of the failure loads of a laminate is a highly controversial issue and remains one of the most challenging areas of current research.

It is apparent from the above discussion that the scope of research on the constitutive behaviour of composite laminates may be divided into four main sequential subjects:

- Behaviour of the undamaged laminate, i.e. pre-failure.

- Onset of damage, i.e. first ply or initial failure.

- Behaviour of the damaged laminate, i.e. post first ply failure.

- Ultimate failure.

The remainder of this section gives a brief review of the available literature on the analytical treatment of the topics itemized above.

2.3 Constitutive Modelling of Undamaged Composites

Analytical studies of the problem of mechanical behaviour of composite materials have been approached from any one of three basic levels, namely, the micromechanics level, the minimechanics level and the macromechanics level. The linear-range properties of composites, approached from all three levels, are quite well understood and well documented in all the standard texts on mechanics of composites (see for example the survey article by Hashin (1983)). On the other hand, the nonlinear behaviour of fibre composites is much more complicated and its rigorous treatment did not start until the early 1970s. The complexity of nonlinear response exhibited by composites helps to explain the diversified methodologies employed by numerous investigators in formulating constitutive theories for these materials. Unless otherwise stated, the discussion in this section is concerned with the behaviour of a single ply.

2.3.1 Micromechanics Approach

Rigorous micromechanical models based on the mathematical theory of plasticity have appeared in the literature. Notable among these are the finite element approaches of Adams (1970, 1974), Foye and Baker (1971), Foye (1973), Lin et al. (1972) and Dvorak et al. (1973, 1974) to determine initial

yield surfaces and subsequent stress-strain curves of unidirectionally-reinforced composites. Aboudi (1984) considered a model of a square array of fibres with square sections in terms of linear approximating fields including viscoplastic effects. In a recent paper Aboudi (1986) summarized his constitutive theory and gave a list of references of previous works. All the above papers take into account the complicated geometry of the composite on the microscale. Although such detailed investigations are essential for an understanding of the inelastic behaviour of FRMs they are unfortunately very complicated and require a relatively large computer facility and significant amounts of computer time. Thus, they can be prohibitively expensive to utilize extensively in the stress analysis of large scale structures.

2.3.2 Minimechanics Approach

Approaches in this category typically relate stresses to strains in terms of physical parameters such as the fibre volume content and the material properties of the fibre and the matrix. These stresses and strains are most often average (or composite) values over representative volume elements which are large compared to typical phase region dimensions (e.g. fibre diameters and spacings). Analyses based on this approach are therefore not truly micromechanical, since they do not provide a description of the local stress and strain gradients within the composite. Hence the term minimechanics is used here to encompass all such approaches.

The general groundwork for determination of overall mechanical properties of FRMs from their constituents has been laid out by Hill (1964) for a class of transversely isotropic materials with elastic fibres and elasto-

plastic matrices. Using a self-consistent scheme (SCS)*, bounds were obtained for the overall moduli and flow stress at any stage of deformation. Based on the deformation theory of plasticity and SCS, Huang (1971) predicted the overall transverse elastic-plastic uniaxial stress-strain curve for a unidirectional FRM comprised of rigid fibres and an elastic-plastic matrix. Dvorak and Bahei-el-din (1979) modified the SCS of Hill in calculating internal stress fields, overall and local yield surfaces, instantaneous moduli, thermal coefficients, plastic strains and thermal microstresses for transversely isotropic materials. Dvorak and Bahei-el-din (1982) later used a simple model to arrive at three dimensional constitutive relations for elastic-plastic deformation of unidirectional fibrous composites. In their approximate treatment, which simplifies the geometry of the microstructure, each of the fibres is assumed to be of very small diameter, so that although the fibres occupy a finite volume fraction of the composite, they do not interfere with matrix deformation in the transverse and longitudinal directions. The fibres were regarded as elastic embedded in an isotropic elastoplastic matrix of Mises-type with kinematic hardening. As a result, analytical expressions were obtained for the yield conditions, hardening rules, and flow rules for the composite aggregate in terms of local properties and volume fractions of the phases. In a subsequent paper Bahei-el-din and Dvorak (1982) used their model of elastic-plastic behaviour of unidirectional FRM to derive constitutive equations of laminate plates under in-plane mechanical loading. Analytical calculations based on their model were compared with selected experimental results on Boron/Aluminum

---

*For a description of this scheme and further references see p. 59 of Christensen (1979).

(B/Al) laminates. In order to obtain good agreement they had to use plastic properties of the matrix that departed significantly from those of the true unreinforced aluminum. The reasons for this discrepancy were attributed to the inherent deficiencies in their material model.

Min (1981) used a similarly simple model to arrive at a plane stress description of the elastoplastic response of unidirectionally reinforced metal matrix composites. In this study, based on Hoffman's model (1979), the fibre was assumed to have stiffness only in the axial direction, whereas the matrix was considered to be an elastic-perfectly plastic material obeying the von Mises yield criterion and its associated flow rule. This led to a work-hardening type response for the overall behaviour of the composite similar to that reported by Bahei-el-din and Dvorak. A few numerical examples were presented and shown to compare favourably with the results of experiments performed on Graphite/Aluminum (Gr/Al) composites under simple in-plane uniaxial and biaxial loading conditions.

2.3.3 Macromechanics Approach

In this section we shall be primarily concerned with "continuum" theories which describe the behaviour of the FRM on the macroscopic scale. The models to be discussed treat the composite as a material in its own right, without direct reference to the properties of the individual constituents. In these models the FRM is regarded as an anisotropic continuum, with appropriate overall (average) properties known from experiments or micromechanical analyses.

The several macroscopic approaches for defining the stress-strain behaviour of FRMs under various stress states can be conveniently classified as belonging to five main groups:

  i)   Linear Elasticity

  ii)   Nonlinear Elasticity

  iii) Viscoelasticity

  iv)   Incremental Plasticity

  v)   Endochronic Plasticity.

The following outlines some of the existing constitutive models under the above headings.

i)   Linear Elasticity

In spite of its shortcomings, the linear elasticity theory is by far the most commonly used material model for composites in the prefailure range. The emphasis on linear elasticity reflects its usefulness and importance, not only as a basic theory but also for providing the means to develop practical design methods. The basic concept of linear elasticity as applied to FRMs is well established (see for example Jones (1975)). The corresponding design aspects are also well advanced. By no means, however, can all practical FRMs be idealized as behaving according to linear elasticity theory. Many types of composite materials involve constitutive behaviour that is distinctly nonlinear (elastic or inelastic) in at least one of the principal material directions. The following deals with theories that cover such non-linearities.

ii)   Nonlinear Elasticity

Contemporary FRMs generally consist of elastic brittle fibres such as glass, boron or graphite in relatively soft matrix materials such as epoxy or aluminum. For these matrix materials it is reasonable to anticipate that at a certain loading state the matrix will begin to exhibit nonlinear effects.

The degree of nonlinearity varies from composite to composite depending on the type of matrix material. Polymer matrix composites reinforced by unidirectional fibres usually exhibit an appreciable amount of nonlinearity in shear and only a slight nonlinearity in tension transverse to the fibres. On the other hand, metal matrix composites such as B/Al have strong transverse and shear nonlinearities. The nonlinearities for all of these materials are more pronounced with increasing temperature.

Various investigators have attempted to include mechanical property nonlinearities in analysis of composite materials. Petit and Waddoups (1969) devised an incremental method (using a piecewise linear approximation) for nonlinear analysis of laminates. According to this method, an increment of average laminate stress (or stresses) is placed on the laminate, and by using the initial laminate compliance matrix, the first increment in the laminate strains is calculated with the assumption that the laminate behaves linearly over the applied stress increment. The increment in the laminate strains is added to any previous strains to determine the current total laminate strain. As the incremental loading proceeds, the individual ply strains are monitored, and, by referring to the basic ply stress-strain curves, the corresponding ply tangent moduli and stiffnesses for the strain levels present are calculated. The Petit-Waddoups method requires far too many input data and their incremental scheme is unduly complicated.

Starting with a complementary energy density function for a linear elastic material, Hahn and Tsai (1973) added a fourth order term in shear to model the nonlinear shear behaviour and regarded all other stress-strain curves as linear. The method which was applicable to unidirectional layers, was subsequently extended to laminated composites by Hahn (1973). Hashin,

Bagchi and Rosen (1974) proposed a deformation type theory* in conjunction with the Ramberg-Osgood (1943) representation of stress-strain relations to approximate the nonlinearities. In their analysis the strains in each ply were split into elastic and inelastic components. Furthermore, the transverse and shear stresses were allowed to interact in the inelastic range while inelastic strains in the fibre direction were neglected. The deformation theory used in their analysis has the obvious deficiency of failing to account for load-history effects and of possibly causing continuity and uniqueness problems in the case of nonproportional loading (see for example Kachanov, 1971, p. 54). Sandhu (1976) introduced an incremental method that used piecewise cubic spline interpolation functions to represent the basic nonlinear stress-strain data. Like the Petit and Waddoups' analysis, Sandhu's method required the complete ply tensile and compressive stress-strain data under longitudinal, transverse and shear loading as input. Sandhu's model attempted to compensate for the triaxial stress effect (which was absent in Petit-Waddoups' model) by defining equivalent strains. A slight inconvenience of the Sandhu's analysis is that it requires biaxial loading to determine normal and transverse tangent moduli for plane stress loading. The model also lacks provisions for stress interaction in shear. Jones and Morgan (1977) developed a material model in which the nonlinear mechanical properties were expressed as functions of the strain energy

---

*The deformation theory (also called J_2 deformation theory, octahedral shear deformation, total theory) developed in 1924 by Hencky assumes that there is a one-to-one correspondence between the stress and strain. It is known that in the case of proportional loading, that is, all stresses at a point grow simultaneously in a fixed ratio to one another, deformation theory is simply an integration of the incremental plasticity theory. It has also been shown by Kachanov (1971) that the governing equation of deformation theory corresponds to a nonlinear elastic constitutive representation.

density. They argued that under multiaxial loading the strain energy capacity of the material can exceed the uniaxial strain energy capacities. Using some ad-hoc modifications (to prevent the material from violating thermodynamic constraints), they extrapolated the stress-strain and mechanical property-strain energy curves in a rather complicated manner. The complexity of this method did not prove to produce better results when compared with the Hahn-Tsai method.

Nahas (1984) employed a technique similar to that of Sandhu in addition to the secant modulus concept to predict the nonlinear behaviour of laminates. Recently, Takahashi and Chou (1987) adopted the piecewise linear approximation of Petit and Waddoups and used Fourier series expansion of the experimental results to model the nonlinear shear stress-strain relations of individual plies.

iii) Viscoelasticity

Composite materials which have one or more polymeric constituents (such as resinous matrix materials) exhibit a considerable amount of time-dependent mechanical behaviour. This behaviour, termed viscoelasticity, increases in significance with elevated temperature. In the case of metallic matrix materials, such as aluminum, time-dependent effects are generally negligible unless elevated temperature or high strain rate conditions are considered.

A summary and review of the literature on viscoelastic behaviour and analysis of composites are given by Schapery (1974). More recent developments in this field can be found in the survey article by Hashin (1983).

iv) <u>Incremental Plasticity</u>

All the macroscopic constitutive models mentioned so far suffer from certain inherent limitations. In particular they cannot predict dissipative (irreversible) effects characterized by permanent strain accumulation, a shortcoming that becomes apparent when the material experiences unloading at large stresses. The incremental theory of plasticity is a well developed constitutive representation that accounts, in principle, for the stress history dependent behaviour and residual strains due to unloading. A more extensive discussion of the incremental theory of plasticity is given in Chapter 3.

While considerable work apparently has been done in the area of composite elasticity, the study of its elastoplastic behaviour is still very limited. Studies of plastically anisotropic materials in the context of the incremental theory of plasticity were begun by Hill (1950), who first postulated the form of a yield condition based on the von-Mises criterion for isotropic plastic materials. Hill's yield condition was devised to account for the differences of yield stress in rolled steel sheet in the rolling and transverse directions. In his formulation, Hill introduced six parameters to account for orthotropic symmetry of the material. However, he considered only isotropic hardening which results in a proportional change of the six orthotropic parameters during hardening. Hu (1956) extended Hill's theory to the analysis of plastic flow of anisotropic bodies with strain-hardening. In this work the anisotropic parameters of the yield criterion were considered as constant during plastic deformation. Hu (1958) generalized the Tresca maximum shear stress criterion to study the plastic flow of anisotropic bodies. Whang (1969) generalized Hill's criterion by suggesting a

non-proportional rule for changing the anisotropic parameters during the hardening process. This was based on the assumption that for equal amounts of plastic work produced during stress-strain tests in each of the principal directions, the effective stress level reached would be the same. Whang's approach was used by Valliappan (1971) in the finite element solutions of several anisotropic elasto-plastic structures.

Shih and Lee (1978) proposed an extension of Hill's formulation to account for the distortion of the yield surface for differing strengths in tension and compression and the effective size of the loading surface. The anisotropic parameters of the yield function were determined from monotonic loading tests on Zircaloy materials. It was observed that these parameters, which were responsible for the distortion of the yield surface, tended to reach constant values with increasing plastic strain. Griffin, Kamat and Herakovich (1981) employed Hill's criterion and its associated flow rule in a three dimensional finite element program to analyze the inelastic tensile response of unidirectional off-axis FRMs. The Ramberg-Osgood representation was used to approximate the basic stress-strain relations. For the purpose of computing the hardening modulus (i.e. the slope of the effective stress versus effective plastic strain diagram) proportional loading was assumed. Such assumptions lack physical arguments. The method suggested is rather complicated and requires much experimental data for the evaluation of various parameters. Kenaga, Doyle and Sun (1987) used a plane stress orthotropic elastic-plastic formulation based on a four parameter quadratic yield function to characterize the nonlinear behaviour of unidirectional B/Al FRMs. A number of off-axis tensile tests were performed and a trial and error procedure was employed to determine the anisotropic parameters that best fitted the data. Leewood, Doyle and Sun (1987) implemented the above

formulation in a two-dimensional finite element program to analyze the elastic-plastic behaviour of multilayer laminates.

Higher order (than quadratic) yield functions for anisotropic materials have also been suggested by some authors (e.g. Dubey and Hillier (1972); Gotoh (1977); and Rees (1984)).

The theories described above may be interpreted as generalizations of plastic flow theories for isotropic materials, with enough arbitrary material parameters built in to account for as many classes of material symmetry as desired. These theories thus contain no elements which can account physically for the presence of fibres in a ductile matrix. A survey of the literature, however, reveals that theoretical analyses have appeared which recognize the presence of stiff fibres by constraining the deformation of an essentially isotropic plastic material. In this manner the difficulties associated with anisotropic plasticity are avoided. The basic idea of representing a FRM by a continuum model of this nature originated with the paper by Adkins and Rivlin (1955) who treated the problem of a rubber-like incompressible material reinforced with inextensible fibres. Mulhern, Rogers and Spencer (1967) adopted a somewhat similar procedure as Adkins and Rivlin, but applied it to plastic rather than elastic solids. They proposed a continuum model for describing the mechanical behaviour of a rigid-plastic material reinforced by a single family of inextensible fibres. Whereas Mulhern et al. (1967) treated the composite as a transversely isotropic rigid plastic solid, Prager (1969) viewed the composite as consisting of an isotropic rigid-plastic matrix constrained by inextensible fibres. Mulhern, Rogers and Spencer (1969) later relaxed the rigidity assumption and permitted elastic composite strains in the fibre direction. While the aforementioned papers are based on Mises isotropic yield condition or on its anisotropic

modification by Hill (1950), Lance and Robinson (1971) developed a model of an incompressible rigid-plastic material of the type assumed by Mulhern et al., but obeying an anisotropic modification of Tresca's yield condition. Dvorak and Rao (1976) proposed a continuum theory for axisymmetric plastic deformation of unidirectional fibrous composites, consisting of elastic fibres and an elastic-perfectly plastic matrix. Their theory accounted for both the plastic extensibility of the composite in the fibre direction, and for the plastic dilatation (in the presence of elastic deformation of the fibres). It should be emphasized that, in all the above papers, the fibres are assumed to have a constraining effect on the yielding of the matrix. Such details as fibre stresses (i.e. the part of the overall stress carried by fibres themselves) have been ignored. The theories suggested are therefore continuum theories and must not be confused with the minimechanics approaches outlined in section 2.3.2.

v)   Endochronic Plasticity

In the preceding section, the classical incremental theory of plasticity was used as the basis for developing constitutive models for FRMs. Fundamentally, the incremental theory assumes the existence of a yield criterion coupled with a hardening rule to define the subsequent yield surfaces. However, it is often difficult to determine the precise values of the yield stresses and define appropriate hardening rules. A theory that does not require the existence of a yield condition and is therefore free from hardening rules, is the endochronic theory of plasticity developed originally by Valanis (1971) for the description of mechanical behaviour of metals. Using Valanis' concept, Pindera and Herakovich (1983) extended the theory to transversely isotropic media in order to describe the response of graphite-

polyimide off-axis tensile coupons under monotonic and cyclic loading. They demonstrated the applicability of the endochronic theory by obtaining good correlation with the observed experimental data. It should be noted, however, that the endochronic theory is not without its limitations and some serious criticisms of it has been raised by Rivlin (1981).

2.4 Initial Failure

Failure criteria for composite materials are more difficult to postulate than for isotropic materials. The analytical determination of the strength of composites on the basis of micromechanics methods is extremely complex, perhaps to the point of being regarded as an intractable problem. On the other hand, it is also impractical to resolve the problem by experimentation alone since the number of tests required to develop the full failure surface would be extremely large. The remaining alternative is to construct analytical failure criteria in terms of macrovariables, such as average stresses or strains.

Over the last twenty years, a significant number of failure criteria for many anisotropic materials have been proposed. Extensive surveys of the criteria as applied to composite materials are presented by Tsai and Hahn (1975), Wu (1974), Rowlands (1985), Nahas (1986), Craddock and Champagne (1985), Fan (1987), and Labossiere and Neale (1987a). All the existing failure criteria tend to be phenomenological and empirical in nature, not mechanistic. The intended use of most of these criteria was mainly the prediction of the strength in "single layers" of FRMs under complex loading conditions. None of the available anisotropic strength criteria represents observed results sufficiently accurately to be employed confidently by themselves in practice. Several of the theories suffer from the inconvenience of

requiring biaxial information as basic input data. Some of the most popular failure criteria will be discussed in the following.

The simplest failure criteria are the maximum stress and maximum strain criteria. According to these theories failure of a layer occurs when any single stress or strain component in the principal material axes directions reaches its corresponding ultimate value regardless of the values of the other components. The maximum stress (strain) criteria are not realistic since they disregard the combined effects of stresses (strains) on failure,* and therefore overestimate the strength of the material under combined stress (strain). Both criteria, however, are simple to utilize in practice and are capable of determining the mode of failure of the failed ply. The latter facilitates the study of the behaviour of the laminate after the first ply failure.

A convenient mathematical representation of failure criteria that accounts for the interaction of stresses (or strains) is in terms of polynomials in stress (or strains). It is then necessary to determine the coefficients of the polynomial in terms of test results which can be conveniently obtained in the laboratory, such as uniaxial tension or compression, pure shear, etc. In one of the first contributions to the subject Tsai (1965) assumed that Hill's (1950) quadratic yield criterion for orthotropic plastic materials could be used as a failure criterion. Hoffman (1967) added linear terms to account for different tensile and compressive ultimate stresses. The disadvantage of these criteria is that they are based on the assumption that hydrostatic pressure has no effect on the failure.

---

*It should be noted that although the maximum strain criterion is an independent mode criterion in strain space it accounts for the interaction of stresses (due to the Poisson ratio effect) in stress space.

While such an assumption may be a good approximation for initial yielding of a metal, it is certainly not valid for FRMs. Realizing the shortcomings of the previous failure criteria Tsai and Wu (1971) proposed a general tensor polynominal criterion in terms of stresses. In their notation failure of the material will occur when the following condition is met,

$$F_i \sigma_i + F_{ij} \sigma_i \sigma_j + F_{ijk} \sigma_i \sigma_j \sigma_k + \ldots = 1 \quad (i,j,k = 1,2,\ldots,6) \qquad (2.1)$$

Here σ_i are the components of the stress tensor and the coefficients F_i, F_{ij}, F_{ijk}, etc. are the components of the strength tensors, calculated from experimental data. All components are referred to the material principal axes and the following contracted tensor notation (in the sense of Green) is used,

$$\sigma_1 = \sigma_{11} \; ; \quad \sigma_2 = \sigma_{22} \; ; \quad \sigma_3 = \sigma_{33}$$
$$\sigma_4 = \sigma_{23} \; ; \quad \sigma_5 = \sigma_{13} \; ; \quad \sigma_6 = \sigma_{12} \qquad (2.2)$$

Thus F_i and σ_i are second order tensors. Similarly, F_{ij} is a fourth order tensor with 21 independent components. All higher-order tensors appearing in Eq. (2.1) follow the same general character. Tensorial criteria similar to that of Tsai-Wu had been proposed earlier in the Russian literature (see for example Rowlands (1985)). Although the polynomial (2.1) can be expanded to any degree, the number of strength parameters rises considerably for each additional degree included. To reduce the number of experiments required to obtain the strength parameters, usually only linear and quadratic terms are retained.* In this case all of the coefficients in Eq. (2.1), except the

---

*Some authors have advocated the inclusion of higher order terms (see for example Tennyson et al. (1978) and Ashkenazi (1965)), but the effort in determining the corresponding strength parameters hardly justifies the gain in accuracy.

cross term coefficients, F_{12}, F_{13} and F_{23}, can be found from simple, single stress component tests. Tsai and Wu propose to determine the cross term coefficients by running biaxial failure tests. Unfortunately, such tests are complicated and expensive. Indeed it should be expected that the interaction parameters, will be dependent upon the signs of the stresses and thus will not be unique (see the discussion of quadratic failure criteria by Wu (1974)). Moreover, the allowable values of these parameters are limited by bounding conditions to ensure that the failure envelope is closed (see Section 3 for details). Recently, Labossiere and Neale (1987b) have proposed alternative methods of calculating the strength parameters.

Reddy and Pandey (1987) have examined the accuracy of the various failure criteria discussed above in predicting the initial failure (or first ply failure) of laminated composite plates under in-plane or bending loads. They concluded that all these failure criteria were equivalent in their prediction of failure when laminates were subjected to in-plane load. For laminates subjected to bending, the maximum strain and Hill's criteria were found to predict different failure location and failure loads to the other criteria.

The Tsai-Wu tensorial failure criterion has the advantage of being invariant under coordinate transformation. Furthermore, Wu (1974) has shown that all other stress based failure theories (including the maximum stress criterion) are the degenerate cases of the tensor polynomial criterion given by Eq. (2.1). A major shortcoming of these polynomial-based failure criteria, however, is that they primarily predict the onset, but not the mode, of failure. In view of the diverse failure mechanisms that are operative in a composite material, this shortcoming is particularly severe. Identification of the mode of damage is a required feature if the failure criterion is to be useful for progressive failure analysis of fibre composite

laminates by computational procedures. Motivated by the foregoing need, Hashin (1980) proposed separate quadratic failure criterion to distinguish between the fibre dominated failure mode and the matrix dominated failure mode in unidirectional FRMs. These criteria had different forms for tensile and compressive stresses. One of the advantages of Hashin's approach was that troublesome biaxial test data were not needed for the evaluation of various strength parameters. It should also be noted that Hashin's failure criteria were intended to identify only the failure modes within a single ply (i.e. intralaminar modes of failure). Subsequently, Lee (1982) used a similar criterion to distinguish delamination analytically from other modes. Another way of differentiating between the modes of failure has been to ascribe failure to either matrix or fibre depending on the relative magnitude of the various terms appearing in Eq. (2.1) (see for example, Chiu (1969)).

2.5 Constitutive Modelling of Damaged Composites

The major damage which develops in laminates under static or cyclic loading is in the form of interlaminar and intralaminar cracks. The former develop gradually and slowly between the plies. The latter appear suddenly and in large numbers in plies in which the stresses reach critical values defined by the initial failure criteria. The main macroscopic effect of such cracks on laminate properties is reduction of stiffness.

Many approaches have been used in the past to model the behaviour of damaged (or cracked) laminates. Attention has mostly been directed towards the effect of intralaminar cracks on the load carrying capacity of laminates under in-plane loading conditions. Depending upon the mode of failure predicted by the failure criteria, many authors have suggested a softening of response in the direction in which the failure has occurred. Petit and

Waddoups (1969) modelled the softening by giving the tangent moduli rela-
tively high negative values. Chiu (1969) considered instantaneous stress
relaxation in the failed layers. Such post-failure models have been used by
many authors (see for example the survey article by Nahas (1986)). Swanson
and Christoforou (1987) proposed an empirical expression, in terms of an
effective strain, for softening due to matrix cracking. Chang and Chang
(1987) assumed that upon matrix cracking in a unidirectional layer, only the
transverse modulus and the Poisson's ratio reduce to zero while the proper-
ties in the other directions remain unchanged. For fibre failure they
postulated that both the longitudinal and shear moduli reduce according to
the Weibull distribution, whereas the transverse modulus and Poisson's ratio
vanish.

Attention in recent years has focused on the rigorous determination of
stiffness reduction, primarily for the case of transverse tension cracking in
the matrix. The analyses have been concerned mainly with cross-ply laminates
in which only the 90° plies are cracked. A precise estimate of the stiffness
reductions for laminates with general layups is presently not available.
Perhaps the simplest model is that of Highsmith and Reifsneider (1982) who
devised a simple shear lag method to evaluate stiffness reduction due to
cracks. Another method of analysis is due to Laws, Dvorak and Hejazi (1983)
who employed the self-consistent scheme for the prediction of the effective
stiffness of a cracked ply. This method is based on the solution of the
problem of a single crack embedded in an infinite medium. A different
approach which was proposed by Talreja (1985, 1986) is based on a continuum
damage theory in which the material is characterized by a set of vector
fields each representing a damage mode. The resulting constitutive equations
contain numerous parameters which must be determined experimentally. Hashin

(1985,1986,1987) used the variational method on the basis of the principle of minimum complementary energy for the analysis of cracked laminates.

The major shortcoming of these so-called rigorous models is that they lack generality of the loading and configuration, and their actual use is often complicated by the requirement for numerous experimentally determined quantities.

2.6 Ultimate Failure

The final point to be addressed is the ultimate failure of laminates. The problem of ultimate failure in laminates can be approached by monitoring the growth of damage zones until failure occurs either by excessive debonding or fibre fracture of primary load-carrying plies.

A number of progressive failure analyses have been presented in the literature. These require as input information the complete constitutive properties of the individual plies, and use the classical lamination theory (CLT) to trace the overall load-displacement response up to the ultimate state. Among the most recent study in this area are the papers by Lee (1982), Sandhu et al. (1983), Swanson and Christoforou (1987), Ochoa and Engblom (1987), Takahashi and Chou (1987), and Chang and Chang (1987).

One of the very few failure criteria which has successfully been applied to the laminate as a "whole" is the Puppo-Evenson (1972) quadratic failure criterion. This theory is a direct laminate analysis which makes no constitutive assumption and does not involve lamination theory. It has been shown by Hütter, Schelling and Krauss (1974) that for glass/epoxy laminates loaded biaxially, the Puppo and Evensen analysis predicts the observed failure results quite well.

CHAPTER 3

THEORETICAL FOUNDATIONS OF THE PROPOSED CONSTITUTIVE MODEL

3.1 Introduction

The primary objective of the present chapter is to develop a relatively comprehensive constitutive model for progressive failure analysis of laminated composite structures comprising layers of unidirectional and/or bidirectional (i.e. woven fabric) FRMs.

The model, which attempts to cover the entire stress history, is essentially representative of the mechanical behaviour of one layer. To this end, the first part of this chapter is devoted to the derivation of the constitutive equations for single layers of unidirectional and bidirectional FRM. In the final part these equations are combined with classical lamination theory to form the complete constitutive relations for multilayer laminates. For conciseness and brevity, the formulations are expressed in tensorial (indicial) notation, wherever possible. Matrix constitutive equations are also presented for direct finite element implementation, details of which are provided in Chapter 4.

3.2 Descriptive Outline of the Model

Physically, the nonlinear and/or irreversible deformation of FRMs can be caused by inherent material nonlinearities of the individual constituents, damage accumulation due to fibre or matrix cracking, interfacial debonding, or any combination of the above. These phenomena may be described macroscopically within the framework of plasticity theory, thus providing the impetus for the elastic-plastic-failure model proposed here.

It is instructive to present first a descriptive outline of the func-
tioning of the model before its analytical formulation. We attempt to
describe the behaviour of FRMs in terms of the "classical incremental theory
of plasticity". In order to do this, we ignore the detailed structure of the
material and assume that it is permissible to consider stress and strain as
averages taken throughout a representative volume which is itself taken to
correspond to a point in a continuum. We stay entirely within the most fami-
liar framework of incremental plasticity, with small displacements and no
viscosity, creep or thermoelasticity. Moreover, only the mechanical beha-
viour of the material under static or quasi-static loading will be considered
(i.e. strain rate effects on yielding are ignored). It will be assumed that
any degradation which occurs due to ply yielding or ply failure is restricted
to that ply and is not transmitted to adjacent plies. Also no attempt will
be made to model the interlaminar effects.

The model proposed in this study may best be divided into three regimes:
the elastic regime, the plastic regime and the post-failure regime. In this
model the linear elastic stress-strain relation is used first until the
combined state of stress reaches an initial yield surface which marks the
beginning of plastic flow. Further loading produces plastic response until
failure is reached. For simplicity the initial yield criterion and the fail-
ure criterion are assumed to have similar functional forms in stress space.
Between the initial yielding state and the failure state, the constitutive
relations are expressed in incremental form based on the associated flow rule
of plasticity theory. When failure is reached it is ascribed to either
matrix or fibre depending on the relative magnitude of the various stress
ratios appearing in the criterion. To simulate post-failure behaviour, two
types of failure modes are defined, namely, brittle and ductile. For the

brittle fracture mode, the layer is assumed to lose its entire rigidity and strength in the dominant stress direction. For the ductile fracture mode, the layer retains its strength but loses all of its stiffness in the failure direction.

Different stages of the proposed elastic-plastic-fracture model mentioned above can be illustrated schematically on an idealized uniaxial stress-strain curve shown in Fig. 3.1.

In what follows a complete set of elastoplastic constitutive relations will first be developed in a general form, appropriate for any orthotropic material whose behaviour falls within the framework of time and temperature independent incremental plasticity. These formulations will subsequently be specialized to the single layers of unidirectional and bidirectional FRMs under plane stress, since the latter is the condition that normally prevails in plies of a laminate sufficiently distant from singularities.

3.3 General Formulation of the Single Layer Constitutive Equations

3.3.1 Elastic Regime

In the initial loading state, the FRM layer is treated as a homogeneous and orthotroipc linear elastic continuum. Let x_1, x_2 and x_3 denote a local orthogonal Cartesian axes, the axes of x_1 and x_2 being in the mid-plane of the layer and x_3 in the thickness direction. These axes coincide with the principal axes of orthotropy. All subsequent discussions and derivations will be referred to this local coordinate system.

In the linear elastic range there is a one-to-one analytical relation between the stress tensor σ_{ij} and the strain tensor e_{ij}. This can be expressed as (Sokolnikoff, 1956)

$$\sigma_{ij} = C^e_{ijk\ell} \, e_{k\ell} \qquad (i,j,k,\ell = 1,2,3) \qquad (3.1)$$

where $C^e_{ijk\ell}$ is a fourth order stiffness tensor whose components are the elastic constants, or moduli of the material, and repeated indices imply summation. Equation (3.1) is a natural generalization of Hooke's law, and it is used in all developments of the linear theory of elasticity.

Inasmuch as the components σ_{ij} and e_{ij} are symmetric, the tensor of elastic constants $C^e_{ijk\ell}$ is symmetric with respect to the first two and the last two indices, i.e.

$$C^e_{ijk\ell} = C^e_{jik\ell} = C^e_{ij\ell k} = C^e_{ji\ell k} \qquad (3.2)$$

Such symmetry considerations reduce the maximum number of independent elastic constants from 81 to 36.

Green (1839) asserted that for an elastic body there exists a potential function Φ with the property

$$\sigma_{ij} = \partial\Phi/\partial e_{ij} \qquad (3.3)$$

For a linear elastic body, Φ coincides with the strain-energy density function so that

$$\Phi = 1/2 \, C^e_{ijk\ell} \, e_{ij} \, e_{k\ell} = 1/2 \, \sigma_{ij} \, e_{ij} \qquad (3.4)$$

where Eq. (3.1) is used in the last step.

It can be deduced from Eqs. (3.3) and (3.4) that the order of the pairs of subscripts ij and kℓ are interchangeable, so that

$$C^e_{ijk\ell} = C^e_{k\ell ij} \qquad\qquad (3.5)$$

Thus, under the above restriction, the 36 independent elastic constants can now be reduced to 21 such constants for the most general case of an anisotropic elastic body. If there are elastic symmetries in certain directions of the material, then the number of independent constants $C^e_{ijk\ell}$ in Eq. (3.1) can be further reduced.

To avoid dealing with double sums, it is convenient to write Hooke's law in contracted notation as

$$\sigma_i = C^e_{ij}\epsilon_j \qquad (i,j = 1,2,\ldots,6) \qquad\qquad (3.6)$$

The relationships between the contracted and tensor notations are given in Table 3.1 below.

Table 3.1 Comparison between tensor, engineering and contracted notation for stresses and strains.

Stresses		Strains		
Tensor	Contracted	Tensor	Engineering	Contracted
σ_{11}	σ_1	e_{11}	ϵ_{11}	ϵ_1
σ_{22}	σ_2	e_{22}	ϵ_{22}	ϵ_2
σ_{33}	σ_3	e_{33}	ϵ_{33}	ϵ_3
$\sigma_{23} = \tau_{23}$	σ_4	$2e_{23}$	γ_{23}	ϵ_4
$\sigma_{31} = \tau_{31}$	σ_5	$2e_{31}$	γ_{31}	ϵ_5
$\sigma_{12} = \tau_{12}$	σ_6	$2e_{12}$	γ_{12}	ϵ_6

If the material has two mutually perpendicular planes of elastic symmetry, it is considered orthotropic. For such materials, there are only nine independent elastic constants C_{ij}^{e}, and the stress-strain relation (Eq. 3.6) in matrix form becomes

$$
\begin{bmatrix} \sigma_1 \\ \sigma_2 \\ \sigma_3 \\ \sigma_4 \\ \sigma_5 \\ \sigma_6 \end{bmatrix} = \begin{bmatrix} C_{11}^{e} & C_{12}^{e} & C_{13}^{e} & 0 & 0 & 0 \\ & C_{22}^{e} & C_{23}^{e} & 0 & 0 & 0 \\ & & C_{33}^{e} & 0 & 0 & 0 \\ & & & C_{44}^{e} & 0 & 0 \\ & & & & C_{55}^{e} & 0 \\ \text{Symmetric} & & & & & C_{66}^{e} \end{bmatrix} \begin{bmatrix} \epsilon_1 \\ \epsilon_2 \\ \epsilon_3 \\ \epsilon_4 \\ \epsilon_5 \\ \epsilon_6 \end{bmatrix} \tag{3.7}
$$

Assuming that the material coefficients remain constant during the deformation process, the incremental elastic constitutive relationship takes the following form

$$
d\sigma_i = C_{ij}^{e} \, d\epsilon_j \qquad (i,j = 1,2,\ldots,6) \tag{3.8}
$$

where $d\sigma_i$ and $d\epsilon_i$ are the stress- and strain-increment tensors.

3.3.2 Plastic Regime

A theory of plasticity is a procedure by which a set of constitutive equations for multiaxial stress-states can be derived from uniaxial stress-strain test data. Such a theory accounts, in principle, for the stress history dependent behaviour. Dissipative response characterized by permanent strain accumulation can be evaluated. The theory accounts for

unloading and reloading, and for the interaction of stresses. Some references on the subject of plasticity are the books by Hill (1950), Kachanov (1971), Mendelson (1968), and the review article by Naghdi (1960).

The following four basic ingredients of plasticity theory are proposed for use with FRMs. In addition, item (v) is added to describe the onset of failure:

i)   An initial yield surface, bounding the part of the stress space within which deformation is purely elastic.

ii) A hardening rule, specifying the modification of the yield surface in the course of plastic deformation.

iii) A flow law, indicating the direction of the incremental plastic strain vector.

iv) A plastic modulus or hardening modulus, i.e. the ratio between increments of "effective stress" and "effective plastic strain". This ratio is assumed to be independent of loading direction.

v)   A failure surface, defining an upper bound of the plastic regime in stress space.

In what follows, the analytical formulation of the foregoing items will be presented.

i)   <u>Initial yield</u>

The simplest generalization of the yield condition for plastically anisotropic materials is the general quadratic function given by (cf. Baltov and Sawczuk, 1965; Shih and Lee, 1978)

$$f(\sigma_{ij}, \alpha_{ij}, A_{ijk\ell}, k) = 0 \qquad (3.9a)$$

where

$$f \equiv A_{ijk\ell}(\sigma_{ij} - \alpha_{ij})(\sigma_{k\ell} - \alpha_{k\ell}) - k^2 \qquad (3.9b)$$

In Eq. (3.9b), $A_{ijk\ell}(i,j,k,\ell = 1,2,3)$ denotes the fourth order tensor of anisotropic strength parameters which describes the shape of the yield surface, and the tensor α_{ij} describes the origin of the yield surface. The effective size of the yield surface is given by the scalar parameter k which stands for a reference yield stress.

In contracted notation Eq. (3.9a,b) can be rewritten as

$$f(\sigma_i, \alpha_i, A_{ij}, k) \equiv A_{ij}(\sigma_i - \alpha_i)(\sigma_j - \alpha_j) - k^2 = 0 \quad (i,j = 1,2,\ldots,6) \quad (3.9c)$$

Generally, yield stresses are different in tension and compression. It should be noted that α_{ij} in Eq. (3.9b) (or α_j in Eq. (3.9c)) accounts for the strength differential between tensile and compressive yield stresses by shifting the origin of the yield surface.

Since the material cannot distinguish between positive and negative shear stresses (provided that the reference frame coincides with the principal axes of orthotropy), all odd powers (one, in this case) of shear stress terms in Eq. (3.9c) must vanish.

From the above arguments and symmetry considerations, one can write A_{ij} and α_i in the following matrix form

$$[A] = \begin{bmatrix} A_{11} & A_{12} & A_{13} & 0 & 0 & 0 \\ & A_{22} & A_{23} & 0 & 0 & 0 \\ & & A_{33} & 0 & 0 & 0 \\ & & & A_{44} & 0 & 0 \\ & & & & A_{55} & 0 \\ \text{Symmetric} & & & & & A_{66} \end{bmatrix} \qquad (3.10)$$

$$\{\alpha\} = \{\alpha_1 \ \alpha_2 \ \alpha_3 \ 0 \ 0 \ 0\}^T$$

The function which expresses the initial yield conditions for an orthotropic material can be defined as

$$f_0 \ (\sigma_i, \ \alpha_i^0, \ A_{ij}^0, \ k_0) = 0 \qquad (3.11)$$

where the suffix $_0$ denotes the initial value of the quantity to which it is attached.

The parameters A_{ij}^0, α_i^0 and k_0 must be obtained from experiments. Appendix A provides the details of evaluating these parameters.

ii) <u>Subsequent yield and hardening rule</u>

After initial yielding, it is necessary to define conditions for subsequent yielding of the material under changing load. Because stress states outside the yield surface are not admissible, an increase in load must be accounted for in one of two ways. In an ideal plastic material the point of interest merely translates on the unchanged initial yield surface, while if some form of hardening is allowed, the yield surface will change shape and/or position in a manner dictated by the hardening rule and the stress point will be somewhere on the subsequent yield surface.

The progressive deformation of the material is described in terms of evolution of the family of yield (or loading) surfaces given by

$$f(\sigma_i, \alpha_i(\kappa), A_{ij}(\kappa), \ k(\kappa)) = 0 \qquad (3.12)$$

where κ termed the hardening parameter is a suitably defined plastic internal variable which can be related to some measure of plastic deformation or plastic work.

Relative to an arbitrary point in stress space, a state of "loading" is specified by

$$f = 0; \quad d\kappa \neq 0 \; ; \quad \text{and} \quad (\partial f/\partial \sigma_i) \, d\sigma_i > 0$$

During "neutral loading"

$$f = 0; \quad d\kappa = 0; \quad \text{and} \quad (\partial f/\partial \sigma_i) \, d\sigma_i = 0$$

Finally during "unloading" we have

$$f = 0; \quad d\kappa = 0; \quad \text{and} \quad (\partial f/\partial \sigma_i) \, d\sigma_i < 0$$

By allowing α_i, A_{ij} and k in Eq. (3.12) to vary as some function of the hardening parameter κ various kinds of hardening models can be simulated.

The two principal models of strain hardening behaviour that have been developed are the "kinematic" and "isotropic" hardening models. Isotropic hardening occurs when the initial yield surface expands uniformly during plastic flow. For kinematic hardening the yield surface does not change its initial shape and orientation but translates in the stress space like a rigid body. This concept was introduced by Prager (1955) and later modified by Ziegler (1959). The kinematic hardening model accounts for the Bauschinger

effect*, which is an experimentally observed phenomenon under cyclic loading situations.

When $k(\kappa)$ = constant (i.e., $\partial k/\partial \kappa = 0$) and $A_{ij}(\kappa)$ = constant (i.e., $\partial A_{ij}/\partial \kappa = 0$) in Eq. (3.12), we obtain the case of kinematic work-hardening. If on the other hand $\partial \alpha_i/\partial \kappa = 0$; $\partial A_{ij}/\partial \kappa = 0$ and $k(\kappa)$ is a monotonically increasing function, isotropic workhardening occurs. The latter can alternatively be attained by allowing the A_{ij} parameters to vary in a proportional manner while $\partial \alpha_i/\partial \kappa = 0$ and $\partial k/\partial \kappa = 0$.

More recently, attempts have been made at combining the two preceding models in a mixed hardening formulation (Axelsson and Samuelsson, 1979), in order to obtain a more realistic representation of elastoplastic behaviour. In this case, the yield surface experiences translation and uniform expansion in all directions, i.e. it retains its original shape.

General "anisotropic" hardening can be introduced by letting all the parameters α_i, A_{ij} and k vary with κ. Such a theory accounts for changes in the shape of the yield locus during plastic deformation, a feature that is absent in the hardening models discussed so far. It should be noted that the kinematic hardening model is a special case of anisotropic hardening whereby the anisotropy is induced by Bauschinger effect.

In the present study, special types of isotropic and anisotropic hardening models are used. The latter allows for a nonproportional change of the yield values and thus leads to a distorted shape of the yield surface (i.e., $\partial A_{ij}/\partial \kappa \neq$ constant) while $\partial \alpha_i/\partial \kappa = 0$ and $\partial k/\partial \kappa =$ constant. The mathematical details of these models are presented in Appendix B.

---

*The Bauschinger effect refers to a particular type of directional anisotropy induced by plastic deformation, namely, that an initial plastic deformation of one sign reduces the resistance of the material with respect to a subsequent plastic deformation of the opposite sign.

iii) <u>Flow rule</u>

After initial yielding the material behaviour will be partly elastic (recoverable) and partly plastic (irrecoverable). It is a fundamental assumption in the infinitesimal theory of plasticity that the increment of the total strain tensor in the plastic range may be decomposed into elastic and plastic components $d\epsilon_i^e$ and $d\epsilon_i^p$ by simple superposition, so that

$$d\epsilon_i = d\epsilon_i^e + d\epsilon_i^p \qquad (i = 1,2,\ldots,6) \qquad (3.13)$$

The elastic strain increment is related to the stress increment by the generalized Hooke's law (Eq. (3.8)), i.e.

$$d\sigma_i = C_{ij}^e \, d\epsilon_j^e \qquad (i,j = 1,2,\ldots,6) \qquad (3.14)$$

In order to derive the relationship between the plastic strain increment and the stress increment a further assumption about the material must be made. In particular it will be assumed that the plastic strain increment is proportional to the stress gradient of a function, g, termed the plastic potential*, so that

$$d\epsilon_i^p = d\lambda \, \frac{\partial g}{\partial \sigma_i} \qquad (3.15)$$

---

*Plastic potential function is analogous to the potential function in ideal fluid flow and the strain- or complementary-energy density function in linear elasticity. A theoretical basis for its existence is developed by Hill (1950).

where $d\lambda$ is a positive scalar parameter which can vary throughout the deformation process. Eq. (3.15) is termed the "flow rule" since it governs the plastic flow after yielding. The gradient of the potential surface $\partial g/\partial \sigma_i$ defines the direction of the plastic strain increment vector $d\epsilon_i^p$, while the length is determined by $d\lambda$. The flow rule is termed "associated" if the plastic potential surface has the same shape as the current yield or loading surface, i.e. $f \equiv g$ (cf. Bland, 1957). The latter has a special significance in the mathematical theory of plasticity, since for this case certain variational principles and uniqueness theorems can be formulated.

Since there is very little experimental evidence on subsequent yield surfaces, especially for FRMs, the associated flow rule will be applied in the following work. In this case Eq. (3.15) becomes

$$d\epsilon_i^p = d\lambda \frac{\partial f}{\partial \sigma_i} \qquad (3.16)$$

Eq. (3.16) is also termed the normality condition since $\partial f/\partial \sigma_i$ is a vector directed outward and normal to the yield surface at the stress point under consideration.

iv) Effective stress and effective strain

For the work-hardening theory of plasticity to be of any practical use, we must relate the hardening parameter κ in the loading function (Eq. (3.12)) to experimental uniaxial stress-strain curves. To this end we are looking for some stress variable, called "effective stress", which is a function of the stresses, and some strain variable, called "effective strain", which is a function of the plastic strains, so that they can be used to correlate the test results obtained by different loading programs.

If from here on the strength differential in tension and compression is ignored (i.e., $\alpha_i = 0$) partly for the sake of simplicity and also due to a lack of adequate knowledge of the post-yield behaviour of FRMs, it is then convenient to define the effective stress $\bar{\sigma}$ as follows:

$$\bar{\sigma}^2 = A_{ij}\sigma_i\sigma_j \qquad (i,j = 1,2,\ldots,6) \qquad (3.17)$$

Therefore the loading function can be rewritten as

$$f(\sigma_i, A_{ij}(\kappa), k(\kappa)) \equiv \bar{\sigma}^2(\sigma_i, A_{ij}(\kappa)) - k^2(\kappa) = 0 \qquad (3.18)$$

The definition of effective plastic strain $\bar{\epsilon}^P$ is not quite as simple. Two methods are generally used. One defines the effective plastic strain increment in terms of the specific plastic work increment, dW^P, in the form

$$dW^P = \sigma_i \, d\epsilon_i^P \qquad (3.19)$$

$$= k \, d\bar{\epsilon}^P$$

The second method defines the effective plastic strain increment as a metric in the space of plastic strains ϵ_i^P. In this case we can intuitively write an expression for $d\bar{\epsilon}^P$ as

$$(d\bar{\epsilon}^P)^2 = A_{ij}^* \, d\epsilon_i^P \, d\epsilon_j^P \qquad (3.20)$$

where A_{ij}^* is a matrix of coefficients. It is shown in Appendix C that A_{ij}^* is in fact the inverse of the matrix A_{ij} provided $|A_{ij}| \neq 0$.

The hardening parameter κ appearing in the loading function (Eq. (3.12)) is commonly defined either as

$$\kappa = \bar{\epsilon}^p = \int d\bar{\epsilon}^p \qquad (3.21a)$$

or

$$\kappa = W^p = \int \sigma_i \, d\epsilon_i^p \qquad (3.21b)$$

where the integrations are performed over appropriate strain paths. The first definition complies with the strain hardening hypothesis while the second is in accord with the work hardening hypothesis. In either case κ is a history dependent parameter. For algebraic convenience the strain-hardening hypothesis is adopted in the present study. Accordingly, the effective yield stress-effective plastic strain relation has the general form

$$k = H(\bar{\epsilon}^p) \qquad (3.22)$$

Then upon differentiation we obtain the slope

$$H' = \frac{dk}{d\bar{\epsilon}^p} \qquad (3.23)$$

evaluated at the current value of the effective yield stress k. The function H, and its derivative H' (termed the plastic or hardening modulus associated with the rate of expansion of the yield surface) are derivable from a generalized effective stress-effective strain diagram which is usually identified with one of the stress-strain curves along the principal material directions. For a bilinear stress-strain diagram adopted in this study, H' is a constant and we have

$$k = k_0 + H'\bar{\epsilon}^p$$

With a view to determining $d\lambda$, we use the flow rule (Eq. (3.16)) in Eq. (3.20) to obtain

$$(d\bar{\epsilon}^p)^2 = A^*_{ij} \, (d\lambda)^2 \, \frac{\partial f}{\partial \sigma_i} \, \frac{\partial f}{\partial \sigma_j} \tag{3.24}$$

Now from Eqs. (3.17) and (3.18) we have

$$\frac{\partial f}{\partial \sigma_i} = 2 \, k \, a_i \tag{3.25}$$

where

$$a_i = \frac{\partial \bar{\sigma}}{\partial \sigma_i} = \frac{1}{k} \, A_{ij} \, \sigma_j \tag{3.26}$$

are the components of a plastic flow vector in the stress space, $\sigma_1, \sigma_2, \ldots, \sigma_6$.

Introducing Eqs. (3.25) and (3.26) into Eq. (3.24) and noting that $A_{ik} A^*_{kj} = \delta_{ij}$[†] (see Appendix C), yields

$$d\lambda = \frac{d\bar{\epsilon}^p}{2k} \tag{3.27}$$

With the aid of Eqs. (3.25) and (3.27), the flow rule given by Eq. (3.16) may be re-expressed as

$$d\epsilon^p_i = d\bar{\epsilon}^p \, a_i \tag{3.28}$$

We can now proceed with the derivation of the incremental elastoplastic stress-strain relationships.

[†] δ_{ij} is the Kronnecker-delta defined as, $\delta_{ij} = \begin{cases} 0 & \text{for } i \neq j \\ 1 & \text{for } i = j \end{cases}$

During plastic loading, both initial yield and subsequent stress states must satisfy the yield condition, i.e. df = 0. Therefore, plastic flow is governed by the following consistency condition*

$$df = \frac{\partial f}{\partial \sigma_i} d\sigma_i + \frac{\partial f}{\partial A_{ij}} dA_{ij} + \frac{\partial f}{\partial k} dk = 0 \qquad (3.29)$$

It is interesting to note that in all the previous work on anisotropic plasticity (e.g. Whang, 1969; Valliappan, 1971) the term $\partial f/\partial A_{ij}$ was not included in the formulation even though the assumption of varying A_{ij}'s was made. Consistent with the strain hardening hypothesis given by Eq. (3.21a), the parameters A_{ij} and k can in general be functions only of the accumulated effective plastic strain $\bar{\epsilon}^p$. Thus, we may write

$$dk = H' \, d\bar{\epsilon}^p$$

$$(3.30)$$

$$dA_{ij} = \frac{\partial A_{ij}}{\partial k} dk = \frac{\partial A_{ij}}{\partial k} H' \, d\bar{\epsilon}^p$$

Also from Eqs. (3.13) and (3.14) we can write the stress increment $d\sigma_i$ as

$$d\sigma_i = C^e_{ij} (d\epsilon_j - d\epsilon^p_j) \qquad (3.31)$$

Recalling the flow rule given by Eq. (3.28), the above equation can be recast into the following form

---

*This is the term used by Prager (1949) which demands that loading from a plastic state must lead to another plastic state.

$$d\sigma_i = C^e_{ij} (d\epsilon_j - a_j \, d\bar{\epsilon}^p)$$ (3.32)

Substituting Eqs. (3.30) and (3.32) into Eq. (3.29) and noting that

$$\frac{\partial f}{\partial \sigma_i} = 2k \, a_i \quad ; \quad \frac{\partial f}{\partial A_{ij}} = \sigma_i \sigma_j \quad \text{and} \quad \frac{\partial f}{\partial k} = -2k$$ (3.33)

one can rewrite the consistency condition (Eq. (3.29)) as

$$d\bar{\epsilon}^p = \frac{a_i C^e_{ij}}{\mu H' + a_m C^e_{mn} a_n} \, d\epsilon_j$$ (3.34)

where all the indices take on the values 1,2,...,6 and the parameter μ is given by

$$\mu = 1 - \frac{1}{2k} \sigma_i \sigma_j \frac{\partial A_{ij}}{\partial k}$$ (3.35)

Finally, substitution of Eq. (3.34) in Eq. (3.32) leads to the following elastoplastic constitutive equations

$$d\sigma_i = C^{ep}_{ij} \, d\epsilon_j = (C^e_{ij} - C^p_{ij}) \, d\epsilon_j$$ (3.36)

where C^{ep}_{ij} is the elastoplastic material stiffness tensor and C^p_{ij} is the plastic material stiffness tensor defined as

$$C^p_{ij} = \frac{C^e_{ik} \, a_k \, a_\ell \, C^e_{\ell j}}{\mu H' + a_m \, C^e_{mn} \, a_n}$$ (3.37)

The negative sign appearing in Eq. (3.36) clearly represents the degradation of the material stiffness due to plastic flow.

v)   Failure

A failure criterion defines the maximum strength of the FRM layer under any possible combination of stresses. It is assumed that this criterion is not influenced by the deformation history (i.e. it is path-independent) and can be postulated a priori. Unless otherwise stated, in the present study the failure surface is assumed to have a similar functional form to that of the yield locus, i.e.

$$f_u(\sigma_i, A_{ij}^u, k_u) \equiv A_{ij}^u \sigma_i \sigma_j - k_u^2 = 0 \qquad (3.38)$$

where the suffix u stands for the ultimate values of the quantities to which it is attached. The parameters A_{ij}^u and k_u are material constants which can be related to the ultimate stresses obtained from the same basic tests used to obtain the yield values.

Criteria of the type given above predict the onset of failure but provide no information regarding the modes of failure. The latter are important in studying the behaviour of the material beyond initial failure. The failure mode identification procedure used in the present study will be fully discussed in section 3.4 for plane stress situations.

3.3.3 Post-Failure Regime

To complete the constitutive model, we also need to define the post-failure behaviour for different failure modes. For FRMs, failure may take one of two forms, namely, fibre fracture or matrix cracking. Several approaches can be employed for crack modelling in the post-failure region.

These may be classified as the smeared cracking model, and the discrete cracking model. The particular choice of the model depends upon the purpose of the analysis. In general, if overall load-deflection behaviour is desired, without regard to completely realistic crack patterns and local stresses, the smeared-crack model is probably the best choice. If detailed local behaviour is of interest the use of the discrete model may prove necessary. However, for most structural engineering applications, the smeared cracking model is generally adopted. Such representation, which is favoured in the present work, assumes that the cracked composite remains a continuum, i.e. the cracks are smeared out in a continuous fashion. The effects of such cracks on the behaviour of the failed layer is the reduction of stiffness and/or strength in certain directions.

The fibre fracture is assumed to cause a loss in load carrying capacity (i.e. strength and stiffness) in the fibre direction. This corresponds with the brittle fracture mode shown in Fig. 3.1. Matrix cracking; on the other hand, is assumed to be caused by shear and/or transverse tension. These cracks are formed parallel to the fibre directions as shown schematically in Fig. 3.2. When the cracked layer is within a multilayer laminate the crack opening displacements will be constrained by the adjacent layers. This leads to a gradual loss of load carrying capacity or softening of the failed layer in the overall sense. The extent of softening, marked by the slope of the descending part of the stress-strain curve, is generally dependent on the orientation of the adjacent plies in a laminate, i.e. it is laminate-dependent. This leads to considerable complications in the development of continuum constitutive theories for FRM layers beyond initial failure. In the present work the two extreme cases of brittle and ductile fracture models

shown in Fig. 3.1 are considered sufficient to serve as bounds to the actual behaviour after matrix cracking.

The details of the post-failure modelling under plane stress conditions are outlined in Section 3.4 for unidirectional and bidirectional layers.

3.4 Plane Stress Formulation of the Single Layer Constitutive Equations

The plies of a laminate are generally under the state of plane stress at sufficient distance from the free edges. Therefore the discussion in this section will be devoted to specialization of the preceding constitutive equations to plane stress situations. Under such conditions, the through-thickness stresses can be neglected (i.e., $\sigma_3=\sigma_4=\sigma_5=0$).

3.4.1 Elastic Regime

The elastic constitutive relation given by Eq. (3.7) may now be written as:

$$
\begin{bmatrix} \sigma_1 \\ \sigma_2 \\ \sigma_6 \end{bmatrix} =
\begin{bmatrix} Q_{11}^e & Q_{12}^e & 0 \\ Q_{21}^e & Q_{22}^e & 0 \\ 0 & 0 & Q_{66}^e \end{bmatrix}
\begin{bmatrix} \epsilon_1 \\ \epsilon_2 \\ \epsilon_6 \end{bmatrix}
\tag{3.39}
$$

where the components of the reduced elastic stiffness matrix Q_{ij}^e can be related to the C_{ij}^e constants by using $\sigma_3 = 0$ in Eq. (3.7). Thus

$$
Q_{11}^e = C_{11}^e - C_{13}^{e\,2}/C_{33}^e
$$

$$
Q_{12}^e = Q_{21}^e = C_{12}^e - C_{12}^e C_{23}^e/C_{33}^e
$$

$$
Q_{22}^e = C_{22}^e - C_{23}^{e\,2}/C_{33}^e
\tag{3.40}
$$

$$
Q_{66}^e = C_{66}^e
$$

The Q_{ij}^e coefficients can also be represented in the more common engineering form as (see e.g. Jones, 1975)

$$Q_{11}^e = E_1/(1-\nu_{12}\nu_{21})$$

$$Q_{22}^e = E_2/(1-\nu_{12}\nu_{21})$$

$$Q_{12}^e = Q_{21}^e = \nu_{21}E_1/(1-\nu_{12}\nu_{21}) \qquad (3.41)$$

$$Q_{66}^e = G$$

where E_1 and E_2 are the elastic moduli in the x_1 and x_2 directions, respectively; ν_{12}, ν_{21} are Poisson's ratios; and G is the in-plane shear modulus. In the notation for Poisson's ratios the first index refers to the direction of imposed strain and the second index refers to the response direction. The Poisson's ratios ν_{12} and ν_{21} are related through the reciprocal relationship

$$\nu_{12}E_2 = \nu_{21}E_1 \qquad (3.42)$$

leaving a total of four independent elastic constants to describe the planar orthotropy.

In symbolic matrix notation, the incremental elastic constitutive relationship for the plane orthotropic case is

$$\{d\sigma\} = [Q^e] \{d\epsilon\} \qquad (3.43)$$

where

$$\{\sigma\} = \{\sigma_1 \ \sigma_2 \ \sigma_6\}^T$$

<div align="right">(3.44)</div>

$$\{\epsilon\} = \{\epsilon_1 \ \epsilon_2 \ \epsilon_6\}^T$$

are the stress and strain vectors and $[Q^e]$ is the 3 x 3 elastic material stiffness matrix.

3.4.2 Plastic Regime

The yield criterion given by Eq. (3.18) can now be written in matrix notation as

$$f(\{\sigma\},[A],k) \equiv \bar{\sigma}^2(\{\sigma\},[A]) - k^2 = 0 \qquad (3.45)$$

where

$$\bar{\sigma}^2(\{\sigma\},[A]) = \{\sigma\}^T [A] \{\sigma\} \qquad (3.46)$$

and

$$[A] = \begin{bmatrix} A_{11} & A_{12} & 0 \\ A_{12} & A_{22} & 0 \\ 0 & 0 & A_{66} \end{bmatrix} \qquad (3.47)$$

Although any polynomial in the form of Eq. (3.45) represents a surface in the stress space, not all the surfaces are admissible yield surfaces. A geometric interpretation is useful for examining the constraints on the form of Eq. (3.45). Specifically, in the plane stress state, open-ended yield surfaces are physically impossible since they imply infinite strength for

some state of stress.* To ensure the boundedness of the yield surface in the $\sigma_1, \sigma_2, \sigma_6$ stress space we must have

$$A_{ij}\sigma_i\sigma_j > 0 \qquad (i,j = 1,2,\ldots,6) \qquad (3.48)$$

for an arbitrary stress tensor σ_i. Mathematically, the inequality (3.48) implies that the matrix of anisotropic strength parameters [A] has to be positive definite. Since [A] is symmetric, the necessary and sufficient conditions for it to be positive definite are that all its principal minors be positive. Thus, the components of [A] must satisfy the following inequalities:

$$A_{11}A_{22} - A_{12}^2 > 0$$

$$A_{11}A_{66} > 0 \qquad (3.49)$$

$$A_{22}A_{66} > 0$$

Geometrically, the positive definiteness of [A] ensures that the yield surface is an ellipsoid. The interaction parameter A_{12} defines the angular orientation of the ellipsoid (with respect to the σ_1 and σ_2 axes), and determines the lengths of its major and minor axes. The range of allowable values for A_{12}, however, is limited by the bounding conditions (3.49) and this in turn can often result in unsatisfactory yield (or failure) surfaces.

---

* In three-dimensional states of stress a loading state exists for which most materials exhibit essentially infinite strength. In fact, any criterion neglecting the effect of hydrostatic stress, such as the von Mises criterion (cf. Mendelson, 1968), is such a case.

The incremental elastoplastic constitutive relations given by Eqs. (3.36) and (3.37) can be expressed in matrix notation as:

$$\{d\sigma\} = [Q^{ep}]\{d\epsilon\} = ([Q^e] - [Q^p])\{d\epsilon\}$$

$$= ([Q^e] - \frac{[Q^e]\{a\}\{a\}^T[Q^e]}{\mu H' + \{a\}^T[Q^e]\{a\}}) \{d\epsilon\} \qquad (3.50)$$

where $[Q^p]$ and $[Q^{ep}]$ are the plane stress plastic and elastoplastic material stiffness matrices; and

$$\{a\} = 1/k \ [A]\{\sigma\}$$

$$(3.51)$$

$$\mu = 1 - 1/2k \ \{\sigma\}^T \ [\partial A/\partial k] \ \{\sigma\}$$

The treatment of unidirectional (U/D) and bidirectional (B/D) layers differs in the way their yield (and failure) surfaces are defined. Otherwise the above formulations are common to both these cases. We shall now define separate yield (and failure) functions for U/D and B/D layers.

(a) Bidirectional layers

Let us consider the plane stress form of Hill's yield criterion (1950) which reads (see Appendix A):

$$(\frac{\sigma_1}{X})^2 + (\frac{\sigma_2}{Y})^2 - (\frac{1}{X^2} + \frac{1}{Y^2} - \frac{1}{Z^2})\sigma_1\sigma_2 + (\frac{\sigma_6}{S})^2 = 1 \qquad (3.52)$$

where X,Y,Z are the yield stresses under uniaxial loading along each of the three principal axes of anisotropy (Fig. 3.3a); and S is the corresponding

yield value of in-plane shear stress σ_6. In the absence of information about Z, the yield stress U for uniaxial tension at 45° to the fibres can be used to obtain an estimate for Z (see Appendix A). Under these circumstances, comparing Eqs. (3.45) and (3.52) for the four test conditions gives

$$A_{11} = \frac{k^2}{X^2} ; \qquad A_{22} = \frac{k^2}{Y^2} ; \qquad A_{66} = \frac{k^2}{S^2} ; \qquad \text{and}$$

$$(3.53)$$

$$A_{12} = [\frac{4}{U^2} - (\frac{1}{X^2} + \frac{1}{Y^2} + \frac{1}{S^2})]\, k^2$$

One of the disadvantages of this criterion is that it requires four material constants to define the yield function, and quite often four separate tests are not available. In addition for many materials it proved difficult to satisfy Eq. (3.49) i.e. the boundedness criteria. This motivated a search for a criterion that required fewer input data for its evaluation and did not have as restrictive a condition as that given by Eq. (3.49).

The Puppo-Evensen criterion (1972) (which was originally suggested for the prediction of failure in multilayer laminates) satisfies the above requirements and also possesses features that are ideal for modelling a wide range of bidirectional FRMs. This criterion, in the plane stress case, can be written as:

$$(\frac{\sigma_1}{X})^2 - \Lambda(\frac{X}{Y})\frac{\sigma_1}{X}\frac{\sigma_2}{Y} + \Lambda(\frac{\sigma_2}{Y})^2 + (\frac{\sigma_6}{S})^2 = 1 \qquad (3.54a)$$

$$\Lambda(\frac{\sigma_1}{X})^2 - \Lambda(\frac{Y}{X})\frac{\sigma_1}{X}\frac{\sigma_2}{Y} + (\frac{\sigma_2}{Y})^2 + (\frac{\sigma_6}{S})^2 = 1 \qquad (3.54b)$$

where

$$\Lambda = 3S^2/XY \qquad\qquad (3.54c)$$

Thus, in this case the matrix of anisotropic strength parameters takes one of the following two forms depending on which one of the criteria (3.54a) or (3.54b) is dominant (i.e. corresponds with the greater effective stress $\bar{\sigma}$):

$$[A] = k^2 \begin{bmatrix} \dfrac{1}{X^2} & -\dfrac{3}{2}\dfrac{S^2}{XY^3} & 0 \\[2ex] & 3\dfrac{S^2}{XY^3} & 0 \\[2ex] \text{Symm.} & & \dfrac{1}{S^2} \end{bmatrix} \qquad (3.55a)$$

$$[A] = k^2 \begin{bmatrix} 3\dfrac{S^2}{X^3Y} & -\dfrac{3}{2}\dfrac{S^2}{X^3Y} & 0 \\[2ex] & \dfrac{1}{Y^2} & 0 \\[2ex] \text{Symm.} & & \dfrac{1}{S^2} \end{bmatrix} \qquad (3.55b)$$

Figuratively, Eqs. (3.54 a,b) describe a pair of ellipsoids in the three dimensional stress space $(\sigma_1,\sigma_2,\sigma_6)$. The yield surface is taken to be the inner surface resulting from the intersection of these ellipsoids. The parameter Λ is numerically equal to unity for an isotropic material obeying the von Mises yield criterion (i.e. $X=Y=\sqrt{3}\,S$) and tends to zero for the case of a fabric-like material made up of strong fibres in the x_1 and x_2 directions but with very weak matrix material. In the former case, the yield surface reduces to the von Mises ellipse and in the latter it approaches the square shape (i.e., non-interacting stresses) in the $\sigma_6 = 0$ plane. A typical bi-directionally-reinforced material falls somewhere in between these two extreme cases, i.e. $0 < \Lambda < 1$. Fig. 3.4 illustrates the progressive change

of the yield surface in the $\sigma_6 = 0$ plane, for some representative values of the parameter Λ. The surfaces are plotted for the particular case of equal strength fibres, i.e. $X = Y$.

The condition for the boundedness of the yield surface (Eq. (3.49)) now becomes

$$S^2 < \frac{4}{3} \frac{X^3}{Y}$$

and
(3.56)

$$S^2 < \frac{4}{3} \frac{Y^3}{X}$$

For strongly anisotropic materials (e.g. unidirectional composites in which $X \gg Y$) at least one of the inequalities in (3.56) may be violated. This makes the 3-parameter Puppo-Evensen's criterion unsuitable for prediction of yielding in U/D materials. The following is devoted to treatment of such materials.

b)   Unidirectional layers

Here we propose the 3-parameter Hill's criterion for transversely isotropic medium. This extension of Hill's criterion, which was first suggested by Azzi and Tsai (1965), is based on the concept that the unidirectional fibres (aligned in the x_1 direction as shown in Fig. 3.3b) are randomly distributed and hence the properties in the x_2 and x_3 directions are the same. Thus $Y = Z$ and the 4-parameter Hill's criterion given by Eq. (3.52) reduces to

$$\left(\frac{\sigma_1}{X}\right)^2 + \left(\frac{\sigma_2}{Y}\right)^2 - \frac{\sigma_1\sigma_2}{X^2} + \left(\frac{\sigma_6}{S}\right)^2 = 1 \tag{3.57}$$

The matrix [A] now reads:

$$[A] = k^2 \begin{bmatrix} \dfrac{1}{X^2} & -\dfrac{1}{2}\dfrac{1}{X^2} & 0 \\ & \dfrac{1}{Y^2} & 0 \\ \text{Symm.} & & \dfrac{1}{S^2} \end{bmatrix} \qquad (3.58)$$

It can be shown that the surface represented by Eq. (3.57) satisfies the closure conditions of Eq. (3.49), provided that $Y < 2X$. The latter condition is readily met by the unidirectional FRMs for which $X > Y$.

It should be noted that when Eqs. (3.54 a,b) and (3.57) are used as initial yield criteria the quantities X, Y, S and k are replaced by their initial values X_0, Y_0, S_0 and k_0. During subsequent yielding, if the evolution of the yield surface follows the anisotropic hardening model described in Appendix B, then the individual yield values in terms of the current effective yield stress k become

$$X^2(k) = \frac{E_{p_1}}{H'} (k^2 - k_0^2) + X_0^2$$

$$(3.59)$$

$$Y^2(k) = \frac{E_{p_2}}{H'} (k^2 - k_0^2) + Y_0^2$$

$$S^2(k) = \frac{G_p}{H'} (k^2 - k_0^2) + S_0^2$$

where E_{p_1}, E_{p_2} and G_p are the plastic moduli in the x_1-direction, x_2-direction, and in-plane shear respectively. These moduli remain constant

for the bilinear stress-strain curves considered here and can be expressed in terms of the elastic and tangent moduli as (see Appendix B)

$$E_{p_1} = \frac{E_1 E_{T_1}}{E_1 - E_{T_1}}$$

$$E_{p_2} = \frac{E_2 E_{T_2}}{E_2 - E_{T_2}} \tag{3.60}$$

$$G_p = \frac{G G_T}{G - G_T}$$

In order to use Eqs. (3.54a,b) and (3.57) as failure criteria, X,Y,S and k must be replaced by their ultimate values X_u, Y_u, S_u and k_u. Failure is ascirbed to either the matrix or fibre depending on the relative magnitude of the various stress ratio terms appearing in the failure criterion. The failure mode identification procedure is shown in Table 3.2, for both U/D and B/D layers.

Table 3.2 Failure Identification Procedure

Layer Type	Condition	Failure Mode
Unidirectional	$\left\|\frac{\sigma_1}{X_u}\right\| > \left\|\frac{\sigma_2}{Y_u}\right\|$ and $\left\|\frac{\sigma_1}{X_u}\right\| > \left\|\frac{\sigma_6}{S_u}\right\|$	fibre
	Otherwise $\left\|\frac{\sigma_2}{Y_u}\right\| > \left\|\frac{\sigma_6}{S_u}\right\|$	matrix (tensile)
	$\left\|\frac{\sigma_6}{S_u}\right\| > \left\|\frac{\sigma_2}{Y_u}\right\|$	matrix (shear)
Bidirectional	$\|\sigma_1/X_u\|$ is greatest $\quad$ $\|\sigma_2/Y_u\|$ is greatest $\quad$ $\|\sigma_6/S_u\|$ is greatest	fibre in x_1 $\quad$ fibre in x_2 $\quad$ matrix

3.4.3 Post-Failure Regime

After failure, new incremental constitutive relationships must be derived. This is accomplished by modifying the elasticity matrix $[Q^e]$ such that at the failure location the material cannot carry any additional tensile stress normal to the crack plane or shear stress parallel to the crack plane. Table 3.3 summarizes the form of the post-failure elasticity matrix (denoted by $[Q^f]$) for both U/D and B/D layers.

Table 3.3. Post-Failure Incremental Constitutive Matrix $[Q^f]$ for Both Brittle and Ductile Failure Models

Layer Type	Failure Mode	$[Q^f]$
Uni-directional	Fibre (x_1-direction)	$Q_{22}^f = E_2$; all other $Q_{ij}^f = 0$
	Matrix	$Q_{11}^f = E_1$; all other $Q_{ij}^f = 0$
Bi-directional	Fibre (x_1-direction)	$Q_{22}^f = E_2$; all other $Q_{ij}^f = 0$
	Fibre (x_2-direction)	$Q_{11}^f = E_1$; all other $Q_{ij}^f = 0$
	Matrix	$\left.\begin{array}{l} Q_{11}^f = E_1 \\ \text{and} \\ Q_{22}^f = E_2 \end{array}\right]$ all other $Q_{ij}^f = 0$

These matrices apply whether the failure process is assumed to be brittle or ductile. However, in the former case the relevant stress components on the cracked planes just before failure must be removed abruptly and redistributed to adjacent uncracked material of the entire structure. The vector of released stresses (denoted by $\{\sigma^f\}$) is tabulated in Table 3.4

for various cases. It should be noted that for the ductile mode of fracture $\{\sigma^f\}$ vanishes.

Table 3.4 Released Stress Vector $\{\sigma^f\}$ During Brittle Type of Failure

Layer Type	Failure Mode	$[\sigma^f]$
Uni-directional	Fibre (x_1-direction)	$\{\sigma_1, 0, \sigma_6\}^T$
	Matrix	$\{0, \sigma_2, \sigma_6\}^T$
Bi-directional	Fibre (x_1-direction)	$\{\sigma_1, 0, \sigma_6\}^T$
	Fibre (x_2-direction)	$\{0, \sigma_2, \sigma_6\}^T$
	Matrix	$\{0, 0, \sigma_6\}^T$

3.5 Multilayer Laminates

The constitutive equations for single layers of FRM developed in the previous sections are now applied to laminates comprising a number of layers to determine laminate response. In the following a laminate subjected to a general state of membrane stress will be treated. The equations which are developed define the overall response of a laminate under a given set of membrane loads. Because of the potential for plastic flow in each layer the governing equations are presented in differential form.

Let the laminate consist of homogeneous orthotropic thin layers, each exhibiting plane stress behaviour. The incremental elastic and elastoplastic constitutive relations in principal material coordinates (i.e. x_1, x_2) for a single layer are given by Eqs. (3.43) and (3.50), respectively. In any other coordinate system in the plane of the layer (say x,y in Fig. 3.5), the incremental stress-strain relations can be written as

$$
\begin{bmatrix} d\sigma_x \\ d\sigma_y \\ d\tau_{xy} \end{bmatrix} = [Q'] \begin{bmatrix} d\epsilon_x \\ d\epsilon_y \\ d\gamma_{xy} \end{bmatrix}
\tag{3.61}
$$

where

$$
\begin{bmatrix} d\sigma_x \\ d\sigma_y \\ d\tau_{xy} \end{bmatrix} = [T]^T \begin{bmatrix} d\sigma_1 \\ d\sigma_2 \\ d\sigma_6 \end{bmatrix}
$$

$$
\tag{3.62}
$$

$$
\begin{bmatrix} d\epsilon_x \\ d\epsilon_y \\ \frac{1}{2} d\gamma_{xy} \end{bmatrix} = [T]^T \begin{bmatrix} d\epsilon_1 \\ d\epsilon_2 \\ \frac{1}{2} d\epsilon_6 \end{bmatrix}
$$

$$
[Q'] = [T]^T [Q][T]
$$

and [T] is the transformation matrix given by

$$
[T] = \begin{bmatrix} \cos^2\theta & \sin^2\theta & \frac{1}{2}\sin2\theta \\ \sin^2\theta & \cos^2\theta & -\frac{1}{2}\sin2\theta \\ -\sin2\theta & \sin2\theta & \cos2\theta \end{bmatrix}
\tag{3.63}
$$

with θ being the angle "from" the x-axis "to" the x_1-axis (see Fig. 3.5).

In Eq. (3.62) [Q] stands for elastic, elastoplastic and post-failure constitutive matrices, whichever is appropriate.

The incremental stress-strain relations in arbitrary coordinates given by Eq. (3.61), are useful in the definition of the laminate stiffnesses because of the arbitrary orientation of the constituent layers. Eq. (3.61) can be thought of as a set of constitutive relations for the kth layer of a multilayered laminate, and thus can be written as

$${d\sigma'}_k = [Q']_k {d\epsilon'}_k \qquad (3.64)$$

where

$${\sigma'} = {\sigma_x \ \sigma_y \ \tau_{xy}}^T$$

$$\qquad (3.65)$$

$${\epsilon'} = {\epsilon_x \ \epsilon_y \ \gamma_{xy}}^T$$

The laminate is assumed to consist of perfectly bonded layers and the displacements are continuous across the layer boundaries (interfaces) so that no layer can slip relative to another. It is further assumed that the stresses in any layer are constant, but different in the different layers. These are the usual type of assumptions made in the classical lamination theory (see e.g. Jones, 1975).

A typical laminate is pictured in Fig. 3.6 along with its deformed shape. Let the laminate be referred to a fixed system of coordinates x, y and z as shown in Fig. 3.6. This will henceforth be referred to as the laminate or structural coordinate system. The incremental stress-strain relations for each layer can be expressed as

$${d\sigma'}_k = [Q']_k {d\epsilon'^{\circ}} \qquad (3.66)$$

where ${d\epsilon'^{\circ}}$ is the laminate strain increment vector, which is the same for each layer.

The resultant laminate forces per unit width are obtained by integrating the stress components of each layer through the total thickness of the laminate. In the incremental sense, they will take the following form:

$$\begin{bmatrix} dN_x \\ dN_y \\ dN_{xy} \end{bmatrix} = \int_{-t/2}^{t/2} \begin{bmatrix} d\sigma_x \\ d\sigma_y \\ d\tau_{xy} \end{bmatrix}_k dz \qquad (3.67)$$

Since the stresses are constant through the thickness of each layer then this becomes

$$\begin{bmatrix} dN_x \\ dN_y \\ dN_{xy} \end{bmatrix} = \sum_{k=1}^{n} \begin{bmatrix} d\sigma_x \\ d\sigma_y \\ d\tau_{xy} \end{bmatrix}_k t_k \qquad (3.68)$$

where t_k is the thickness of the kth layer, and n is the total number of layers. When the layer incremental stress-strain relations, Eq. (3.66), are substituted in Eq. (3.68), the resulting incremental laminate force-strain relations take the following form:

$$\begin{bmatrix} dN_x \\ dN_y \\ dN_{xy} \end{bmatrix} = \sum_{k=1}^{n} [Q']_k t_k \begin{bmatrix} d\epsilon_x^\circ \\ d\epsilon_y^\circ \\ d\gamma_{xy}^\circ \end{bmatrix} \qquad (3.69a)$$

or

$$\{dN\} = \sum_{k=1}^{n} [Q']_k t_k \{d\epsilon'^\circ\} \qquad (3.69b)$$

The overall response of the laminate will be affected by each layer's stiffness contribution $[Q']_k$. During elastic deformation, $[Q']_k = [Q'^e]_k$,

and during elastoplastic deformation $[Q']_k = [Q'^{ep}]_k$.

It should be noted that the analysis given above is based on plane stress conditions in individual layers. This is a valid assumption if:

a)   The loads on the laminate are statically equivalent to in-plane forces (membrane forces) and produce neither bending nor twisting moments.

b)   The laminate has a certain "stacking sequence" of layers which defines a so-called symmetric laminate.

c)   The "free-edge effects" are negligible.

The "stacking sequence" referred to in (b) is an arrangement in which the laminate has a middle plane of geometrical and material symmetry. The layers are arranged in pairs with respect to the plane of symmetry. The layers of such pair have equal thicknesses, same distances from middle plane, and are of the same material with identical orientation of material axes, θ. In a non-symmetric laminate application of membrane forces will in general produce bending and twisting of the layers and thus a plane state of stress will not be realized.

The "free edge effects" referred to in (c) are confined to a "boundary layer" which extends inward from the free edge to a distance approximately equal to the laminate thickness. Within this region, the interlaminar stresses become pronounced and the laminate is in a three-dimensional state of stress (cf. Pipes and Pagano, 1970).

CHAPTER 4

FINITE ELEMENT FORMULATION

4.1 Introduction

In recent years, the finite element method has emerged as the most powerful general method of structural analysis and has provided engineers with a tool of very wide applicability. Indeed, without this computational tool, it is very difficult and expensive to gain insight into the nonlinear behaviour of materials in general and laminated FRMs in particular.

The following discussion is mainly concerned with the numerical implementation of the elastic-plastic-failure model (developed in the previous chapter) into a displacement based finite element program COMPLY (COMposite PLastic Yielding). The chapter is divided into three parts. The first part briefly describes the basic steps of the finite element analysis. In the second part the technique adopted for solution of nonlinear equilibrium equations is outlined. The third and final part presents the numerical technique implemented to perform the required computations for the proposed constitutive model.

4.2 Governing Equations of Finite Element Analysis

The principles of the finite element method are now well established (Zienkiewicz, 1971) and will not be discussed here in great detail. In this section we summarize briefly the general technique used in the finite element method for solving problems with material nonlinearity. In deriving the basic equations of the current finite element analysis a two dimensional isoparametric formulation is used throughout.

Relations describing the approximate equilibrium equations will be presented here. The outline of the numerical scheme used to solve these generally nonlinear equations will be deferred to Section 4.3.

4.2.1 Isoparametric element Representation

It is generally thought that the isoparametric numerically integrated element is more efficient and accurate in elasto-plastic analysis than simple low order elements (Nayak and Zienkiewicz, 1972; Nagtegaal et al., 1974). For this reason, the conventional 8-node (quadratic) isoparametric element is implemented in the finite element code COMPLY. Isoparametric elements are those for which the functional representation of deformation is employed in representation of the element geometry. A typical curved element with the nodal points being numbered for the purposes of discussions is shown in Fig. 4.1. Also shown in the same figure is the parent element of square shape with coordiates ξ, η, ranging from -1 to 1 on their boundaries. If u and v denote the in-plane displacements in the x and y directions respectively, then the variation of displacement within an element can be written as

$$u = \sum_{i=1}^{8} \phi_i u_i \; ; \qquad v = \sum_{i=1}^{8} \phi_i v_i \qquad (4.1)$$

where u_i, v_i are the nodal displacement variables for the ith node, and ϕ_i are the associated shape functions given by

• For corner nodes:

$$\phi_i = \frac{1}{4} (1 + \xi\xi_i)(1 + \eta\eta_i)(\xi\xi_i + \eta\eta_i - 1) \qquad (i = 1,3,5,7)$$

• For midside nodes:

$$\phi_i = \frac{\xi_i^2}{4}(1 + \xi\xi_i)(1 - \eta^2) + \frac{\eta_i^2}{4}(1 + \eta\eta_i)(1 - \xi) \quad (i = 2,4,6,8) \quad (4.2)$$

in which ξ_i, η_i are the nodal coordinates in the ξ-η plane.

By definition of isoparametric elements the above shape functions are also used to map the element geometry in the x-y plane, i.e.

$$x = \sum_{i=1}^{8} \phi_i x_i \quad ; \quad y = \sum_{i=1}^{8} \phi_i y_i \quad (4.3)$$

where x_i, y_i are the coordinates of the nodes in the x-y plane.

4.2.2 Element Stiffness Formulation

The basic step in any finite element analysis is the derivation of the nodal force-displacement relationship. To derive this relation we must satisfy three conditions no matter what type or shape of element is involved. These are:

i) The compatibility condition (i.e. strain-displacement relations)

ii) The equilibrium condition

iii) The stress-strain relations

i) <u>Strain-Displacement Relations</u>

Let $\{\delta_i\}^e = \{u_i, v_i\}^T$ be the vector of nodal displacement variables for the ith node of a typical element e in the finite element mesh. The in-plane strain field within this element, $\{\epsilon'\}^e = \{\epsilon_x, \epsilon_y, \gamma_{xy}\}^T$, is then related to the nodal point displacement vector as

$${\{\epsilon\}}^e = \sum_{i=1}^{8} [B_i] \{\delta_i\}^e = [B] \{\delta\}^e \tag{4.4}$$

where $[B_i]$ is the strain-displacement matrix* for the ith node given by

$$[B_i] = \begin{bmatrix} \partial\phi_i/\partial x & 0 \\ 0 & \partial\phi_i/\partial y \\ \partial\phi_i/\partial y & \partial\phi_i/\partial x \end{bmatrix} \qquad (i = 1,2,\ldots,8) \tag{4.5}$$

and

$$[B] = [[B_1],[B_2],\ldots,[B_8]]$$
$$\{\delta\}^e = \{u_1, v_1, u_2, \ldots, v_8\}^T$$

The Cartesian shape function derivatives used in Eq. (4.5) may be expressed in terms of the ξ,η derivatives of ϕ_i by the transformation

$$\begin{bmatrix} \partial\phi_i/\partial x \\ \partial\phi_i/\partial y \end{bmatrix} = [J]^{-1} \begin{bmatrix} \partial\phi_i/\partial\xi \\ \partial\phi_i/\partial\eta \end{bmatrix} \tag{4.6}$$

where $[J]^{-1}$ is the inverse of the Jacobian matrix

$$[J] = \begin{bmatrix} \partial x/\partial\xi & \partial y/\partial\xi \\ \partial x/\partial\eta & \partial y/\partial\eta \end{bmatrix} = \begin{bmatrix} \sum_{i=1}^{8} \dfrac{\partial\phi_i}{\partial\xi} x_i & \sum_{i=1}^{8} \dfrac{\partial\phi_i}{\partial\xi} y_i \\ \sum_{i=1}^{8} \dfrac{\partial\phi_i}{\partial\eta} x_i & \sum_{i=1}^{8} \dfrac{\partial\phi_i}{\partial\eta} y_i \end{bmatrix} \tag{4.7}$$

---

*Consideration here is limited to small deformation situations where the strains can be assumed to be infinitesimal (i.e. Lagrangian and Eulerian geometric descriptions coincide) and the strain-displacement matrix remains constant during the deformation process.

ii) Equilibrium Condition

By applying the principle of virtual work or any other similar energy principle, the equilibrium equation for a single element can be written as

$$\int_{V^e} [B]^T \{\sigma'\}^e \, dV = \{F\}^e \qquad (4.8)$$

where $\{\sigma'\}^e = \{\sigma_x, \sigma_y, \tau_{xy}\}^T$ is the elemental stress vector, $\{F\}^e$ is the consistent (external) load vector and V_i^e is the elemental volume.

iii) Constitutive Relations

Before a solution can proceed further, a constitutive relationship between $\{\sigma'\}^e$ of Eq. (4.8) and $\{\epsilon'\}^e$ of Eq. (4.4) has to be established. For the present plane stress analysis of laminated FRMs, the material nonlinearity is incorporated into the stress-strain relation in the following incremental form

$$\{d\sigma'\}_k^e = [Q']_k^e \{d\epsilon'\}_k^e = [Q']_k^e \{d\epsilon'\circ\}^e \qquad (4.9)$$

where $[Q']_k$ is the constitutive matrix (for the current stress level) associated with the kth layer of the laminate (see Eq. (3.66)). Substituting Eq. (4.9) in the incremental form of Eq. (4.8) and using Eqs. (4.4) and (3.69b) gives for each element

$$\{dF\}^e = \int_{A^e} [B]^T \{dN\}^e dA = [K_T] \{d\delta\}^e \qquad (4.10)$$

where

$$[K_T]^e = \sum_{k=1}^{n} t_k \int_{A^e} [B]^T [Q']_k^e [B] \, dx \, dy \qquad (4.11)$$

is the element tangential stiffness matrix. In Eq. (4.11) A^e denotes the surface area of the element under consideration and the summation is taken over the total number of layers, n, through the thickness. Due to the nonlinear nature of the integrand in Eq. (4.11), the integration must be carried out numerically. This will be attempted in the following.

Using the transformation relation

$$dxdy = det[J] \, d\xi d\eta \qquad (4.12)$$

where det[J] is the determinant of the Jacobian matrix [J], we can rewrite Eq. (4.11) as

$$[K_T]^e = \sum_{k=1}^{n} t_k \int_{-1}^{1} \int_{-1}^{1} [H]_k^e \, d\xi d\eta \qquad (4.13)$$

where $[H]_k^e$ is defined as

$$[H]_k^e = [H(\xi,\eta)]_k^e = [B]^T [Q']_k^e [B] \, det \, [J] \qquad (4.14)$$

Now, using Gaussian quadrature with q x q sampling points the element tangent stiffness matrix can be evaluated as

$$[K_T]^e = \sum_{k=1}^{n} \sum_{j=1}^{q} \sum_{i=1}^{q} [H(\xi_i,\eta_j)]_k^e \, t_k \, W_i \, W_j \qquad (4.15)$$

where (ξ_i, η_i) is a sampling position within the element and W_i, W_j are the associated weighting factors.

With regard to one dimensional integrals, q Gauss evaluation points are sufficient to integrate exactly a polynomial of degree (2q-1). Table 4.1 offers a brief summary of some of the details of Gaussian quadrature.

Table 4.1   Sampling Coordinates and Weighting Factors for One-Dimensional Gaussian Quadrature

$$\int_{-1}^{+1} H(\xi)\, d\xi = \sum_{i=1}^{q} W_i\, H(\xi_i)$$

q	i	ξ_i	W_i
1 (linear)	1	0	2
2 (cubic)	1	$+ 1/\sqrt{3}$	1
	2	$- 1/\sqrt{3}$	1
3 (quintic)	1	0	8/9
	2	$+ \sqrt{3/5}$	5/9
	3	$- \sqrt{3/5}$	5/9

4.2.3 Structural Stiffness Formulation

Once the element stiffness matrices $[K_T]^e$ have been calculated in the global (structural or laminate) coordinates, the structural tangent stiffness matrix $[K_T]$, which relates the load increment {dF} to the nodal displacement increment {dδ} of the complete structure, can be formed by the systematic addition of element stiffnesses. Thus

$$\{dF\} = [K_T]\, \{d\delta\} \tag{4.16}$$

4.3 Numerical Solution of Nonlinear Equilibrium Equations

A large number of numerical schemes have been proposed in the literature for the integration of equations (4.16), all of which are based on piecewise linearization of the nonlinear equations over a finite number of steps. The two main categories of methods are purely iterative or purely incremental. In the incremental (step by step) method the structure is loaded in small increments and for every step of loading a new structural stiffness matrix is calculated from the updated material (constitutive) matrices. However, since the flow theory of plasticity is based on "differential" steps and the load must be added in "finite" steps, the stiffness of the structure is easily overestimated and the equilibrium conditions are violated. In this case the incremental procedure must be combined with a suitable iterative process in order to satisfy equilibrium at each load step. During the general stage of the incremental/iterative solution process, the equilibrium equations (4.16) will not be exactly satisfied and a system of residual (unbalanced) forces $\{\psi\}$ will exist such that

$$\{\psi(\delta)\}_r = \{F\} - \{P(\delta)\}_r \qquad (4.17)$$

in which the subscript r signifies the iteration cycle number within a particular load increment and $\{P\} = \{P(\delta)\}$ is the internal equivalent force vector given by

$$\{P\} = \int_V [B]^T \{\sigma'\} dV = \int_A [B]^T \{N\} dA \qquad (4.18)$$

where the integrations are carried out over the whole structure using the usual element-by-element procedure and standard assembly rules. Note that in Eqs. (4.17) and (4.18) the total (accumulated) level as opposed to

incremental level of various force and stress quantities are considered. Also due to the nonlinearity of the problem the integrations in Eq. (4.18) must be carried out numerically by the Gaussian quadrature scheme described earlier.

Let us now consider the Taylor series expansion of $\{\psi\}_r$ about $\{\delta\}_{r-1}$ (i.e. the known solution from previous iteration) so that

$$\{\psi\}_r = \{\psi\}_{r-1} + \frac{\partial \{\psi\}}{\partial \{\delta\}} \bigg|_{\{\delta\}_{r-1}} (\{\delta\}_r - \{\delta\}_{r-1}) + \ldots \ldots \qquad (4.19)$$

Putting

$$\{\Delta\delta\} = \{\delta\}_r - \{\delta\}_{r-1} \qquad (4.20)$$

and then truncating the expansion to the linear term yields

$$\{\psi\}_r = \{\psi\}_{r-1} - [K_T]_{r-1} \{\Delta\delta\} \qquad (4.21)$$

where

$$[K_T]_{r-1} = \frac{\partial \{P\}}{\partial \{\delta\}} \bigg|_{\{\delta\}_{r-1}} = - \frac{\partial \{\psi\}}{\partial \{\delta\}} \bigg|_{\{\delta\}_{r-1}} \qquad (4.22)$$

is the tangential stiffness matrix of the entire structure evaluated at the beginning of the rth iteration. This is calculated using the element by element assembly of stiffnesses given by Eqs. (4.11) or (4.15).

It is desired that $\{\psi\}_r = 0$, thus

$$[K_T]_{r-1} \{\Delta\delta\} = \{\psi\}_{r-1} \qquad (4.23)$$

This is the linear incremental equilibrium equation wherein the residuals $\{\psi\}$ can be visualized as corrective nodal forces required to bring the assumed displacement pattern into nodal equilibrium. The set of simultaneous equations (4.23) can be solved* for $\{\Delta\delta\}$ and the improved solution will be

$$\{\delta\}_r = \{\delta\}_{r-1} + \{\Delta\delta\} \qquad (4.24)$$

The updated displacements $\{\delta\}_r$ are used to evaluate the current stresses $\{\sigma\}_r$ and hence the residual forces $\{\psi\}_r$ from Eqs. (4.17). The iteration process is repeated until these residual forces practically vanish, or equivalently that $\{\delta\}_{r-1}$ and $\{\delta\}_r$ are sufficiently close. For the purposes of this study we will assume that the numerical process has converged if (Owen and Hinton, 1980)

$$\frac{\|\{\psi\}_r\|}{\|\{F\}\|} = [\frac{\{\psi\}_r^T \{\psi\}_r}{\{F\}^T \{F\}}]^{1/2} \leq \text{TOLER} \qquad (4.25)$$

where TOLER is a small preset tolerance limit. The criterion (4.25) states that convergence occurs if the Euclidian norm of the residual forces becomes less than TOLER times the norm of the total applied forces.

The above iterative procedure, often termed the Newton-Raphson method, is illustrated schematically in Fig. 4.2 for a single variable situation. It should be noted that in this scheme the tangent stiffness matrix $[K_T]$ is updated and solution of the full equation system is obtained for each iteration. A variant on the above algorithm is offered by the "initial stiffness" scheme in which the original structural stiffness matrix is employed at each

---

*In the current computer code COMPLY the solution method is based on the Gaussian elimination procedure.

stage of the iteration process. This reduces the computational costs per iteration but unfortunately also reduces the rate of convergence of the process. In practice the optimum algorithm is generally provided by updating the stiffnesses at selected iterative intervals only (Owen and Hinton, 1980). In the present work the pure Newton-Raphson method is employed whereby the tangent stiffness matrix is re-evaluated at each iteration of each load increment.

The complete sequence of the iterative process described above is summarized in Table 4.2.

Table 4.2 Sequence of the Iterative Solution Technique

1.	Begin new load increments, $\{F\} = \{F\} + \{\Delta F\}$. Set iteration counter $r = 1$ and $\{\psi\}_{r-1} = \{\Delta F\} + \{\psi\}$, where $\{\psi\}$ is the equilibrium correction from previous increment.
2.	Evaluate the new tangential stiffness matrix $[K_T]_{r-1}$.
3.	Solve $[K_T]_{r-1} \{\Delta\delta\} = \{\psi\}_{r-1}$ by Gauss elimination.
4.	Set $\{\delta\}_r = \{\delta\}_{r-1} + \{\Delta\delta\}$.
5.	For each Gauss point calculate the increment in strain $\{\Delta\epsilon'^0\} = [B]\{\Delta\delta\}$.
6.	Estimate the increments in stress at each Gauss point in each layer $\{\Delta\sigma'\}^k = [Q']^k\{\Delta\epsilon'^0\}$ and hence evaluate the total stress value $\{\sigma'\}_r^k = \{\sigma'\}_{r-1}^k + \{\Delta\sigma'\}^k$. The stresses $\{\sigma'\}_r^k$ must be adjusted to account for any plastic behaviour or failure of the layer (see Section 4.4).
7.	Evaluate the stress resultants $\{N\}_r = \sum\limits_{k=1}^{n} \{\sigma'\}_r^k t_k$ at each Gauss point.
8.	Determine the residual force vector $$\{\psi\}_r = \{F\} - \int_A [B]^T\{N\}_r dA.$$
9.	If convergence is achieved according to criterion (4.25), set $\{\psi\} = \{\psi\}_r$ and go to step (1) to perform the next load increment. Otherwise set $r = r+1$ and go to step (2) to perform the next iteration.

4.4 Numerical Implementation of the Anisotropic Elastic-Plastic-Failure Model

As was observed in the previous section, the finite element scheme solves the displacement equations of equilibrium in an incremental fashion. Hence, the constitutive laws presented earlier (Chapter 3) that dealt with differential (infinitesimal) stress and strain quantities must now be used approximately to relate small but finite increments in stresses and strains. A finite element model may consist of several sampling points (layers and Gauss points) at which the plasticity computations are performed for every load step and corrective iteration. Analyses of such models must permit relatively large load steps to maintain efficiency of the solution. These large increments place severe demands on the plasticity routines to maintain accuracy, numerical stability and efficiency. The importance of the precision with which constitutive elastoplastic relations are integrated has motivated a number of recent studies, e.g. (Krieg and Krieg, 1977; Schreyer et al., 1979; Ortiz and Popov, 1985; Franchi and Genna, 1987; Dodds, 1987). The generalized trapezoidal rule as described by Ortiz and Popov (1985) encompasses the three most popular methods for integration of the elasto-plastic constitutive equations. These methods are known as: (1) tangent predictor-radial corrector; (2) mean normal or secant stiffness; and (3) elastic predictor-radial return. In the present work the first method is employed to integrate the incremental stress-strain law. As shown by Schreyer et al. (1979) this method, if used with subincrementation of the strain increment vector (as in the present analysis), is very accurate for plane stress conditions. It is the aim of this section to outline the stress computation technique used in the current finite element program COMPLY. The

numerical procedure describing the failure and post-failure stress analyses will also be covered.

4.4.1 Elastic-Plastic Formulation

During each iteration of each load increment an element, or part of an element, may yield. All stress and strain quantities are monitored at each Gaussian integration point in every layer of every element. Consequently an element can behave elastically at some points and elastic-plastically at others. For every iteration of a given load increment it is necessary to adjust the stress and strain terms until the yield criterion and the constitutive laws are satisfied. The procedure adopted is described below.

Consider the situation existing (at a point*) for the rth iteration of any particular load increment. The stress components $\{\sigma\}_{r-1}$ and the parameters describing the yield surface are all known from the solution at the end of the $(r-1)^{th}$ iteration. Also known are the components of the new strain increments $\{\Delta\epsilon'^{\circ}\}$. The latter, which is given in the overall (laminate) coordinate system, must appropriately be transformed (using Eqs. (3.62) and (3.63)) to give the incremental strain components in the principal material directions. Such transformation is essential since the yield and failure criteria described earlier (Chapter 3) involve the stress and strain components, which are referred to the material coordinates of a particular layer. For the purposes of the following discussion we assume that all the stress and strain quantities have already been transformed to the material

---

*It is understood that the stress computation is performed for every point (i.e. for each Gauss station in every layer) involved in numerical integration over the volume. Thus suffixes e and k previously used to denote generic elements and layers, respectively, will henceforth be suppressed for clarity.

coordinates of the point under consideration. Thus, in what follows,
$\{\Delta\epsilon\} = \{\Delta\epsilon_1, \Delta\epsilon_2, \Delta\epsilon_6\}^T$; $\{\Delta\sigma\} = \{\Delta\sigma_1, \Delta\sigma_2, \Delta\sigma_6\}^T$.

In the first step of the numerical algorithm, an elastic estimate $\{\Delta\sigma^e\}$ for the stress increment is computed as

$$\{\Delta\sigma^e\} = [Q^e]\{\Delta\epsilon\} \qquad (4.26)$$

A set of elastic trial stresses $\{\sigma^e\}_r$ is then calculated by accumulating the total stress. The result is

$$\{\sigma^e\}_r = \{\sigma\}_{r-1} + \{\Delta\sigma^e\} \qquad (4.27)$$

These trial stresses are then tested with respect to the initial yield surface

$$f_0(\{\sigma\},[A^0],k_0) \equiv \bar{\sigma}^2(\{\sigma\},[A^0]) - k_0^2 = 0 \qquad (4.28)$$

where the matrix $[A^0]$ is given by Eqs. (3.55a,b) or (3.58) (in which the yield stresses, X,Y,S and k are replaced by their initial values X_0, Y_0, S_0 and k_0) depending on whether the layer is bidirectional or unidirectional, respectively.

If the trial stresses do not violate the yield criterion (4.28), i.e. $f_0(\{\sigma^e\}_r, [A^0], k_0) \leq 0$, then the elastic behaviour assumption holds and the final stresses $\{\sigma\}_r$ at the end of the rth iteration are indeed $\{\sigma^e\}_r$. Otherwise, the initial yield surface has been crossed during the trial stress incrementation. This is shown schematically in Fig. 4.3. If $\{\sigma^c\}$ denotes

the stress state at the point where the assumed stress path comes into contact with the initial yield surface, then we can write

$$\{\sigma^C\} = \{\sigma\}_{r-1} + \beta\{\Delta\sigma^e\} \; ; \qquad 0 \le \beta < 1 \qquad (4.29)$$

where $\beta\{\Delta\sigma^e\}$ is the portion of the stress increment at which the plastic behaviour is first encountered, i.e. $f_0 \, (\{\sigma^C\},[A^o],k_0) = 0$. This condition leads to a quadratic equation for the determination of β. However, a simple approximate value of β can be obtained by a linear interpolation in $\bar{\sigma}$ (Owen and Hinton, 1980), that is,

$$\beta \approx \frac{k_0 - \bar{\sigma}_{r-1}}{\bar{\sigma}_r^e - \bar{\sigma}_{r-1}} \qquad (4.30)$$

where $\bar{\sigma}_r^e = \{\sigma^e\}_r^T [A^o] \{\sigma^e\}_r$, and $\bar{\sigma}_{r-1} = \{\sigma\}_{r-1}^T [A^o] \{\sigma\}_{r-1}$. It should be observed that the path from $\{\sigma\}_{r-1}$ to $\{\sigma^C\}$ constitutes fully elastic response. The remaining portion of stress, $(1-\beta)\{\Delta\sigma^e\}$ results in a stress state that lies outside the initial yield surface and consequently must be adjusted by allowing plastic deformation to occur. Once β has been determined from Eq. (4.30), the plastic stress increment can be calculated as

$$\{\Delta\sigma^p\} = \int_{\beta\{\Delta\epsilon\}}^{\{\Delta\epsilon\}} [Q^p] \{d\epsilon\} \qquad (4.31)$$

This plastic stress increment is required to restore the assumed elastic stress increment

$$\{\Delta\sigma^e\} = \int_0^{\{\Delta\epsilon\}} [Q^e]\{d\epsilon\} = [Q^e]\{\Delta\epsilon\} \qquad (4.32)$$

to the correct elastoplastic values as required by the constitutive equation (3.50). Therefore, substituting incremental changes for infinitesimals in Eq. (3.50), we have

$$\{\Delta\sigma\} = \int_0^{\{\Delta\epsilon\}} ([Q^e] - [Q^p])\{d\epsilon\} = \int_0^{\beta\{\Delta\epsilon\}} [Q^e]\{d\epsilon\} + \int_{\beta\{\Delta\epsilon\}}^{\{\Delta\epsilon\}} ([Q^e] - [Q^p])\{d\epsilon\}$$

$$= \int_0^{\{\Delta\epsilon\}} [Q^e]\{d\epsilon\} - \int_{\beta\{\Delta\epsilon\}}^{\{\Delta\epsilon\}} [Q^p]\{d\epsilon\} = \{\Delta\sigma^e\} - \{\Delta\sigma^p\} \qquad (4.33)$$

The construction of the elastoplastic stress increment vector $\{\Delta\sigma\}$ is illustrated schematically in Fig. 4.3. If $\{\Delta\epsilon^p\}$ denotes the vector of plastic strain increments, which is unknown at this stage, then in view of the relation

$$\{\Delta\sigma\} = [Q^e](\{\Delta\epsilon\} - \{\Delta\epsilon^p\}) \qquad (4.34)$$

and Eq. (4.33), one can write

$$\{\Delta\sigma^p\} = [Q^e]\{\Delta\epsilon^p\} \qquad (4.35)$$

Since the plastic material stiffness $[Q^p]$ varies with the current state of stress, the computation of the plastic stress increment given by Eq. (4.31) requires a numerical integration. Various algorithms have been

designed for this purpose. The simplest approximation of Eq. (4.31) is obtained by using a one-step, forward Euler integration method:

$$\{\Delta\sigma^p\} \simeq (1-\beta)[Q^p]\{\Delta\epsilon\} \tag{4.36}$$

The integration process used above is admissible if small load (and strain) increments are applied. The fact that the direction of the plastic flow is only correct in the beginning of the increment can lead to a significant error in the final orientation of the stress vector in the stress space. Therefore to allow for relatively large load (and strain) increments a more accurate integration procedure is desirable. This can be achieved by dividing the elasto-plastic portion of the strain increment vector, $(1-\beta)\{\Delta\epsilon\}$ into M equal sub-increments and reforming the plastic matrix $[Q^p]$ at the beginning of each subincrement. Accordingly, for each subinterval we have

$$\{\Delta\epsilon\}_m = \{\Delta\epsilon\}/M \tag{4.37}$$

and

$$\{\Delta\sigma^e\}_m = (1-\beta)[Q^e]\{\Delta\epsilon\}_m = \{\Delta\sigma^e\}/M$$

$$\tag{4.38}$$

$$\{\Delta\sigma^p\}_m = (1-\beta)[Q^p]\{\Delta\epsilon\}_m = \{\Delta\sigma^p\}/M$$

where $\{\Delta\epsilon\}_m$, $\{\Delta\sigma^e\}_m$ and $\{\Delta\sigma^p\}_m$ are the mth strain, elastic stress and plastic stress subincrements, respectively. The input quantities used in the calculation of $[Q^p]$ (see Eq. 3.50) are the accumulated (total) stress components $\{\sigma\}_{m-1}$, the effective yield stress k_{m-1}; the anisotropic parameters $[A(k)]_{m-1}$ and μ_{m-1}, all of which are evaluated at the end of the $(m-1)^{th}$ subincrement.

It should be noted that for m = 1 (i.e. at the onset of workhardening), we have

$$\{\sigma\}_0 = \{\sigma^c\}$$

$$[A(k)]_0 = [A^0] \qquad (4.39)$$

$$\mu_0 = 1 - \frac{1}{2k_0} \{\sigma^c\}^T \left[\frac{\partial A}{\partial k}\right]\Big|_{k=k_0} \{\sigma^c\}$$

The yield stress k is updated according to the amount of plastic work produced during the mth subincrement. For the bilinear stress-strain representation considered in this study one can write

$$k_m = k_{m-1} + H' \, \Delta W^P / k_{m-1} \qquad (4.40)$$

where

$$\Delta W^P = \{\sigma\}_{m-1}^T \{\Delta\epsilon^P\}_m \qquad (4.41)$$

is the increment of plastic work done per unit volume. In Eq. (4.41) the vector of plastic strain increments $\{\Delta\epsilon^P\}_m$ can be determined from Eq. (4.35) as follows

$$\{\Delta\epsilon^P\}_m = [Q^e]^{-1} \{\Delta\sigma^P\}_m \qquad (4.42)$$

In order to update the anisotropic parameters $[A(k)]$ we adopt the approach of Jensen et al. (1966) or Whang (1969), the details of which are

outlined in Appendix B. According to this method the new levels of yield stress X,Y and S reached during plastic flow are (see Eq. 3.59):

$$X_m^2 = \frac{E_{p_1}}{H'} [k_m^2 - k_0^2] + X_0^2$$

$$Y_m^2 = \frac{E_{p_2}}{H'} [k_m^2 - k_0^2] + Y_0^2 \qquad (4.43)$$

$$S_m^2 = \frac{G_p}{H'} [k_m^2 - k_0^2] + S_0^2$$

It should be emphasized that any one of the stress-strain curves, $\sigma_1 - \epsilon_1$, $\sigma_2 - \epsilon_2$ and $\sigma_6 - \epsilon_6$ can be prescribed as the effective stress $(\bar{\sigma})$ - effective strain $(\bar{\epsilon})$ diagram, i.e. the analysis is independent of the choice made.

Having established the updated values of the yield stresses, the matrix of anisotropic parameters $[A]_m$ at the end of the mth subincrement can be found from Eqs. (3.55a,b) or (3.58), as the case may be.* The updated yield function now becomes

$$f_m(\{\sigma\}_m, [A]_m, k_m) \equiv \{\sigma\}_m^T [A]_m \{\sigma\}_m - k_m^2 \qquad (4.44)$$

In general, the stress state $\{\sigma\}_m$ will be outside the updated yield surface and we expect $f_m \neq 0$. This small departure from the yield surface will be cumulative. To prevent artificial hardening, a correction must be made to restore the stresses to the correct yield surface. Such a correction is

---

*The updated anisotropic parameters must always be tested with respect to the inequalities (3.49) to check for the boundedness of the new yield surface.

achieved by simply scaling the stresses $\{\sigma\}_m$ to the yield surface. The appropriate scaling factor is readily seen to be

$$s = k_m / \sqrt{\{\sigma\}_m^T [A]_m \{\sigma\}_m} \qquad (4.45)$$

The above process is repeated for all subincrements leading to the following expression for the stresses at the end of the rth iteration

$$\{\sigma\}_r = \{\sigma\}_{r-1} + \beta\{\Delta\sigma^e\} + \sum_{m=1}^{M} (\{\Delta\sigma^e\}_m - \{\Delta\sigma^P\}_m) \qquad (4.46)$$

where $\{\Delta\sigma^e\}_m$, $\{\Delta\sigma^P\}_m$ are given by Eq. (4.38) in terms of the known strain increment vector $\{\Delta\epsilon\}$. Obviously the greater the number of steps M into which the plastic portion of strain increment $(1-\beta)\{\Delta\epsilon\}$ is divided, the greater the accuracy. However, the expense of reforming $[Q^P]$ and updating the stresses for many steps, may lead to excessive computation times. Clearly a balance must be sought and to this end several criteria have been proposed to select an optimum number of subincrements M. Schreyer et al. (1979) select M by limiting the angular difference between a normal vector $\{\partial f/\partial\sigma\}_0$ at the current contact point $\{\sigma^c\}$ and a normal vector $\{\partial f/\partial\sigma\}_1$ at the contact point computed with a single step (i.e., $M=1$) estimate. This angle which measures the change in plastic flow direction (due to curvature of the yield surface) within an increment, is calculated as

$$\omega = \cos^{-1}\left[\frac{\{\frac{\partial f}{\partial\sigma}\}_0^T \{\frac{\partial f}{\partial\sigma}\}_1}{|\{\frac{\partial f}{\partial\sigma}\}_0||\{\frac{\partial f}{\partial\sigma}\}_1|} \right] \qquad (4.47)$$

where $| |$ indicates the magnitude of a vector.

Schreyer et al. (1979) offered the following simple formula for the number of subincrements:

$$M = 1 + \omega/\ell \qquad (4.48)$$

where ω is given in degrees and ℓ is a postive number chosen on the basis of numerical experience. Alternative criteria for determination of M are given by Bushnell (1976), Nyssen (1981), and Owen and Hinton (1980). However, that of Schreyer et al is preferred in the present study.

It should be remarked in passing that for integration points that have already yielded in the previous iteration $\{\sigma\}_{r-1} = \{\sigma^c\}$, i.e. $\beta = 0$ and the stress computation procedure described above applies identically. Also during the iterative process, if the effective stress at a Gauss point falls below the yield value at the end of the previous load increment, that point is assumed to be elastically unloading, i.e. $\{\Delta\sigma^p\} = 0$.

This concludes the numerical implementation of the elastic-plastic region of the constitutive model. The next subsection is devoted to the numerical treatment of failure and post-failure behaviour.

4.4.2 Post-Failure Formulation

In each constant strain increment $\{\Delta\epsilon\}$, the updated state of stress $\{\sigma\}_r$ at an integration point of a finite element needs to be examined with respect to the failure criterion

$$f_u (\{\sigma\},[A^u],k_u) \equiv \{\sigma\}^T [A^u] \{\sigma\} - k_u^2 = 0 \qquad (4.49)$$

where the matrix $[A^u]$ is given by Eqs. (3.55a,b) and (3.58) for B/D and U/D layers, respectively, with X_u, Y_u, S_u and k_u replacing X,Y,S and k.

If the stress combination violates the failure criterion, then cracks are defined in the regions of the integration point under consideration. To account for the presence of cracks in succeeding iterations (or increments of loading), the post-failure elasticity matrix $[Q^f]$ tabulated in Table 3.3 is used so that at that integration point the element cannot carry any more increments of stress in certain directions. This is a common feature for both brittle and ductile fracture models as described in Chapter 3. Therefore, once failure occurs, the subsequent incremental stress-strain relationship can be written as

$$\{\Delta\sigma\} = [Q^f] \{\Delta\epsilon\} \tag{4.50a}$$

if the behaviour is elastic, or

$$\{\Delta\sigma\} = ([Q^f] - \frac{[Q^f]\{a\}\{a\}^T[Q^f]}{\mu H' + \{a\}^T[Q^f]\{a\}}) \{\Delta\epsilon\} \tag{4.50b}$$

if the behaviour is plastic.

If the failure is of brittle type, however, the appropriate stresses (normal or parallel to the crack, as the case may be) at the integration point just before failure are released completely* and thereafter the point is assumed to lose its resistance against any further deformation in the

---

*In most situations where failure occurs in the primary load-carrying part of the structure, the stresses must be released gradually to facilitate convergence of the iterative process.

failure direction. In this case, the nodal point released-force vector in the structure (or laminate) coordinate system can be written as

$$\{R\} = \int_V [B]^T [T]^T \{\sigma^f\} \, dV \qquad (4.51)$$

where the vector of released stresses $\{\sigma^f\}$ is tabulated in Table 3.4 for various brittle modes of failure. The residual force vector $\{\psi\}$ now takes on the following form

$$\{\psi\} = \{F\} + \{R\} - \{P\} \qquad (4.52)$$

The released forces $\{R\}$ can therefore be interpreted as known nodal loads, which in addition to the actual external loads $\{F\}$, must be equilibriated by the internal forces $\{P\}$. This corresponds to the redistribution of the released stresses from failed integration points to unfailed points of the entire structure. During the process of stress redistribution, another point may fail even though the applied load $\{F\}$ remains constant. If the failure spreads throughout the structure, a singular or negative structural stiffness matrix may appear. Or, the Newton-Raphson iteration of unbalanced external forces may become divergent and an equilibrium state cannot be reached. For these cases, the structure is considered to have collapsed and the computation is terminated.

To obtain the collapse load within narrow limits the size of load increments must be refined when the structure is about to collapse. Use of the restart facility included in the present code is particularly useful in this respect.

CHAPTER 5

NUMERICAL RESULTS AND DISCUSSIONS

5.1 Introduction

A general theory of the inelasticity of FRMs has been outlined in the preceding chapters which would appear to exhibit considerable potential as a basis for a systematic model of the observed material behaviour. To completely fulfill the objectives of this thesis, it remains to check the ability of the proposed theory to reproduce (within the bounds of the theoretical assumptions) the available data and the suitability of the model for use in finite element computations. In this chapter, these issues are addressed by comparing some tests of the model to experimental data and various other numerical results.

There are three major portions of this chapter. In the first portion the general performance and functioning of the finite element code COMPLY is validated by conducting numerical analyses of a few well known example problems involving isotropic materials. These problems merely serve to verify the isotropic elastoplastic analysis capability of the COMPLY program before it can be applied with confidence to problems involving anisotropic layered media. The second portion of the chapter is concerned with the application of the computer program to selected laminate coupon specimens subjected to various loading conditions. The objective of this numerical study is to determine the adequacy of the proposed constitutive model in describing the basic response characteristics of laminated FRMs. The third and final portion of the chapter covers the finite element (in-plane) analyses of laminated composite plates with centered circular hole. This geometry, which provides non-uniform yielding as well as multi-axial stress states, is

an ideal application for tracing the overall load-deflection response in the post-failure realm (i.e. beyond the failure of one element) and consequently testing the capability of the COMPLY program in performing progressive failure analysis of laminated structures.

To facilitate comparison to experiment, theory and other numerical techniques, a large number of problems have been chosen from works in the open literature. Since these problems do not come from any single source they have not been originally specified in one unified unit system. In order to make an easy comparison with these results, the units as specified in the original source have been adopted.

5.2 Verification of the Finite Element Program

In order to assess the accuracy of elastoplastic solutions obtained by the finite element code COMPLY, it is necessary to consider problems that have solutions of known validity. In this section we investigate three such problems all of which involve isotropic materials obeying the von Mises' yield criterion. The first example considers an infinitely long thick-walled cylinder loaded by an internal pressure causing elasto-plastic deformations. In the second example the capability of the program to handle more complex (non-proportional) loading paths is tested by conducting the analysis of a thin-walled tube subjected to combined torsion and tension. The last example investigates the elasto-plastic behaviour of a thin sheet containing a circular hole under remote uniform tension. The purpose of the problems considered in this section is to examine the development of plastic deformation, thus no limit is specified for failure strains and stresses.

5.2.1 Thick-Walled Isotropic Cylinder Under Internal Pressure

The cylinder is assumed to be infinitely long so that the condition of plane strain prevails in the axial direction. The material is elastic-perfectly plastic obeying the von Mises' yield criterion. Earlier solutions to this problem has been obtained by Hodge and White (1950) using finite differences, and by Hill (1950) who employed the Tresca yield criterion in order to simplify the solution of the governing equations. Graphical representations of the solution have also been given by Prager and Hodge (1951). In the following, these solutions, regarded as exact, form the basis of comparison with the present numerical results.

Due to axial symmetry, only a quarter of the cylinder needs to be considered. The cylinder shown in Fig. 5.1 was analyzed with the program COMPLY using the same type of finite element (i.e., 8-noded isoparametric element) and the same element subdivision as that of Owen and Hinton (1980). The following numerical values were assigned to the geometric and material parameters involved:

Inner radius, $a = 100$ mm

Outer radius, $b = 200$ mm

Elastic modulus, $E = 2.1 \times 10^5$ MPa

Poisson's ratio, $\nu = 0.3$

Uniaxial yield stress, $\sigma_0 = 240$ MPa

Plastic modulus, $H' = 0$

The solution was obtained using a 2 x 2 Gauss integration rule. The internal pressure, P, was gradually increased until the plastic collapse of the cylinder was attained at P = 185 MPa. The latter is marked by the divergence of the iterative process for an incremental load increase. Figure 5.2 shows

that the calculated pressure-radial displacement curve falls slightly below that obtained by Hodge and White (1950). For comparison, it is interesting to note that the exact values of the initial and ultimate (collapse) pressure levels are 104 and 192 MPa, respectively. The spreading of the plastic zone, corresponding to selected load levels P = 80, 120, 140 and 180 MPa, is shown in Fig. 5.3, where the yielded Gauss points are indicated by full squares. Figure 5.4 depicts the circumferential (hoop) stress, σ_θ distribution for the above specified pressures values. The peaks on the theoretical curves mark the position of the elasto-plastic boundaries. A reasonably good agreement between the numercial and exact solution is evident.

5.2.2 Combined Tension and Torsion of an Isotropic Thin-Walled Tube

The physical problem being solved is that of a thin-walled cylindrical tube which is subjected to axial tension and torsion. We consider a tube which is first stressed in tension from a stress free state to incipient yield and is subsequently twisted under constant axial stress. At a given value of the shear stress, τ, the extensional strain ϵ and the shear strain γ are given by the relationships

$$\epsilon = \frac{\sigma_0}{2H'} \ln \left[1 + \frac{3\tau^2}{\sigma_0{}^2} \right] + \frac{\sigma_0}{E} \qquad (5.1)$$

$$\gamma = \frac{3}{H'} \left[\tau - \frac{\sigma_0}{\sqrt{3}} \tan^{-1} (\tau\sqrt{3}/\sigma_0) \right] + \frac{\tau}{G} \qquad (5.2)$$

where G is the elastic shear modulus for $\nu = 0.3$. The above exact solution for isotropic hardening materials has been derived by Hill (1950). We can use it here to quantify our finite element solution errors. Since the stress distribution in the tube, remote from the ends, is constant everywhere (i.e.

no spatial variation), a single material point is sufficient to model the problem. This can be accomplished by a single plane stress isoparametric element. The numerical model together with the loading path is shown in Fig. 5.5 while the material constants are listed below:

$$E = 28300 \text{ ksi}$$
$$E_T = 280 \text{ ksi}$$
$$\nu = 0.3$$
$$\sigma_0 = 26.25 \text{ ksi}$$

The coordinates of the points O, A and B along the load path are tabulated in Table 5.1. All the data used in the present analysis is taken from Dodds (1987) who adopted the elastic predictor-radial return algorithm for the stress computations.

Table 5.1 Load Path Data for Tension-Torsion Test on an Isotropic Tube

Points in Fig. 5.5	σ (ksi)	τ (ksi)
O	0	0
A	26.25	0
B	26.25	24

Since the elastoplastic nonlinearities are very severe in the case considered, this problem can provide a benchmarking example for testing the accuracy of our nonlinear finite element code.

To compute the solution, the axial stress was increased to σ_0 in the first load step. The shear stress was then increased to 24 ksi using a constant size increment $\Delta \tau$. Two analyses were performed corresponding to

$\Delta\tau$ = 2 ksi and $\Delta\tau$ = 4 ksi. Considering the nonlinearities involved, the latter load increments are rather large leading to a severe test of the present numerical method. A tolerance of 0.01% was used to ensure the convergence of the iterative solution at each load step. Table 5.2 compares the computed and exact strains. A graphical representation of the exact strain path along with the present results is also provided in Fig. 5.6.

Table 5.2   Exact and Computed Strains for Combined Tension and Torsion of an Isotropic Tube

τ (ksi)	Exact		$\Delta\tau$ = 2.0 ksi		$\Delta\tau$ = 4.0 ksi	
	$\epsilon \times 10^2$	$\gamma \times 10^2$	$\epsilon \times 10^2$	$\gamma \times 10^2$	$\epsilon \times 10^2$	$\gamma \times 10^2$
0	0.093	0.000	0.093	0.000	0.093	0.000
4	0.405	0.131	0.408	0.126	0.404	0.179
8	1.234	0.752	1.251	0.684	1.250	0.712
12	2.352	2.073	2.400	1.926	2.420	1.891
16	3.568	4.057	3.654	3.838	3.707	3.737
20	4.773	6.572	4.897	6.296	4.987	6.139
24	5.917	9.482	6.076	9.164	6.200	8.964

5.2.3 Perforated Isotropic Sheet Subjected to Remote Uniform Tension

A thin perforated sheet with isotropic elastoplastic material properties is modelled and analyzed numerically for the case of a uniformly distributed load applied at the edges remote from the hole. This problem is of interest for two important reasons. First, it is one of the few non-trivial problems for which adequate theoretical and experimental solutions exist. Second, it provides a benchmark from which orthotropic elastoplastic behaviour can be gauged. The dimensions of the specimen, applied loads and the coordinate axis employed are shown in Fig. 5.7. Because of the symmetry of loading and geometry, a quarter of the plate (shaded region of Fig. 5.7) is modelled by

finite elements. A typical finite element mesh used in the computations is shown in Fig. 5.8. The mesh consists of 48 isoparametric elements with a total of 177 nodes. The material used is an aluminum alloy 57S whose stress-strain curve and its bilinear approximation are shown in Fig. 5.9. The material constants are as follows:

$$E = 7000 \text{ kg/mm}^2 \quad (9956 \text{ ksi})$$

$$\nu = 0.3$$

$$H' = 225 \text{ kg/mm}^2 \quad (320 \text{ ksi})$$

$$\sigma_0 = 24.3 \text{ kg/mm}^2 \quad (34.5 \text{ ksi})$$

The above data correspond to those used in the experimental work of Theocaris and Marketos (1964). Utilizing birefringent coatings bonded on the surface of the specimen together with the electrical analogy method and the plastic incompressibility assumption, they determined the complete elastoplastic response of the perforated strip. A body of literature containing finite element solutions of the same problem are also available; notable among which are the works of Marcal and King (1967) and Zienkiewicz, Valliappan and King (1969). These earlier approaches employed the constant strain triangular element to discretize the specimen and used the "tangent stiffness" and the "initial strain/stress" schemes, respectively, in their finite element solution algorithms. In Fig. 5.10 the development of the maximum strain (at the Gauss integration point closest to the hole and the x-axis) is compared with the experimental results of Theocaris and Marketos (1964) and the above referenced finite element solutions. In the figure σ_{mean} stands for the mean applied stress along the x-axis which, for the particular geometry considered, takes the value $2\sigma_\infty$. The results were obtained using a 3 x 3

Gauss integration rule. We observe that in general the numerical models predict a curve somewhat lower (i.e. more flexible) than the experimental one. This is in spite of the fact that all the numerical models used a stiff representation of the material law. Yield of the first Gauss point takes place at a remote load of $\sigma_\infty = 0.23 \, \sigma_0$. This is reasonable since for the case where the ratio of the plate width to the diameter of the hole is equal to 2 the elastic stress concentration factor is approximately 4.3 (see Howland, 1930). The single step solution shown in Fig. 5.10 is evidence of the fact that the results are insensitive to the magnitude of the load increment, thus supporting the findings of Zienkiewicz et al. (1969). The effect of varying the number of Gauss points and refinement of the mesh were also investigated. Specifically, two analyses were performed, one employing a 2 point Gauss rule with the same mesh as in Fig. 5.8 and the other using a 2 point Gauss rule with a finer mesh consisting of 80 elements and 281 nodal points. The differences in the results were so small as to be indiscernable in Fig. 5.10 and have not been explicitly included in the figure for the sake of clarity.

Figure 5.11 shows the development of the plastic zone around the hole, as the applied remote load is increased. The calculations were made in five load increments (in the plastic range) essentially coinciding with those of Theocaris and Marketos (1964). The depiction of plastic zone growth is accomplished by placing a full square at each of the yielded Gauss points. The plastic zone boundaries which were found by Theocaris and Marketos (1964) are also shown in Fig. 5.11 by solid curves. We note that the pattern of the plastic zone and its evolution obtained in the present work are similar to those reported earlier with the exception of the loading case $\sigma_\infty = 0.47 \, \sigma_0$.

However, a closer examination reveals that for a slightly higher value of the load given by $\sigma_\infty = 0.49\ \sigma_0$, yielding initiates at the free edge (note that no experimental results were available at this load level for direct comparison) and progresses inward in much the same way as that observed by Theocaris and Marketos (1964) for $\sigma_\infty = 0.47\ \sigma_0$.

Contours of effective stress are presented in Fig. 5.12. This figure provides the location of initial yield and the direction of subsequent plastic flow. It can be seen that the contours are consistent with the plastic zone patterns shown in Fig. 5.11.

Finally in Fig. 5.13 we compare the strain (ϵ_y) and stress (σ_y) distributions at the net section (i.e. along the x axis) with the experimental values for the applied stress $\sigma_\infty = 0.47\ \sigma_0$. It can be seen that the trends exhibited by the finite element result are consistent with the experiment. The greatest deviation occur for the ϵ_y strain distribution near the hole where the model overpredicts the experiment. However, this is consistent with the previous numerical predictions.

5.2.4 Conclusions

The numerical examples investigated in this section provide sufficient evidence of the accuracy of the present finite element code COMPLY in analyzing various problems with isotropic elastoplastic material properties. It is now possible to apply the code with confidence to some anisotropic problems. This task is undertaken in the remainder of this chapter.

5.3 Response Prediction of Laminated Composite Coupons

In this section the effectiveness of the proposed constitutive model is verified for a number of loading paths imposed on different types of

laminated FRM coupons. Throughout this section consideration is given to a material point remote from the edges of the coupon specimen, so that the stress distribution can be taken as constant everywhere. Accordingly a single element representation is used in the following analyses. The objective of this section is to examine the capability of the model to accurately reproduce a broad sample of experimental records, both uniaxial and biaxial, with monotonic and cyclic loading, including proportional and nonproportional stress paths.

5.3.1 Uniaxial Loading

As a first test of the proposed model, the program COMPLY is used to predict the nonlinear response of tensile specimens. A series of laminates of Boron/Epoxy (B/Ep) U/D composites for which experimental data had been obtained by Petit and Waddoups (1969) are examined numerically. Figures 5.14 to 5.16 show the three basic stress-strain curves (i.e. longitudinal tension, transverse tension, and in-plane shear) for a single layer of U/D B/Ep composite under investigation. To properly identify the material parameters required as input to the model, these basic stress-strain curves have been fitted with bilinear curves (shown by solid lines in Figs. 5.14 to 5.16). The crosses in these and subsequent curves indicate the stress and strain level at which ultimate failure occurs. The resulting material constants used as input to COMPLY are given in Table 5.3.

Figures 5.17 to 5.25 show predicted and experimental results of tensile tests on a variety of B/Ep laminates. The results of analytical models due to Hashin et al. (1974) and Petit and Waddoups (1969) are also added for comparison. Hashin's model is based on the deformation theory of plasticity while Petit's model is nonlinear elastic (see Section 2.3.3). In Fig. 5.17

Table 5.3 Input Material Properties for a Single Layer of U/D B/Ep

Elastic (ksi)	Plastic (ksi)	Failure (ksi)
E_1 = 30000 E_2 = 3080 ν_{12} = 0.3 (unitless) G = 1000	E_{T_1} = 26100 E_{T_2} = 2200 G_T = 180 X_0 = 132.5 Y_0 = 9 S_0 = 10	X_u = 200 Y_u = 12.5 S_u = 18.6

the experimental stress-strain curve for a $[0°/90°]_s$* cross-ply B/Ep laminate is compared to the results of the present analysis. Though the analysis requires only two distinct layers, at least four plies would be required for symmetric layup. Both brittle and ductile modes of failure were investigated. It appears that these extreme types of post-failure models have provided a good bound to the actual behaviour after tensile matrix cracking in the 90° ply. The ultimate failure is associated with fibre fracture in the 0° ply.

The result for the case of a $[\pm45°]_s$ angle-ply laminate is shown in Fig. 5.18. As is seen, the present model predicts very closely the ultimate strength and general shape of the experimental curve. The highly nonlinear nature of the response in this case is caused by the presence of a considerable amount of shear strain in the plies of the laminate. It should be noted

---

*In the notation for laminate orientation used in this thesis the ply angles are separated by a slash with the entire layup enclosed within square brackets. The 0° ply has its fibres along the loading direction. Where there is more than one ply at any given angle, the number of plies at that angle is denoted by a numerical subscript within the brackets. Subscript s outside the brackets means that the layup is symmetric about the mid-surface.

that for this particular laminate and in general all angle-ply laminates of the form $[\pm\theta]_s$ ultimate failure coincides with the failure of one layer.

Figure 5.19(a) presents the stress-strain curves for the $[\pm30°]_s$ laminate. It can be seen that the Hill's failure criterion (Eq. (3.57)) underpredicts the ultimate strength of this laminate. However, by observing the stress paths in one of the plies, say the +30° ply, (Fig. 5.19(b)) it can be inferred that the ultimate failure of the $[\pm30°]_s$ laminate is caused by compression in the transverse direction before failure could occur in the fibre direction. Since Hill's criterion does not account for the strength differential between tension and compression, and that the transverse compressive strength is in this case about three times higher than the tensile strength, the use of the maximum stress failure criterion allows us to trace the response curve to the second cross indicated in Fig. 5.19(a). The corresponding stress paths are shown in Fig. 5.19(c). It should be noted that the Hill's criterion was still used as the yield criterion in the analyses whether or not it was used to indicate failure.

The results of the present computations for a $[\pm60°]_s$ laminate of B/Ep are compared to prior analytical and experimental results in Fig. 5.20. The shapes of the curves are in good agreement with the experimental curves showing a more nonlinear behaviour than either of the analytical results. The ultimate failure in this case occurred from tension in the transverse direction.

Figure 5.21(a) displays the response results for a $[\pm20°]_s$ laminate of B/Ep. It can be observed again that there is a relatively large difference between the measured ultimate strength and the present predictions based on Hill's failure criterion. As can be seen from the stress path diagram shown in Fig. 5.21(b) the predicted mode of failure is that of compression in the

transverse direction (i.e. compressive matrix failure). By adopting the maximum stress failure criterion (which accounts for the actual compressive strength) the predicted mode of failure shifts to that of fibre failure (Fig. 5.21(c)). This is in fact the type of failure exhibited by the test specimen as reported in the paper by Petit and Waddoups (1969).

Figure 5.22 presents results for the case of a quasi-isotropic $[0°/±45°/90°]_s^*$ laminate of B/Ep. All the results, including the present predictions, show a relatively insignificant amount of nonlinearity. At σ_x = 60 ksi the 90° layer fails in transverse tension. The ±45° layers remain intact until the 0° layer fails in the fibre mode thereby causing the ultimate failure of the laminate. A very similar result is presented in Fig. 5.23 for the quasi-isotropic laminate formed from the $[0°/±60°]_s$ layup. As seen in the figure, the experimental results and analytical predictions are in excellent agreement. According to the analytical results, ultimate laminate failure was due to failure occurring almost simultaneously in the 0° ply in the fibre direction and in the ±60° plies in the transverse direction. It is worth noting that for the two quasi-isotropic laminates discussed above the results of the brittle post-failure model showed no perceptible difference when compared to the ductile model and hence were omitted from the figures.

Figures 5.24 and 5.25 display the stress-strain curves for a $[0°_3/±45°]_s$ (i.e. $[0°/0°/0°/±45°]_s$) laminate tested at 0° and 65° to the 0° ply, respectively. For the 0° test (Fig. 5.24) the numerical and experimental curves

---

*Since we are only concerned with in-plane loadings and also ignore the effects of interlaminar stresses a change of ply stacking sequence is assumed not to cause a change in the laminate response. This applies to all the laminates considered here.

are very close exhibiting good agreement. In this case the laminate ultimate failure was caused by fibre failure in the 0° plies while no failures occurred in the ±45° plies. For the laminate tested at 65° (Fig. 5.25) the present predictions agree reasonably well with the results of Hashin's theory. However, the discrepancy between the observed and predicted failure stress is quite substantial. The cause of this premature failure is not known but may be attributed to interlaminar effects (which have not been included in the present analysis). It should be pointed out that the results shown are for the ductile post-failure model in which case the ultimate failure (marked by fibre failure in the 20° ply) is preceded by tensile matrix failures in the ±65° and -70° plies. When the brittle post-failure model was employed the failure occurred simultaneously in all plies causing the collapse of the laminate at a load level of 30 ksi.

It is of interest to note that for laminates showing extreme nonlinearity due to shear (such as $[\pm 45°]_s$ and $[\pm 60°]_s$) the response curves are sensitive to the choice of the bilinear fit used to approximate the shear stress-strain curve. For the other laminate configurations, particularly the ones having fibres in several directions (including the loading direction) no significant change in results occurs when the bilinear shear stress-strain curve is altered. Given the extent of experimental error and the relative insensitivity of the results to the precise form of the basic stress-strain curves of the individual plies, insisting on precise curve fitting is unwarranted. Instead, a good qualitative agreement with the data should be sought as a means of testing the validity of the model. The results obtained so far serve to indicate that the present model captures the most important trends of laminated FRM behaviour under monotonic tensile loading. It should be remarked in passing that although the external loads in the above examples

grow proportionally, this does not necessarily imply that the internal stress components in a typical layer also grow proportionally (see Figs. 5.19(b,c) and 5.21(b,c)). This raises doubts concerning the validity of the deformation theory offered by Hashin et al. (1974), which necessarily requires proportionality of the stress path.

Figures 5.26 through 5.28 display the stress-strain curves for the case of a polyester resin matrix reinforced by various bidirectional woven glass fibres. The three basic experimental stress-strain curves (extracted from MIL-HDBK-17 (1959)) and their bilinear representations are illustrated in Figs. 5.26(a), 5.27(a) and 5.28(a). The resulting material constants used as input data are tabulated in Table 5.4.

Table 5.4   Input Material Properties for a Single Layer of B/D Glass Fabric/Polyester Resin

Parameter	181 Glass Fabric (ksi)	162 Glass Fabric (ksi)	143 Glass Fabric (ksi)
Elastic			
E_1	2740	2820	5770
E_2	2520	1740	1600
ν_{12}	0	0	0
G	630	570	720
Plastic			
E_{T_1}	2100	600	5770
E_{T_2}	2000	730	430
G_T	190	260	155
X_0	34	32	90
Y_0	25	24	32
S_0	5	4	4.8
Failure			
X_u	49.2	45	90
Y_u	45.3	29.4	11
S_u	13.4	11.6	12

The uniaxial tensile stress-strain responses at 45° to the fibres are shown in Figs. 5.26(b), 5.27(b) and 5.28(b). These are the output of the program COMPLY wherein the Puppo-Evensen yield and failure criteria were used. Since here we are dealing with a single layer of material the initial and ultimate failure coincide. From the figures it can be observed that the experimental curves fall below the predicted curves with the ultimate strain levels reached being under-predicted. In spite of such discrepancies in the results the predicted ultimate stress values are in reasonably good agreement with the experimental values. Notice that the experimental curve in Fig. 5.26(b) does not extend to the failure level and is terminated at strain level of 2%. It is regretable that experimental data for laminates consisting of various oriented layers of B/D FRM are not available in the literature for comparison. This is one area which could certainly benefit from further experimental work.

5.3.2 Biaxial Loading

To further verify the capability of the elastic-plastic-failure model, a few test cases were investigated in which the external loadings were biaxial. In particular we consider the effects of pure internal pressure, and combined torsion/internal pressure loading on the response of $[0°/\pm60°]_s$ laminated tube of U/D Graphite/Epoxy (Gr/Ep) material. The corresponding experimental (and theoretical) work was carried out by Tennyson et al. (1980). As in the preceding examples the three basic stress-strain curves were approximated by bilinear fits resulting in the single ply properties listed in Table 5.5. Note that the longitudinal and transverse stress-strain curves were taken to be linearly elastic right up to failure. Also the nonlinear shear effects appear to be negligible for this material.

Table 5.5 Input Material Properties for a Single Layer of U/D Gr/Ep

Elastic (ksi)	Plastic (ksi)	Failure (ksi)
E_1 = 20500 E_2 = 1400 ν_{12} = 0.26 (unitless) G = 600	E_{T_1} = 20500 E_{T_2} = 1400 G_T = 380 X_0 = 185.6 Y_0 = 7.5 S_0 = 6.8	X_u = 185.6 Y_u = 7.5 S_u = 11.8

A graphical plot of the pressure-strain curve is shown in Fig. 5.29 for the case of internal pressure only. It is worth mentioning that the thickness and the radius of the test tube were 1 in and 0.0343 in, respectively. Both Hill's and maximum stress failure criterion were employed in the analysis. According to the predicted results the initial failure occurred in the $\pm 60°$ plies (from tension in the transverse direction) at pressure levels of about 1.8 ksi and 1.9 ksi for Hill's and the maximum stress criteria respectively. It is apparent from Fig. 5.29 that Tennyson's cubic strength criterion offers a better estimate of the ultimate stress value than either of the two criteria used in the present analysis. However, the shape of the predicted response curve agrees more closely with the experimental data than Tennyson's results. In view of the presence of higher order terms (and hence more basic strength data), it is not surprising that Tennyson's failure criterion provides a more accurate estimate of the maximum load. The question of whether or not the additional complexity (and cost) of evaluating the extra strength parameters is warranted depends on the application.

The effect of a constant pre-torque (19.8 ksi) and internal pressure loading on the response is illustrated in Fig. 5.30. This provides a test

case in which the external loading grows in a nonproportional manner. As can be seen from Fig. 5.30 the results of the present analysis are in reasonable agreement with the experimental data. Based on the present analytical predictions tensile matrix failure occurred first in the -60° ply at a pressure level of 1.1 ksi, according to both the maximum stress and Hill's failure criterion. Subsequent failure occurred in the +60° ply, at a pressure level of 2.02 ksi if the Hill's failure criterion was used, and at 2.6 ksi if the maximum stress criterion was used. The ultimate failure of the laminate occurred shortly afterwards when the 0° ply failed in the fibre direction.

The second example of nonproportional load path is that in which a constant internal pressure (1.1 ksi) was applied while the tube was torsionally loaded to failure. The results are illustrated on a graph of applied torque versus shear strain γ_{xy} in Fig. 5.31. It appears that all the numerical models are overly stiff in comparison with the experimental results. It can also be noted that the ultimate failure stress predicted by the Hill's and the cubic criteria are fairly close and agree better with the experimental data than the predictions of the maximum stress failure criterion.

5.3.3 Cyclic Loading

While the previous examples provide verification of the model under monotonic loading, they do not illustrate the effects of cyclic loading on laminate behaviour. To demonstrate such effects we consider the uniaxial cyclic response of some Boron/Aluminum (B/Al) laminates. The experimental data for comparison with the present results have been extracted from the report by Sova and Poe (1978). To evaluate the input material constants the longitudinal and transverse tensile stress-strain responses of the unidirec-

tional laminate $[0°_6]^*$ were approximated by bilinear curves. Since no experimental data were available for the shear response, the latter was derived from the uniaxial tensile stress strain curve of $[\pm 45°]_s$ laminate This technique is in keeping with the procedure outlined by Rosen (1972) for determination of shear modulus. Accordingly the shear stress and the shear strain in the ply coordinates are given by

$$\sigma_6 = \sigma_x/2$$

$$\epsilon_6 = \epsilon_x - \epsilon_y$$

(5.3)

where σ_x is the tensile stress applied to the $[\pm 45°]_s$ laminate in the x direction (i.e. 0° direction), and ϵ_x, ϵ_y are the corresponding strain components. By choosing a suitable bilinear representation of the tensile stress-strain curve for $[\pm 45°]_s$ laminate one can determine from Eq. (5.3) the necessary parameters of the shear stress-strain curve for a single ply. These are listed in Table 5.6 along with the parameters obtained from longitudinal and transverse stress-strain curves.

Table 5.6 Input Material Properties for a Single Layer of U/D B/Al

Elastic (GPa)	Plastic (GPa)	Failure (GPa)
E_1 = 209.7 E_2 = 107 ν_{12} = 0.2 (unitless) G = 32	E_{T_1} = 202.7 $E_{T_1}^1$ = 24.3 G_T^2 = 1.5 X_0 = 1.2 Y_0 = 0.09 S_0 = 0.045	X_u = 1.7 Y_u = 0.12 S_u = 0.11

---

*It is assumed that the stress-strain response of a single layer of the unidirectional laminate is the same as the response of the total test laminate.

Figure 5.32 presents the uniaxial response prediction of a $[0°/±45°]_s$ B/Al laminate subjected to three load cycles. As may be seen the model captures the relevant features of the response associated with such cyclic loading. Thus, for instance, the residual strains are correctly predicted and the hysteresis loops predicted by the model closely follow the observed pattern. The origin of the unloading hysteretic loops in Fig. 5.32 may be traced back to the ±45° plies which yield in compression upon unloading of the laminate from higher strains. Calculations were also performed for a pure monotonic loading case and essentially the same failure point (shown in Fig. 5.32) was reached. This shows that the load cycles did not affect the ultimate stress and strain level of the laminate, thus supporting the experimental findings of Sova and Poe (1978).

5.3.4 Conclusions

The foregoing numerical simulations of various coupon tests, each representing a typical state of stress, illustrate how the proposed model adequately predicts the basic material response characteristics of laminated FRMS under a variety of in-plane loading conditions. Some cases were reported in which experimental results did not compare very well with the present predictions. These experimental data are, however, quite limited and may be insufficient for drawing conclusions in this regard. A very attractive feature of the model is the fact that it can represent nonlinear behaviour with only a few input material property values being required. For complex loading situations such as nonproportional loading and especially cyclic loadings the present incremental model is superior to the deformation theory model of Hashin et al. (1974).

5.4 Perforated Orthotropic Plates Subjected to Remote Uniform Tension

All the analyses presented in the previous section were applicable to large sheets of laminate, containing no imperfections and thus provide verification of the model in simulating various unnotched coupon tests. To further challenge the model the present section is devoted to the analysis of laminates with a central hole under remote tensile loading. This example exhibits many important effects not tested in the previous applications such as multidimensional stress state, stress gradients and stress concentrations.

In the following section, analyses of various orthotropic sheets with a circular hole are conducted for three distinct loading regimes. These appear under the subheadings of elastic, elastic-plastic and elastic-plastic-failure analyses.

5.4.1 Elastic Analysis

An elastic analysis of the sheet with a circular hole is conducted for two orthotropic materials, namely U/D layers of B/Al and B/Ep FRMs. The former demonstrates mild orthotropy (in the elastic range), while the latter exhibits rather strong orthotropy. Two types of analyses are conducted for each material, one with the fibre direction being oriented along the x-axis (i.e. normal to the load direction), and the other with it along the y-axis (i.e. parallel to the load direction). The theoretical solutions used here for comparison are valid if the size of the opening is small in comparison to the external dimensions (width and length) of the plate. The opening can be considered small if the ratio of the plate width to the diameter of the hole is equal to or greater than 4 (Greszczuk, 1972). To facilitate comparison with theoretical solutions the latter ratio is selected for the plates analyzed in this section.

A quadrant of the plate is modelled by finite elements, as shown in Fig. 5.33, with 64 isoparametric elements and a total of 229 nodal points. For future reference, we designate the Gauss integration point closest to the hole and the x-axis as point "A" and the point at the left corner of the upper edge of the modelled region as point "B". Since linear elastic results are of interest here, let the material constants be listed as follows:

	B/Al	B/Ep
E_1	29.4×10^3 ksi	30.0×10^3 ksi
E_2	19.1×10^3 ksi	3.0×10^3 ksi
ν_{12}	0.169	0.336
G	7.5×10^3 ksi	1.0×10^3 ksi

According to the linear elastic theory (Greszczuk, 1972) the circumferential stress, σ_θ, at the edge of the hole is given by the following expression

$$\frac{\sigma_\theta}{\sigma_\infty} = \frac{(1 + \zeta_1)(1 + \zeta_2)(1 + \zeta_1 + \zeta_2 + 2\cos2\theta)}{(1 + \zeta_1^2 + 2\zeta_1\cos2\theta)(1 + \zeta_2^2 + 2\zeta_2\cos2\theta)} \qquad (5.4)$$

where

$$\zeta_1 = \frac{\{\rho_1 + \rho_2\}^{1/2} - 1}{\{\rho_1 + \rho_2\}^{1/2} + 1}$$

$$(5.5)$$

$$\zeta_2 = \frac{\{\rho_1 - \rho_2\}^{1/2} - 1}{\{\rho_1 - \rho_2\}^{1/2} + 1}$$

where for the case in which the loading direction (y) coincides with the fibre direction (x_1)

$$\rho_1 = \frac{E_2}{2G} - \nu_{12}$$

<div align="right">(5.6)</div>

$$\rho_2 = \{\rho_1^2 - \frac{E_2}{E_1}\}^{1/2}$$

For the case of a plate loaded transverse to the fibre direction the subscripts 1 and 2 in Eq. (5.6) must be interchanged.

The present finite element solutions utilizing 2 x 2 and 3 x 3 Gauss quadratures are compared with the above theoretical predictions in Figs. 5.34 and 5.35, where the circumferential stress distributions at Gauss points close to the hole's edge, $\sigma_\theta/\sigma_\infty$, are plotted against angular location θ. The finite element results are in good agreement with the theory in most locations. Note that the stresses are calculated at the Gauss stations which do not coincide with the hole boundary. It can be seen that the stress concentration factor for B/Al is similar to the isotropic materials (i.e. $\approx$ 3) which is what one would expect since this material is only weakly orthotropic. For the B/Ep material a significant stress concentration in the vicinity of the hole can be observed. This is particularly pronounced when the stiff fibres are oriented along the load direction.

5.4.2 Elastic-Plastic Analysis

[90°] Layer

An experimental study of the elastoplastic response of a U/D B/Al metal matrix composite strip with a circular hole was conducted by Rizzi and reported in the paper by Rizzi et al. (1987). This particular experiment

involved loading a B/Al specimen as shown in Fig. 5.36 with the fibres oriented at 90° to the load. Multiple strain guages were mounted on the front and rear faces of the specimen.

The finite element mesh used to analyze the test specimen is the same as that shown in Fig. 5.33 except that the dimensions were scaled to those of Fig. 5.36. The elastic material properties used here are those determined by Kenaga et al. (1987), as

$$E_1 \ = 29.4 \times 10^3 \ \text{ksi} \qquad (203 \ \text{GPa})$$
$$E_2 \ = 19.1 \times 10^3 \ \text{ksi} \qquad (132 \ \text{GPa})$$
$$\nu_{12} = 0.169$$
$$G \ = 7.49 \times 10^3 \ \text{ksi} \qquad (52 \ \text{GPa})$$

The material properties governing the plasticity of the specimen can be obtained from best-fit bilinear representations of stress-strain curves. A sensitivity analysis revealed that the key material constants affecting the plastic flow characteristics were the yield stress and the tangent modulus transverse to the fibres (x_2 or y direction), i.e. Y_0 and E_{T_2}. Furthermore the shear properties and the properties in the fibre direction were found to have very little influence on the elastic-plastic results. To this end since the shear stress-strain curve for this material was not explicitly given in the available literature, the values S_0 and G_T were taken from Table 5.6, i.e.,

$$S_0 \ = 6.5 \ \text{ksi} \qquad (0.045 \ \text{GPa})$$
$$G_T \ = 220 \ \text{ksi} \qquad (1.5 \ \text{GPa})$$

Along the fibre direction the material behaviour was taken to be purely elastic up to failure (Kenaga et al., 1987). Accordingly,

$$X_0 = X_u = 204 \text{ ksi} \qquad (1.41 \text{ GPa})$$

$$E_{T_1} = E_1 = 29.4 \times 10^3 \text{ ksi} \quad (203 \text{ GPa})$$

Figure 5.37 shows the experimentally determined stress-strain curve transverse to the fibres (Kenaga et al., 1987). Since this curve is highly nonlinear and the parameter Y_0 and E_{T_2} necessary for modelling it can directly affect the results one must first look at the strain range of interest. By examining the experimental results of Rizzi et al. (1987) it was observed that the highest strain (ϵ_y or ϵ_2 measured at the gauge point closest to the hole) level reached was of the order of 0.2%. Therefore in order to simulate the same test results the bilinear representation shown in Fig. 5.37 was selected for the relevant portion of the stress-strain curve. This gave rise to the following values for Y_0 and E_{T_2} (which incidently are very similar to the corresponding values given in Table 5.6)

$$Y_0 = 13.0 \text{ ksi} \qquad (0.09 \text{ GPa})$$

$$E_{T_2} = 4.0 \times 10^3 \text{ ksi} \quad (27.6 \text{ GPa})$$

With the material properties established above the problem was solved for the same load levels reported in Rizzi et al.'s (1987) work using a 2x2 Gauss integration procedure. The distributions of the ϵ_y strain components along the x-axis of the specimen are shown in Fig. 5.38 for all the load steps considered. Incipience of plastic deformation was found to occur at a remote stress σ_∞ of approximately 4 ksi. It can be seen that the test-theory

agreement more than adequately confirms the predictive capability of the COMPLY program for an orthotropic material.

The spreading of the plastic zones and contours of nondimensional effective stress $\bar{\sigma}/k_0$ are depicted in Figs. 5.39 and 5.40 for a representative number of loads. The evolution of plasticity during the successive steps of loading shows an initial spreading across the net section. At the maximum remote stress $\sigma_\infty = 10.7$ ksi, the plastic zone appears to have progressed almost completely across the specimen, forming a certain angle to the net section (i.e. x-axis). The extent of the plastic front seems to be greater away from the net section causing an elastic region to still remain close to the straight boundary of the specimen. Therefore, it is reasonable to assume that little or no permanent strain will be found at the outer strain gauge locations. To substantiate such findings, a direct study of the plastic strains are in order. This can be achieved by unloading[*] the specimen from appropriate load levels. The longitudinal residual strain distributions following unloading from three elastic-plastic remote stresses ($\sigma_\infty = 6$, 7.7 and 10.7 ksi) are plotted along with the experimental results in Fig. 5.41. The agreement between the present numerical solution (solid lines) and the experimental results appears fair. The lack of any substantial residual strains at the outer gauge locations is in keeping with the plastic zone visualization of Fig. 5.39. Overall, the results are indicative of the fact that the proposed material model does a good job of predicting the magnitude and distribution of permanent deformation.

---

[*]Numerically, the unloading is performed by taking a small negative loading step, which allows the elements to become elastic. The small unloading increment also provides an opportunity for re-assembly of the stiffness matrix. The remainder of the load is then removed in the next increment by taking one large unloading step.

For the sake of completeness the residual stress distributions along the net section are illustrated in Fig. 5.42. It is clear from the results that the longitudinal stress component, σ_y, demonstrates a significant compressive (negative) residual value in the vicinity of the hole while the other residual stresses (σ_x, τ_{xy}) are negligible. Such large compressive stresses can be accounted for by noting that the material in the proximity of the net section is permanently deformed, and upon load reversal the surrounding elastic material tends to clamp it down and produce compressive stresses. The curves of σ_y residual stress distribution show relative maxima that tend to move away from the hole with the increase of prior loading.

$[0°/90°]_s$ Laminate

The purpose of this study is to utilize the previously developed computational tools for investigation of the elastic-plastic behaviour of a $[0°/90°]_s$ layup of B/Al plate containing a circular hole. The single layer material properties, geometry of the specimen and the finite element mesh are taken to be the same as that of the preceding example. The plate was subjected to uniaxial in-plane tension. The development of plastic zones in the individual layers are shown in Figs. 5.43 and 5.44 for the 90° and 0° plies respectively. It can be observed that as the loading continues the plastic zone in the 90° layer spreads rapidly across the specimen and almost completely covers it at about 25 ksi. The characteristic shape and growth of the plastic zones in the 0° layer (see Fig. 5.44) is somewhat different in that it extends upward in the loading direction and remains constrained to the immediate vicinity of the hole. This behaviour is understandable, since the major stress component, σ_y, is parallel to the fibres and is not as likely to cause yielding. It is found that at a stress level of 44 ksi the

first failure of the fibres in the 0° layer (at Gauss point A in Fig. 5.33) occurs, i.e. the fibres attain their ultimate tensile strength of 204 ksi. Figures 5.45 and 5.46 present contours of the normalized effective stress, $\bar{\sigma}/k_0$, for the 90° and 0° plies at various load levels. These contours provide the necessary quantitative information regarding the extent of yielding in each layer. For example, contours of value $\bar{\sigma}/k_0 = 1$ show the outline of the elastic-plastic boundary and contours bearing values of $\bar{\sigma}/k_0 > 1$ represent the work-hardened regions.

Bahei-El-Din and Dvorak (1980) have also analyzed a similar problem for a FP/Al metal matrix composite. The development of plastic zones for this analysis is illustrated in Fig. 5.47. Though a direct quantitative comparison cannot be offered due to the different material properties, geometry and loading, the character of the results are the same. It is worth recalling (cf. Chapter 2, Section 2.3.2) that Bahei-El-Din and Dvorak's (1980) material model was based on mini-mechanical concepts as opposed to the simpler macro-mechancial approach adopted in this study. The other macro- mechanical analysis performed by Leewood (1985) (see also Leewood et al., 1987) utilizes a material model developed by Kenaga et al. (1987) which was based on a trial and error approach to determine the anisotropic parameters A_{ij}, that best fitted the data. The present material model, however, is free from such empiricism and can be applied to a wide variety of materials provided the three key stress-strain curves are available.

Figure 5.48 shows the σ_y stress distribution along the x-axis (or rather at Gauss points closest to this axis) for different remote load levels. It can be noted that the elastic analysis underestimates the stress concentration factor for the 0° layer, and overestimates it for the 90° layer. Figure 5.49 shows the longitudinal stress σ_y in the 0° layer at the Gauss point A

(see Fig. 5.33) as a function of the applied load σ_∞. The influence of plastic deformation on the stress concentration factor and the nonlinearity of the curve due to plasticity are particularly obvious from the figure. It can be inferred that plasticity in composite laminates cannot be expected to reduce the level of stress concentration at the free edge. This finding may contradict one's usual expectation of the reduction of stress concentration due to localized yielding such as that prevalent in monolithic metals. The foregoing results support the findings of Bahei-El-Din and Dvorak (1980).

Figure 5.50 shows the overall load (stress) versus deflection (v_B) curve, where v_B refers to the deflection at point B (see Fig. 5.33) in the direction of loading. Also shown in the figure is the residual displacement obtained by unloading the laminate from a load level of 20 ksi. Unloading initially occurred elastically, but before complete unloading to zero overall tension the 90° layer reyielded (in compression) at the six Gauss points closest to the hole perimeter. This accounts for the slight kink in the unloading part of the response curve, a phenomenon which is commonly observed in experiments on laminated metal-matrix composite plates. The residual σ_y stress distributions (along the x-axis) due to unloading from σ_∞ = 20 ksi are illustrated in Fig. 5.51. Notice the significant compressive component of the residual stress in the 90° layer. This behaviour is expected since the 90° layer experiences a substantial amount of permanent deformation.

5.4.3 Elastic-Plastic-Failure Analysis

While the previous section treated the elastoplastic behaviour of ortho-tropic plates with a hole, the attention here is focussed on the extension of the finite element analysis to include failure. Of principal concern in the

following analyses is the prediction of the ultimate failure loads and the progression of damage (i.e. fibre and matrix crackings) prior to the collapse of the laminated structures. Here again the dimensions of the plate and its finite element discretization are those of Fig. 5.33. Although numerical attempts at progressive failure analyses of laminated plates with geometric discontinuities have been made before (Chang and Chang, 1987; Sandhu et al., 1983; Lee, 1982), no experimental verifications of damage patterns were offered. Also, due to the different geometries and lack of sufficient knowledge of material properties (in the full nonlinear range) a direct comparison with these numerical results cannot be made. To this end, present numerical predictions of the failure patterns and collapse loads are made without the benefit of comparison with other sources. The analyses presented here are meant to simulate load-controlled test situations. In light of the different material models for the post-failure regime (brittle and ductile behaviour) the present study is aimed at providing bounds to the actual behaviour of test specimens.

The laminates considered in the following analyses are assumed to be made up of U/D layers of B/Ep with the material properties listed in Table 5.3. The analyses are conducted for [90°], [0°], [0°/90°]$_s$, [±45°]$_s$ and [0°/±45°/90°]$_s$ layups.

[90°] Layer

As the first example, let us consider a single layer with the strong direction perpendicular to the load. The predicted damage progression process at the Gauss points is illustrated in Fig. 5.52 for the ductile post-failure model. It is seen from the figure that matrix failure is

confined to the areas near the stress concentrations. An attempt to increase the applied stress beyond 7 ksi resulted in a singular structural stiffness matrix. This indicates that the entire structure formed a collapse mechanism at this load level. For the brittle failure model the finite element program predicts that the specimen fails catastrophically at a load level of 6 ksi. In other words the first Gauss points to fail precipitate final failure.

[0°] Layer

In this case, a single layer is considered in which the load is in the fibre direction. The spreading of failure zones for the ductile model is shown in Fig. 5.53 where it can be seen that the first appearance of fibre failure happens at the rim of the hole and on the longitudinal axis of the specimen. Similar to the 90° layer no significant damage is predicted prior to final failure at 70 ksi. Once again a brittle type of failure model leads to a sudden collapse of the structure at incipience of failure.

[0°/90°]$_s$ Laminate

Various combinations of post-failure models were considered here for fibre and matrix failure. For the case of brittle fibre failure the gradual, as opposed to sudden, stress release scheme was adopted. Accordingly, the fibre stresses were relaxed over a number of load increments. To facilitate a convergent solution very small load steps had to be used after the first occurrence of fibre failure. During each load step the failed fibre stresses were arbitrarily reduced by 25%. Figure 5.54 shows the corresponding stress path, yield surfaces and the failure surface in the $\sigma_1/X_0 - \sigma_2/Y_0$ plane at Gauss point A (see Fig. 5.33) for the 0° layer. It is worth recording that the numerical stability of brittle type failure solution processes is gener-

ally poor since on initiation of failure part or all of the existing stresses must be eliminated by redistribution.

The load-deflection curve evaluated at point B of the specimen (see Fig. 5.33) is shown in Fig. 5.55 for different material models in the post-failure regime. The corresponding developments of damage zones in the individual layers are depicted in Figs. 5.56 to 5.58, for representative load levels up to the ultimate failure. As can be seen from Figs. 5.56 and 5.57 for the ductile fibre failure models, matrix cracking in the 90° layer tends to propagate both towards the load and across the specimen width. Fibre fracture pattern, however, appears to be discontinuous in nature and remains confined to a narrow band near the hole. For the brittle fibre failure model the damage pattern is markedly different as shown in Fig. 5.58. In this case, damage propagates horizontally leading to the ultimate failure of the specimen by tearing across the net section. It is important to note that here the elements near the first fracture location are further loaded due to stress redistribution. In order to clarify the failure mechanism, the changes in stress distribution for small variations of load level between the initial and ultimate failure loads are shown in Fig. 5.59. Note that the peak stress changes its location as the failure propagates.

$[\pm 45°]_s$ Laminate

The finite element results indicate that the predominant mode of failure in this case is shearing of the matrix. The predicted load-deflection curve is shown in Fig. 5.60 for both ductile and brittle matrix failure. It can be seen that the response is extremely nonlinear owing to the nonlinear shear stress-strain behaviour in each ply (see Fig. 5.16). Initial failure was found to occur at 19.4 ksi. In the brittle failure case the shear stress was

reduced by 50% at every load step following the first failure. A total of 14 load increments (each of magnitude 0.1 ksi) were applied between the initial and final failure load. The predicted patterns of damage in each layer are presented in Figs. 5.61 and 5.62 for ductile and brittle models, respectively. It is clear from these figures that the fracture of the elements starts from the hole and propagates diagonally across the specimen forming a band at 45° to the x-axis. Ultimate failure is seen to be preceded by some scattered fibre fracture in the layers.

$[0°/±45°/90°]_s$ Laminate

The predicted load-deflection curve for this case is shown in Fig. 5.63 for various combinations of brittle and ductile post-failure models assigned to the fibre and matrix. When fibre failure is assumed to be ductile, the ultimate stress level reached appears to be almost independent of the choice of matrix post-failure model. However, when the brittle matrix model is invoked (corresponding to a sudden release of transverse and shear stresses), the specimen exhibits a more nonlinear response. Since the fibres in the 0° layer carry the major portion of the load, a brittle type fibre failure leads to progressive failure of the laminate soon after the first fibre failure occurrs. As a result, the collapse of the laminate is attained without noticeable increase in load-carrying capacity above that of the initial fibre fracture load. This accounts for the plateau in the load-deflection curve (Fig. 5.63) which can be traced using very small load steps until the tangential stiffness matrix becomes singular.

The spread of damage zones in individual layers is illustrated in Figs. 5.64 to 5.66 for representative load levels. It is clear from these figures that for the ductile fibre model the specimen fails gradually with consider-

able damage occurring prior to ultimate failure. Damage in each layer is seen to propagate across the specimen at a rapid rate (Figs. 5.64 and 5.65). For the brittle fibre model the characteristic localized damage around the hole appears to prevail. The brittle fibre-brittle matrix model exhibited a catastrophic failure after initial matrix cracking in the 90° layer. This corresponds to the lower bound on collapse load shown in Fig. 5.63.

5.4.4 Conclusions

The orthotropic elastic capability of the present code, COMPLY, demonstrates good agreement with the theoretical solutions. Close agreements with the experimental results of Rizzi et al. (1987) for a U/D B/Al composite provide further evidence of the adequacy of the proposed orthotropic elastic-plastic formulation and demonstrates the encouraging performance of the present finite element program in this regard. The elastoplastic analyses reveal the strong dependence of plastic flow on the orientation of the principal axes of orthotropy. The present elastic-plastic-failure analyses with various post-failure options should prove to be useful in providing overall bounds on the response history of laminates. The finite element analysis also forms a viable procedure for predicting the damage progression prior to the ultimate failure of composite laminates with stress concentrations. Such capabilities are particularly useful in parametric studies leading to the design of laminates.

CHAPTER 6

SUMMARY AND CONCLUSIONS

6.1 Summary

In almost all of the practical strength analyses of laminated composites in the literature, the stresses used for failure criteria have been determined on the basis of elastic laminate analysis. Use of the elastic theory would, in general, lead to overly stiff predictions, and may result in conservative estimates of the failure loads. The heterogeneous nature of FRMs is such that a variety of possible damage modes exist. Thus, matrix cracking or yielding, fibre fracture, debonding and other inelastic effects can all occur in local regions at relatively low overall stress levels. These nonlinear effects greatly complicate the problem of establishing reliable analyses. In the present study, the problem of nonlinear material behaviour of laminated FRMs was investigated. The primary objective was to model the inelastic behaviour of such materials and to develop a computer program which can be used as an engineering tool in the design and/or analysis of fibre-reinforced composite structures.

In predicting the nonlinear stress-strain behaviour of FRMs, constitutive equations are generally required to cover the entire stress history. To this end, a continuum mechanics approach was utilized herein to develop a relatively simple orthotropic elastic-plastic-failure constitutive model for single layers of FRM undergoing isothermal infinitesimal deformation. The constitutive equations so developed, were then combined using the classical lamination theory, to arrive at the governing response relations for multi-layer laminates. Unidirectional and bidirectional FRM layers were treated within the same general framework with the exception that yielding (and

failure) in these layers was assumed to be governed by different criteria, namely, Hill's and Puppo-Evensen's yield (and failure) criteria, respectively. The proposed plasticity model adopted a 3-parameter quadratic yield surface and the associated flow rule of the rate-independent theory of plasticity. The subsequent loading surfaces were obtained by a non-uniform expansion of the initial yield surface in the stress space. This was achieved by allowing the parameters identifying the initial yield function to vary in a non- proportional manner during plastic flow. A 3-parameter quadratic failure surface similar in form to that of the initial yield surface was defined to mark the upper limit of plastic flow. Once failure was reached, it was identified as fibre or matrix mode of failure depending on the relative magnitude of various stress ratio terms appearing in the failure criterion. In the post-failure modelling, both brittle and ductile type of behaviour were considered in the direction of the offending stress. To completely quantify the proposed elastic-plastic-failure model three pieces of experimental stress-strain curves were required, namely, the uniaxial stress-strain curves along the two principal axes of orthotropy, and the in-plane shear stress- strain curve. Once established, the stress-strain curves were represented by bilinear approximations, thus clearly defining the key parameters under the various loading programs. No provisions were made for the difference between tensile and compressive responses.

Based on the proposed model, constitutive equations were properly formulated. A nonlinear finite element code was subsequently developed to incorporate the derived constitutive equations. The program named COMPLY, was based on the conventional displacement method finite element procedure using two dimensional 8-node isoparametric elements. The nonlinearities in the equilibrium equations were handled by a mixed incremental and Newton-

Raphson iterative procedure. Analysis restart and cyclic loading capabilities were also included to expand the program's usefulness.

The performance of the program and the effectiveness of the model were verified for a number of in-plane loading paths imposed on a wide variety of laminated FRMs with and without geometric discontinuities. The results of numerical simulations were compared with the experimental data available in the literature.

6.2 Concluding Remarks

The favourable agreement between the present numerical predictions and experimental results illustrate the accuracy and versatility of the proposed elastic-plastic-failure model for laminated composites. The model is typical of conventional continuum mechanics theories in that it captures the essence of the material behaviour rather than its detail. In light of this, the model must be applied carefully with the knowledge that the nonlinearities may not actually be due to plastic yielding but to some combination of plasticity, matrix or fibre cracking, fibre pull-out, etc. The relative ease with which the proposed approach can handle nonlinear behaviour is a distinct advantage over current analytical procedures. Indeed the method is sufficiently general that it may be applied to a variety of laminated structures provided either analytical or experimental data are available to describe the stress-strain curves for the constituent plies. As demonstrated in several examples in this thesis, the present theory reasonably predicts the phenomenological behaviour of composites under monotonic and cyclic loading, including proportional and nonproportional stress paths.

The studies conducted herein point to the fact that the global laminate response is a nonlinear superposition of individual layer material proper-

ties. This complex response provides justification for not analyzing the laminate as a whole. In this regard, the present comprehensive constitutive model applied to each layer of a laminate and the subsequent superposition of layer responses via lamination theory appears to offer the most systematic approach. Considering the fact that the proposed material model lends itself to a straightforward computational implementation it may be a viable option for incorporation into general purpose finite element codes for studying the detailed behaviour of anisotropic structures. In the meantime, the present planar finite element program, COMPLY, can be a useful tool in parametric studies of laminated FRMs as part of the design process.

6.3 Further Areas of Research

The topic presents many interesting areas for further detailed investigations. The following briefly outlines a few of these areas of research that are needed to improve or extend the existing theoretical procedure.

Let us observe that because of the simplicity in terms of the necessary input information for implementation, it is possible that the model will not satisfactorily describe in all details some complex loading history responses which may be envisioned. For example, it is conceivable that in certain cases a bilinear representation of the stress-strain curves will not be sufficient to capture the nonlinearities involved. A greater flexiblity of modelling can be achieved by extending the theory to incorporate multilinear stress-strain curves. One basic feature lacking from the present formulation is the description of strength and stiffness differential between tensile and compressive responses. Such differences are of importance for certain types of fibre composites, particularly the ones with carbon contents (e.g. Graphite/Epoxies). An obvious extension of the model would be to include

independent descriptions of tensile and compressive behaviour both initially and subsequently (i.e. Bauschinger effect). The next logical step is to allow for the compressibility of the plastic flow, since plastic volume changes can be important in some types of fibre-reinforced materials. Additional post-failure softening schemes and ply failure criteria should be investigated. This should be combined with careful experimental observations of the failure process.

One of the major causes of failure which is particularly operative in notched laminates, is delamination. This type of failure is often precipitated by high interlaminar stresses that exist within a boundary layer close to the free edge region of the laminate (i.e. hole or notch boundary). These stresses influence the stress concentration around the hole and may play an important role in the yielding and/or failure of laminates. The present finite element program should be extended to take delaminations into account. This is usually achieved by extending the program to three dimensions. However, reliable three-dimensional failure theories are still required to predict the onset and subsequent growth of delamination.

Another useful application of the model would be to study the nonlinear behaviour of plates under bending.

REFERENCES

Aboudi, J. (1984), "Effective Behavior of Inelastic Fibre-Reinforced Composites," Int. J. Engng. Sci., 22, pp. 439-449.

Aboudi, J. (1986), "Elastoplasticity Theory for Composite Materials," Solid Mechanics Archives, 11/3, pp. 141-183.

Adams, D.F. (1970), "Inelastic Analysis of a Unidirectional Composite Subjected to Transverse Normal Loading," J. Comp. Mats., 4, p. 310.

Adams, D.F. (1974), "Elastoplastic Behaviour of Composites," in Mechanics of Composite Materials, Vol. 2 of Composite Materials (Edited by G.R. Sendeckyj), Academic Press, N.Y., pp. 169-208.

Adkins, J.E., and Rivlin, R.S. (1955), "Large Elastic Deformations of Isotropic Materials, X. Reinforcement by Inextensible Cords," Philosophical Transactions, 248, A-944, p. 201.

Ashkenazi, E.K., (1965), "Problems of the Anisotropy of Strength," Mekhanika Polimerov, 1, pp. 79-92, (Polymer Mechanics, 1, pp. 60-70).

Axelsson, K. and Samuelsson, A. (1979), "Finite Element Analysis of Elastic-Plastic Materials Displaying Mixed Hardening," Int. J. Numer. Methods Eng., 14, pp. 211-225.

Azzi, V.D. and Tsai, S.W., (1965), "Anisotropic Strength of Composites", Exp. Mech., 5, pp. 283-288.

Bahaei-El-Din, Y.A. and Dvorak, G.J., (1980), "Plastic Deformation of a Laminated Plate with a Hole", Trans. ASME, J. Appl. Mech., 47, pp. 827-832.

Bahaei-El-Din, Y.A., and Dvorak, G.J. (1982), "Plasticity Analysis of Laminated Composite Plates," Trans. ASME, J. Appl. Mech., 49, pp. 740-746.

Baltov, A. and Sawczuk, A. (1965), "A Rule of Anisotropic Hardening," Acta Mech., 1/2, pp. 81-92.

Bland, D.R. (1957), "The Associated Flow Rule of Plasticity," J. Mech. Phys. Solids, 6, pp. 71-78.

Bushnell, D., (1977), "A Strategy for the Solution of Problems Involving Large Deflections, Plasticity and Creep," Int. J. Numer. Meth. Eng., 11, pp. 683-708.

Chamis, C.C. and Sendeckyj, G.P., (1968), "Critique on Theories Predicting Thermoelastic Properties of Fibrous Composites", J. Comp. Mats., 2, pp. 332-358.

Chang, F.K., and Chang, K.Y. (1987), "A Progressive Damage Model for Laminated Composites Containing Stress Concentrations," J. Comp. Mats., 21, pp. 834-855.

Chiu, K.D. (1969), "Ultimate Strengths of Laminated Composites," J. Comp. Mats., 3, pp. 578-582.

Christensen, R.M. (1979), Mechanics of Composite Materials, John Wiley & Sons.

Christensen, R.M. (1985), "Fibre Reinforced Composite Materials," Appl. Mech. Rev., 38, pp. 1267-1270.

Craddock, J.N. and Champagne, D.J. (1985), "A Comparison of Failure Criteria for Laminated Composite Materials," Proc. 23rd Structural Dynamics and Materials Conference, Orlando, Florida, April 1985, pp. 268-278.

Dodds, R.H., (1987), "Numerical Techniques for Plasticity Computations in Finite Element Analysis", Comput. & Struct., 26 (5), pp. 767-779.

Drucker, D.C., (1975), "Yielding, Flow and Failure", in Inelastic Behaviour of Composite Materials (Edited by C. Herakovich), pp. 1-15.

Dubey, R. and Hillier, M.J., (1972), "Yield Criteria and the Bauschinger Effect for a Plastic Solid", Trans. ASME, J. Basic Eng., 94, pp. 228-230.

Dvorak, G.J., Rao, M.S.M., and Tarn, J.Q. (1973), "Yielding in Unidirectional Composites Under External Loads and Temperature Changes," J. Comp. Mats., 7, pp. 194-217.

Dvorak, G.J., Rao, M.S.M., and Tarn, J.Q. (1974), "Generalized Initial Yield Surfaces for Unidirectional Composites," Trans. ASME, J. Appl. Mech., 41, pp. 249-253.

Dvorak, G.J. and Bahei-El-Din, Y.A. (1979), "Elastic-Plastic Behaviour of Fibrous Composites," J. Mech. Phys. Solids, 27, pp. 51-72.

Dvorak, G.J. and Bahei-El-Din, Y.A. (1982), "Plasticity Analysis of Fibrous Composites," Trans. ASME, J. Appl. Mech., 49, pp. 327-335.

Dvorak, G.J. and Johnson, W.S., (1980), "Fatigue of Metal/Matrix Composites", Int. J. Frac., 16, p. 585.

Fan, W.X. (1987), "On Phenomenological Anisotropic Failure Criteria," Composites Sci. Tech., 28, pp. 269-278.

Foye, R.L. (1973), "Theoretical Post-Yielding Behaviour of Composite Laminates, Part I - Inelastic Micromechanics," J. Comp. Mats., 7, pp. 178-193.

Foye, R.L, and Baker, D.J. (1971), "Design/Analysis Methods for Advanced Composite Structures," AFML-TR-70-299, Vol. I, Analysis; Vol. II, Computer Programs.

Franchi, A. and Genna, F., (1987), "A Numerical Scheme for Integrating the Rate Plasticity Equations with an A Priori Error Control", Comput. Meths. Appl. Mech. Eng., 60, pp. 317-342.

Francis, P.H. and Bert, C.W. (1975), "Composite Material Mechanics: Inelasticity and Failure", Fibre Sci. Tech., 8, pp. 1-19.

Gotoh, M. (1977), "A Theory of Plastic Anisotropy Based on a Yield Function of Fourth Order (Plane Stress State)," Int. J. Mech. Sci., 19, pp. 505-520.

Greszczuk, L.B. (1972), "Stress Concentrations and Failure Criteria for Orthotropic and Anisotropic Plates with Circular Openings", Composite Materials: Testing and Design, 2nd Conference, ASTM STP 497, pp. 363-381.

Griffin, O.H. (1982), "Evaluation of Finite Element Software Packages for Stress Analysis of Laminated Composites," Composites Technology Review, 4, Winter 1982, pp. 136-141.

Griffin, O.H., Kamat, M.P., and Herakovich, C.T. (1981), "Three-dimensional Inelastic Finite Element Analysis of Laminated Composites," J. Comp. Mats., 15, pp. 543-560.

Hahn, H.T. (1973), "Nonlinear Behavior of Laminated Composites," J. Comp. Mats., 7, pp. 257-271.

Hahn, H.T. and Tsai, S.W. (1973), "Nonlinear Elastic Behavior of Unidirectional Composite Laminates," J. Comp. Mats., 7, pp. 102-118.

Hashin, Z. (1980), "Failure Criteria for Unidirectional Fibre Composites," Trans. ASME, J. Appl. Mech., 47, pp. 329-334.

Hashin, Z. (1983), "Analysis of Composite Materials - A Survey," Trans. ASME, J. Appl. Mech., 50, pp. 481-505.

Hashin, Z. (1985), "Analysis of Cracked Laminates: A Variational Approach," Mech. Mater., 4, pp. 121-136.

Hashin, Z. (1986), "Analysis of Stiffness Reduction of Cracked Cross-Ply Laminates," Engng. Frac. Mech., 25, pp. 771-778.

Hashin, Z. (1987), "Analysis of Orthogonally Cracked Laminates Under Tension," Trans. ASME, J. Appl. Mech., 54, pp. 872-879.

Hashin, Z., Bagchi, D. and Rosen, B.W. (1974), "Nonlinear Behavior of Fibre Composite Laminates," NASA Rept. No. CR-2313.

Highsmith, A.L. and Reifsnider, K.L. (1982), "Stiffness-Reduction Mechanisms in Composite Laminates," Damage in Composite Materials (Edited by K.L. Reifsnider), ASTM STP 775, pp. 103-117.

Hill, R. (1950), The Mathematical Theory of Plasticity, Oxford University Press, Oxford.

Hill, R. (1964), "Theory of Mechanical Properties of Fibre-Strengthened Materials: I. Elastic Behavior, II. Inelastic Behavior," J. Mech. Phys. Solids, 12, pp. 199-218.

Hill, R. (1965), "Theory of Mechanical Properties of Fibre-Strengthened Materials: III. Self-Consistent Model," J. Mech. Phys. Solids, 13, pp. 189-198.

Hodge, P.G. and White, G.N., (1950), "A Quantitative Comparison of Flow and Deformation Theories of Plasticity", Trans. ASME, J. Appl. Mech., 17, pp. 180-184.

Hoffman, O. (1967), "The Brittle Strength of Orthotropic Materials," J. Comp. Mats., 1, pp. 200-206.

Hoffman, O. (1979), "A Continuum Model for the Engineering Analysis of Metal Matrix Composites," Modern Developments in Composite Materials and Structures (Edited by J.R. Vinson), American Society of Mechanical Engineers, pp. 101-107.

Howland, R.C.J. (1930), "On the Stresses in the Neighbourhood of a Circular Hole in a Strip Under Tension", Phil. Trans. Roy. Soc., A229, pp. 49-86.

Hu, L.W. (1956), "Studies on Plastic Flow of Anisotropic Metals," Trans. ASME, J. Appl. Mech., 23, pp. 444-450.

Hu, L.W. (1958), "Modified Tesca's Yield Condition and Associated Flow Rules for Anisotropic Materials and Applications," J. Franklin Institute, 265, pp. 187-204.

Huang, W.C. (1971), "Plastic Behaviour of Some Composite Materials," J. Comp. Mats., 5, pp. 320-338.

Hütter, U., Schelling, H., and Krauss, H. (1974), "An Experimental study to Determine Failure Envelope of Composite Materials with Tubular Specimens Under Combined Loads and Comparison Between General Classical Criteria," NATO-AGARD Conference Proceedings No. 163, 39th Meeting of the Structures and Materials Panel in Munich, Germany, 13-19 October 1974, Paper No. 3, pp. 3-11.

Jensen, W.R., Falby, W.E. and Prince, N. (1966), "Matrix Analysis Methods for Anisotropic Inelastic Structures," AFFDL-TR-65-220, Air Force Flight Dynamic Laboratory, Wright-Patterson Air Force Base, Ohio, April 1966.

Jones, R.M. (1975), Mechanics of Composite Materials, McGraw-Hill, New York.

Jones, R.M. and Morgan, H.S. (1977), "Analysis of Nonlinear Stress-Strain Behavior of Fiber-Reinforced Materials," AIAA J., 15, pp. 1669-1676.

Kachanov, L.M. (1971), Foundation of the Theory of Plasticity, North-Holland, Amsterdam.

Kenaga, D., Doyle, J.F. and Sun, C.T. (1987), "The Characterization of Boron/Aluminum Composite in the Nonlinear Range as an Orthotropic Elastic-Plastic Material," J. Comp. Mats., 21, pp. 516-531.

Krieg, R.D. and Krieg, D.B., (1977), "Accuracies of Numerical Solution Methods for the Elastic-Perfectly Plastic Model", J. of Pressure Vessel Tech., 99 (4), pp. 510-515.

Labossiere, P. and Neale, K.W., (1987a), "Macroscopic Failure Criteria for Fibre-Reinforced Composite Materials", Solid Mechanics Archives 12/2, pp. 439-450.

Labossiere, P. and Neale, K.W. (1987b), "On the Determination of the Strength Parameters in the Tensor Polynomial Failure Criterion," J. Strain Analysis, 22, pp. 155-161.

Lance, R.H. and Robinson, D.N. (1971), "A Maximum Shear Stress Theory of Plastic Failure of Fibre-Reinforced Materials," J. Mech. Phys. Solids, 19, pp. 49-60.

Laws, N., Dvorak, G.J. and Hejazi, M. (1983), "Stiffness Changes in Unidirectional Composites Caused by Crack Systems," Mech. Mater., 2, pp. 123-137.

Lee, J.D. (1982), "Three Dimensional Finite Element Analysis of Damage Accumulation in Composite Laminates," Computers & Structures, 15, pp. 335-350.

Leewood, A.R., (1985), "Numerical Studies of Problems in Anisotropic Plasticity", Ph.D. Thesis, School of Aeronautics and Astronautics, Purdue University.

Leewood, A.R., Doyle, J.F. and Sun, C.T. (1987), "Finite Element Program for Analysis of Laminated Anisotropic Elastoplastic Materials," Computers & Structures, 25, pp. 749-758.

Lin, T.H., Salinas, D. and Ito, Y.M. (1972), "Initial Yield Surface of a Unidirectionally Reinforced Composite," Trans. ASME, J. Appl. Mech., 39, pp. 321-326.

Marcal, P.V. and King, I.P., (1967), "Elastic-Plastic Analysis of Two Dimensional Stress Systems by the Finite Element Method", Int. J. Mech. Sci., 9, pp. 143-155.

Mendelson, A. (1968), Plasticity: Theory and Application, MacMillan, London.

MIL-HDBK-17, Plastics for Flight Vehicles, Part I, Reinforced Plastics, U.S. Government Printing Office, Washington, D.C., Nov. 5, 1959.

Mulhern, J.F., Rogers, T.G. and Spencer, A.J.M. (1967), "A Continuum Model for Fibre-Reinforced Plastic Materials," Proc. Roy. Soc., A. 301, pp. 473-492.

Mulhern, J.F., Rogers, T.G. and Spencer, A.J.M. (1969), "A Continuum Theory of a Plastic-Elastic Fibre-Reinforced Material," Int. J. Engng., Sci., 7, pp. 129-152.

Naghdi, P.M. (1960), "Stress-Strain Relations in Plasticity and Thermoplasticity," in Plasticity, ONR Structural Mechanics Series, Proc. of the 2nd Symposium on Naval Structural Mechanics (Edited by E.H. Lee and P.S. Symonds), Pergamon, Elmsford, N.Y., pp. 121-169.

Nagtegaal, J.C., Parks, D.M. and Rice, J.R., (1974), "On Numerically Accurate Finite Element Solutions in the Fully Plastic Range", Comput. Meths. Appl. Mech. Engng., 4, pp. 153-177.

Nahas, M.N. (1986), "Survey of Failure and Post-Failure Theories of Laminated Fiber-Reinforced Composites," J. Composites Technology & Research, 8, pp. 138-153.

Nahas, M.N. (1984), "Analysis of Non-Linear Stress-Strain Response of Laminated Fibre-Reinforced Composites," Fibre Sci. Tech., 20, pp. 297-313.

Nayak, G.C. and Zienkiewicz, O.C., (1972), "Elasto-Plastic Stress Analysis: A Generalization for Various Constitutive Relations Including Strain Softening", Int. J. Numer. Meth. Engng., 15, pp. 113-135.

Nyssen, C., (1981), "An Efficient and Accurate Iterative Method Allowing Large Incremental Steps to Solve Elasto-Plastic Problems," Comput. of Struct., 13, pp. 63-71.

Ochoa, O.O. and Engblom, J.J. (1987), "Analysis of Progressive Failure in Composites," Composites Sci. Tech., 28, pp. 87-102.

Olson, M.D. and Anderson, D.L., (1988), "Modelling Structural Response of Fibre-Reinforced Structures to Air Blast", DRES Contract Report, Dept. of Civil Eng., UBC.

Ortiz, M. and Popov, E.P., (1985), "Accuracy and Stability of Integration Algorithms for Elastoplastic Constitutive Relations", Int. J. Numer. Meth. Eng., 21, pp. 1561-1576.

Owen, D.R.J. and Hinton, E., (1980), "Finite Elements in Plasticity", McGraw-Hill, New York.

Petit, P.H. and Waddoups, M.E. (1969), "A Method of Predicting the Nonlinear Behavior of Laminated Composites," J. Comp. Mats., 3, pp. 2-19.

Pindera, M.J. and Herakovich, C.T. (1983), "An Endochronic Model for the Response of Unidirectional Composites Under Off-Axis Tensile Load," in Mechanics of Composite Materials: Recent Advances, Proceedings IUTAM Symposium on Mechanics of Composite Materials (Edited by Z. Hashin and C.T. Herakovich), Pergamon Press, pp. 367-381.

Pipes, R.B., and Pagano, N.J. (1970), "Interlaminar Stresses in Composite Laminates Under Uniform Axial Extension," J. Comp. Mats., 4, pp. 538-548.

Prager, W., (1949), "Recent Developments in the Mathematical Theory of Plasticity", J. Appl. Phys., 20, pp. 235-241.

Prager, W. (1955), "The Theory of Plasticity: A Survey of Recent Achievements," James Clayton Lecture, Proc. Instn. Mech. Engrs. (London), 169, pp. 41-50.

Prager, W. (1969), "Plastic Failure of Fiber-Reinforced Materials," Trans. ASME, J. Appl. Mech., 36, pp. 770-773.

Prager, W. and Hodge, P.G., (1951), "Theory of Perfectly Plastic Solids", Wiley, New York.

Puppo, A.H. and Evensen, H.A. (1972), "Strength of Anisotropic Materials Under Combined Stresses," AIAA J., 10, pp. 468-474.

Ramberg, W. and Osgood, W.B. (1943), "Description of Stress-Strain Curves by Three Parameters," NASA-TN-902.

Reddy, J.N. and Pandey, A.K. (1987), "A First-Ply Failure Analysis of Composite Laminates," Computers & Structures, 25, pp. 371-393.

Rees, D.W.A. (1984), "An Examination of Yield Surface Distortion and Translation", Acta Mechanica, 52, pp. 15-40.

Rivlin, R.S. (1981), "Some Comments on the Endochronic Theory of Plasticity," Int. J. Solids Struct., 17, pp. 231-248.

Rizzi, S.A., Leewood, A.R., Doyle, J.F. and Sun, C.T., (1987), "Elastic-Plastic Analysis of Boron/Aluminum Composite Under Constrained Plasticity Conditions", J. Comp. Mats., 21, pp. 734-749.

Rosen, B.W., (1972), "A Simple Procedure for Experimental Determination of the Longitudinal Shear Modulus of Unidirectional Composites", J. Comp. Mats., 6, pp. 555-557.

Rowlands, R.E. (1985), "Strength (Failure) Theories and their Experimental Correlation," in Handbook of Composites, Vol. 3: Failure Mechanics of Composites (Edited by G.C. Sih and A.M. Skudra), Elsevier Science Publishers, Amsterdam, pp. 71-125.

Sandhu, R.S. (1976), "Non-Linear Behaviour of Unidirectional and Angle-Ply Laminates," J. Aircraft, 13, pp. 104-111.

Sandhu, R.S., Sendeckyj, G.P. and Gallo, R.L. (1983), "Modelling of the Failure Process in Notched Laminates," in Mechanics of Composite Materials: Recent Advances, Proceedings IUTAM Symposium on Mechanics of Composite Materials (Edited by Z. Hashin and C.T. Herakovich), Pergamon Press, pp. 179-189.

Schapery, R.A. (1974), "Viscoelastic Behaviour and Analysis of Composite Materials," in Mechanics of Composite Materials, Vol. 2 of Composite Materials (Edited by G.P. Sandeckyj), Academic Press, New York, pp. 84-168.

Schreyer, H.L., Kulak, R.F. and Kramer, M.M. (1979), "Accurate Numerical Solutions of Elastic-Plastic Models", Trans. ASME, J. Press. Vessel Tech., 101, pp. 226-234.

Shih, C.F. and Lee, D. (1978), "Further Developments in Anisotropic Plasticity," Trans. ASME, J. Engrg. Mat. and Tech., 100, pp. 294-302.

Smith, C.S. and Chalmers, D.W., (1986), "Design of Ship Superstructures in Fibre-Reinforced Plastic", RINA Spring Meetings, Paper No. 3, pp. 1-12.

Sokolnikoff, I.S. (1956), Mathematical Theory of Elasticity, McGraw-Hill, New York.

Sova, J.A. and Poe, C.C., (1978), "Tensile Stress-Strain Behaviour of Boron/Aluminum Laminates", NASA-TP-1117.

Swanson, S.R. and Christoforou, A.P. (1987), "Progressive Failure in Carbon/Epoxy Laminates Under Biaxial Stress," Trans. ASME, J. Engrg. Mat. and Tech., 109, pp. 12-16.

Takahashi, K. and Chou, T.W. (1987), "Non-Linear Deformation and Failure Behaviour of Carbon/Glass Hybrid Laminates," J. Comp. Mats., 21, pp. 396-420.

Talreja, R. (1985), "A Continuum Mechanics Characterization of Damage in Composite Materials," Proc. Roy. Soc. Lond., A. 399, pp. 195-216.

Talreja, R. (1986), "Stiffness Properties of Composite Laminates with Matrix Cracking and Interior Delamination," Engrg. Frac. Mech., 25, pp. 751-762.

Tennyson, R.C., MacDonald, D. and Nanyaro, A.P. (1978), "Evaluation of the Tensor Polynomial Failure Criterion for Composite Materials," J. Comp. Mats., 12, pp. 63-75.

Tennyson, R.C., Nanyaro, A.P. and Wharram, G.E., (1980), "Application of Cubic Polynomial Strength Criterion to the Failure Analysis of Composite Materials", J. Comp. Mats. Supplement, 14.

Theocaris, P.S. and Marketos, E., (1964), "Elastic-Plastic Analysis of Perforated Thin Strips of a Strain-Hardening Material", J. Mech. Phys. Solids, 12, pp. 377-390.

Tsai, S.W. and Hahn, H.T. (1975), "Failure Analysis of Composite Materials," in Inelastic Behavior of Composite Materials (Edited by C.T. Herakovich), Vol. 13, ASME, New York, pp. 73-96.

Tsai, S.W. (1965), "Strength Characteristics of Composite Materials," NASA CR-224.

Tsai, S.W. and Wu, E.M. (1971), "A General Theory of Strength for Anisotropic Materials," J. Comp. Mats., 5, pp. 58-81.

Valanis, K.C. (1971), "A Theory of Viscoplasticity Without a Yield Surface, I: General Theory; II: Application to Mechanical Behavior of Metals," Arch. Mech., 23, pp. 517-551.

Valliappan, S., (1971), "Elastic-Plastic Analysis of Anisotropic Work-Hardening Materials", University of New South Wales, Kensington, N.S.W., Australia, Report No. R-70.

Whang, B. (1969), "Elasto-Plastic Orthotropic Plates and Shells," Proc. Symp. on Application of Finite Element Method in Civil Engineering, Vanderbilt University Tennessee, pp. 481-515.

Wu, E.M. (1974), "Phenomenological Anisotropic Failure Criterion," in Mechanics of Composite Materials, Vol. 2 of Composite Materials (Edited by G.P. Sendeckyj), Academic Press, New York, pp. 353-431.

Ziegler, H. (1959), "A Modification of Prager's Hardening Rule," Quart. Appl. Math., $\underline{17}$, pp. 55-56.

Zienkiewicz, O.C., (1977), "The Finite Element Method", 3rd Edition, McGraw Hill.

Zienkiewicz, O.C., Valliappan, S. and King, I.P., (1969), "Elasto-Plastic Solutions of Engineering Problems 'Initial Stress', Finite Element Approach", Int. J. Numer. Meth. Eng., $\underline{1}$, pp. 75-100.

APPENDIX A

DETERMINATION OF THE ANISOTROPIC PARAMETERS OF THE YIELD FUNCTION

In order to define the complete yield surface of anisotropic materials, it is required to know the parameters A_{ij}, α_i and k that determine its shape, origin and size, respectively. For the yield function

$$f \equiv A_{ij}(\sigma_i - \alpha_i)(\sigma_j - \alpha_j) - k^2 = 0 \qquad (A.1)$$

a physical interpretation of the A_{ij}, α_i and k may be made in the following manner.

Let Γ_1, Γ_2 and Γ_3 denote the tensile yield stresses in the principal material directions x_1, x_2, and x_3, respectively. Similarly, let the absolute values of the compressive yield stresses along the same axes be denoted by Γ_1', Γ_2' and Γ_3'. Since a direct evaluation of α_i from uniaxial test data is rather cumbersome, it is more convenient to express the yield function as (cf. Shih and Lee, 1978)

$$f \equiv A_{ij} \sigma_i \sigma_j - L_i \sigma_i - \chi = 0 \qquad (A.2)$$

where by comparison with Eq. (A.1), L_i and χ are

$$L_i = 2 A_{ij}\alpha_j$$

$$\qquad (A.3)$$

$$\chi = -A_{ij}\alpha_i\alpha_j + k^2$$

The experimental measurements can now be related to A_{ij} and L_i through Eq. (A.2), and α_i determined from Eq. (A.3). For simple uniaxial tension (and compression) tests in x_1 direction, say, we have $\sigma_1 = \Gamma_1$ (and $\sigma_1 = -\Gamma_1'$) so that

$$A_{11}\Gamma_1^2 - L_1\Gamma_1 = \chi \qquad \text{(tension)}$$

$$\text{(A.4)}$$

$$A_{11}\Gamma_1'^2 + L_1\Gamma_1' = \chi \qquad \text{(compression)}$$

Solving the above equations simultaneously, we obtain

$$A_{11} = \frac{\chi}{\Gamma_1\, \Gamma_1'}$$

$$\text{(A.5)}$$

$$L_1 = \chi\left(\frac{1}{\Gamma_1'} - \frac{1}{\Gamma_1}\right)$$

Similarly, through uniaxial tensile and compressive tests along the x_2 and x_3 axes, we obtain

$$A_{22} = \frac{\chi}{\Gamma_2\, \Gamma_2'} \quad ; \qquad L_2 = \chi\left(\frac{1}{\Gamma_2'} - \frac{1}{\Gamma_2}\right)$$

$$\text{(A.6)}$$

$$A_{33} = \frac{\chi}{\Gamma_3\, \Gamma_3'} \quad ; \qquad L_3 = \chi\left(\frac{1}{\Gamma_3'} - \frac{1}{\Gamma_3}\right)$$

By imposing pure shear in the 3 orthogonal planes, we can relate the A_{ij}'s to the shear yield stresses, Γ_4, Γ_5 and Γ_6 as

$$A_{44} = \frac{\chi}{\Gamma_4^2} \quad ; \quad A_{55} = \frac{\chi}{\Gamma_5^2} \quad ; \quad A_{66} = \frac{\chi}{\Gamma_6^2} \qquad \text{(A.7)}$$

Note that by arbitrarily prescribing one of the anisotropic parameters, the remaining parameters can be scaled with respect to the prescribed value. If for example $A_{11} = 1$ then it follows that $\chi = \Gamma_i \Gamma_i'$ and $k^2 = A_{ij}\alpha_i\alpha_j + \chi$.

The remaining off-diagonal terms in the matrix $[A]$ can be obtained from any biaxial loading condition: tension-tension, compression-compression, tension-compression. However, it is not evident that the values of A_{13}, A_{23}, and A_{12} determined by these different tests will be unique. One remedy to these problems is to assume that the plastic volumetric strain is zero, i.e. $d\epsilon_1^p + d\epsilon_2^p + d\epsilon_3^p = 0$. It is then possible to express the off-diagonal terms of $[A]$ (i.e. A_{ij} for $i \neq j$) as functions of the leading diagonal terms, A_{ii}, in the following way

$$A_{12} = -\frac{1}{2}(A_{11} + A_{22} - A_{33})$$

$$A_{13} = -\frac{1}{2}(A_{11} - A_{22} + A_{33}) \qquad \text{(A.8a)}$$

$$A_{23} = -\frac{1}{2}(-A_{11} + A_{22} + A_{33})$$

Also,

$$L_1 + L_2 + L_3 = 0 \qquad \text{(A.8b)}$$

As a consequence of Eq. (A.8a,b), the A_{ij} and L_i parameters are not all independent and the knowledge of principal components A_{ii} given by Eqs. (A.5) to (A.7) and any two of L_1, L_2, and L_3 is sufficient to completely describe the state of plastic deformation. The assumption of incompressibility of plastic strains is implicit in Hill's (1950) formulation of anisotropic yield criterion. It is interesting to note that the function f reduces to the von

Mises yield criterion when the A_{ij} and L_i parameters assume the following values

$$A_{11} = A_{22} = A_{33} = 1$$
$$A_{12} = A_{13} = A_{23} = -1/2 \qquad\qquad (A.9)$$
$$A_{44} = A_{55} = A_{66} = 3$$
$$L_1 = L_2 = L_3 = 0$$

In the absence of any constraints such as Eq. (A.8), one has to resort to biaxial tests in order to determine the interaction parameters A_{12}, A_{23} and A_{13}. Many authors recommend the use of 45-degree off-axis specimen for the determination of such parameters. This can be done by letting:

$$\sigma_1 = \sigma_2 = \sigma_6 = U/2, \qquad \sigma_3 = \sigma_4 = \sigma_5 = 0 \qquad (A.10)$$

where U is the tensile strength of a 45-degree off-axis specimen. Note that the combined stresses in Eq. (A.10) are applied to the symmetry axes of an orthotropic material. This state of stress is equivalent to a uniaxial tensile stress applied to a reference coordinate system rotated 45 degrees from the material symmetry axes. By introducing Eq. (A.10) into Eq. (A.2), we have

$$\frac{U^2}{4} (A_{11} + A_{22} + 2A_{12} + A_{66}) - \frac{U}{2} (L_1 + L_2) - \chi = 0$$

so that A_{12} can be written in terms of the other known parameters as

$$A_{12} = \frac{2\chi}{U^2} + \frac{2}{U} \ (L_1 + L_2) - \frac{1}{2} \ (A_{11} + A_{22} + A_{66}) \tag{A.11}$$

Similar tests can be performed in order to obtain A_{13} and A_{23}. In all these cases, however, the conditions for closure of the yield surface (see Eq. (3.49)) places a severe restriction on the allowable values of these so-called interaction parameters. In view of these difficulties, Labossiere and Neale (1987) offer alternative methods for determining the A_{ij} parameters.

APPENDIX B

VARIATION OF ANISOTROPIC PARAMETERS WITH STRAIN-HARDENING

It has been shown in Appendix A that the anisotropic parameters of the yield function can be determined from simple tests. However, for a complete description of plastic flow behaviour of anisotropic materials, it is necessary to know the variation of these parameters with plastic strain. To be consistent with the discussion in Chapter 3 the parameter α_i (which accounts for both the initial strength differential and Bauschinger effect) will henceforth be ignored and consideration will be given to the variations of A_{ij} and k only.

Hu (1956) assumed that the A_{ij} parameters remained constant during plastic deformation, while Jensen, Falby and Prince (1966) and later Whang (1969) pointed out that for strain-hardening materials A_{ij} should vary. The objective here is to determine the A_{ij} parameters in such a way that all the stress-strain diagrams in the principal material directions can be reproduced correctly when mapped on to an arbitrary effective stress ($\bar{\sigma}$) – effective plastic strain ($\bar{\epsilon}^p$) diagram. To accomplish this mapping we adopt the method originally developed by Jensen et al (1966). The basic assumption underlying the latter method is that for the same amount of plastic work (W^p) produced during plastic loading in any of the principal material directions the effective yield stress (k) reached will be the same irrespective of the direction of loading.

When the stress-strain diagrams can be represented in bilinear form as shown in Fig. B.1 then the plastic work W^p may be expressed in closed form as (see Fig. B.2)

$$W^P = \int dW^P = \frac{1}{2E_{P_i}} (\Gamma_i^2 - \Gamma_{0i}^2) \quad (i = 1,2,\ldots,6) \quad\quad (B.1)$$

where Γ_{0i} and Γ_i are the initial and subsequent yield values and E_{P_i} is the plastic modulus, all referred to the σ_i-ϵ_i stress-strain diagram. The present formulation allows one of the σ_i-ϵ_i stress-strain diagrams to be arbitrarily chosen as the effective stress-effective strain ($\bar{\sigma}$-$\bar{\epsilon}$) diagram, while the remaining stress-strain curves are then normalized with respect to the prescribed curve.

Equating the plastic work given by Eq. (B.1) to the plastic work done by the effective yield stress,

$$\frac{1}{2H'} (k^2 - k_0^2) = \frac{1}{2E_{P_i}} (\Gamma_i^2 - \Gamma_{0i}^2)$$

or

$$\Gamma_i^2 = \frac{E_{P_i}}{H'} (k^2 - k_0^2) + \Gamma_{0i}^2 \quad (i = 1,2,\ldots,6) \quad\quad (B.2)$$

where H' is the hardening modulus defined by Eq. (3.23), and k_0 is the initial effective yield stress. The plastic moduli E_{P_i} can be determined in terms of the elastic and tangent moduli (E_i and E_{T_i}, respectively) as follows.

Accepting the basic assumption that

$$d\epsilon_i = d\epsilon_i^e + d\epsilon_i^p \quad\quad (B.3)$$

then since for an increment of stress $d\sigma_i$

$$d\epsilon_i = \frac{d\sigma_i}{E_{T_i}} \;; \qquad d\epsilon_i^e = \frac{d\sigma_i}{E_i} \;; \qquad d\epsilon_i^p = \frac{d\sigma_i}{E_{p_i}} \qquad \text{(B.4)}$$

one obtains

$$\frac{1}{E_{p_i}} = \frac{1}{E_{T_i}} - \frac{1}{E_i} \qquad \text{(B.5)}$$

Using Eqs. (A.5) to (A.7) (noting that $\chi = k^2$ and $\Gamma_i' = \Gamma_i$) and (B.4), the anisotropic parameters A_{ii},[†] at any state of plastic deformation described by k, can be obtained as:

$$A_{ii}^0 = \frac{k_0^2}{\Gamma_{0i}^2} \qquad\qquad \text{for } 0 \leq k \leq k_0$$

$$\text{(B.6)}$$

$$A_{ii}(k) = \frac{k^2}{\Gamma_i^2} = k^2 / \left[\frac{E_{p_i}}{H'} (k^2 - k_0^2) + \Gamma_{0i}^2 \right] \quad \text{for } k \geq k_0$$

The variation of A_{ii} with k is shown schematically in Fig. B.3. It is noted that depending on the value of H' (i.e. depending on the choice of normalizing direction) A_{ii} may increase as k increases, and when k gets large the A_{ii} depend only on E_{p_i} and not Γ_{0i}. Following the arguments that led to the form of Eq. (A.11), one can write

---

[†] Note that repeated indices do not imply summation here.

$$A_{12}^0 = 2 \left(\frac{k_0}{U_0}\right)^2 - \frac{1}{2}\left(1 + A_{22}^0 + A_{66}^0\right) , \qquad \text{for } 0 \le k \le k_0$$

$$\text{(B.7)}$$

$$A_{12}(k) = 2 \left(\frac{k}{U}\right)^2 - \frac{1}{2}\left(1 + A_{22}(k) + A_{66}(k)\right) , \quad \text{for } k \ge k_0$$

in which

$$U^2 = \frac{E_{P_{45°}}}{H'}\left(k^2 - k_0^2\right) + U_0^2$$

Thus far the parameters A_{ij} were allowed to vary with the amount of strain-hardening, marked by the value of k. However, it is often convenient, as well as computationally economical to keep these parameters constant at their initial values, A_{ij}^0. To facilitate the latter and yet satisfy the requirement of equal plastic work given by Eq. (B.2) we must have

$$\frac{\partial A_{ii}}{\partial k} = 0$$

or making use of Eq. (B.6)

$$\frac{H'}{E_{P_i}} = \left(\frac{k_0}{\Gamma_{0i}}\right)^2 \qquad (i = 1, 2, \ldots, 6) \qquad \text{(B.8)}$$

The above places constraints on the choice of bilinear fit used to approximate the various σ_i vs ϵ_i curves. Since Eq. (B.8) does not establish unique values of the yield stresses Γ_{0i}, and plastic moduli E_{P_i}, we assume

that one of the stress-strain curves is arbitrarily fitted with the best bilinear representation. For the sake of argument let this be the σ_k vs ϵ_k curve, where k can take one of the values 1 to 6. Therefore, the quantities E_k, Γ_{0_k} and E_{p_k} are assumed to be known. To uniquely define the remaining stress-strain curves it is only necessary to specify three pieces of information for each curve. We have here assumed that all the elastic moduli $E_i (i = 1, 2, \ldots, 6)$ and the location of the ultimate point $(\Gamma_{u_i}, \epsilon_{u_i})$ on the remaining individual σ_i vs ϵ_i curves are defined. With the above information we can establish the following expressions for the tangent moduli E_{T_i}

$$E_{T_i} = \frac{\Gamma_{u_i} - \Gamma_{0_i}}{\epsilon_{u_i} - \Gamma_{0i}/E_i} \qquad (i = 1, 2, \ldots, 6) \qquad (B.9)$$

Eqs. (B.8) and (B.9) combined with (B.5) can be solved for the unknowns Γ_{0i} and E_{T_i}. The result is:

$$\Gamma_{0i} = r_i \Gamma_{0k} \qquad (i \neq k)$$

$$(B.10)$$

$$E_{T_i} = s_i E_i$$

where

$$r_i = \frac{1}{2b_i} [-1 + \sqrt{1 + 4 b_i c_i}]$$

$$(B.11)$$

$$s_i = 1/\left[\frac{E_i}{r_i^2 E_{p_k}} + 1 \right] \qquad (i \neq k)$$

in which

$$b_i = \frac{E_{p_k}}{\Gamma_{0_k}} \left[\epsilon_{u_i} - \frac{\Gamma_{u_i}}{E_i} \right] \qquad (i \neq k)$$

(B.12)

$$c_i = \frac{\Gamma_{u_i}}{\Gamma_{0_k}} \qquad (i \neq k)$$

The constant A_{ij} model described above has been applied to several laminated FRM coupons and the results are documented in the internal report by Olson and Anderson (1988). This model will not be pursued further in this thesis.

APPENDIX C

DERIVATION OF THE EFFECTIVE PLASTIC STRAIN INCREMENT $d\bar{\epsilon}^P$.

Here we drive an expression for the effective plastic strain increment $d\bar{\epsilon}^P$ as a function of plastic strain increments $d\epsilon_i^P$.

For a body deforming plastically, the increment of plastic work per unit volume is

$$dW^P = \sigma_i \, d\epsilon_i^P \qquad (i = 1, 2, \ldots, 6) \qquad (C.1)$$

Using the associated flow rule, Eq. (3.16), in conjunction with Eqs. (3.17) and (3.18) yields

$$d\epsilon_i^P = d\lambda \cdot 2A_{ij} \, \sigma_j \qquad (C.2)$$

Substituting $d\epsilon_i^P$ from Eq. (C.2) into Eq. (C.1)

$$dW^P = 2d\lambda \, \bar{\sigma}^2 = 2 \, d\lambda \, k^2 \qquad (C.3)$$

Defining the increment of effective plastic strain $d\bar{\epsilon}^P$ as

$$dW^P = k \, d\bar{\epsilon}^P \qquad (C.4)$$

the quantity $d\lambda$ is found from Eqs. (C.3) and (C.4) to be

$$d\lambda = \frac{1}{2} \frac{d\bar{\epsilon}^P}{k} \qquad (C.5)$$

Assuming that $|A_{ij}| \neq 0$, then the matrix of anisotropic parameters [A] has an inverse [A*]; and Eq. (C.2) can be inverted to give

$$\sigma_j = A_{ij}^* \, d\epsilon_i^{\,p} \, \frac{1}{2d\lambda} = A_{ij}^* \, d\epsilon_i^{\,p} \, \frac{k}{d\bar{\epsilon}^p} \tag{C.6}$$

where the last step follows from Eq. (C.5).

Using the above stress-plastic strain increment relation we can rewrite $\bar{\sigma}^2$ as

$$\bar{\sigma}^2 = A_{ij} \, \sigma_i \, \sigma_j = \left(\frac{k}{d\bar{\epsilon}^p}\right)^2 A_{ij} \, (A_{ki}^* \, d\epsilon_k^p) \, (A_{\ell j}^* \, d\epsilon_\ell^p) \tag{C.7}$$

$$= k^2$$

which after some tensor manipulation results in

$$(d\bar{\epsilon}^p)^2 = A_{ij}^* \, d\epsilon_i^p \, d\epsilon_j^p \tag{C.8}$$

In the plane stress case, the expression for $d\bar{\epsilon}^p$ can be written explicitly as

$$(d\bar{\epsilon}^p)^2 = \frac{1}{(A_{11}A_{22}-A_{12}{}^2)} \, [A_{22} \, (d\epsilon_1^p)^2 + A_{11} \, (d\epsilon_2^p)^2 \tag{C.9}$$

$$- 2A_{12} \, d\epsilon_1^p \, d\epsilon_2^p] + \frac{1}{A_{66}} \, (d\epsilon_6^p)^2$$

It can be shown in the three dimensional case that the assumption of zero plastic volumetric strain (i.e. $d\epsilon_1^p + d\epsilon_2^p + d\epsilon_3^p = 0$) implies a singular [A] matrix (cf. Shih and Lee, 1978). Under these circumstances the above procedure for obtaining $d\bar{\epsilon}^p$ fails, and resort must be made to a different technique (cf. Hu, 1956).
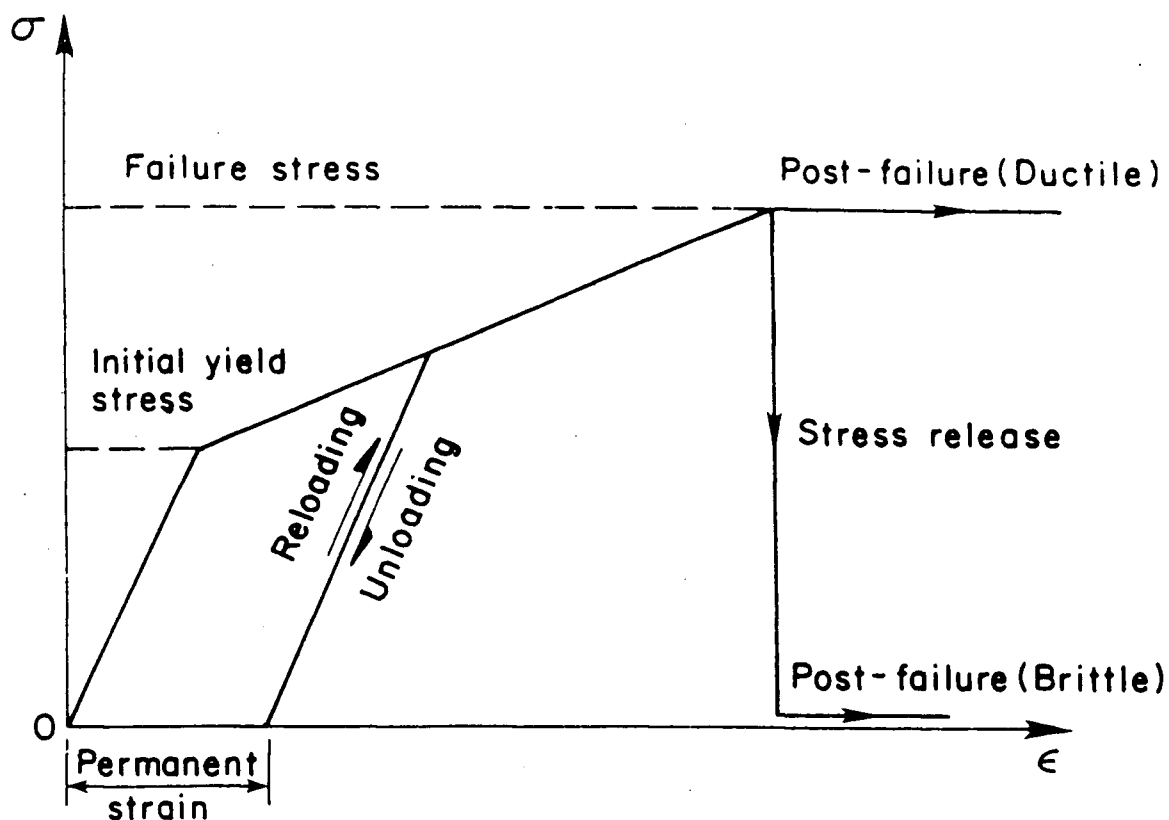
Fig. 3.1 — Idealized stress — strain curve showing different stages
of the proposed elastic—plastic—failure model
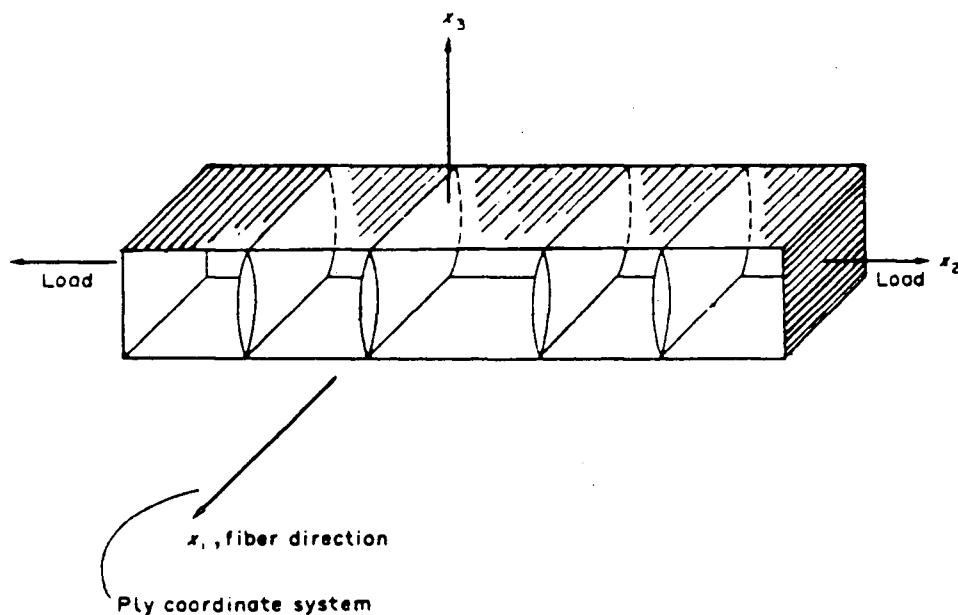
Fig. 3.2 — Transverse matrix cracking in a single layer of U/D FRM
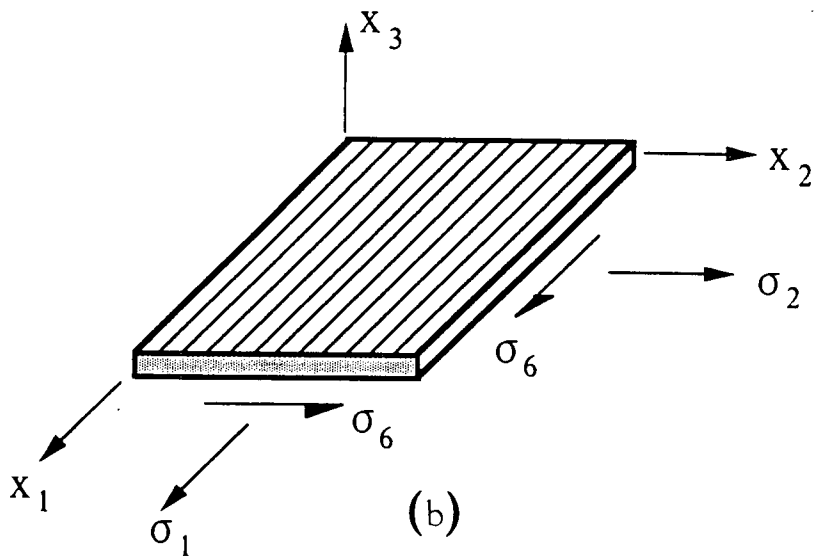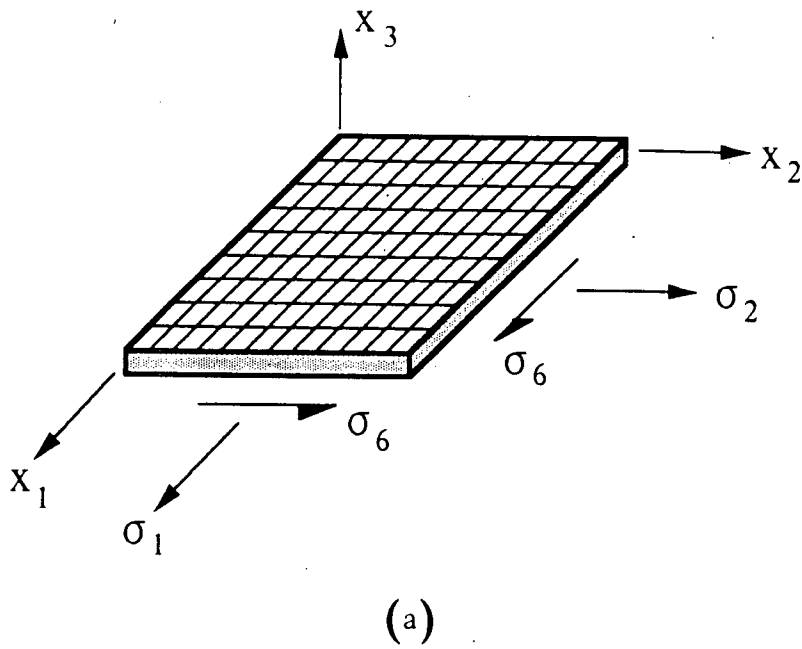
Fig. 3.3 – Nomenclature for single layers of FRM :

a — Bidirectional
b — Unidirectional
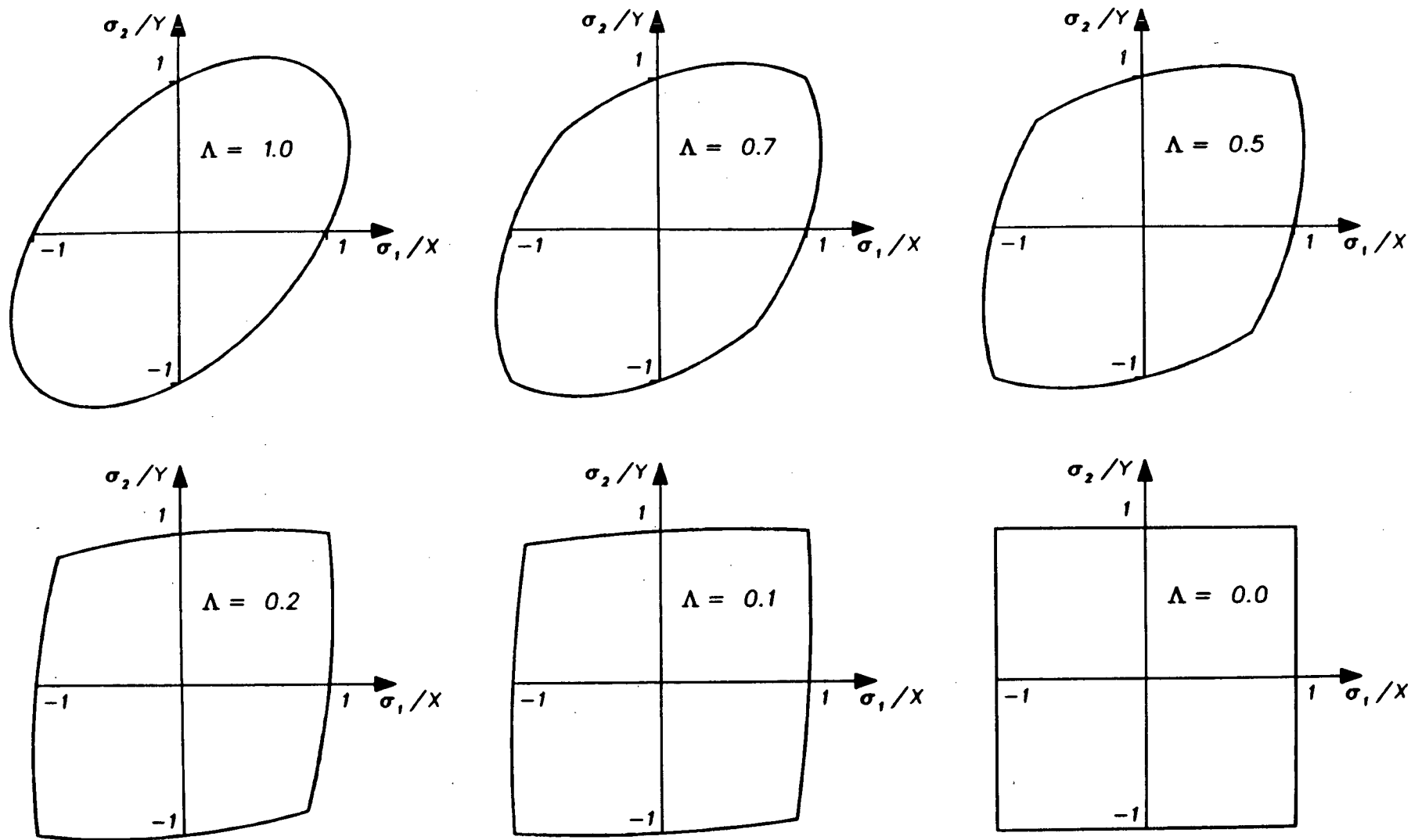
Fig 3.4 — Puppo — Evensen yield surfaces in the $\sigma_6 = 0$ plane for bi-directional layers with $X = Y$ and various values of the parameter Λ
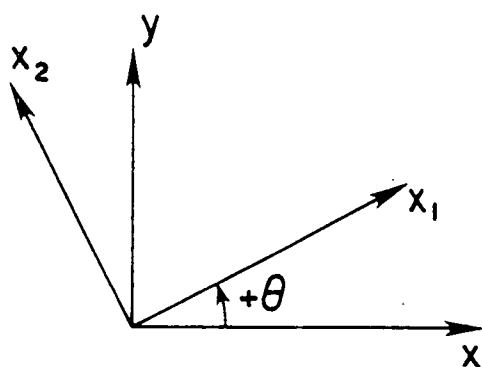
Fig. 3.5 — Orientation of layer coordinate axes with respect to laminate coordinates
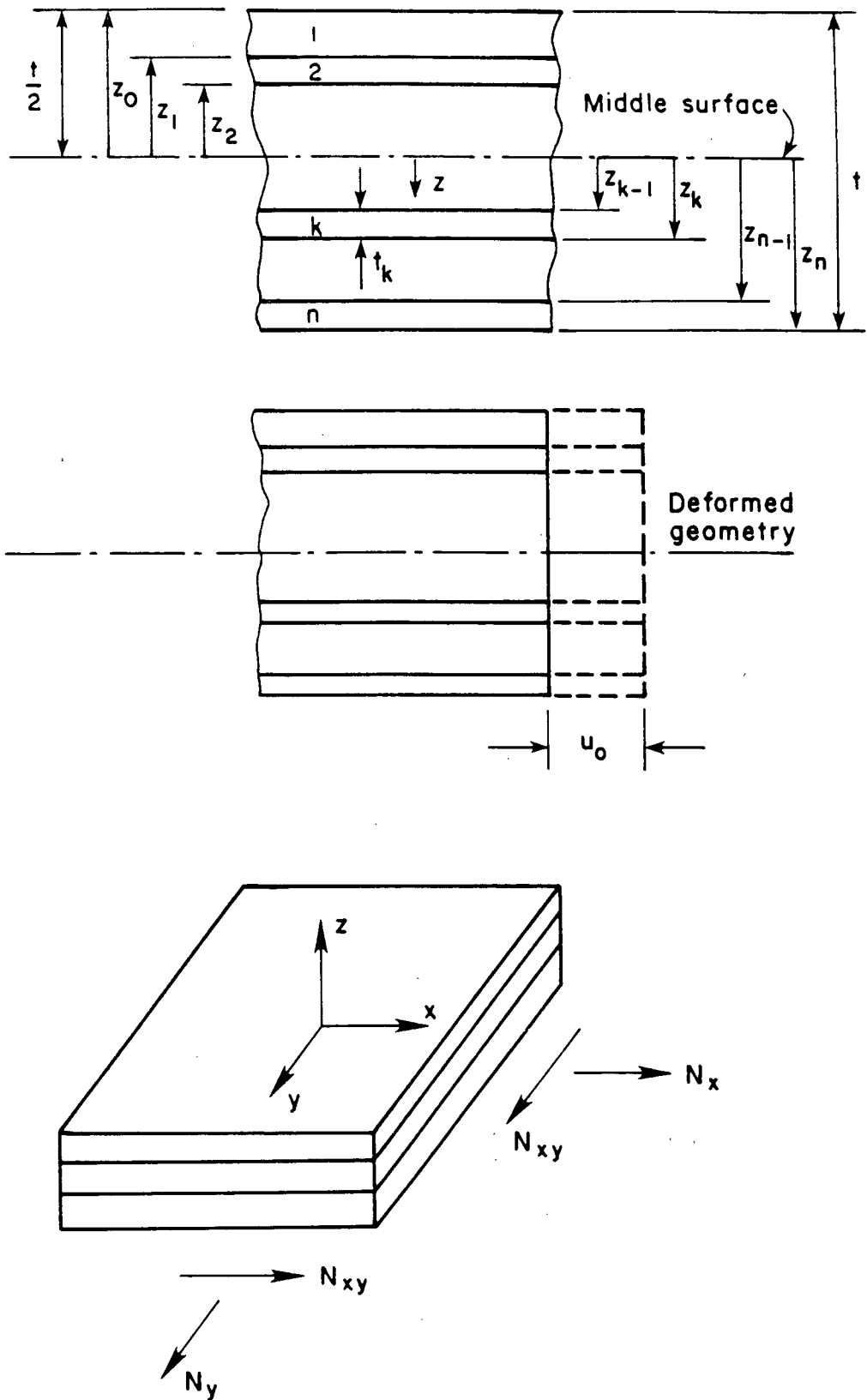
Fig. 3.6 — Illustration of an n-layered laminate along with a typical in-plane deformed geometry
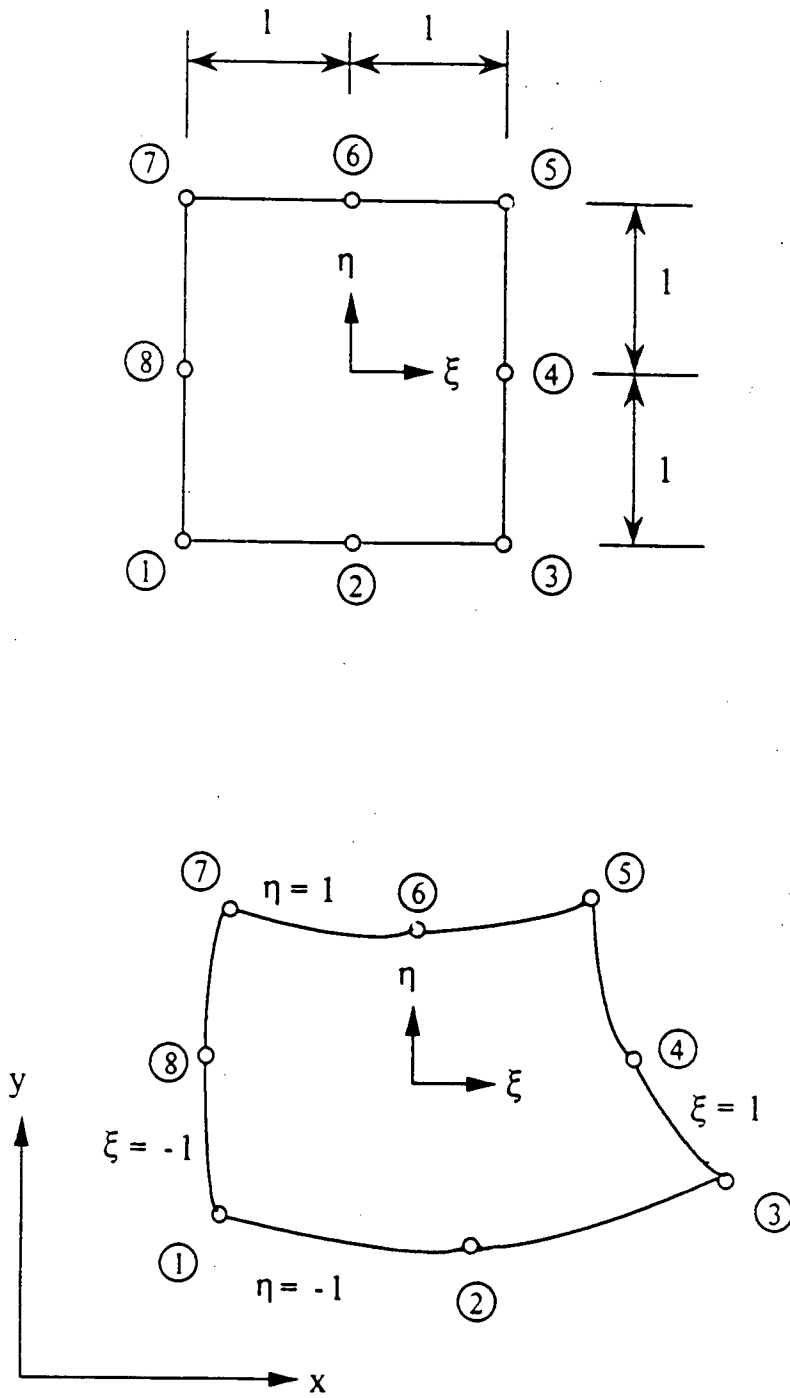
Fig. 4.1 — Quadratic isoparametric element
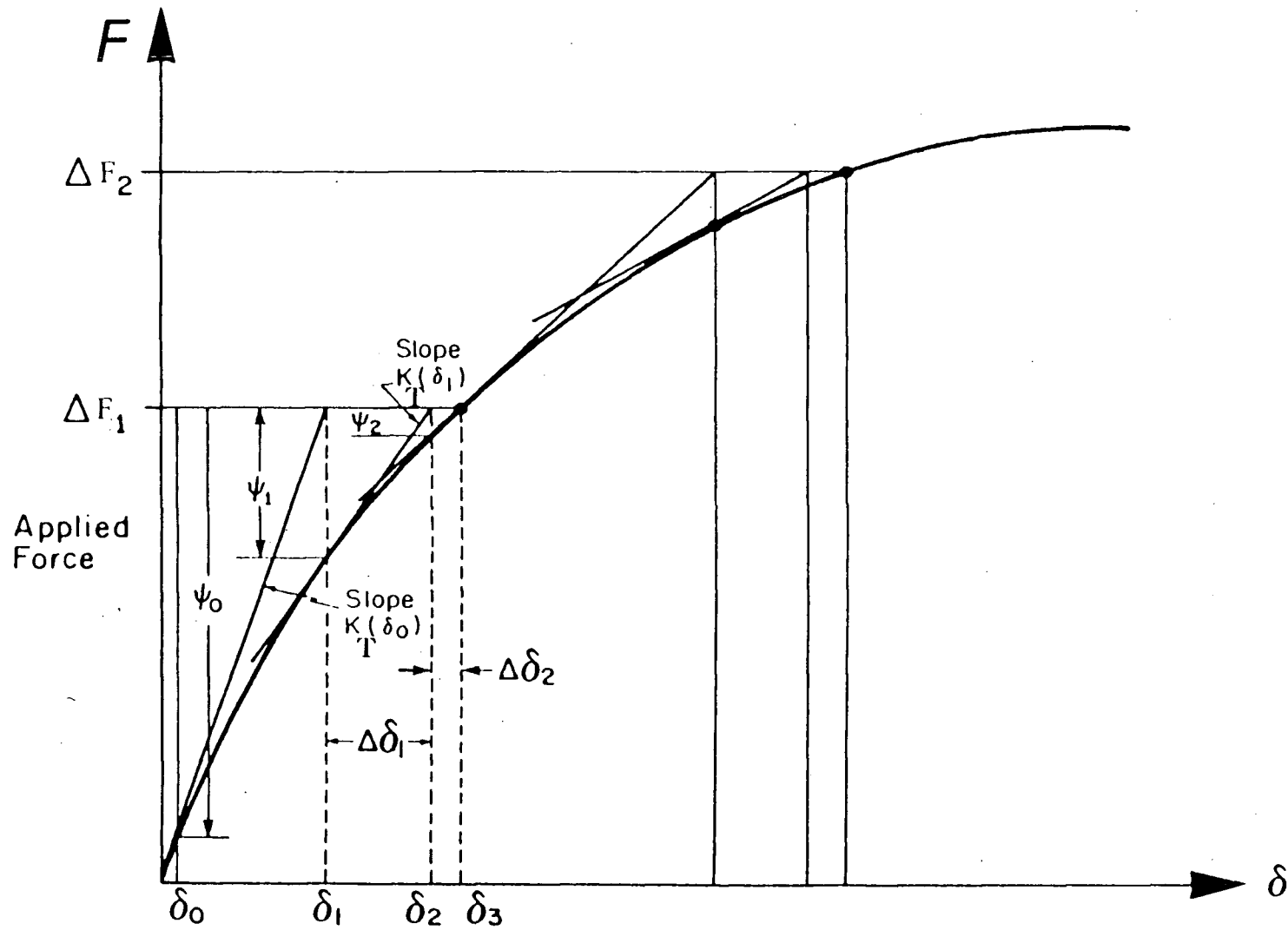
Fig. 4.2 – Tangent stiffness method for a single variable problem
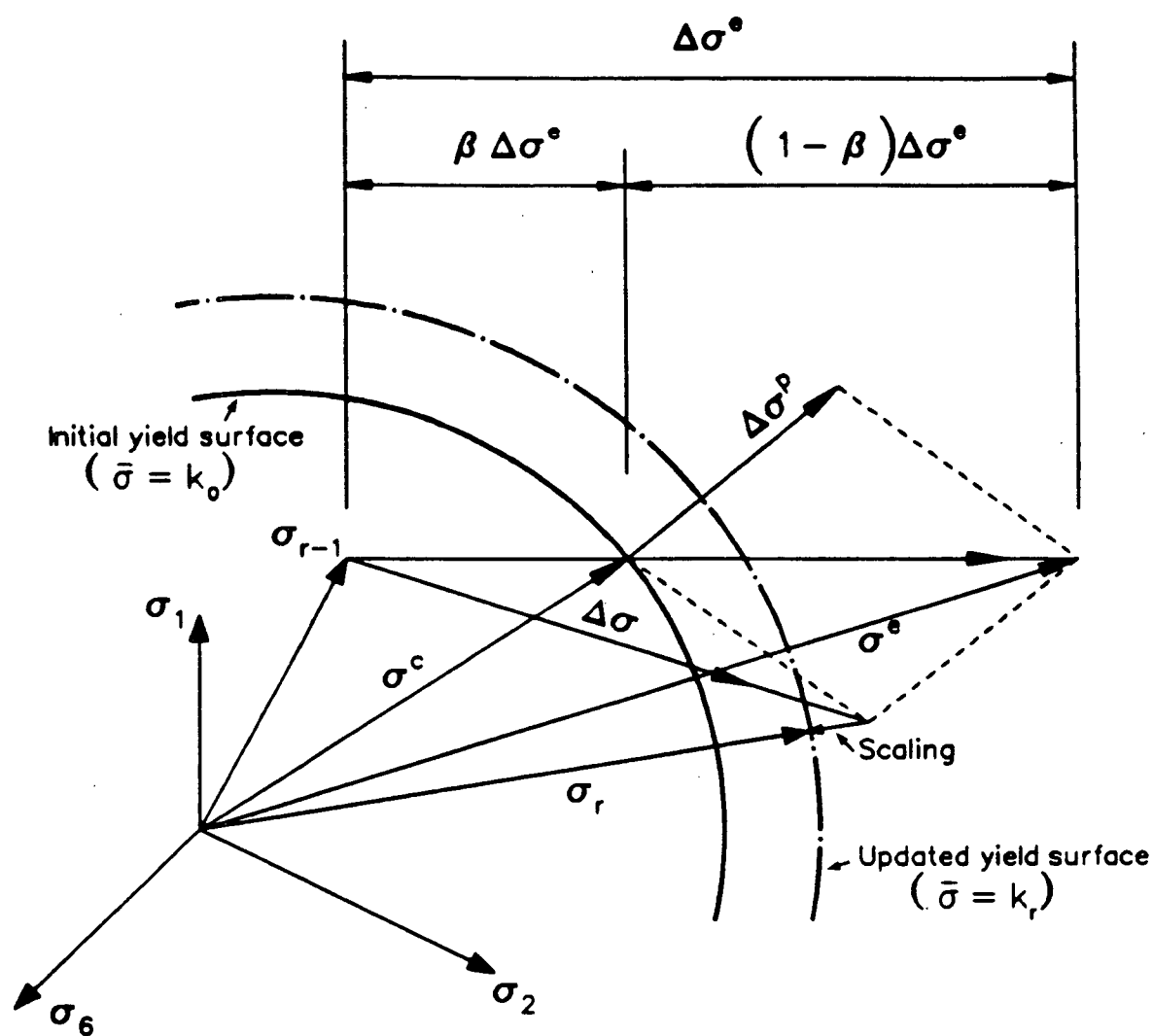
Fig 4.3 — Incremental elastoplastic stress computation for an initially elastic point
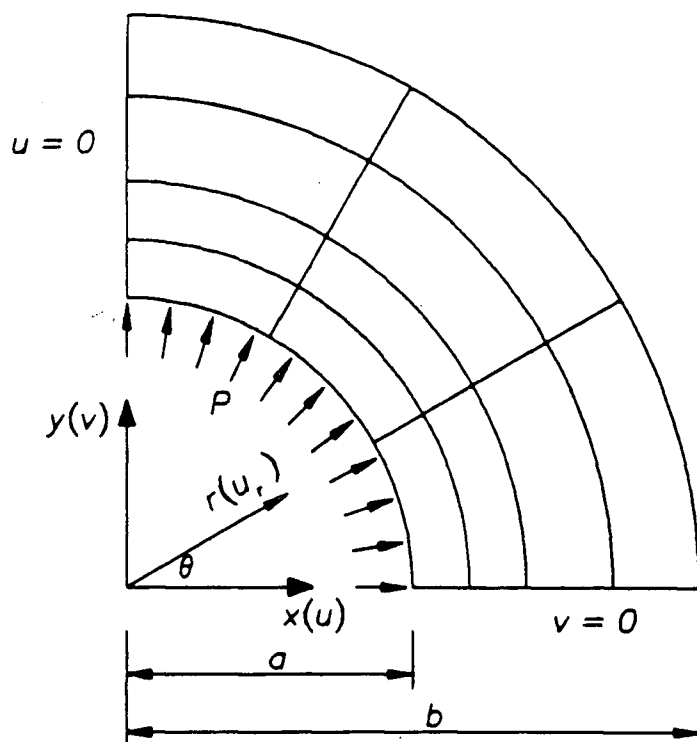
Fig. 5.1 — Finite element mesh for the analysis of an isotropic cylinder
under elastoplastic internal pressure
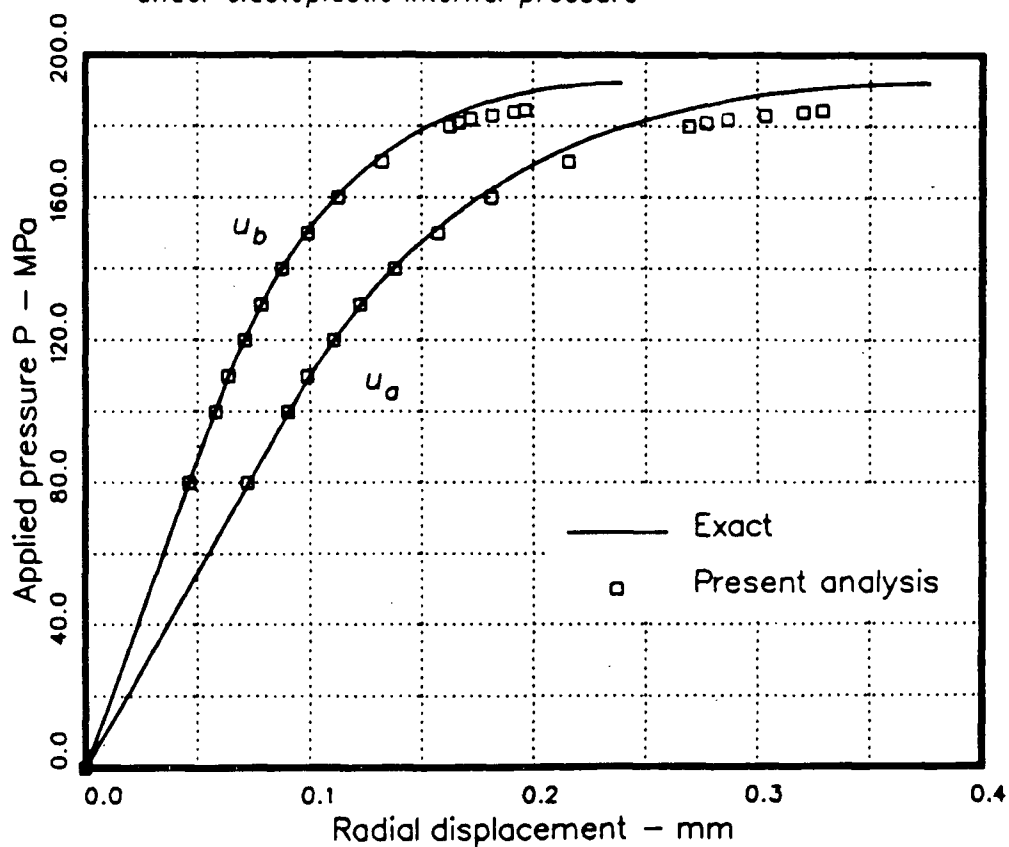
Fig. 5.2 — Pressure P versus inner and outer wall displacements u_a and u_b
for the problem of Fig. 5.1

P = 80.0 MPa

P = 120.0 MPa

P = 140.0 MPa

P = 180.0 MPa
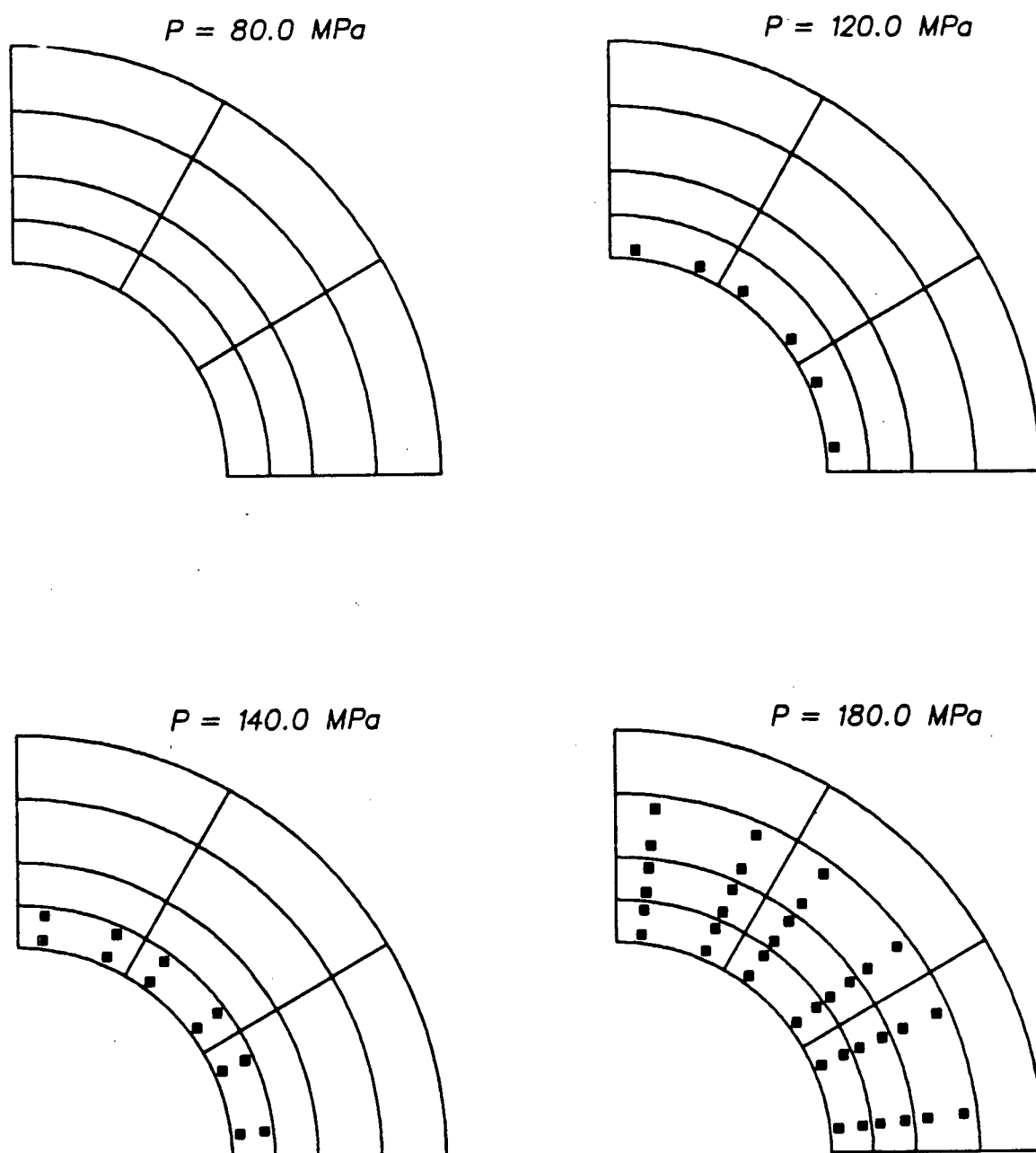
Fig. 5.3 – Progression of yielding for the problem of Fig. 5.1
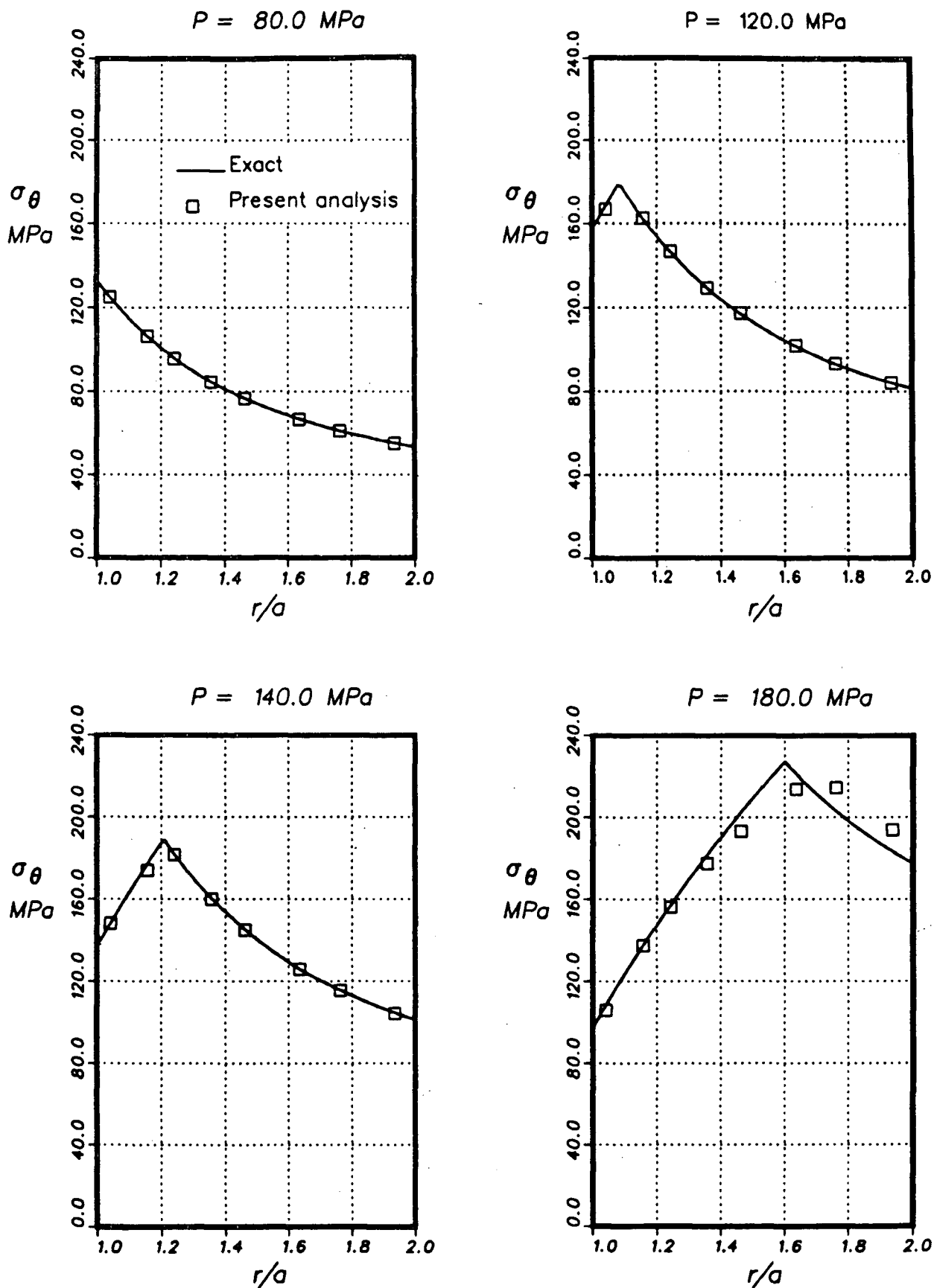
Fig. 5.4 – Radial distribution of hoop stress at various pressures for the problem of Fig. 5.1
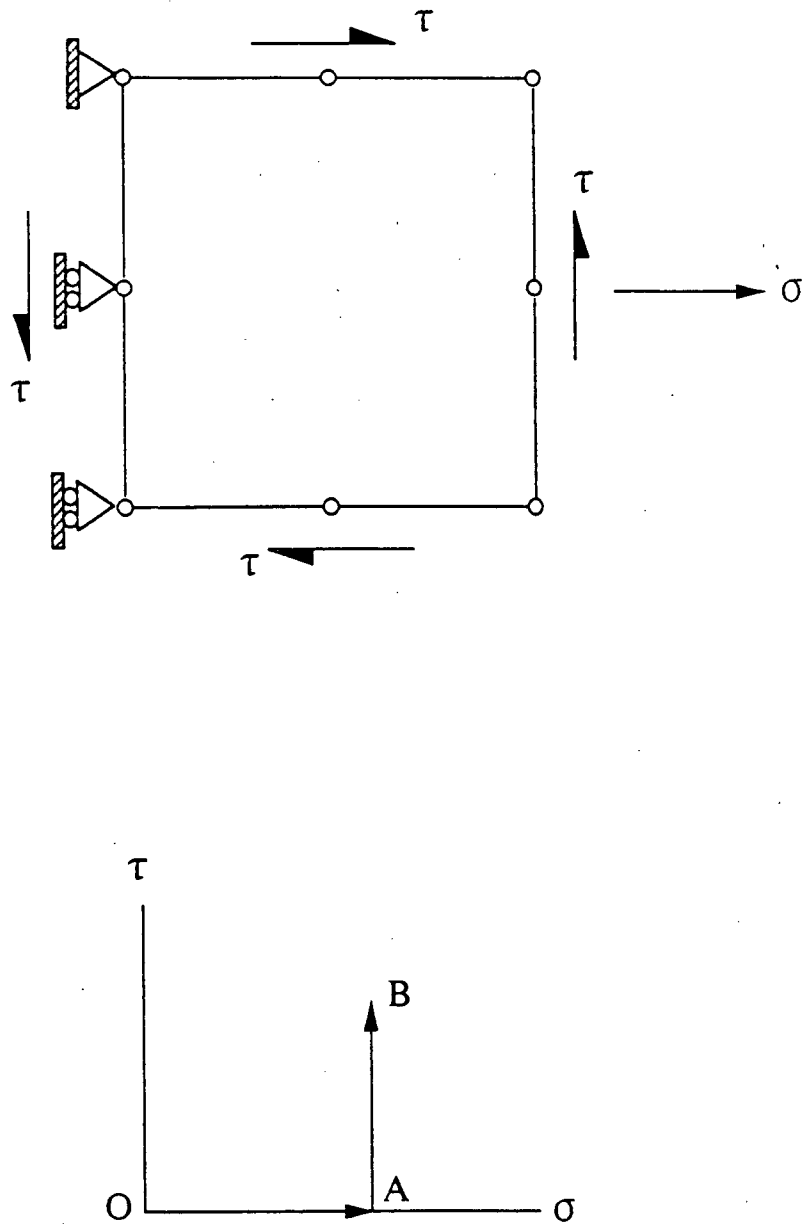
Fig. 5.5 — Numerical model and the stress path for the analysis of an isotropic thin — walled tube subjected to combined tension and torsion
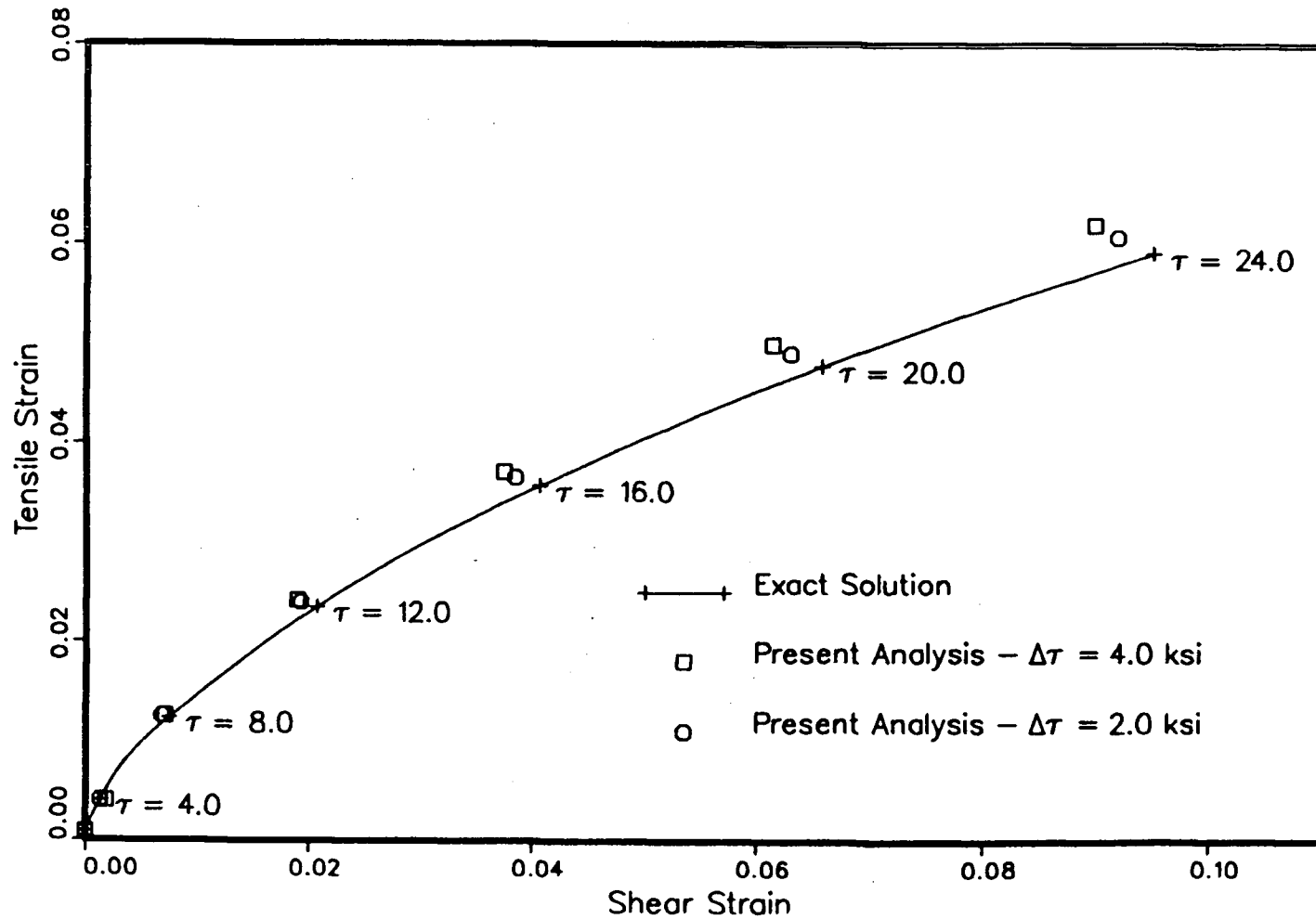
Fig. 5.6 — *Strain path for an isotropic thin tube subjected to combined tension and torsion*
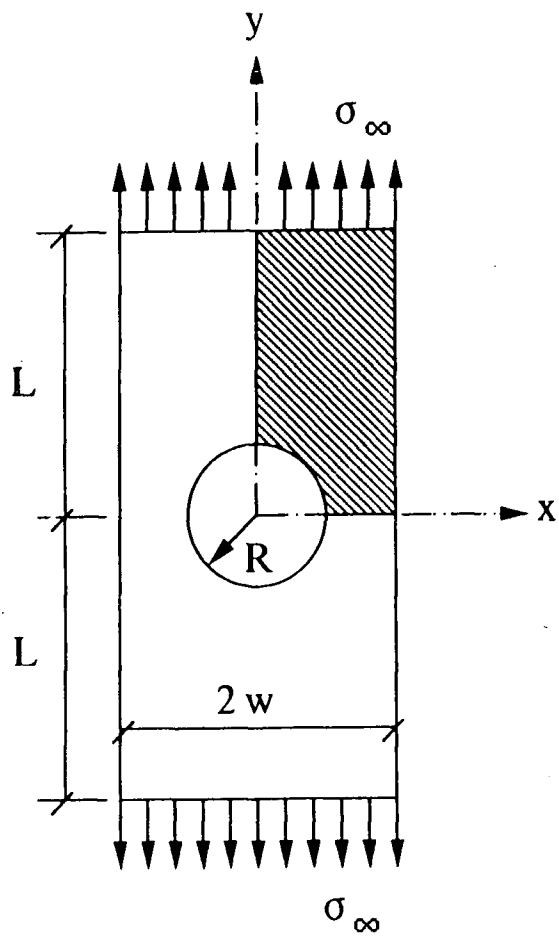
Fig. 5.7 — Nomenclature for the perforated
plate problem

σ_∞

$L = 20$ mm

No. of elements = 48

No. of nodes = 177

$u = 0$

y,v

$R = 5$ mm

x,u

$v = 0$

$w = 10$ mm
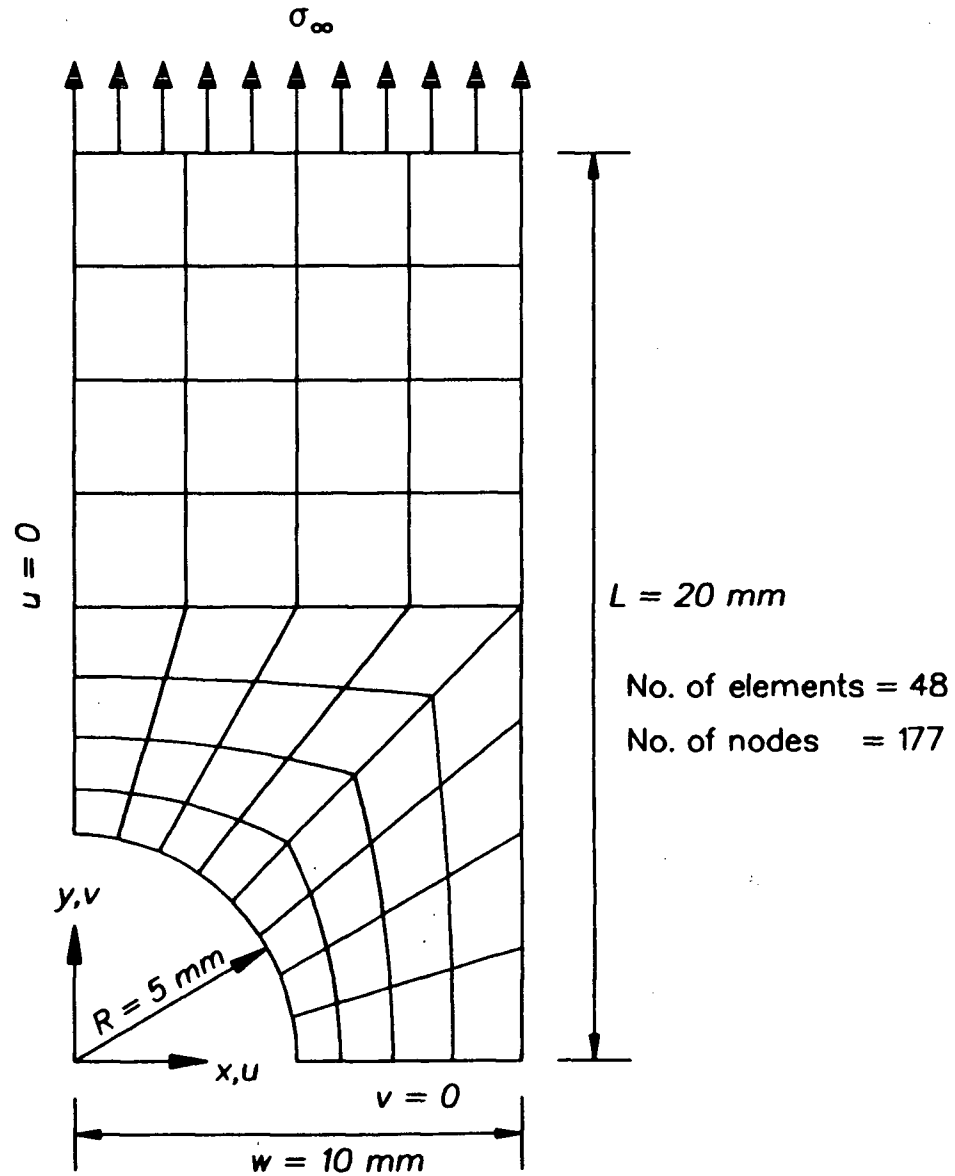
Fig. 5.8 — Finite element mesh used to analyze a quadrant of Fig. 5.7
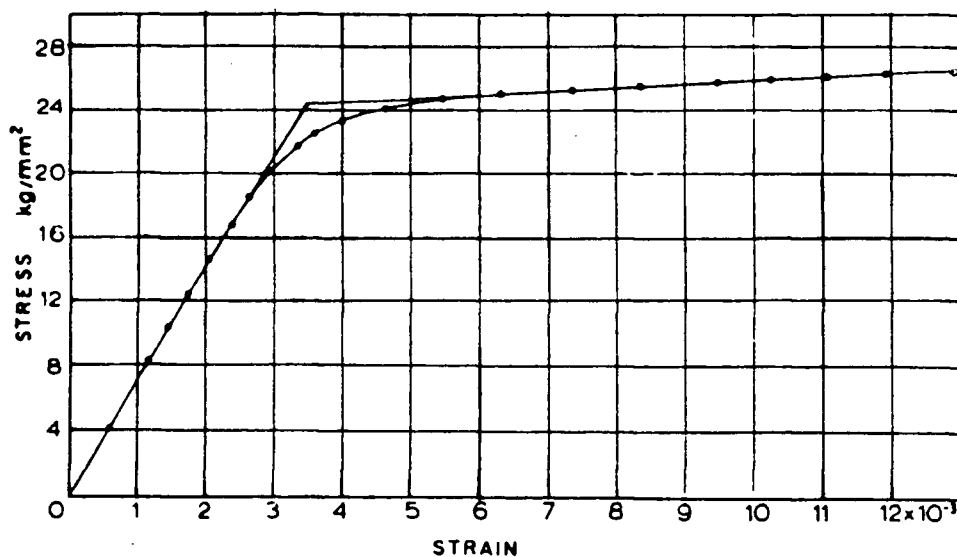
Fig. 5.9 — The stress — strain curve in pure tension for Aluminum alloy 57S
[Theocaris and Marketos , 1964]
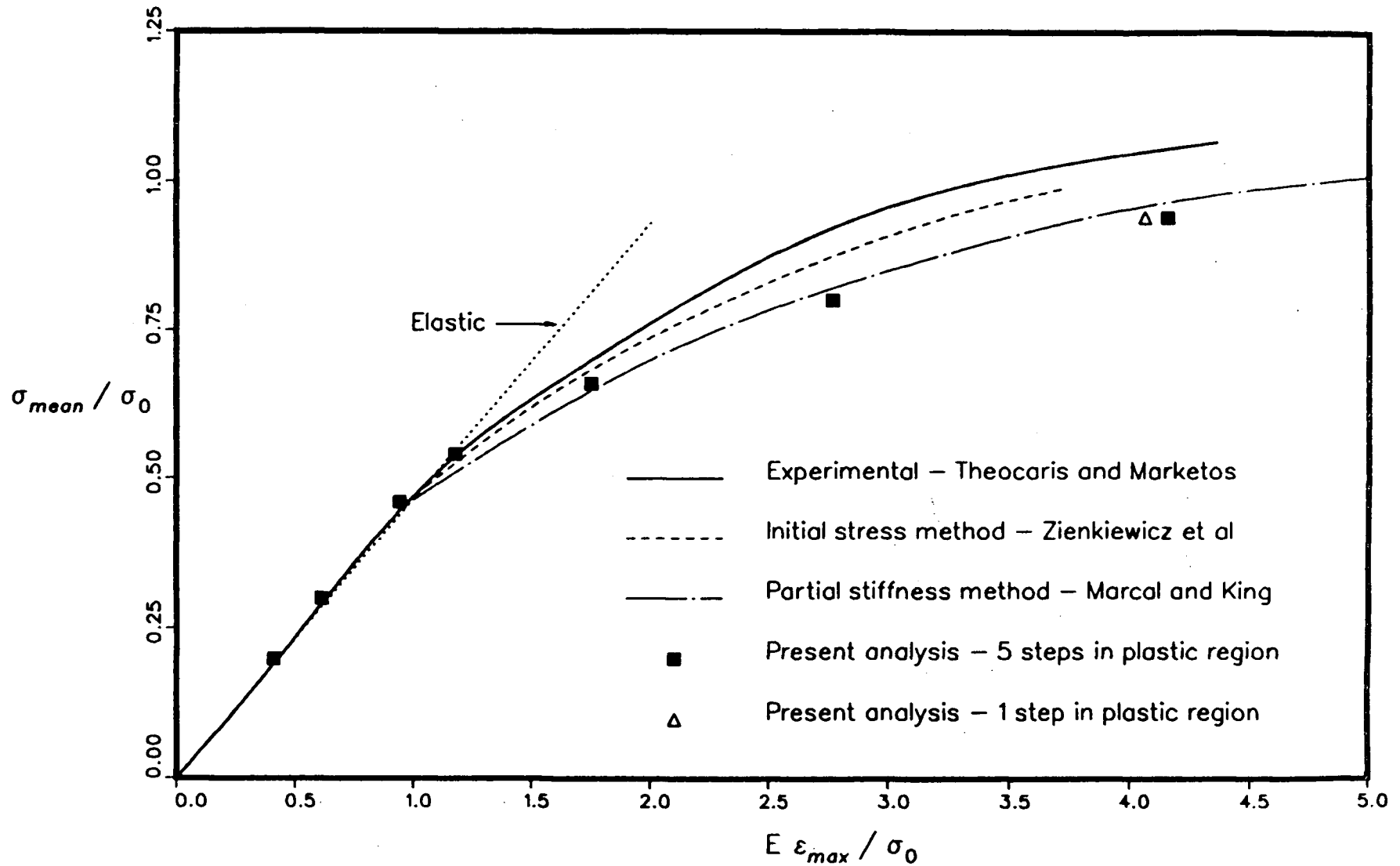
Fig. 5.10 – Nondimensional graph of mean stress against maximum strain for the isotropic perforated plate shown in Fig. 5.8
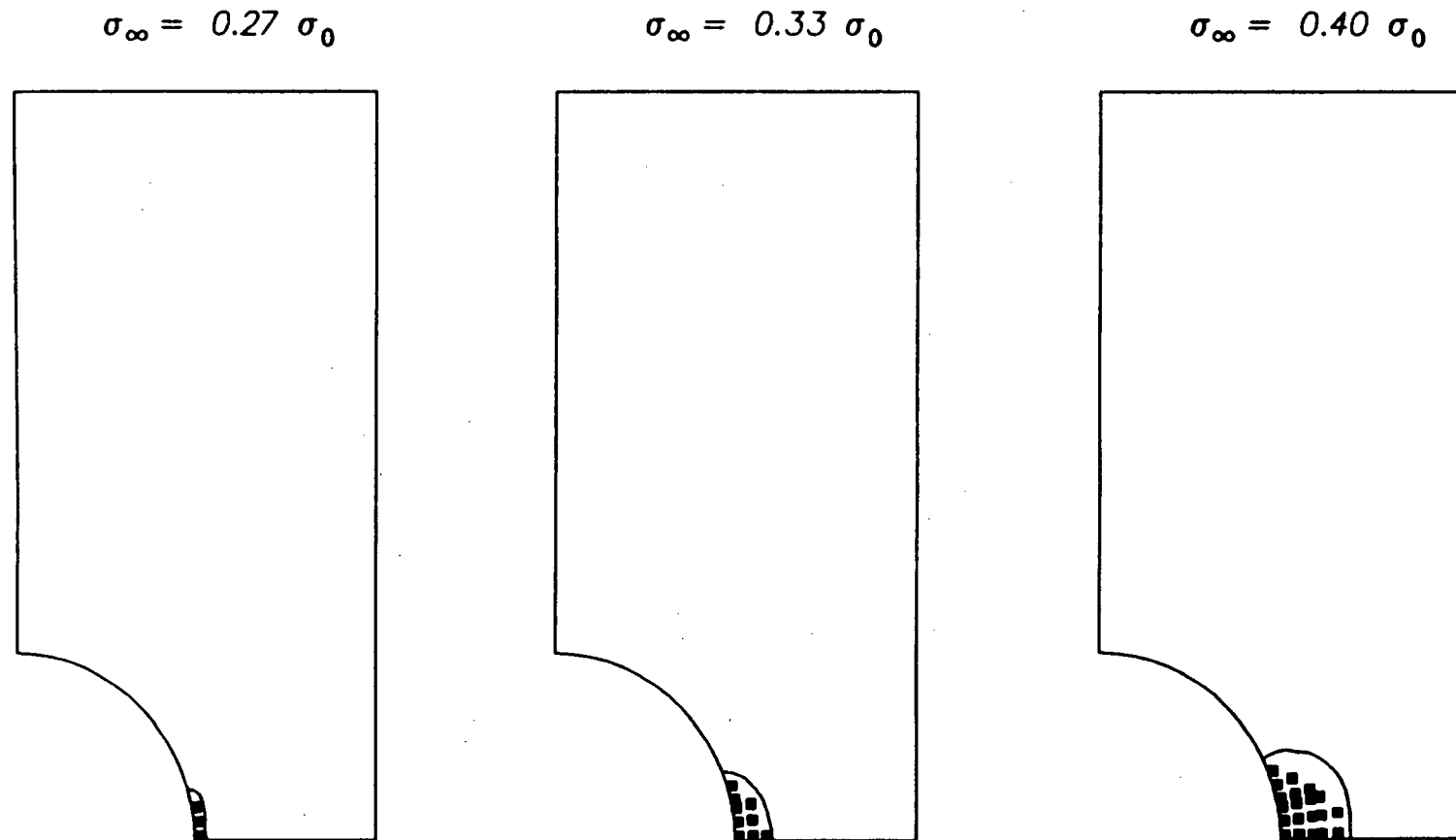
$$\sigma_\infty = 0.27 \ \sigma_0 \qquad\qquad \sigma_\infty = 0.33 \ \sigma_0 \qquad\qquad \sigma_\infty = 0.40 \ \sigma_0$$

Fig. 5.11 — Comparison of the computed and experimentally determined plastic zone growth for the isotropic perforated plate subjected to elastoplastic loading
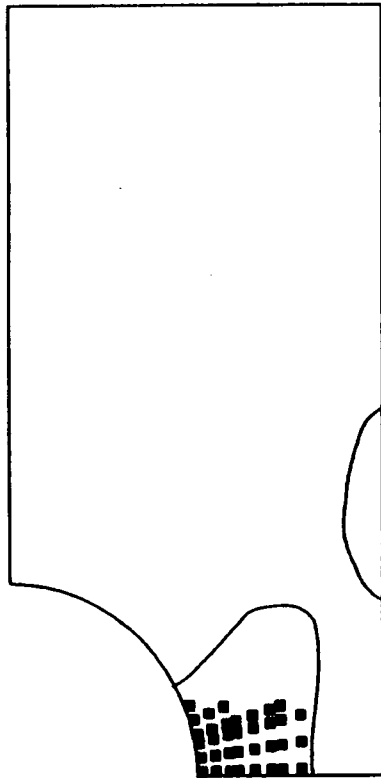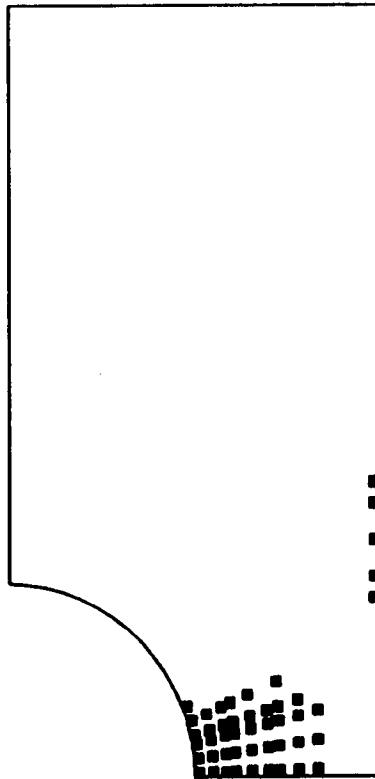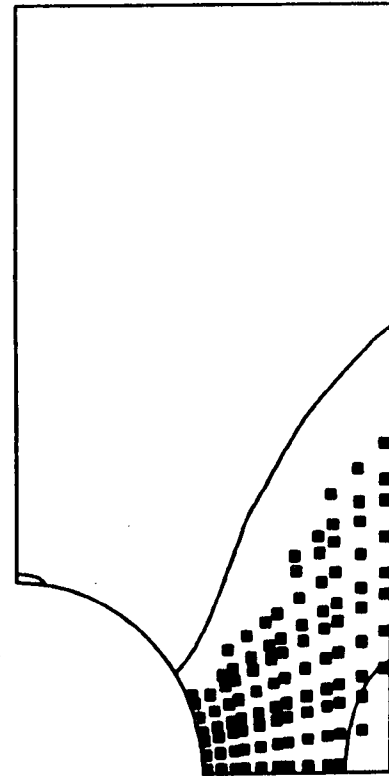
$$\sigma_\infty = 0.47 \ \sigma_0 \qquad\qquad \sigma_\infty = 0.49 \ \sigma_0 \qquad\qquad \sigma_\infty = 0.534 \ \sigma_0$$

Fig. 5.11 – continued
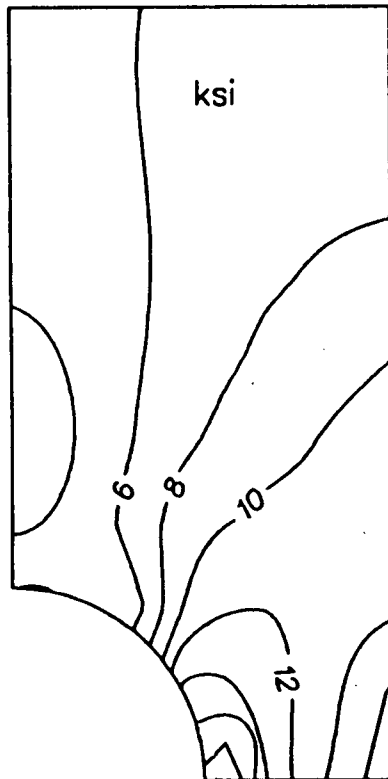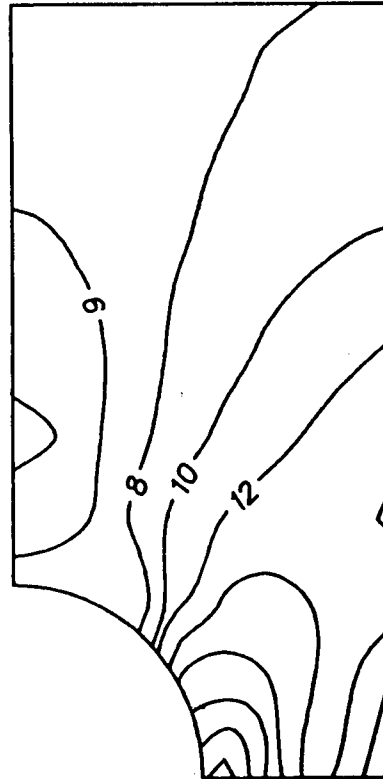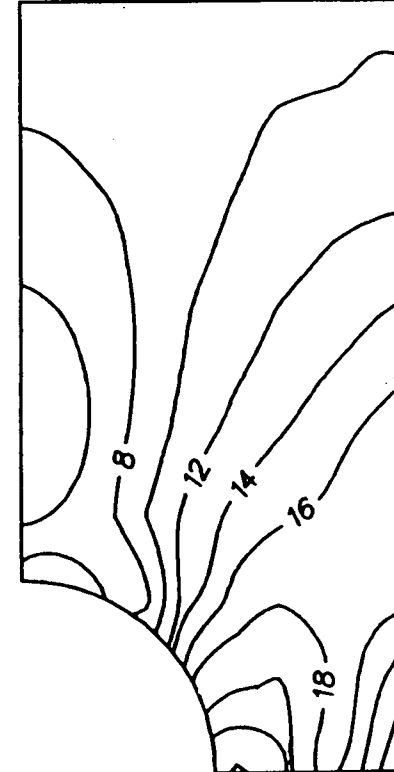
*Fig. 5.12 — Effective stress contours at various load levels for the isotropic
perforated plate subjected to elastoplastic loading*
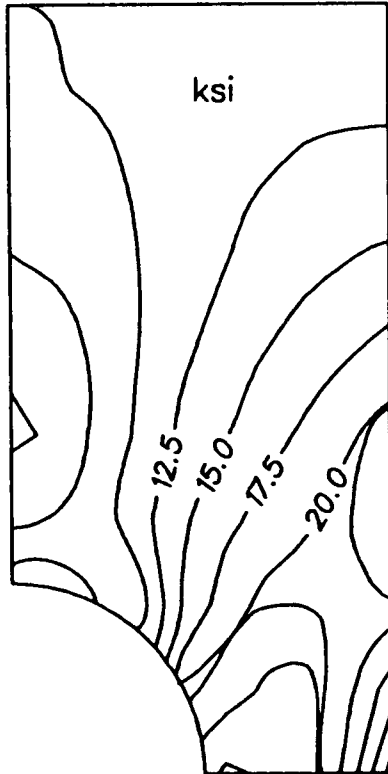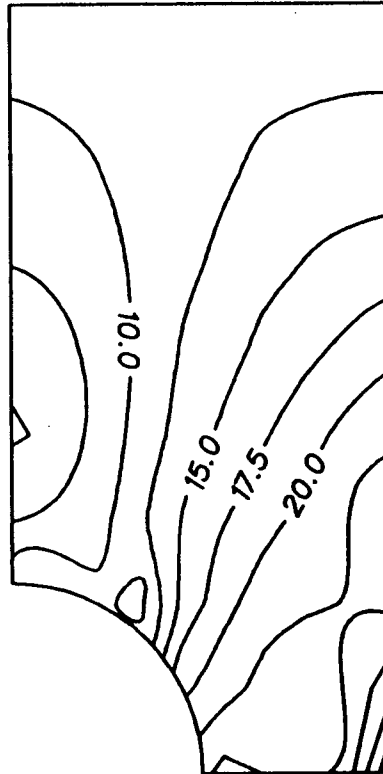
$\sigma_\infty = 0.47 \ \sigma_0$ $\sigma_\infty = 0.49 \ \sigma_0$ $\sigma_\infty = 0.534 \ \sigma_0$
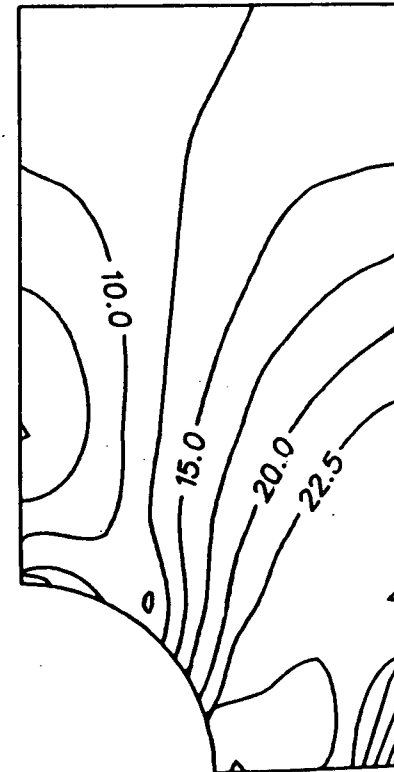
Fig. 5.12 – continued
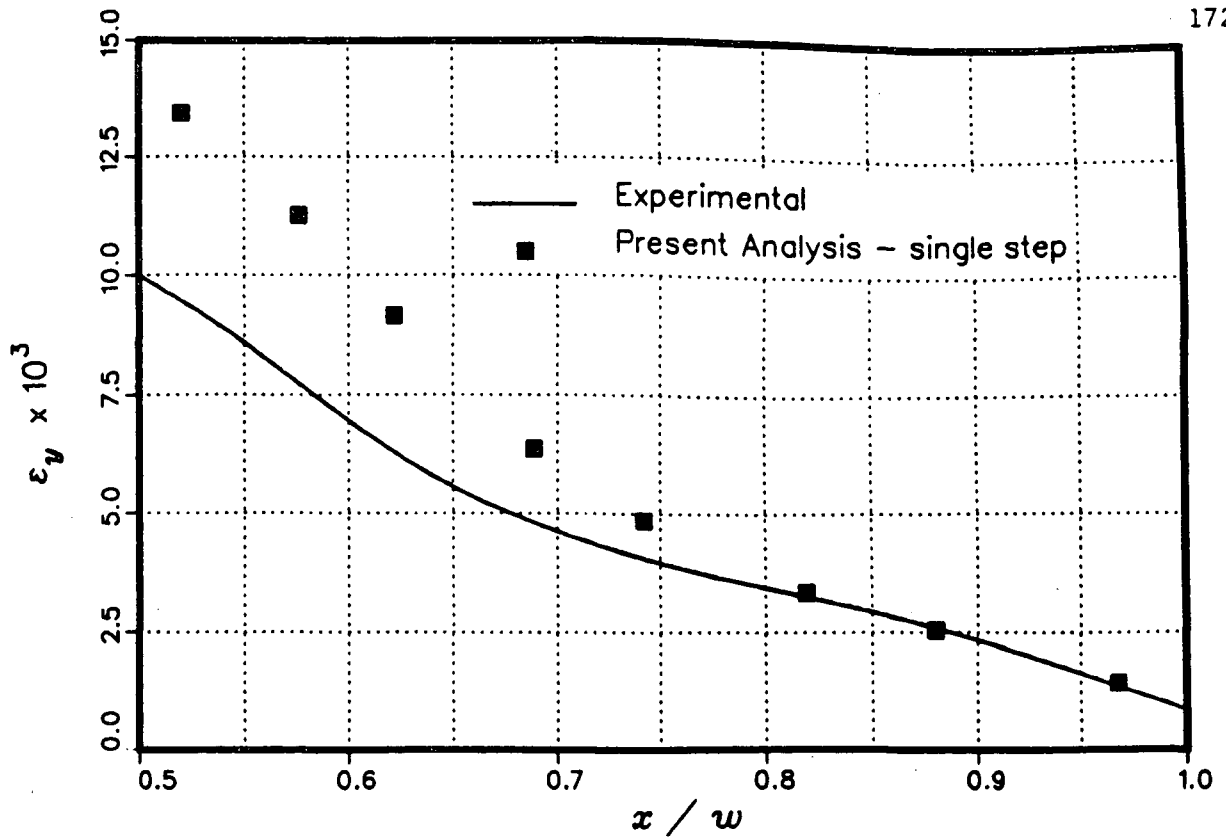
Fig. 5.13 a – Strain profile at the net section for the isotropic perforated plate subjected to $\sigma_\infty = 0.47 \, \sigma_0$
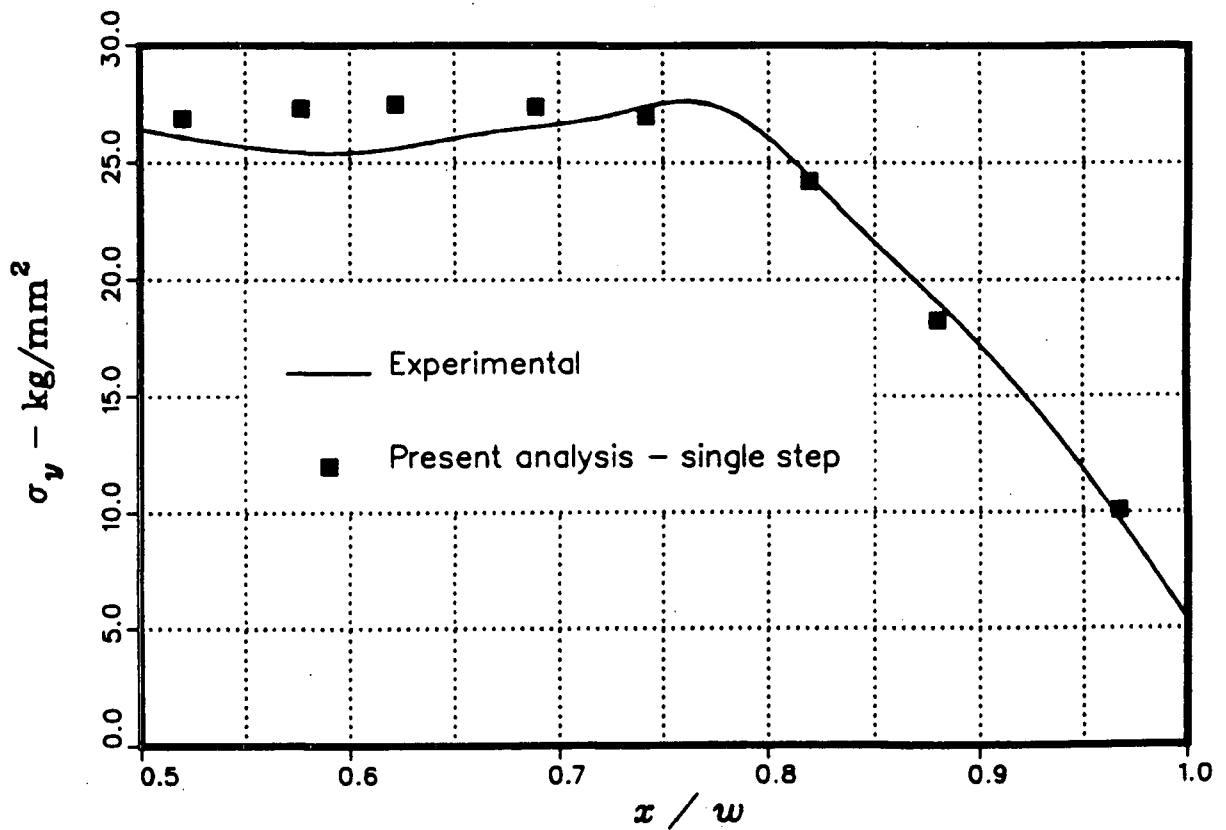
Fig. 5.13 b – Stress profile at the net section for the isotropic perforated plate subjected to $\sigma_\infty = 0.47 \, \sigma_0$
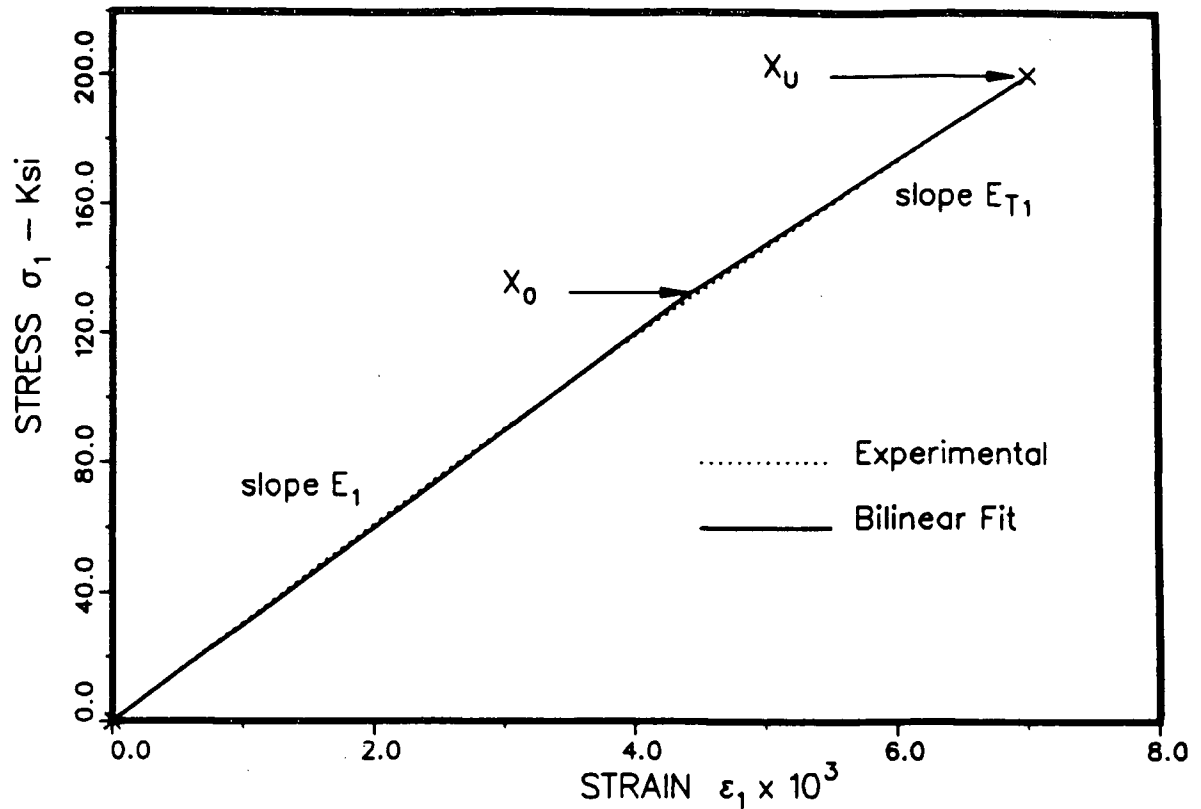
Fig. 5.14 — Longitudinal tensile stress — strain curve for a single layer of U/D Boron/Epoxy
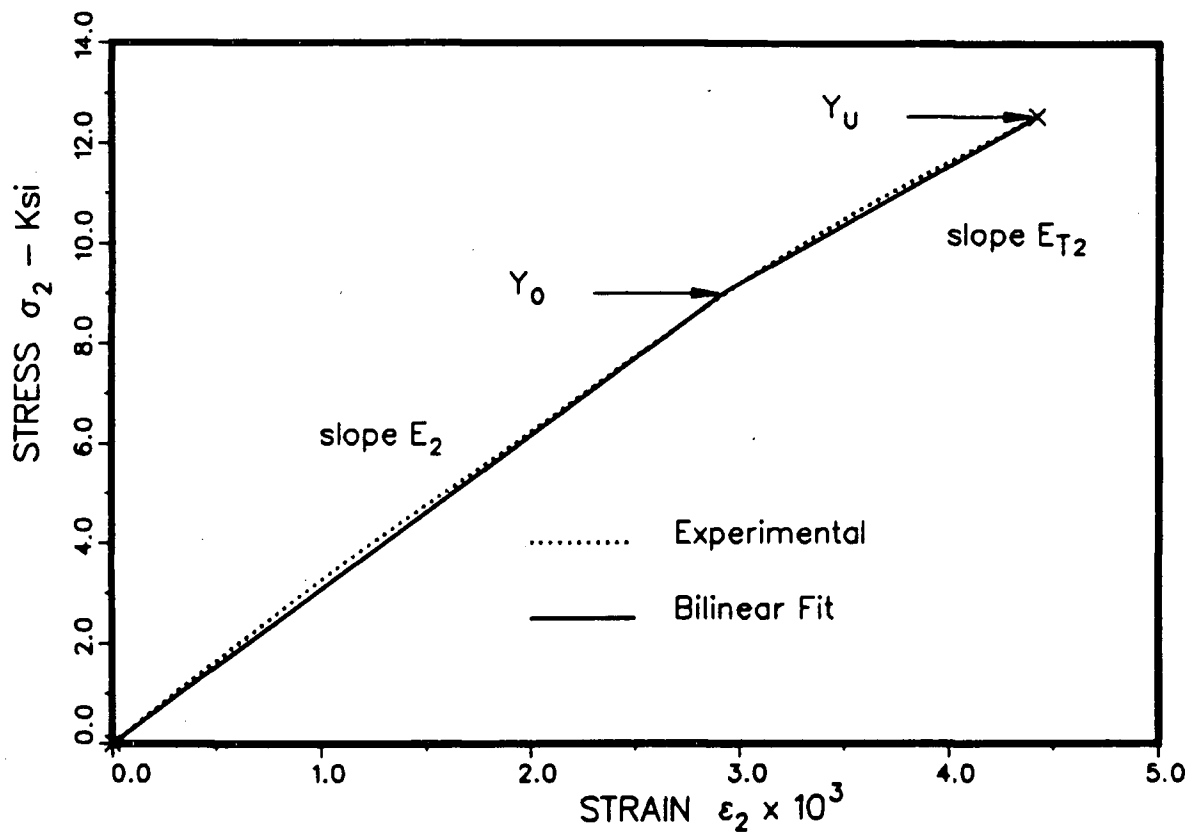
Fig. 5.15 — Transverse tensile stress — strain curve for a single layer of U/D Boron/Epoxy
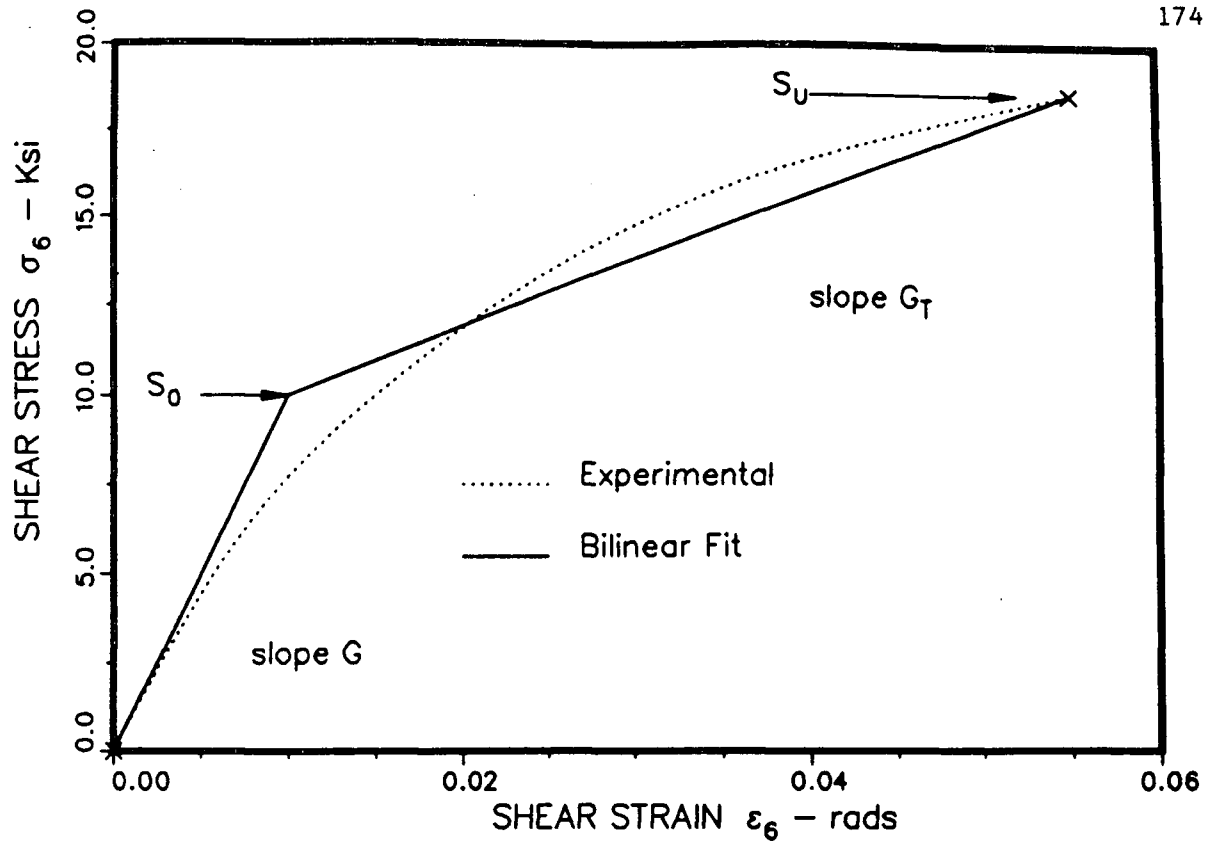
Fig. 5.16 — Shear stress — strain curve for a single layer of U/D Boron/Epoxy
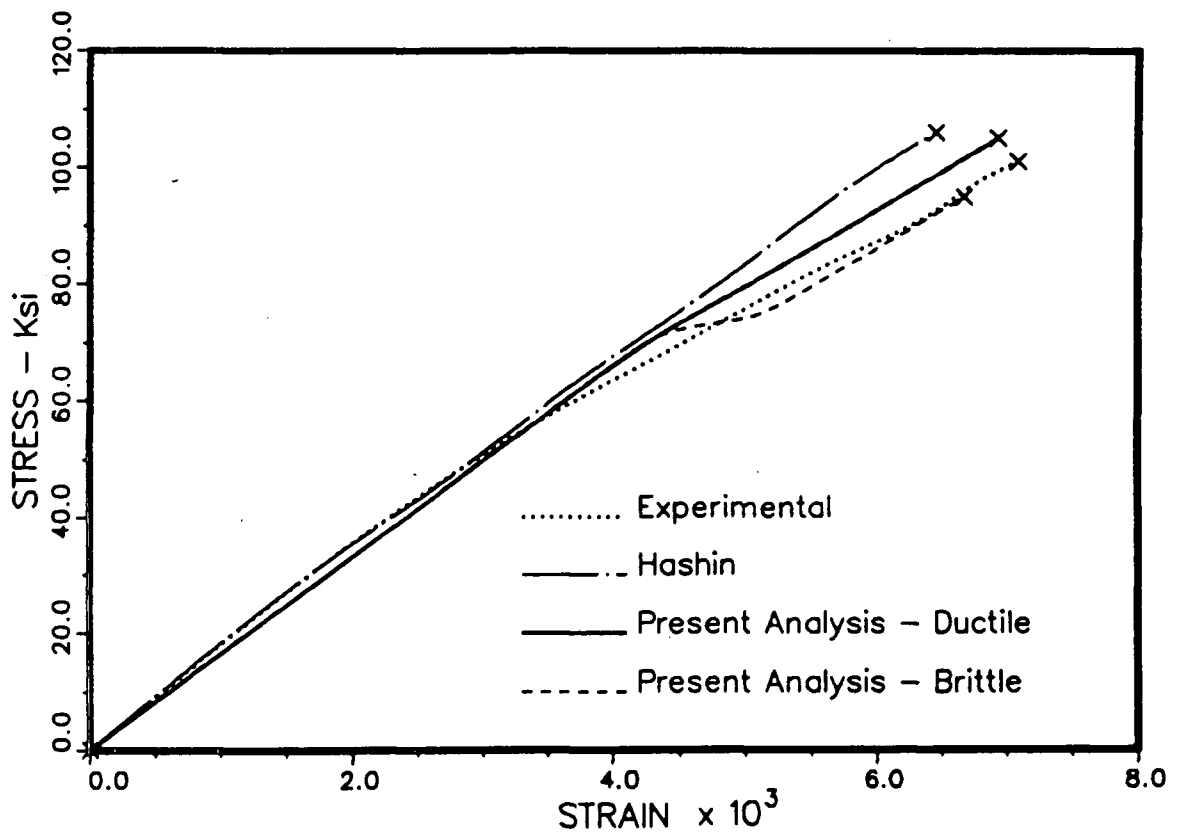
Fig. 5.17 — Tensile stress — strain curve for [0/90] Boron/Epoxy laminate
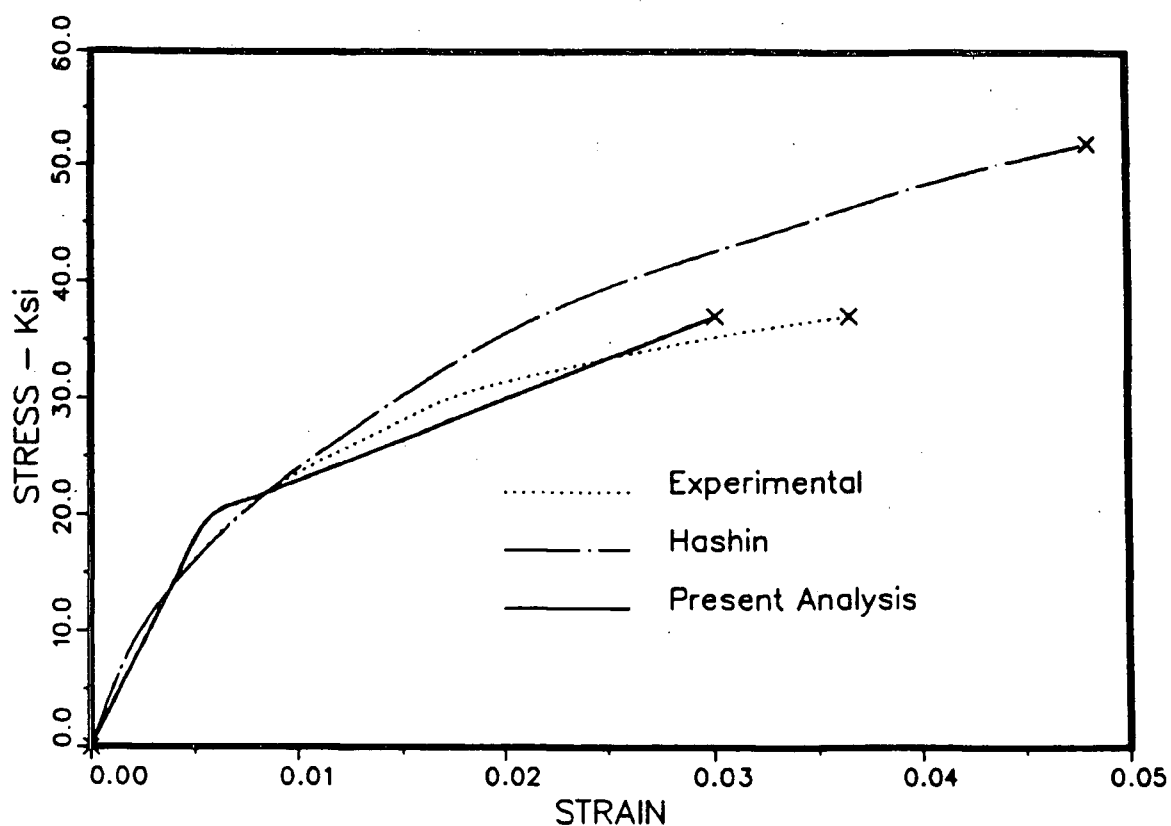
Fig 5.18 — Tensile stress — strain curve for [+45/−45] Boron/Epoxy laminate
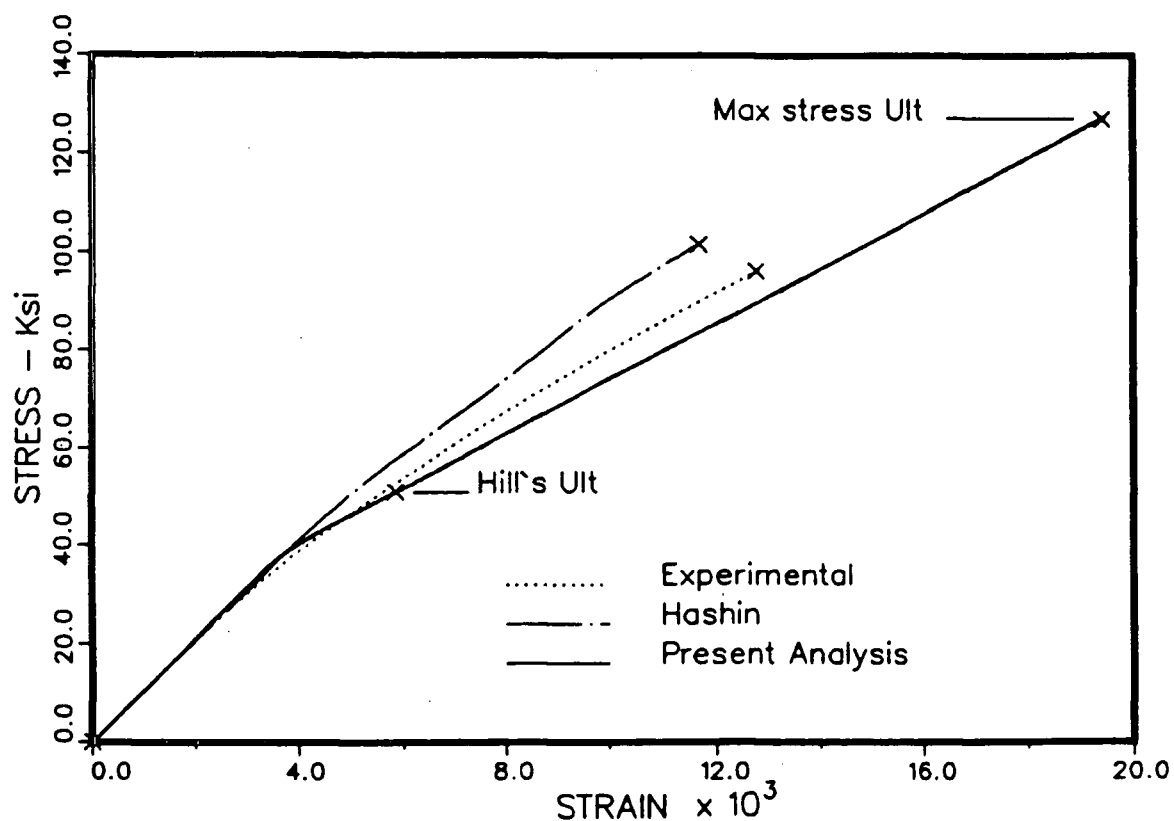
Fig. 5.19 a — Tensile stress — strain curve for [+30/−30] Boron/Epoxy laminate
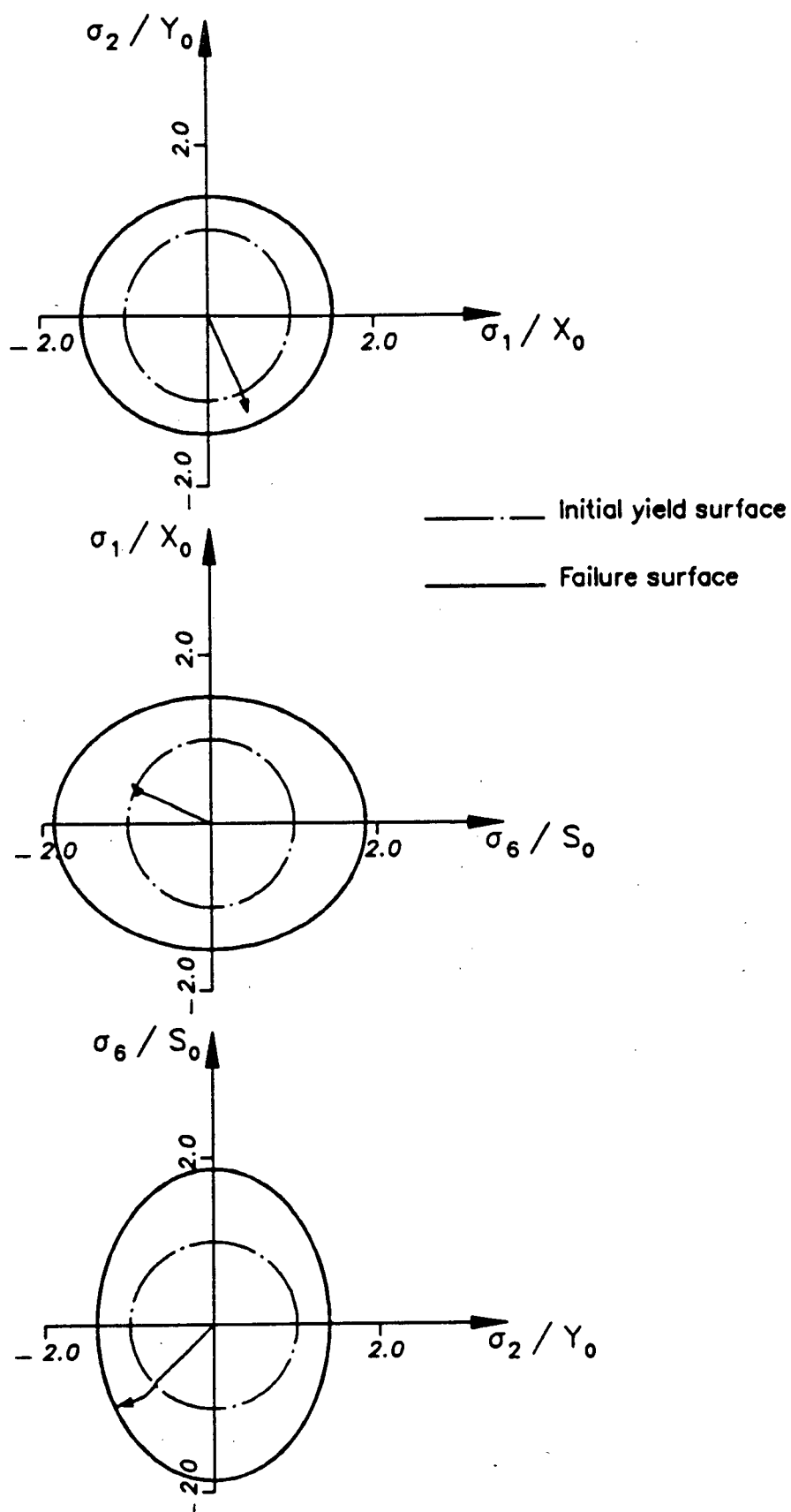
Fig. 5.19 b — Stress paths in the +30 deg layer during uniaxial loading of [+30/−30] B/Ep laminate : Hill's failure criterion
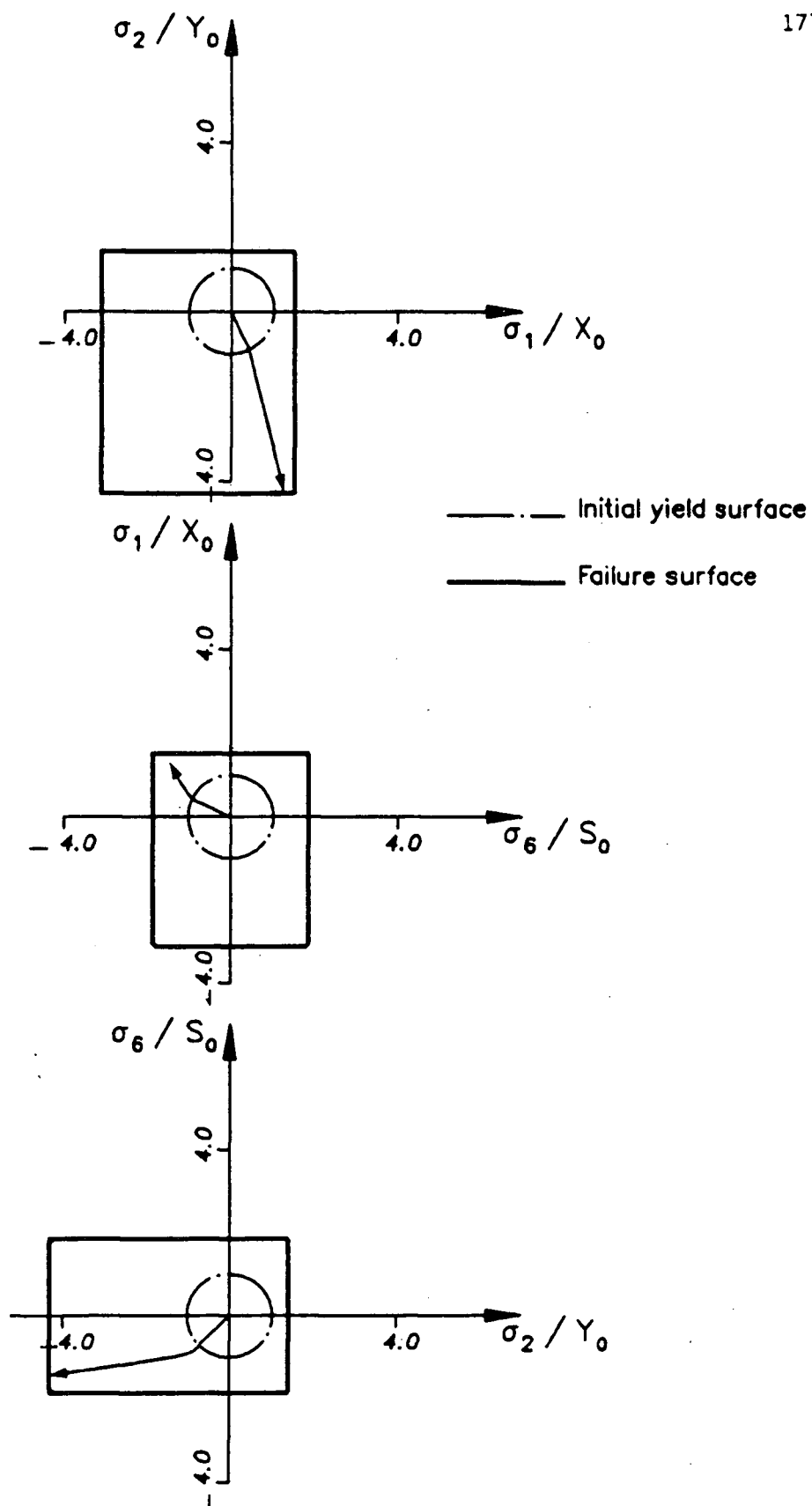
Fig. 5.19 c — Stress paths in the +30 deg layer during uniaxial loading of [+30/−30] B/Ep laminate : Maximum stress failure criterion
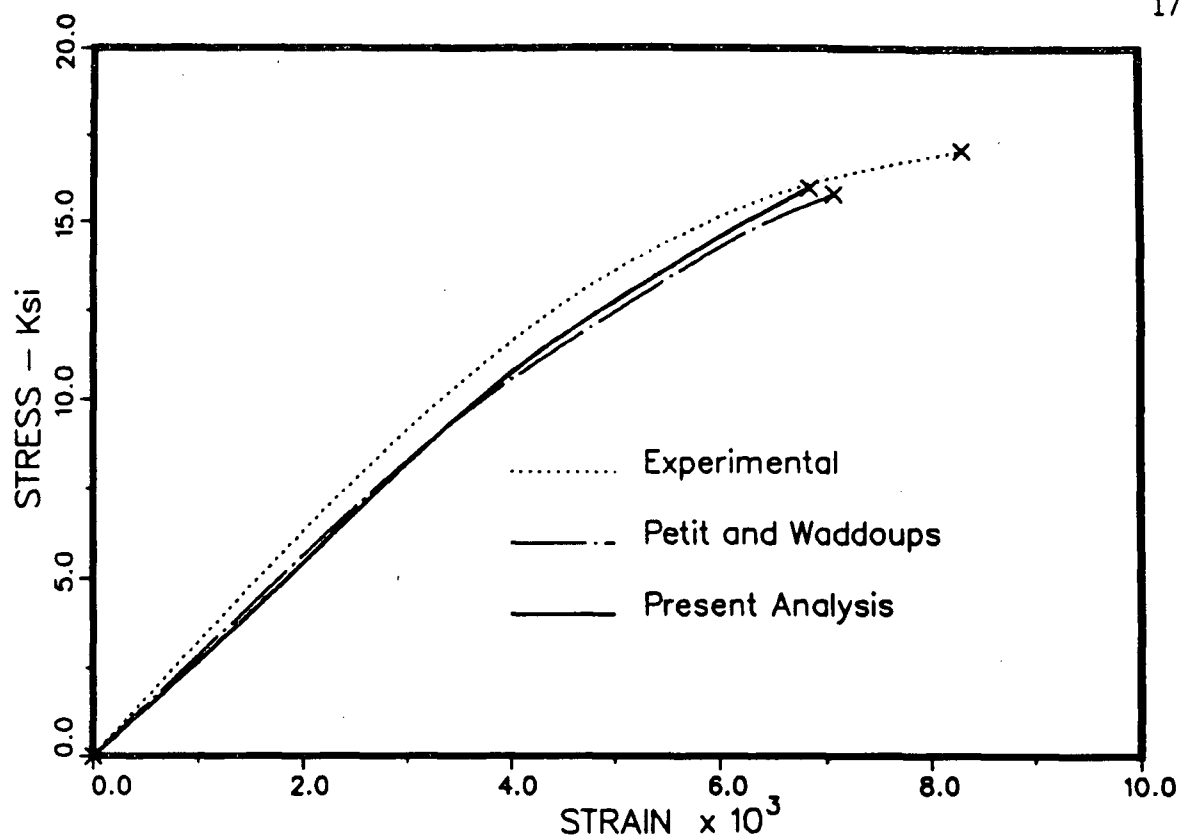
Fig. 5.20 — Tensile stress — strain curve for [+60/-60] Boron/Epoxy laminate
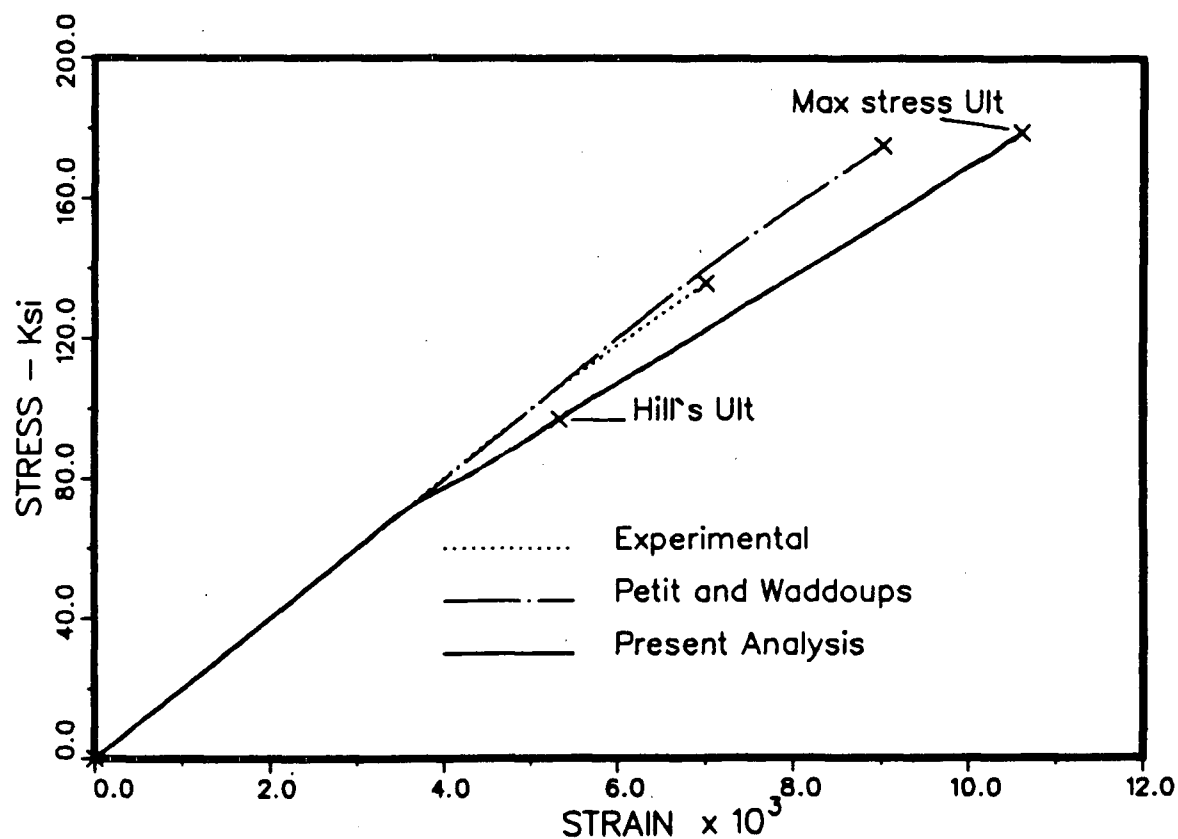
Fig. 5.21 a — Tensile stress — strain curve for [+20/-20] Boron/Epoxy laminate
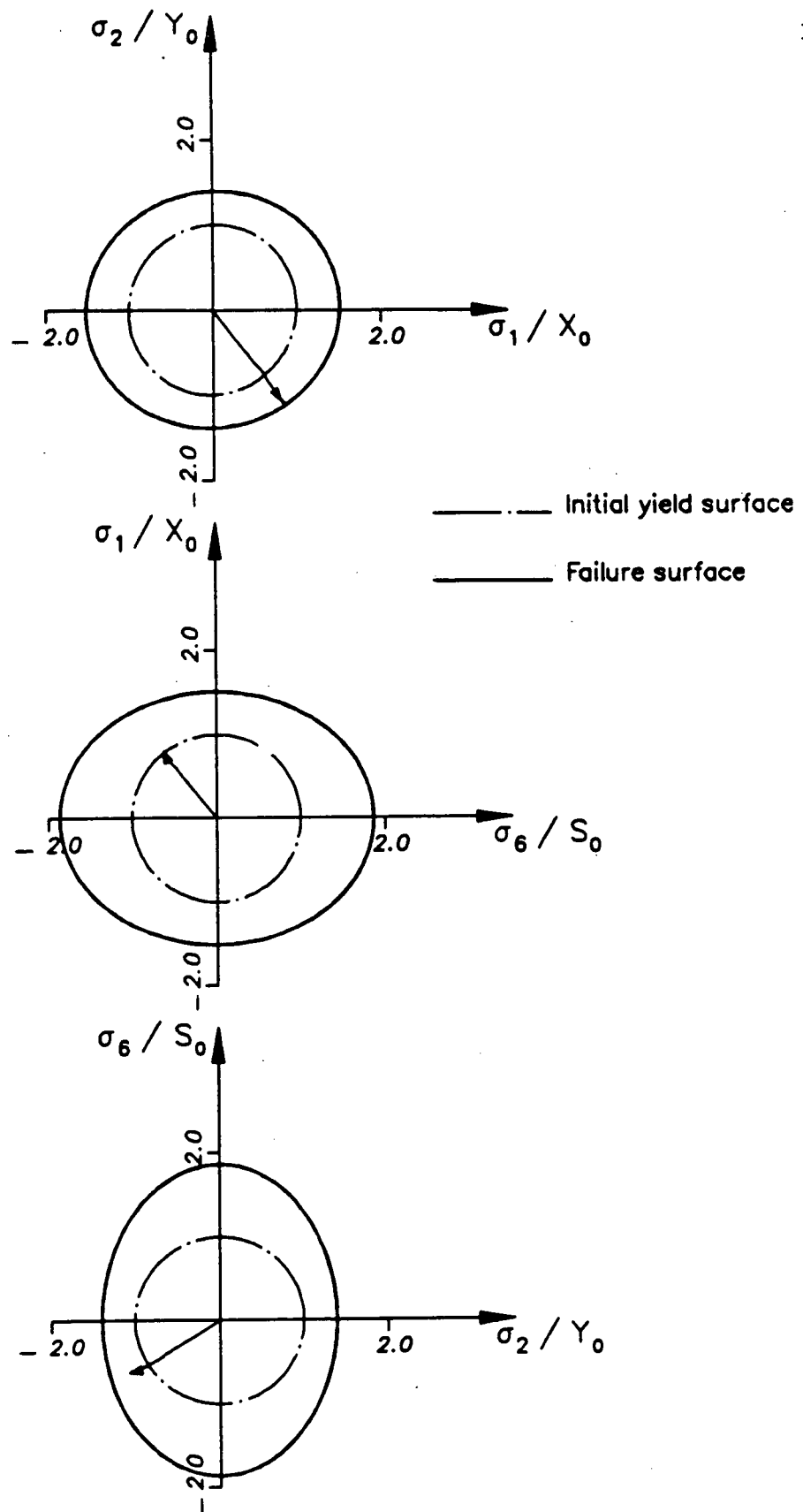
Fig. 5.21 b — Stress paths in the +20 deg layer during uniaxial loading
of [+20/−20] B/Ep laminate : Hill's failure criterion
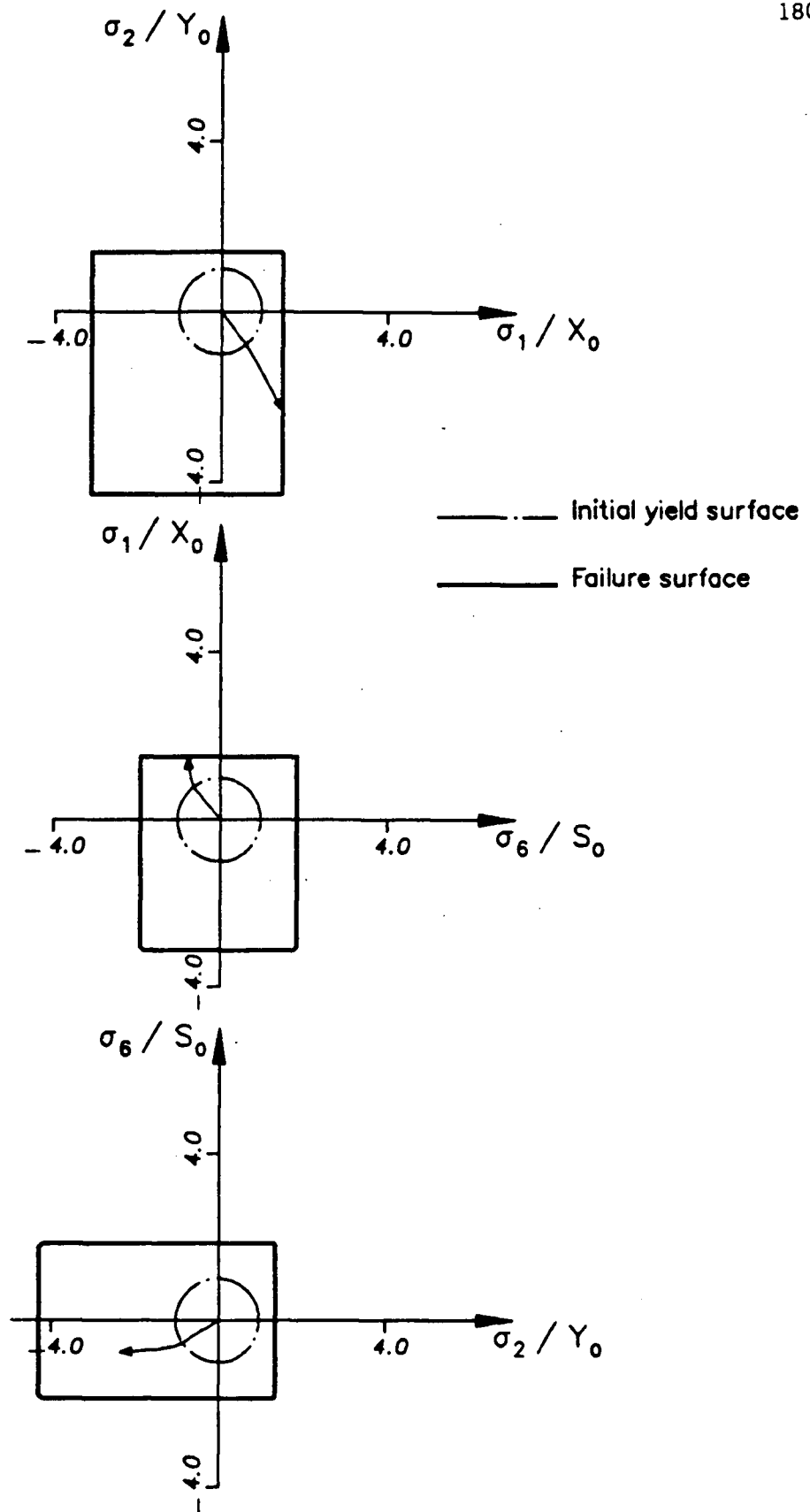
Fig. 5.21 c — Stress paths in the +20 deg layer during uniaxial loading
of [+20/−20] B/Ep laminate : Maximum stress failure criterion
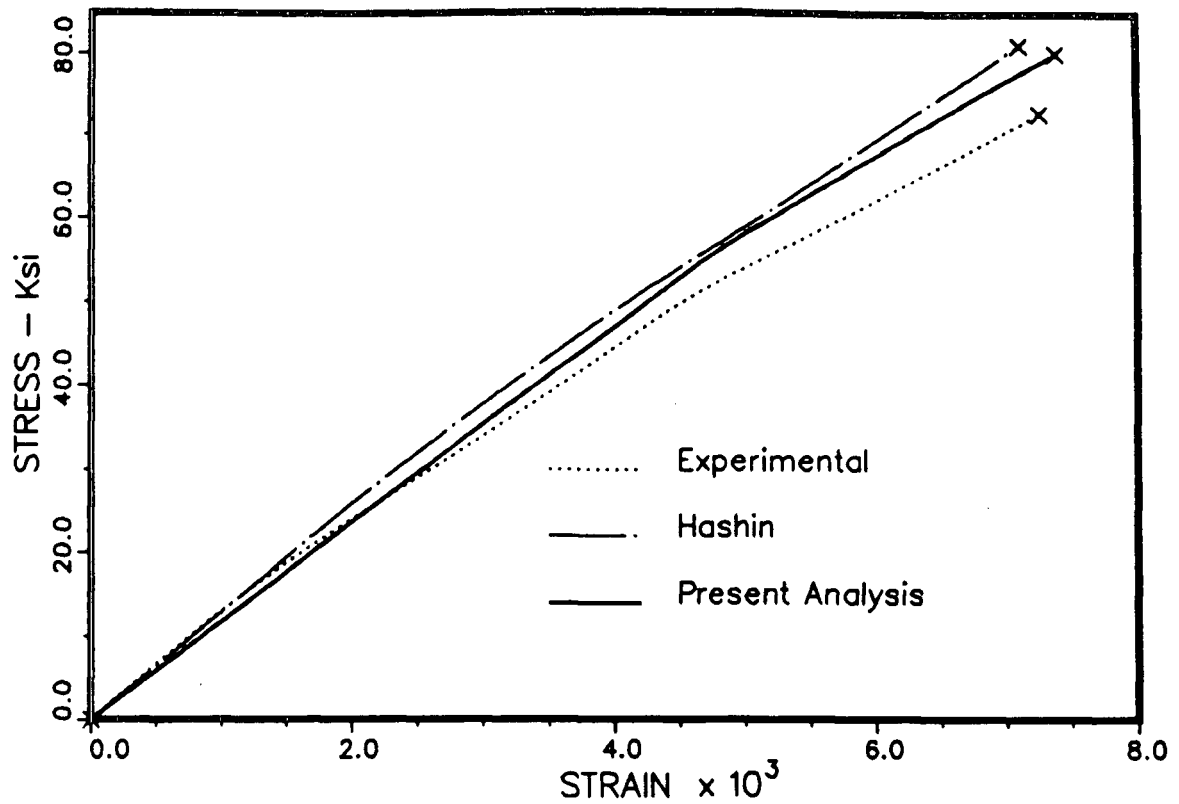
Fig. 5.22 – Tensile stress – strain curve for [0/+45/−45/90] Boron/Epoxy laminate
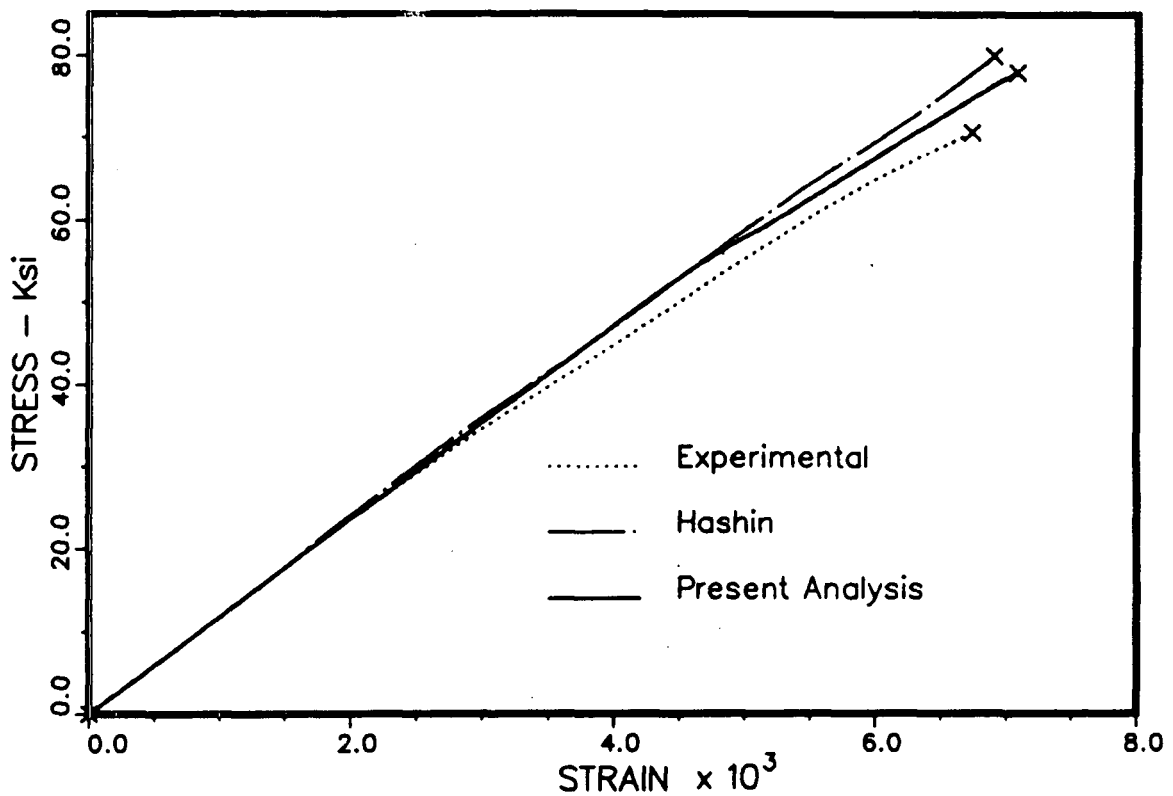
Fig. 5.23 – Tensile stress – strain curve for [0/+60/−60] Boron/Epoxy laminate
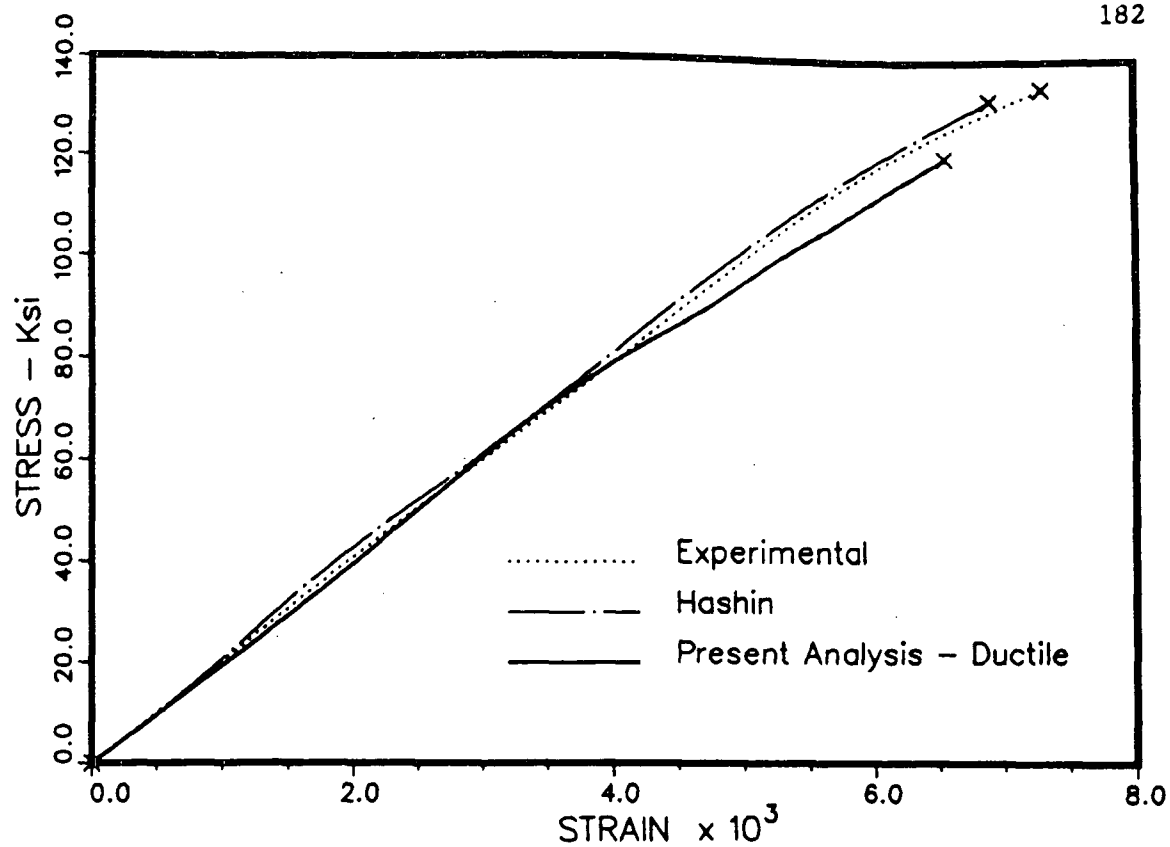
Fig. 5.24 — Tensile stress — strain curve for [0₃ /45/—45] Boron/Epoxy laminate
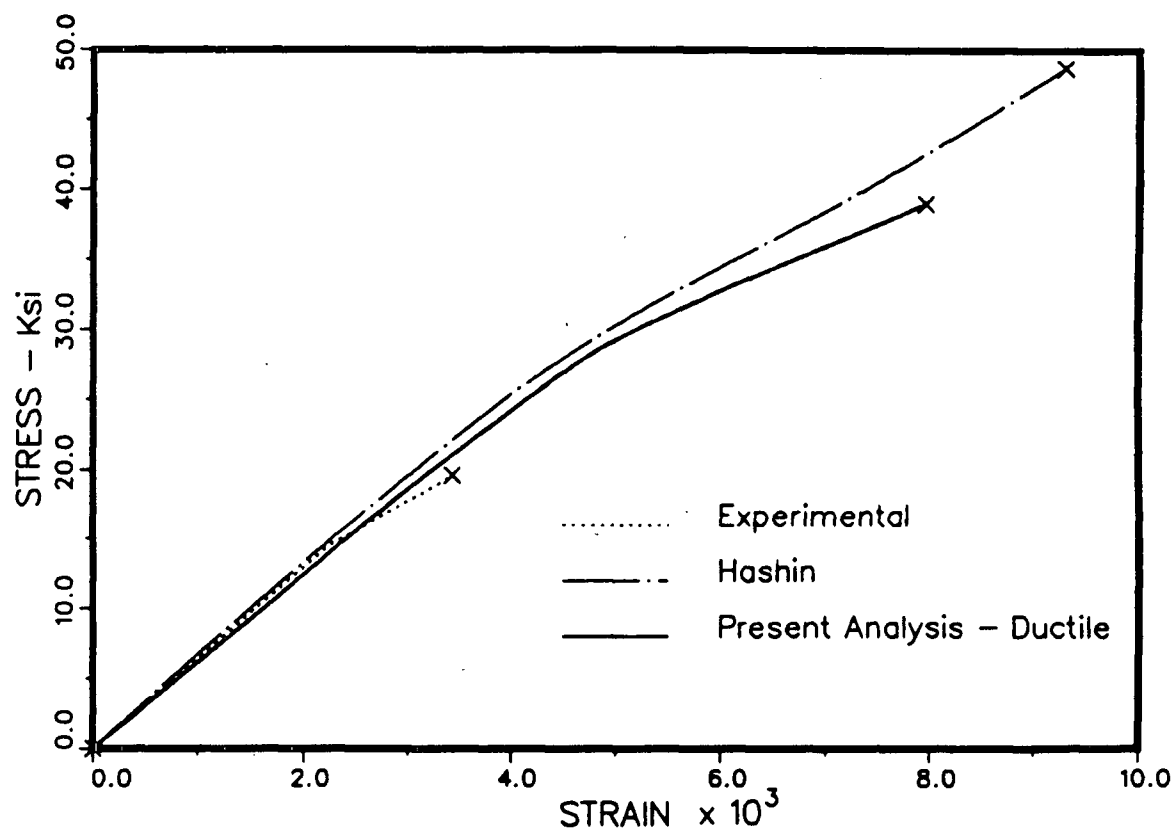
Fig. 5.25 — Tensile stress — strain curve for [65₃ /20/—70] Boron/Epoxy laminate
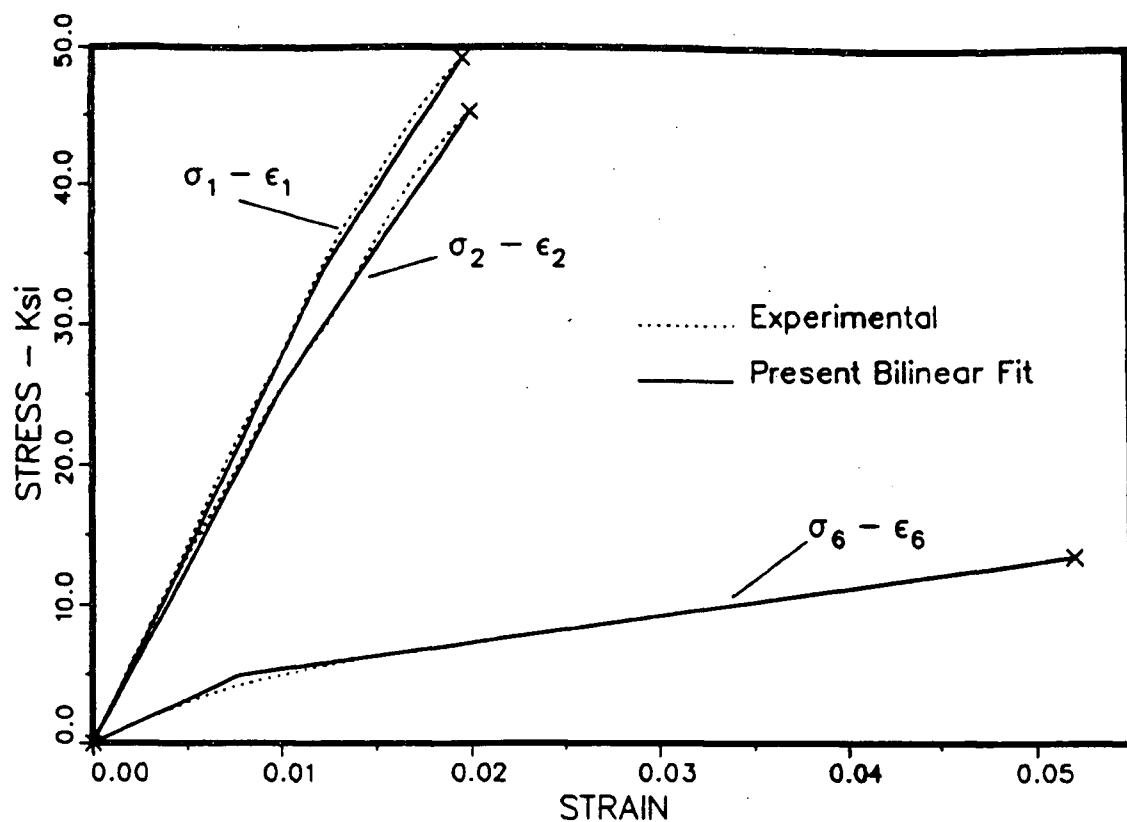
*Fig. 5.26 a — Basic Stress — Strain curves for a B/D layer made of
181 glass fabric and polyester resin*
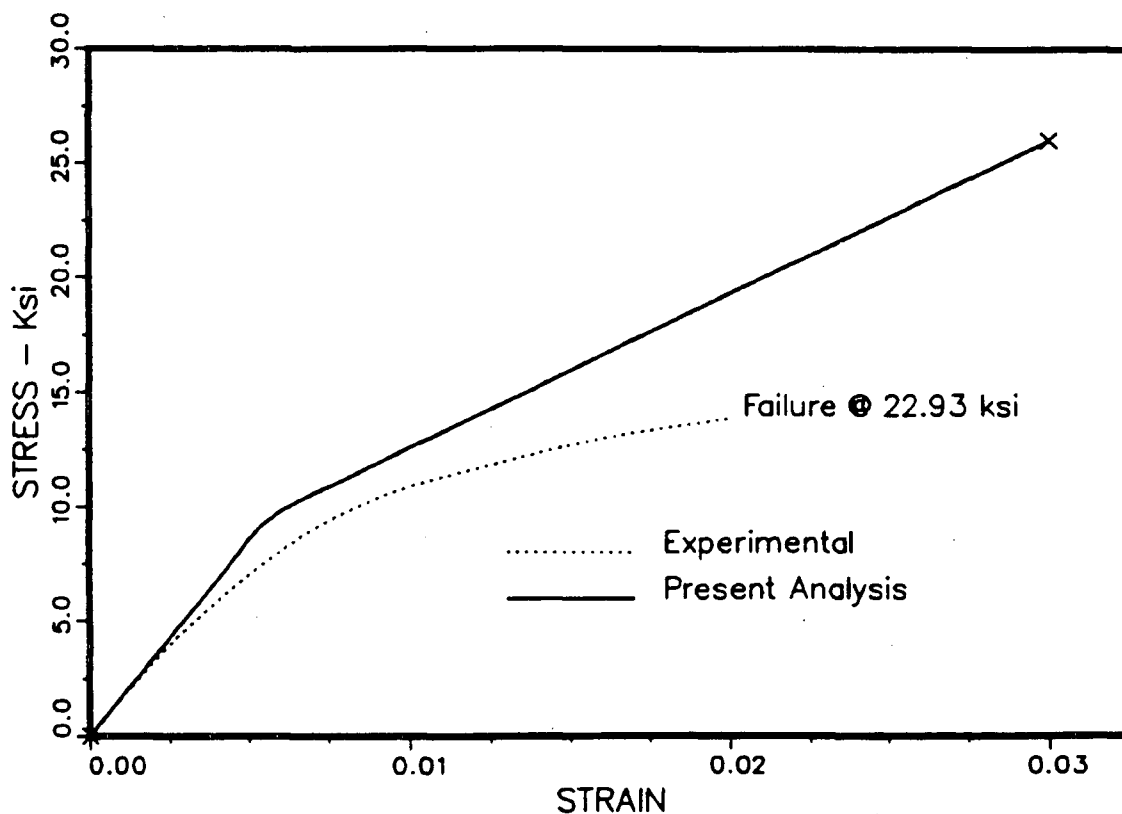
*Fig. 5.26 b — Tensile Stress — Strain curve at 45 deg to the fibre directions for
the material of Fig. 5.26 a*
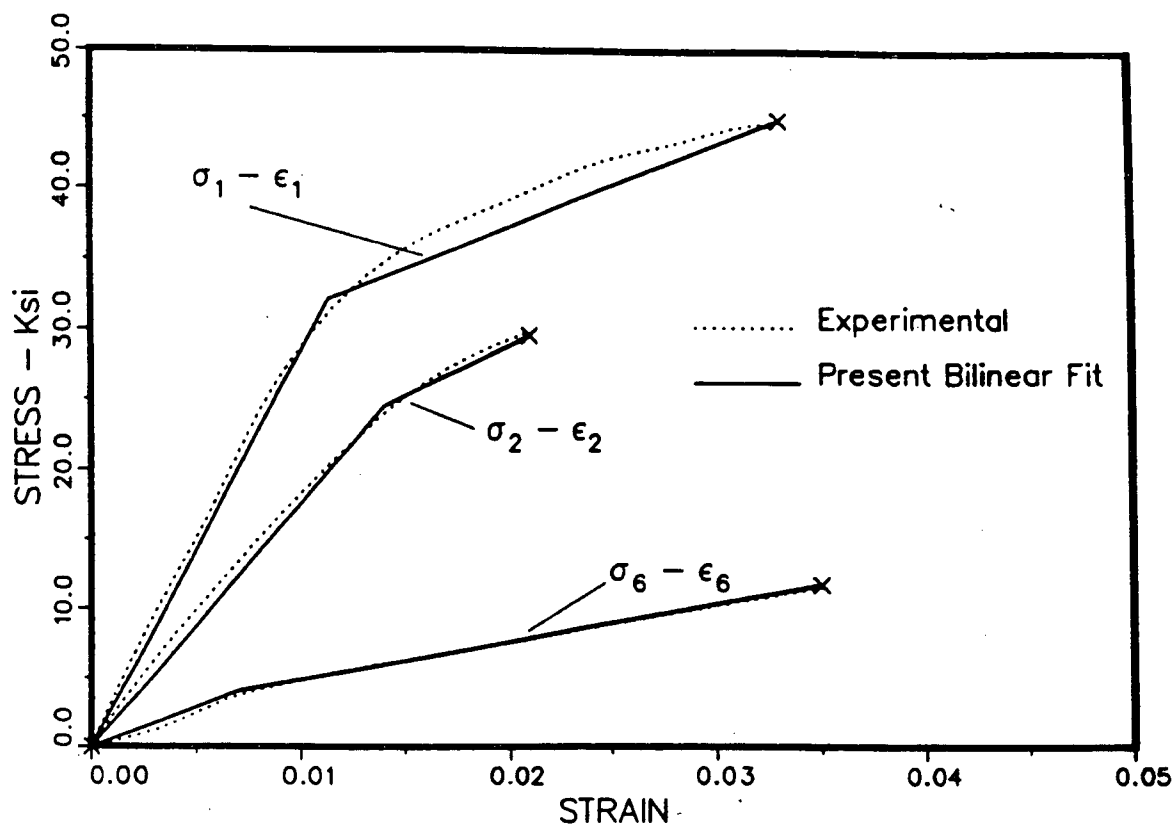
*Fig. 5.27 a — Basic Stress — Strain curves for a B/D layer made of
162 glass fabric and polyester resin*
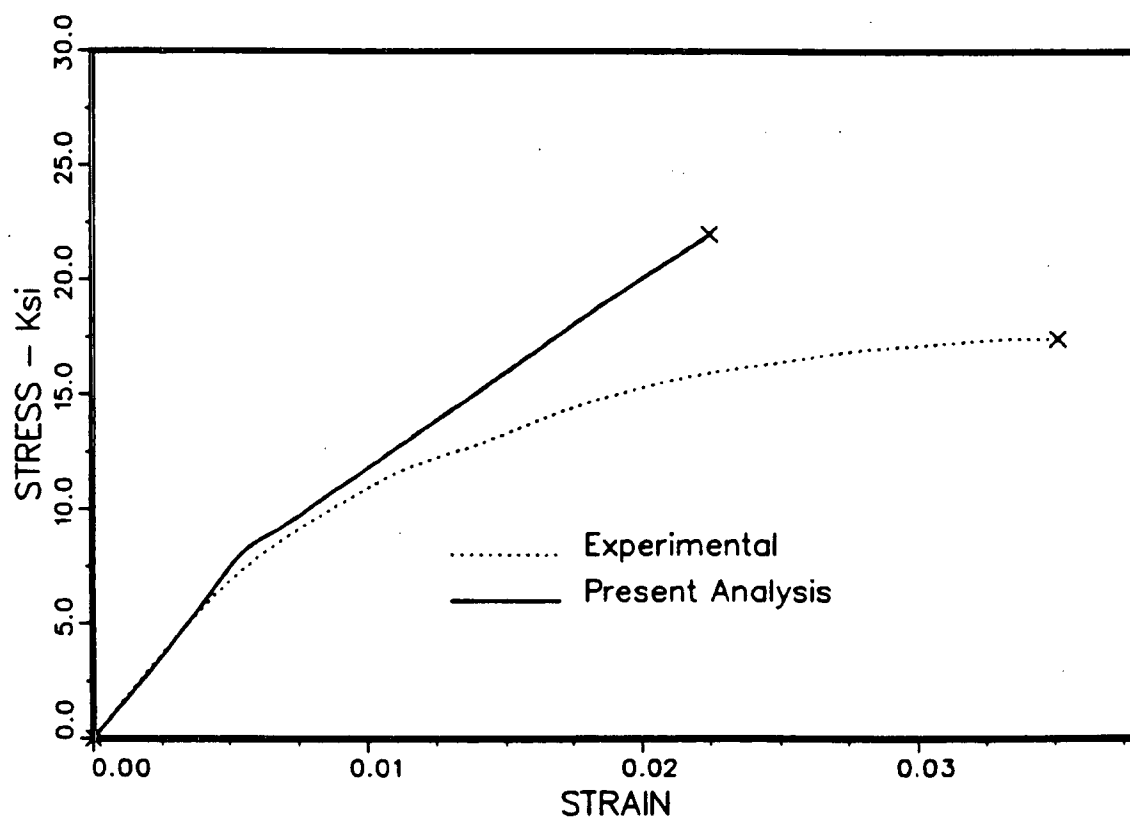
*Fig. 5.27 b — Tensile Stress — Strain curve at 45 deg to the fibre directions for
the material of Fig. 5.27 a*
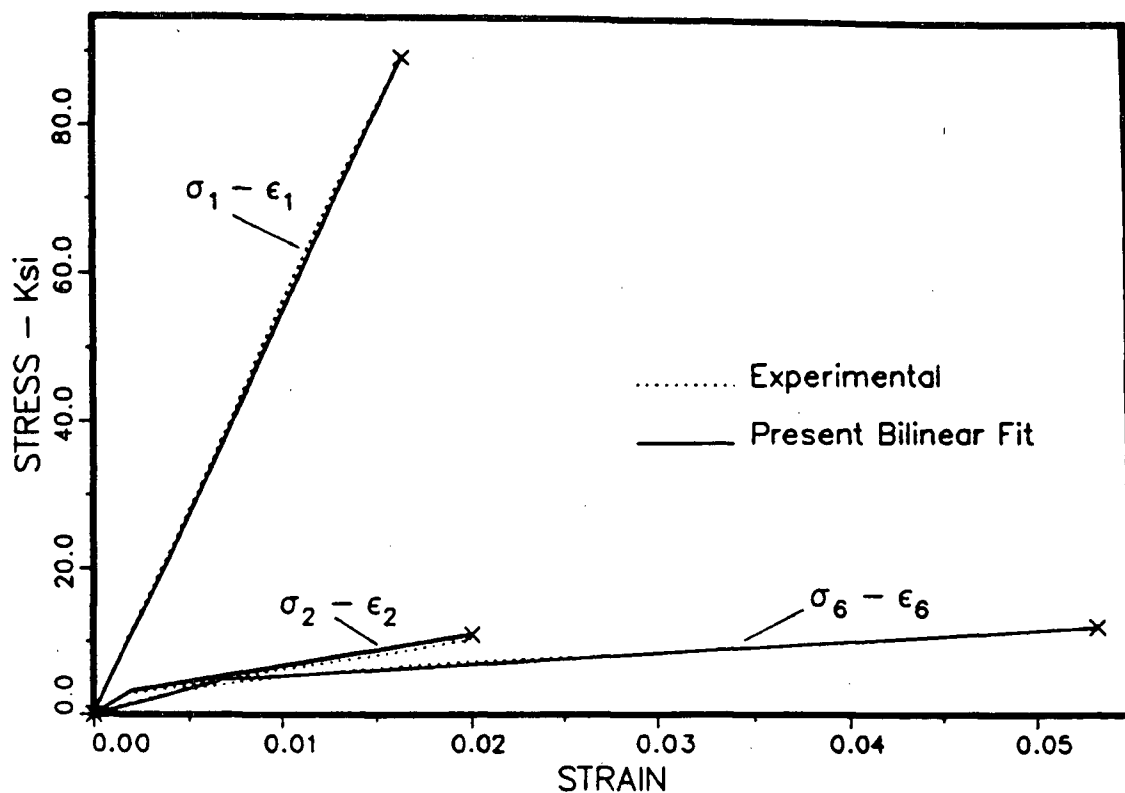
Fig. 5.28 a — Basic Stress — Strain curves for a B/D layer made of
143 glass fabric and polyester resin
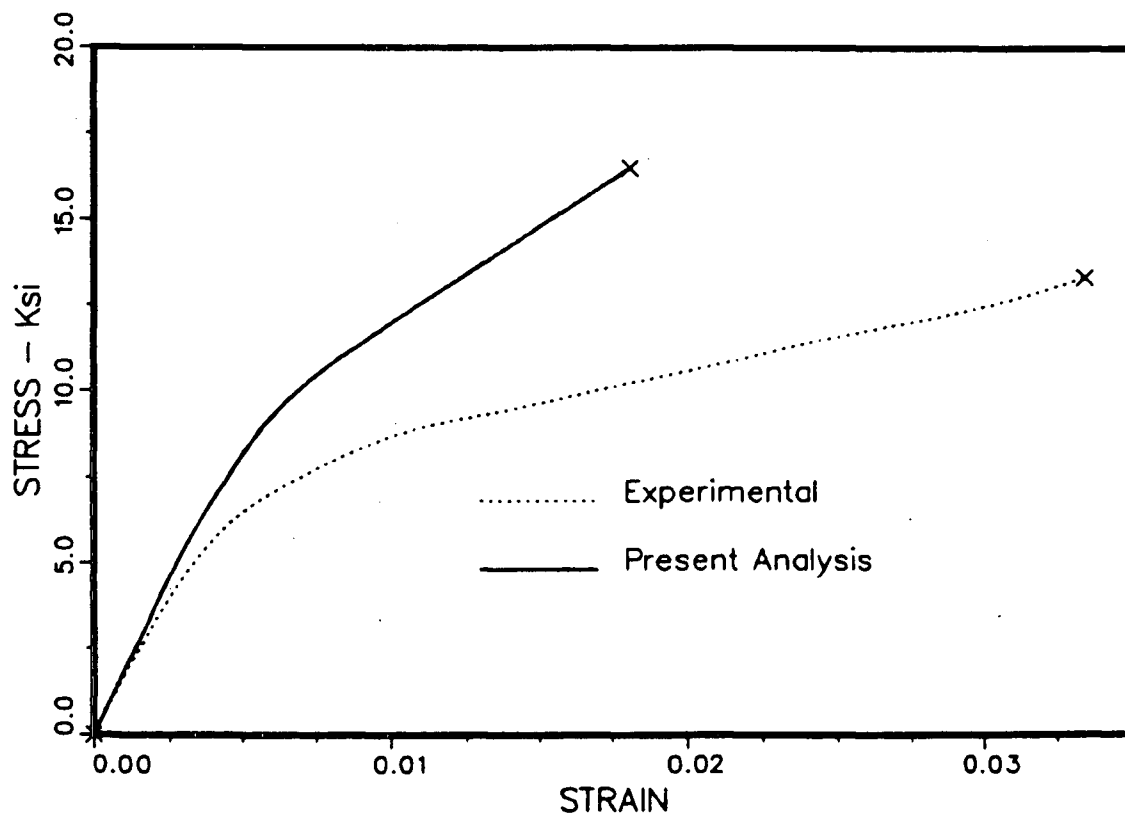
Fig. 5.28 b — Tensile Stress — Strain curve at 45 deg to the fibre directions for
the material of Fig. 5.28 a
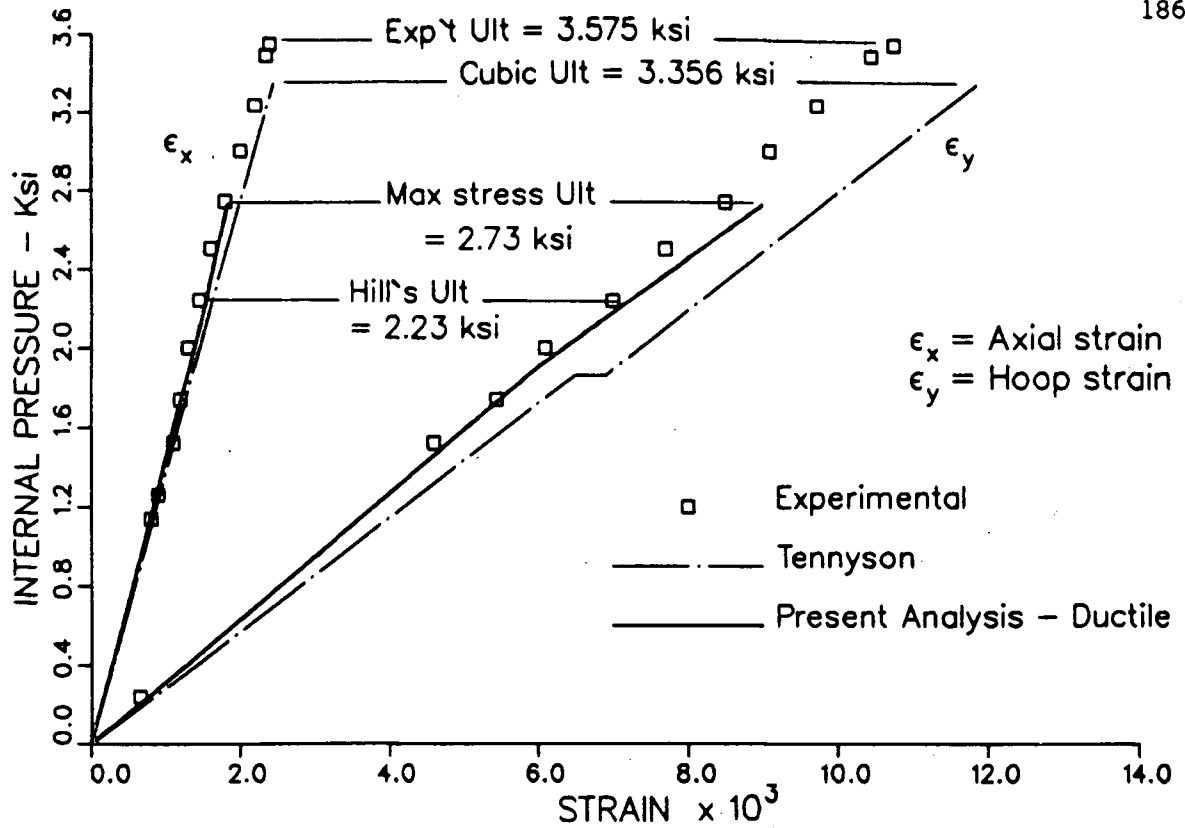
Fig. 5.29 — Pressure — strain curve for [0/60/−60] Gr/Ep tube under internal pressure
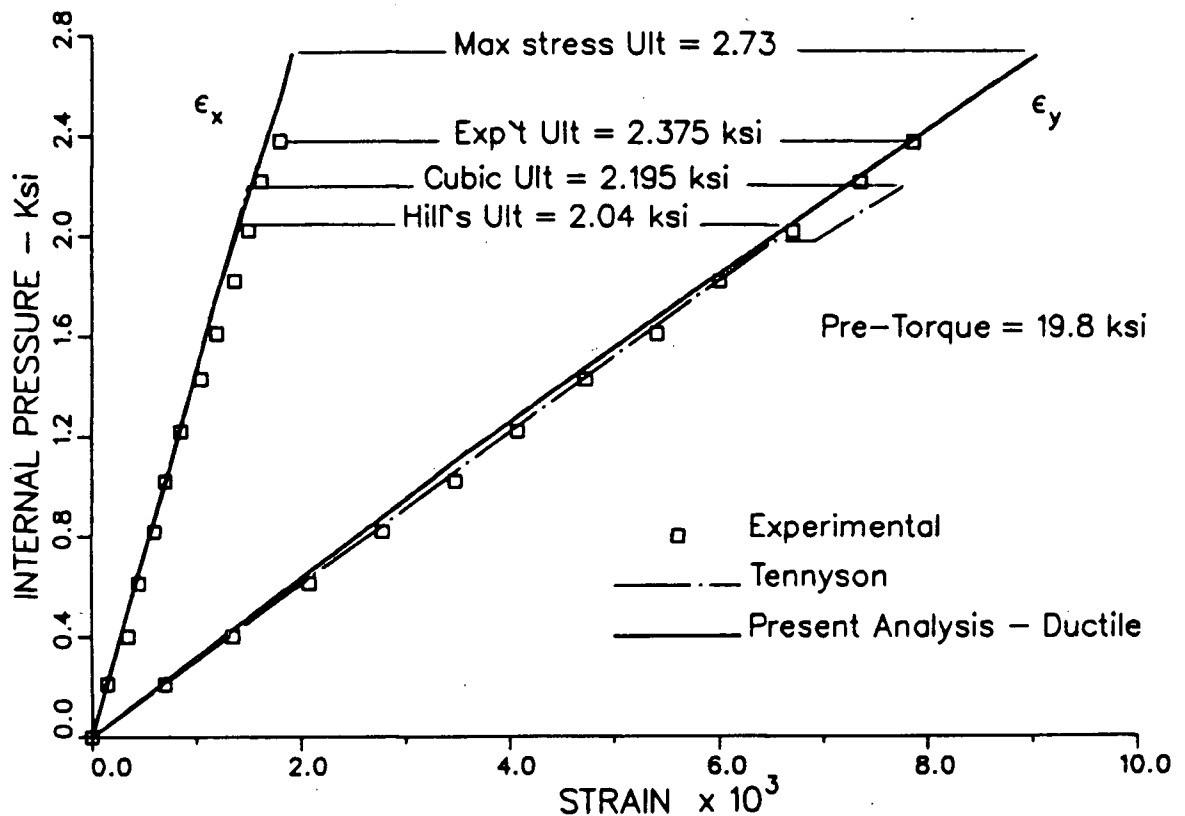
Fig. 5.30 — Pressure — strain curve for [0/60/−60] Gr/Ep tube under combined internal pressure and pre−torque
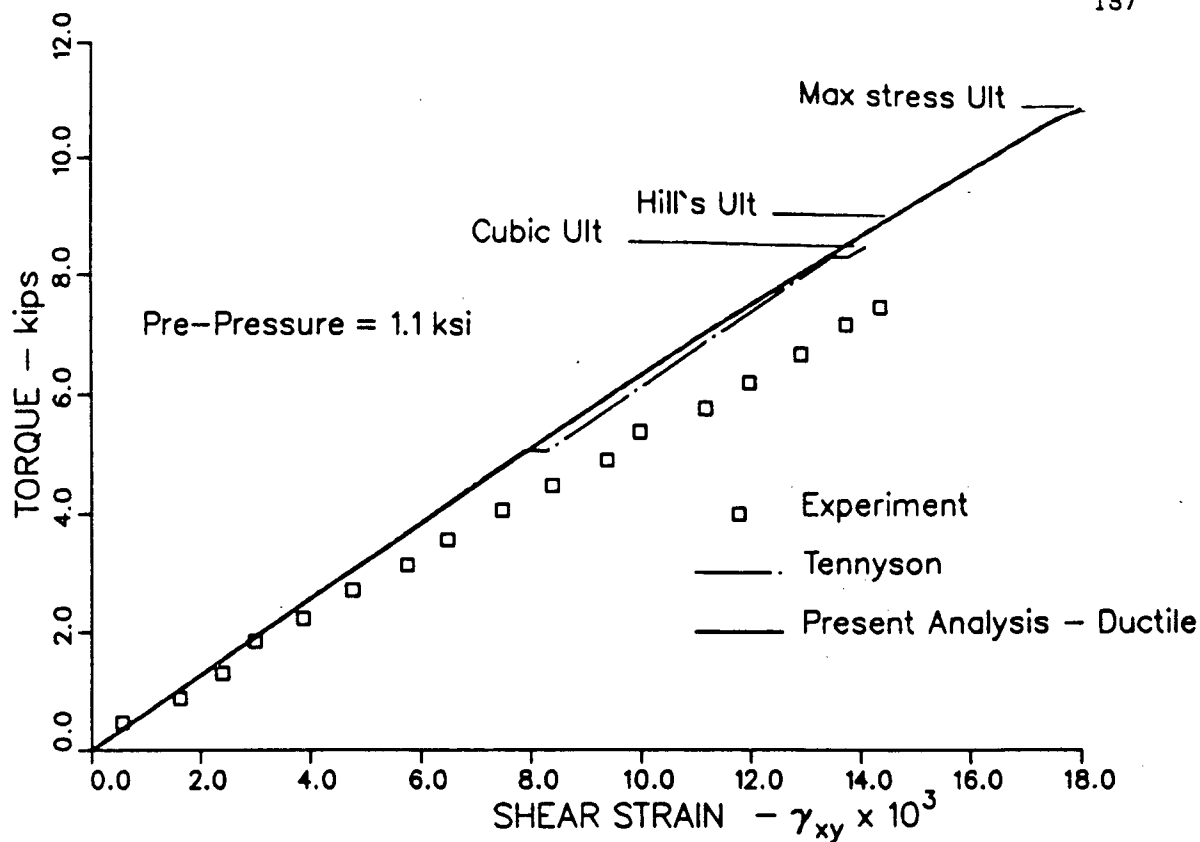
Fig. 5.31 – Torque – shear strain curve for [0/60/–60] Gr/Ep tube with pre-
load of internal pressure
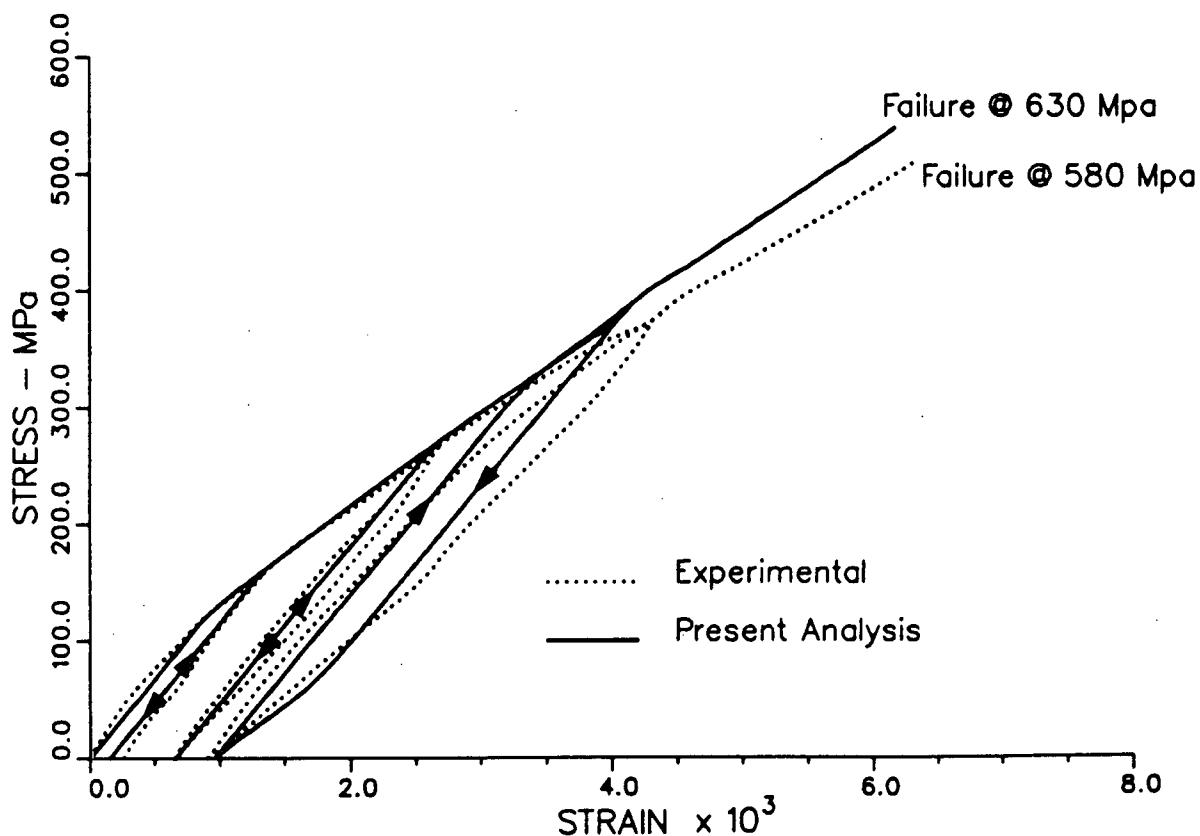
Fig. 5.32 – Tensile stress – strain curve for [0/45/–45] B/Al laminate under
three load cycles
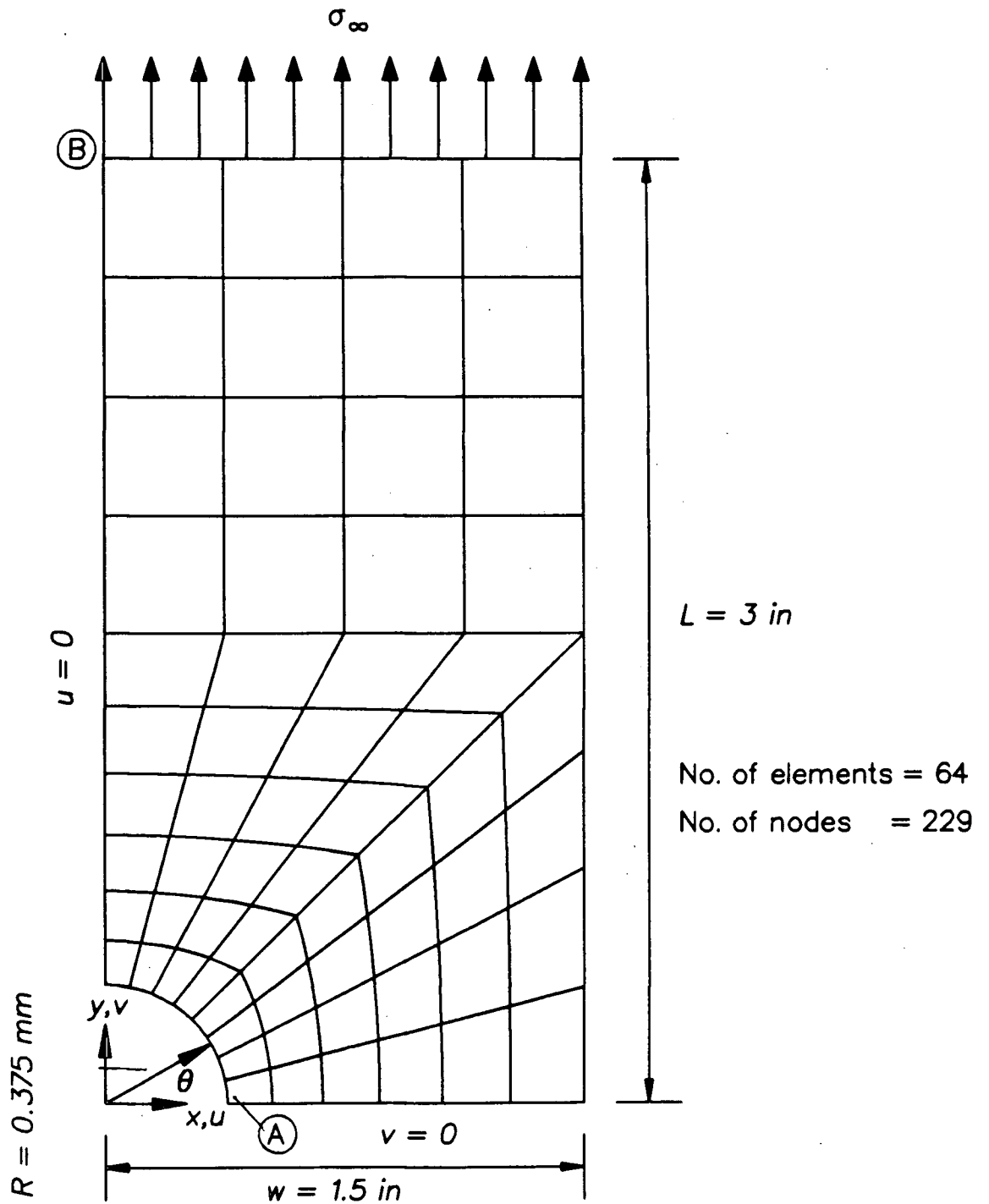
Fig. 5.33 — Geometry and the finite element model for a quadrant
of an orthotropic perforated sheet
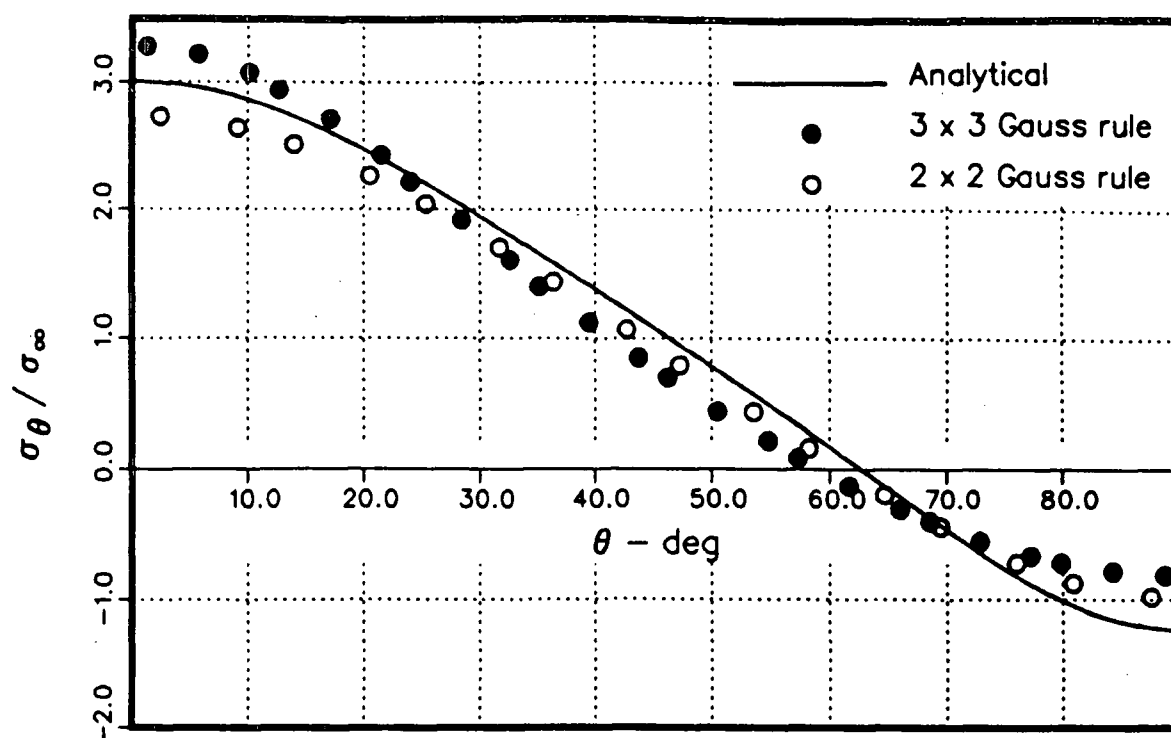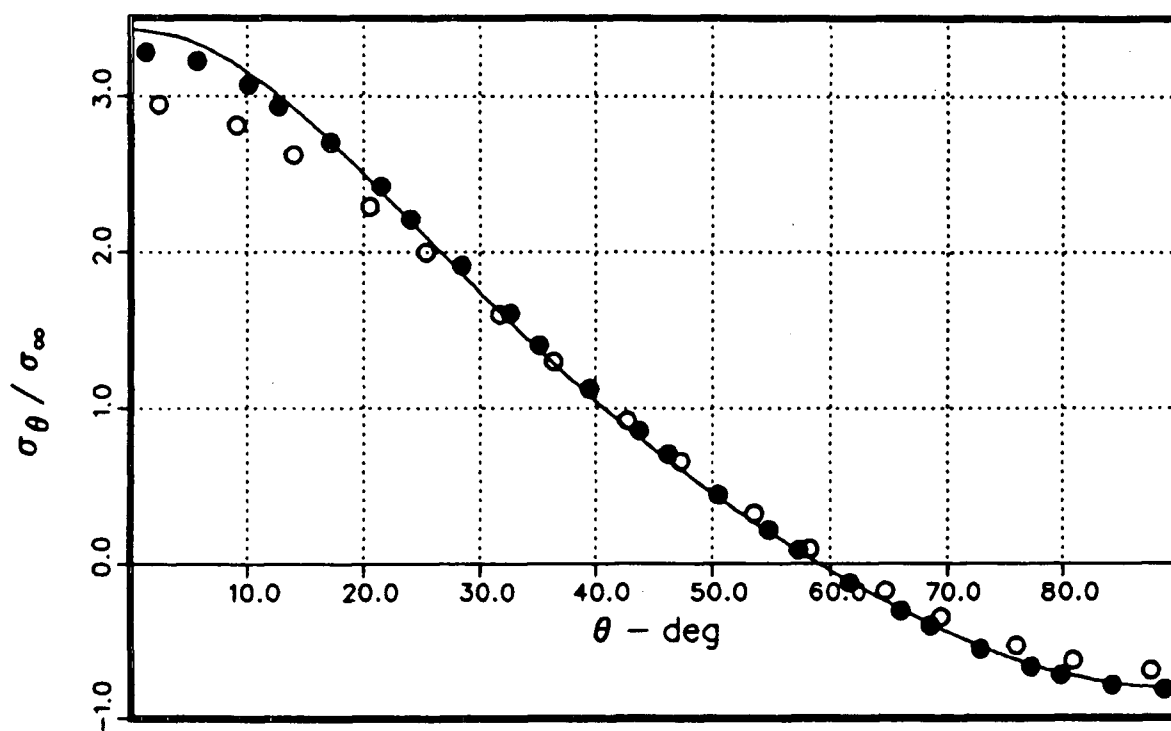
Fig. 5.34 — *Elastic circumferential stress distribution around the hole for a U/D B/Al layer : a — Fibres perpendicular to the load direction b — Fibres along the load direction*
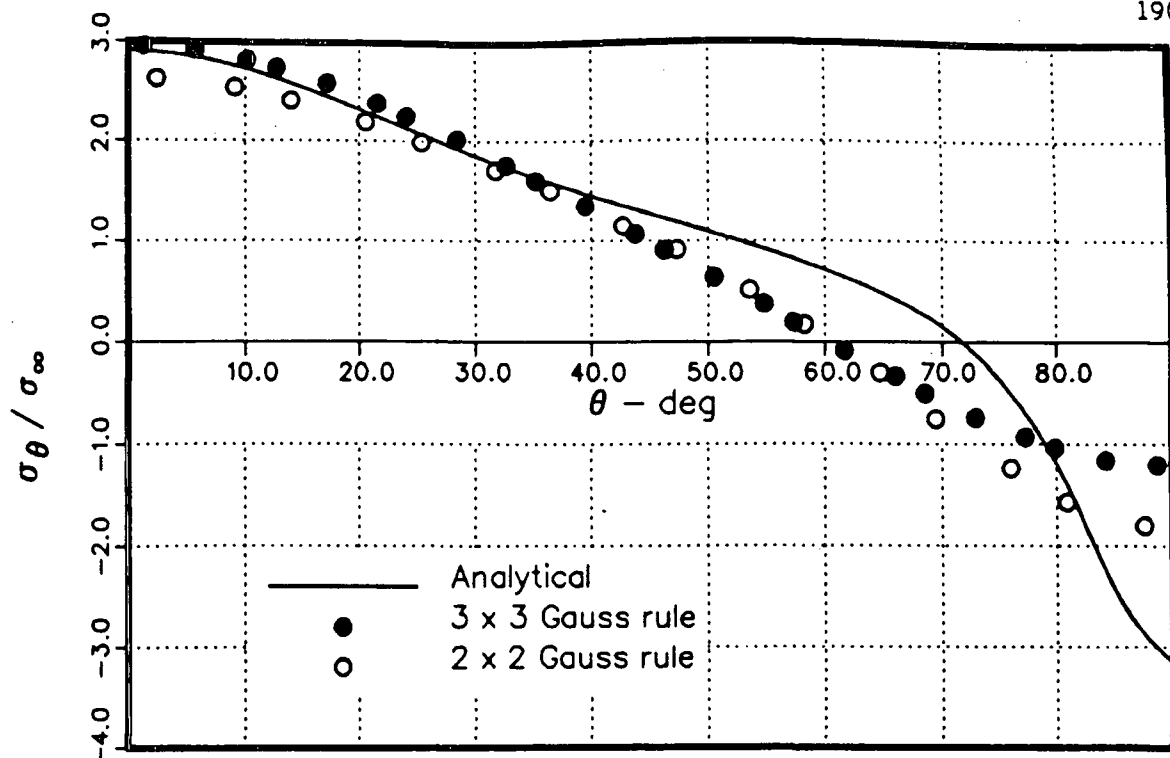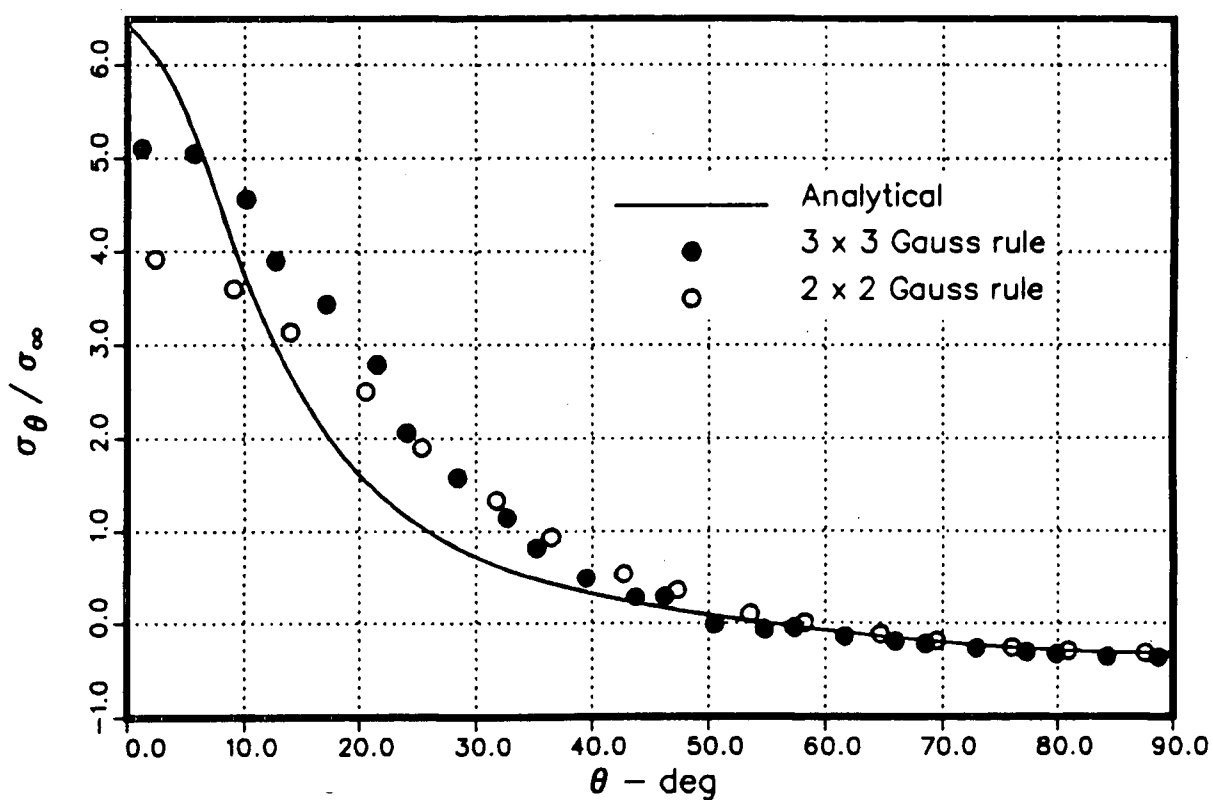
Fig. 5.35 — Elastic circumferential stress distribution around the hole for a
U/D B/Ep layer : a — Fibres perpendicular to the load direction
b — Fibres along the load direction
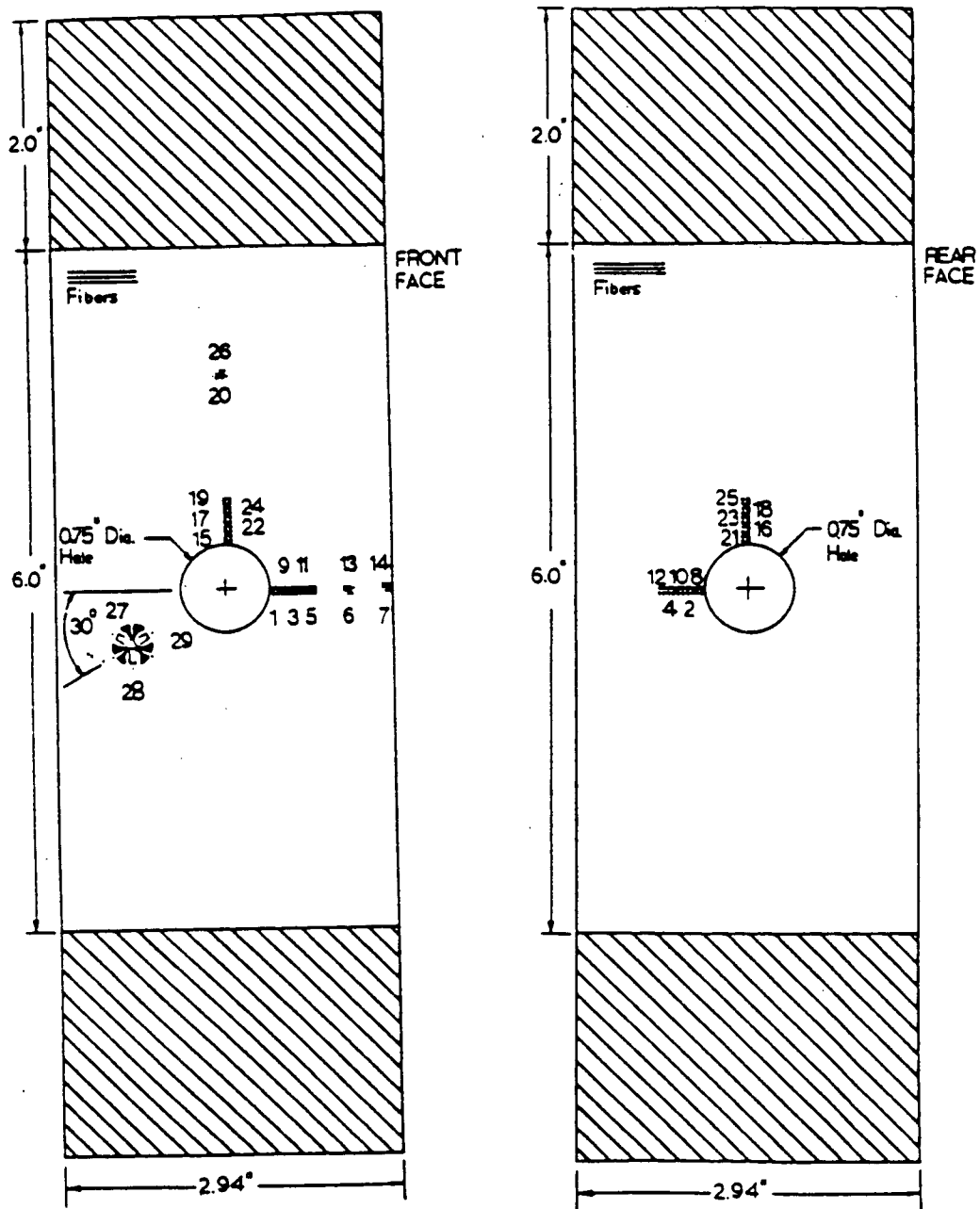
Fig. 5.36 — Geometry of the test specimen used by [Rizzi et al ,1987] for experimental determination of the stress—strain behaviour of a perforated 90—deg U/D B/Al layer
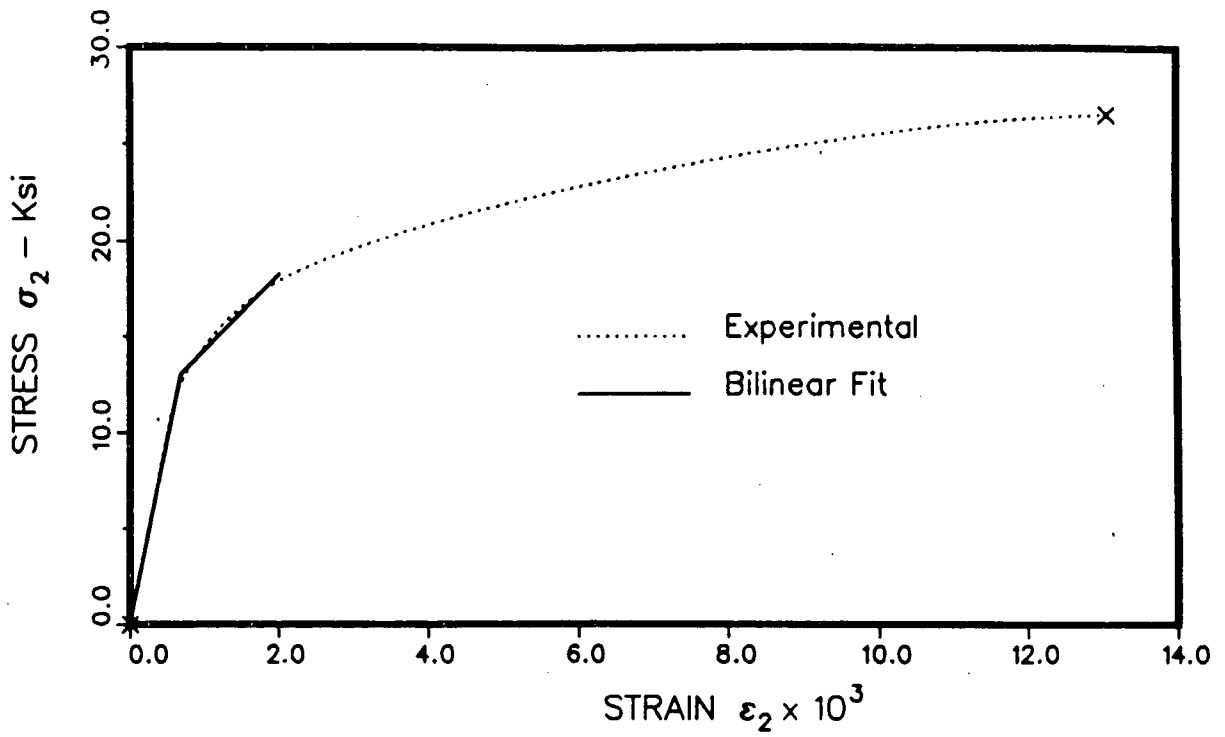
Fig. 5.37 – Transverse tensile stress – strain curve for a single layer of U/D B/Al
[Kenaga et al , 1987]
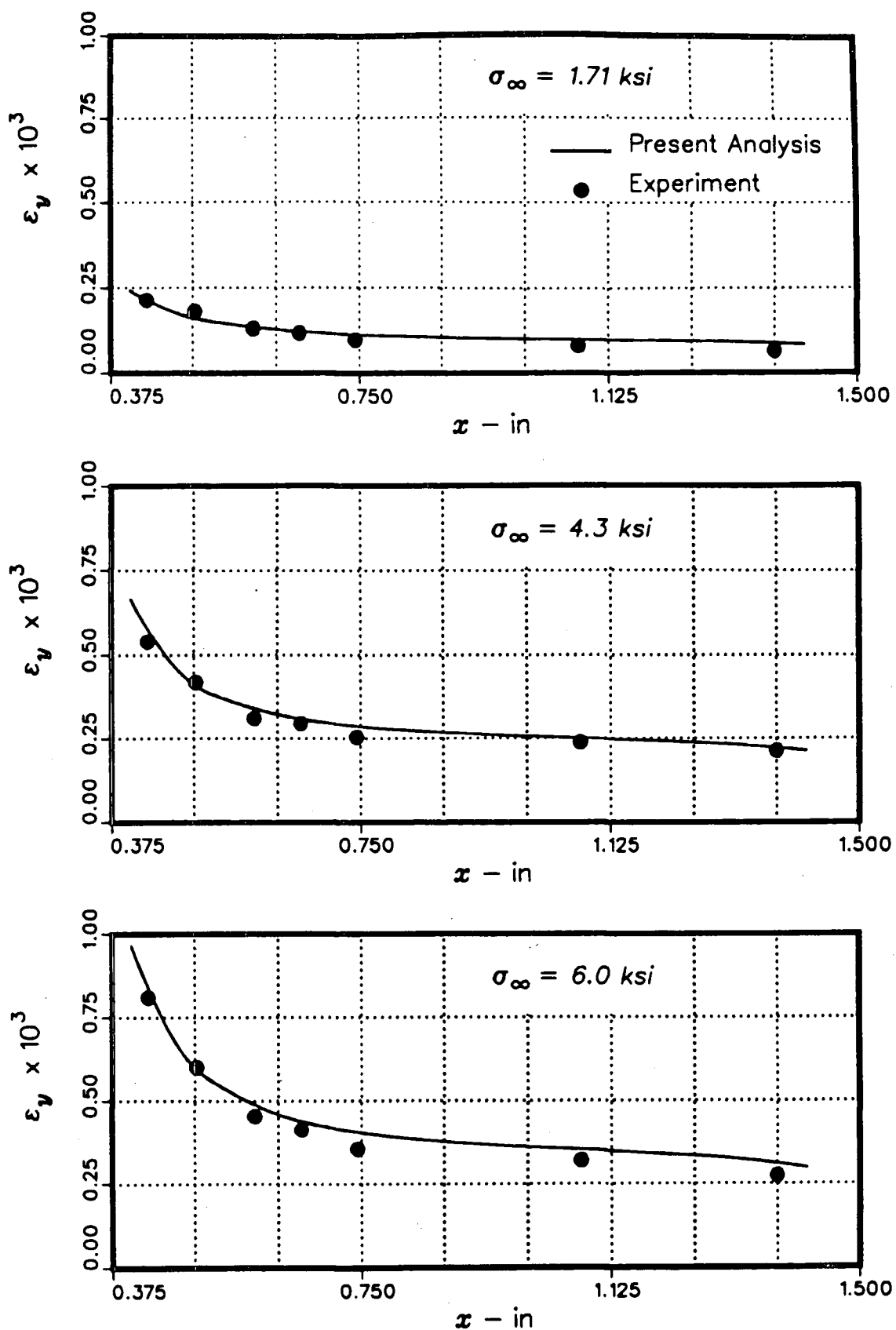
Fig. 5.38 — Longitudinal strain distribution along the net section for various
remote load levels imposed on a perforated 90 — deg layer
of U/D B/Al

Fig. 5.38 — continued

$\sigma_\infty = 6.0 \; ksi$

$\sigma_\infty = 7.7 \; ksi$

$\sigma_\infty = 9.4 \; ksi$

$\sigma_\infty = 10.7 \; ksi$
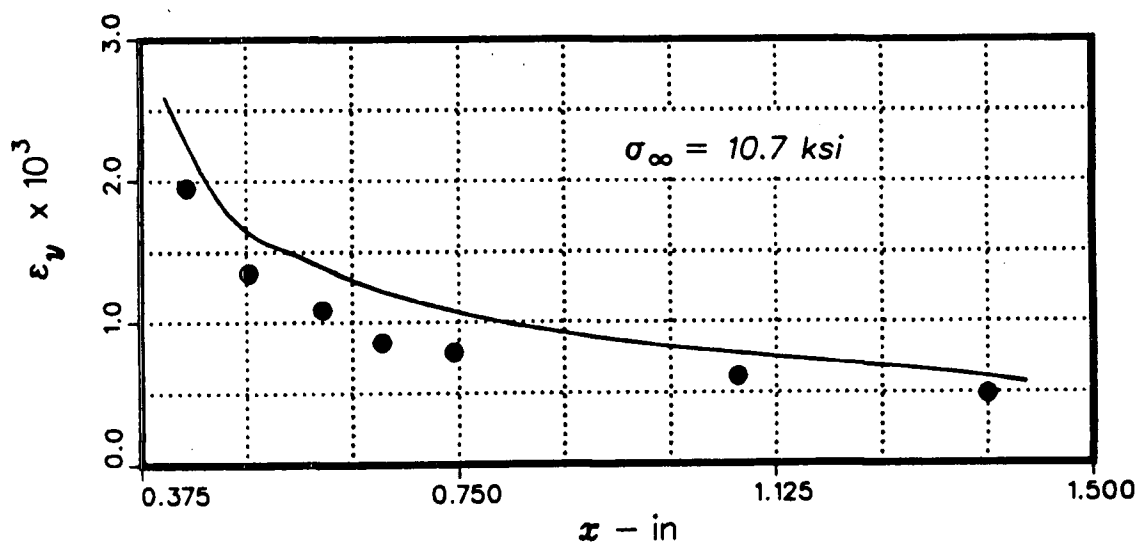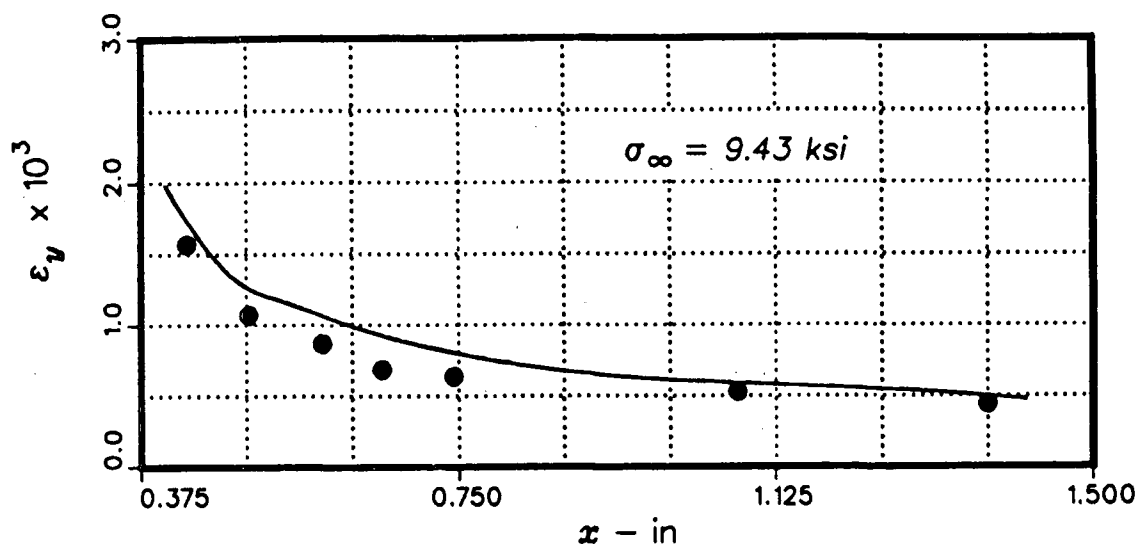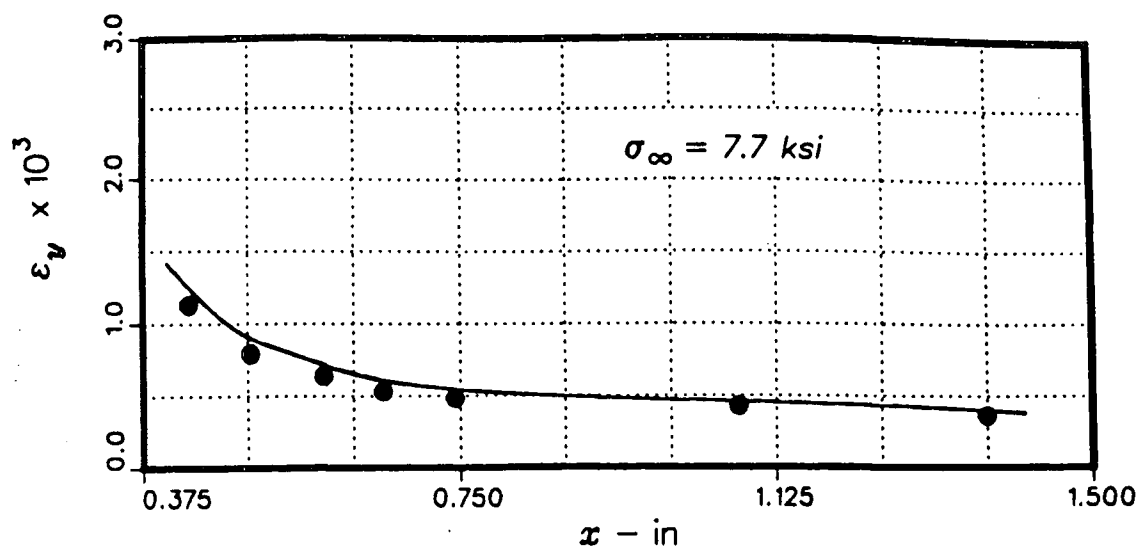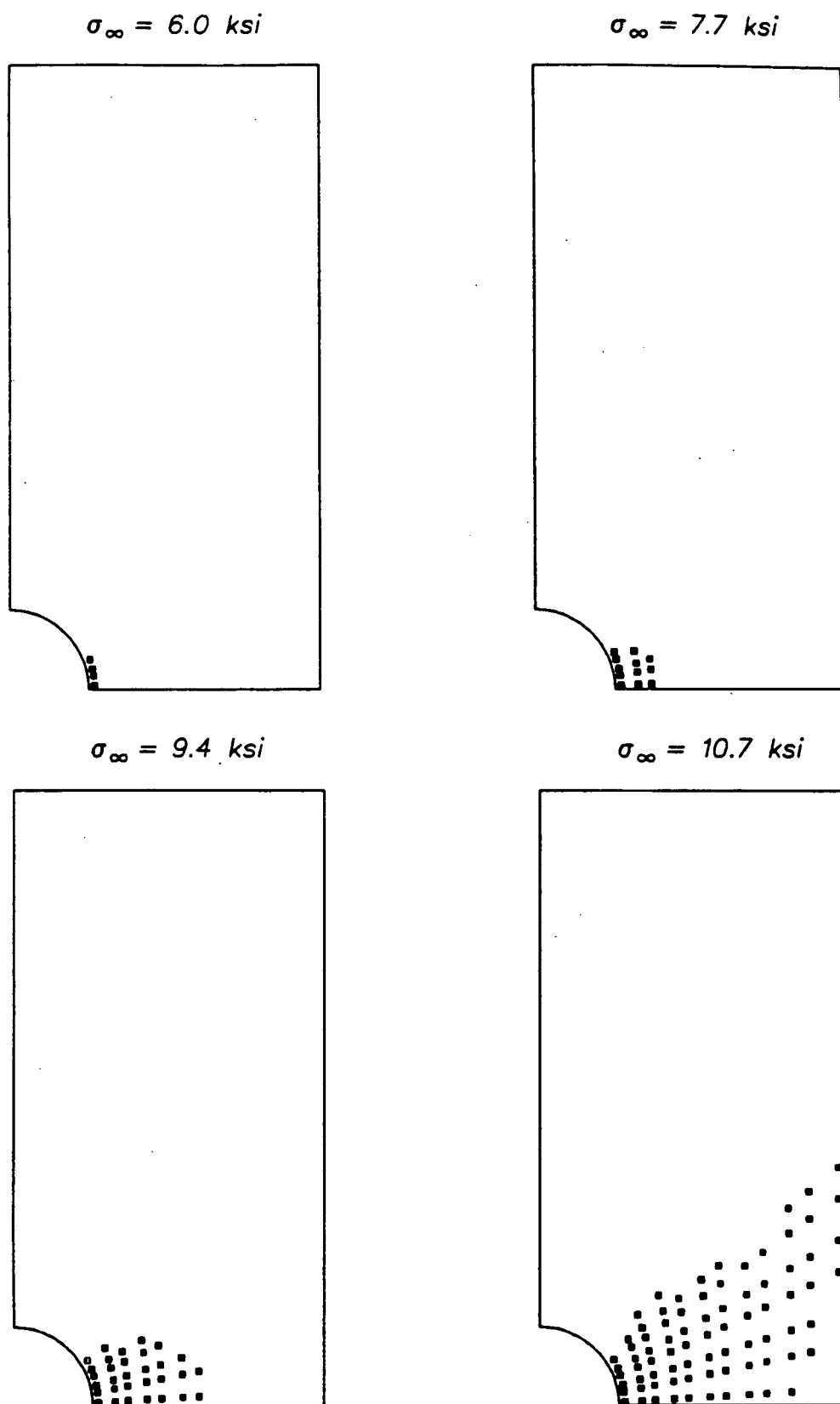
Fig. 5.39 — Development of plastic zones for a perforated 90-deg U/D B/Al layer subjected to elastoplastic loading
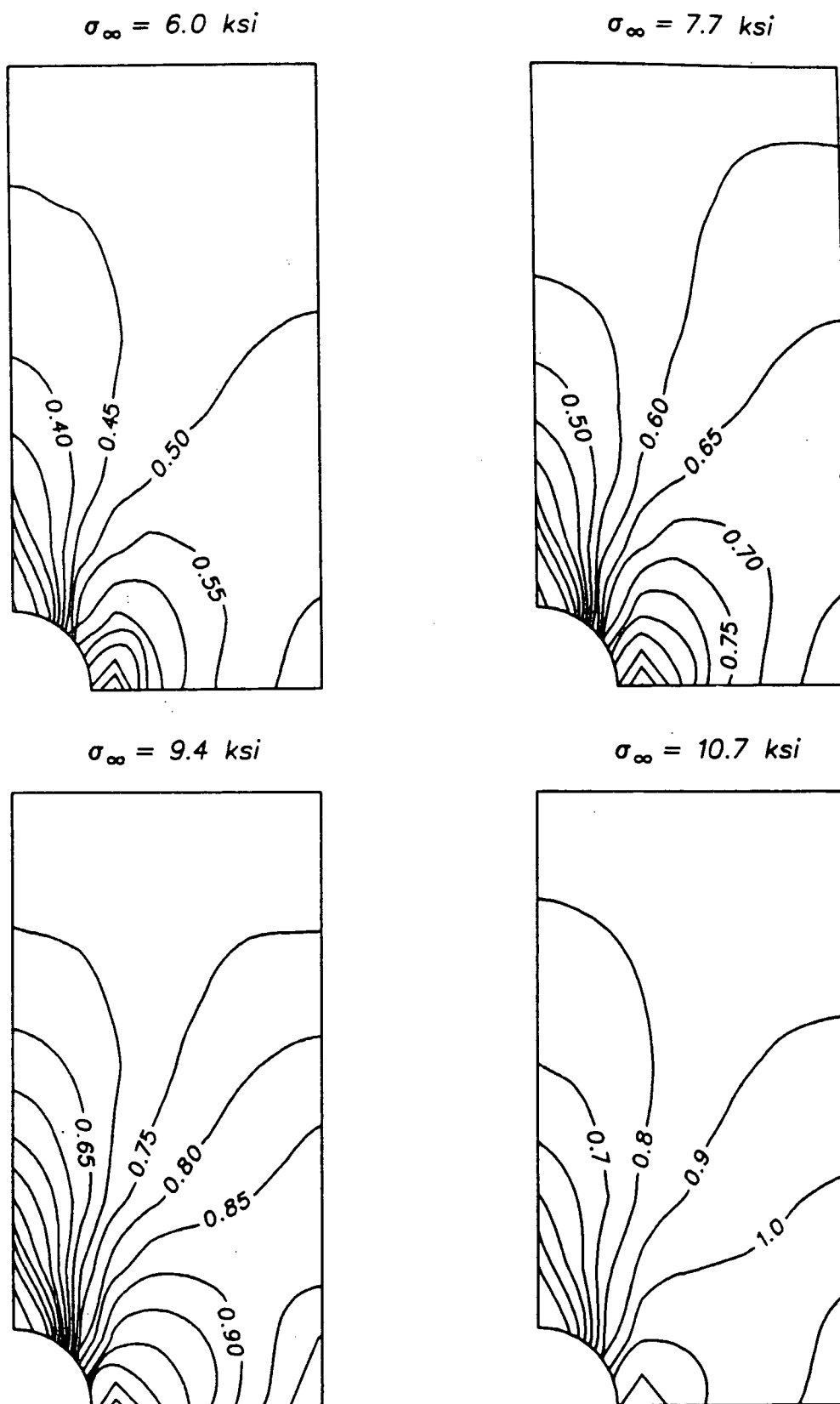
Fig. 5.40 — Nondimensional effective stress contours for a perforated 90-deg U/D B/Al layer subjected to elastoplastic loading
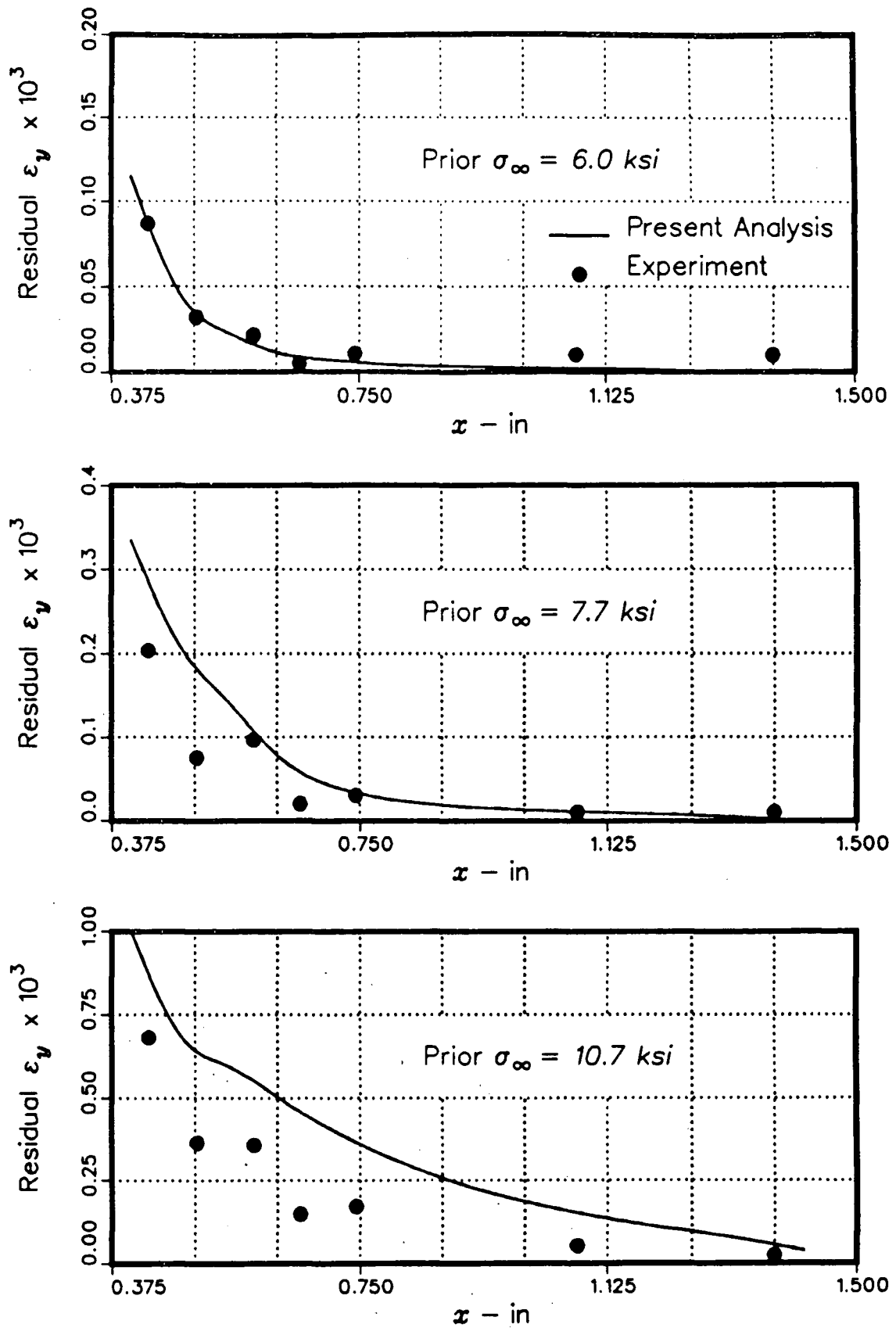
Fig. 5.41 — Residual longitudinal strain distribution along the
net section of a perforated 90-deg layer of U/D B/Al
after unloading from various load levels
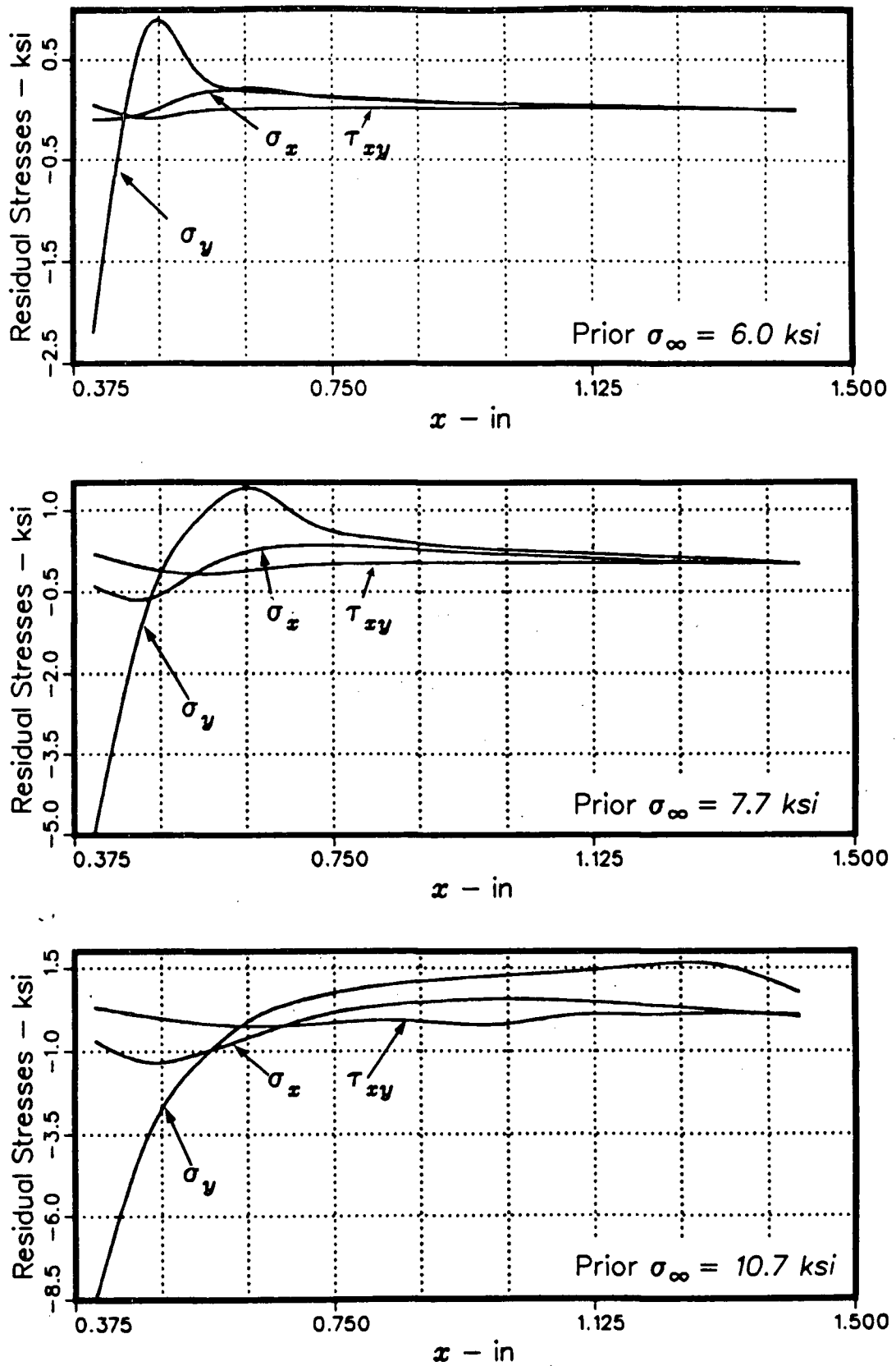
Fig. 5.42 — Distribution of residual stress components along
the net section of a perforated 90-deg layer of
U/D B/Al after unloading from various load levels

$\sigma_\infty = 6.0$ ksi

$\sigma_\infty = 10.0$ ksi

$\sigma_\infty = 15.0$ ksi

$\sigma_\infty = 17.0$ ksi
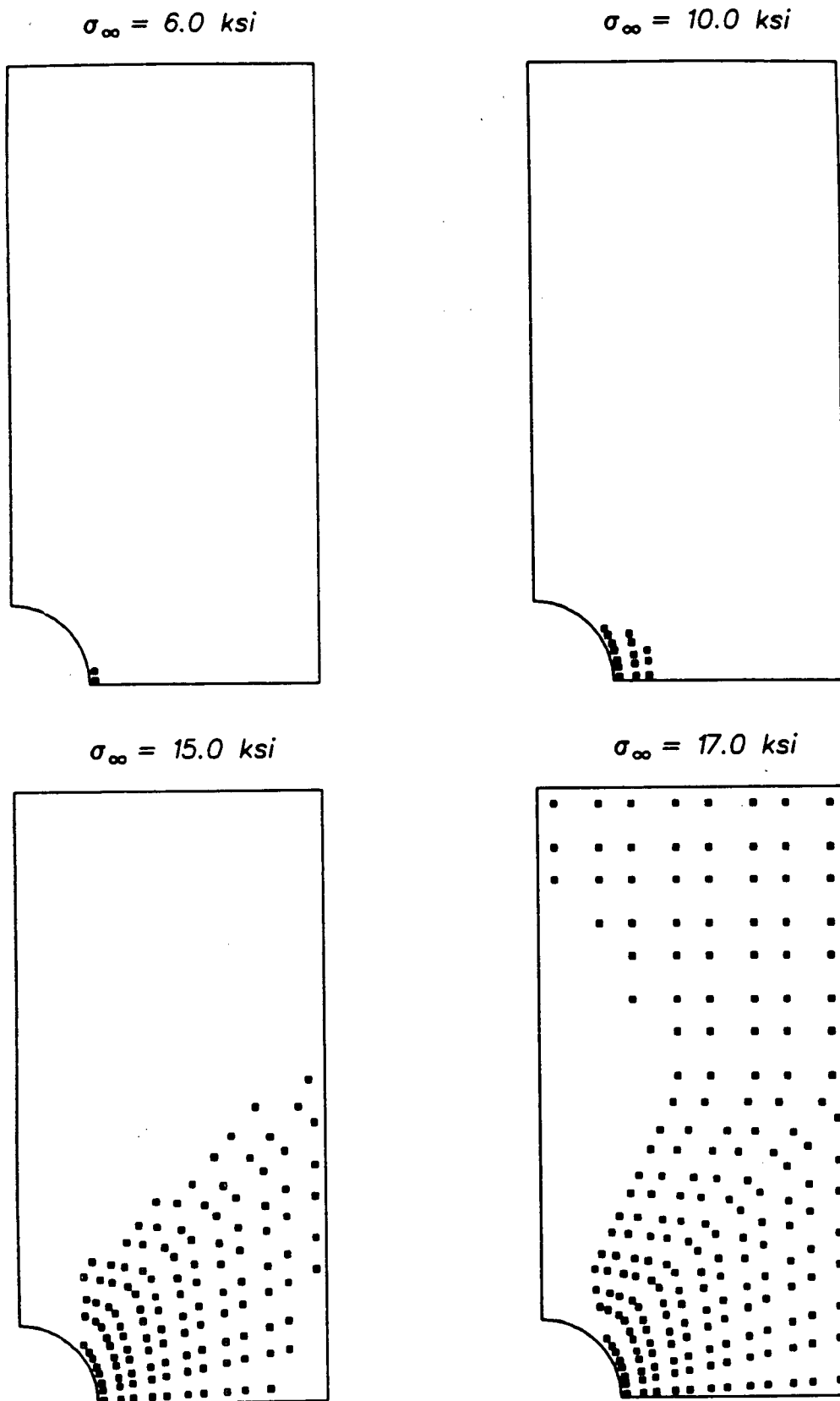
Fig. 5.43 — Development of plastic zones in the 90-deg layer of a perforated [0/90] B/Al laminate subjected to elastoplastic loading
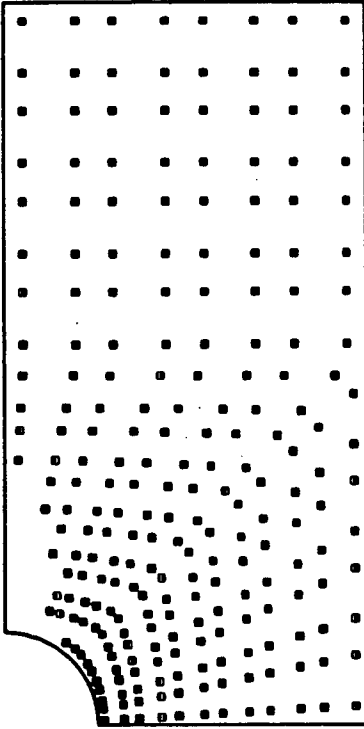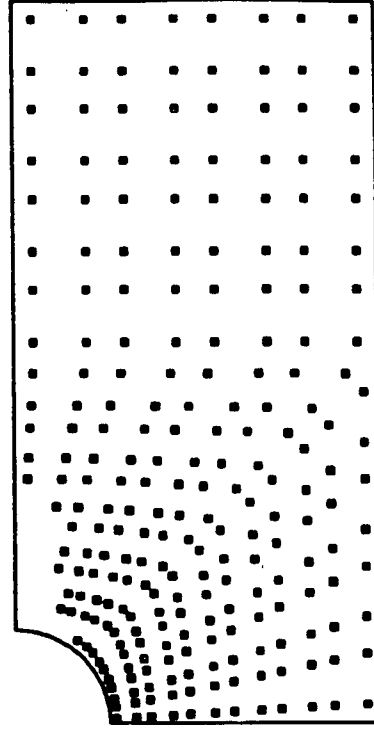
$\sigma_\infty = 25.0$ ksi
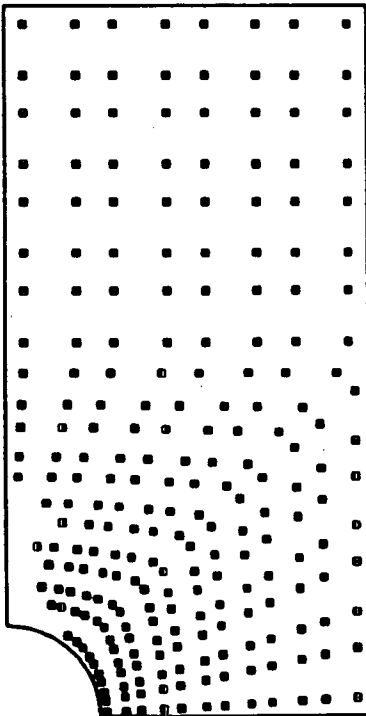
$\sigma_\infty = 30.0$ ksi

$\sigma_\infty = 35.0$ ksi

$\sigma_\infty = 40.0$ ksi

Fig. 5.43 — continued

$\sigma_\infty = 6.0 \ ksi$

$\sigma_\infty = 10.0 \ ksi$

$\sigma_\infty = 15.0 \ ksi$

$\sigma_\infty = 17.0 \ ksi$
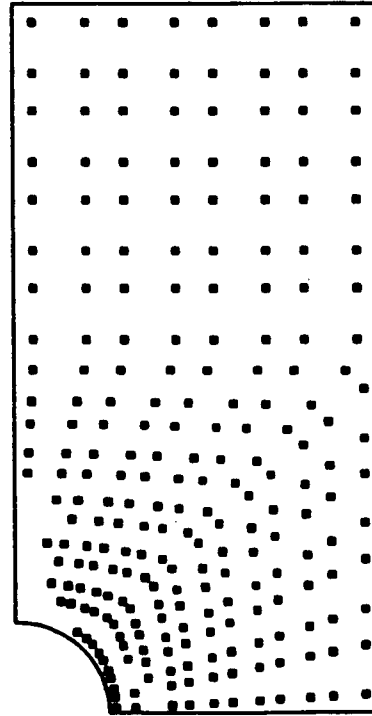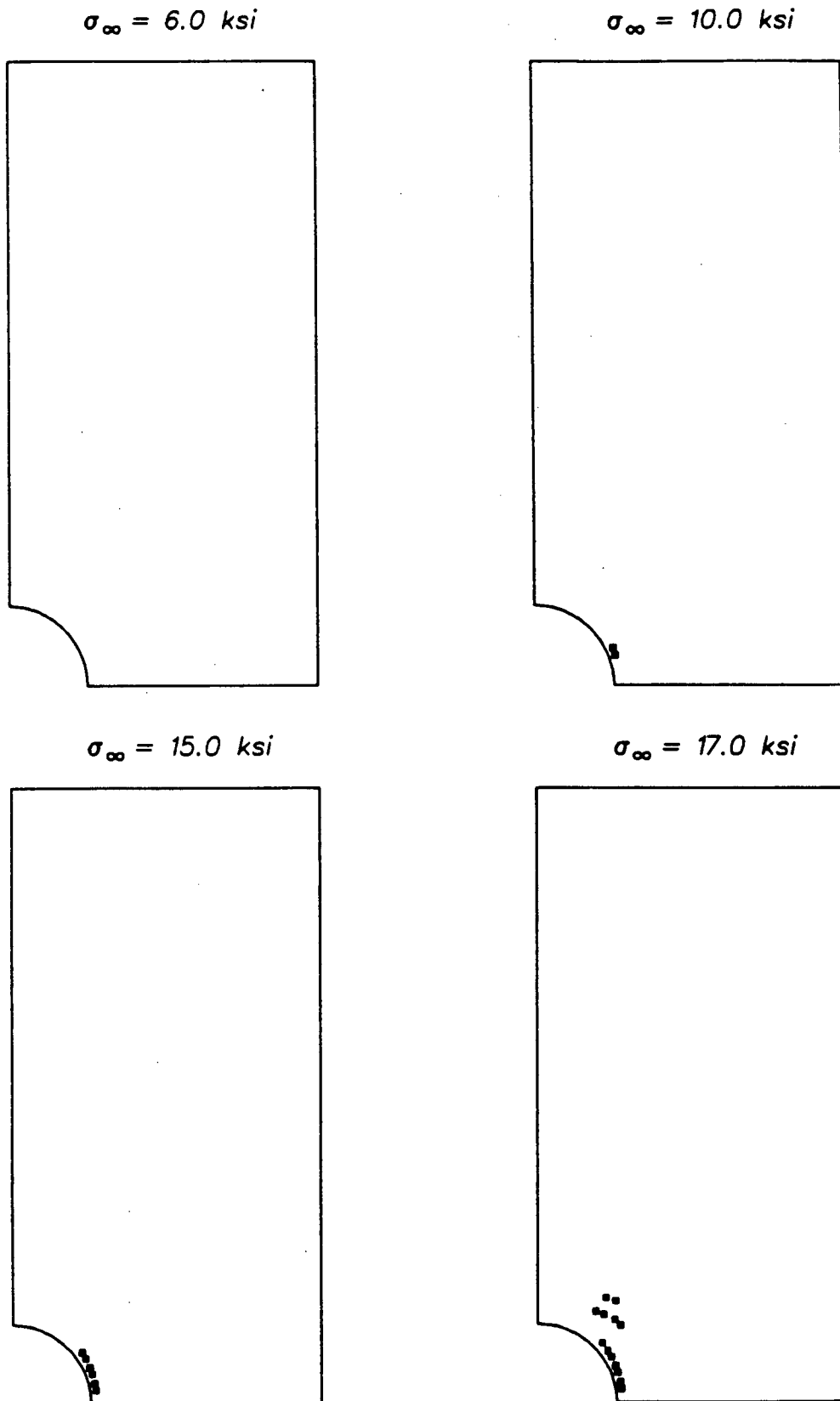
Fig. 5.44 – Development of plastic zones in the 0–deg layer of a perforated [0/90] B/Al laminate subjected to elastoplastic loading
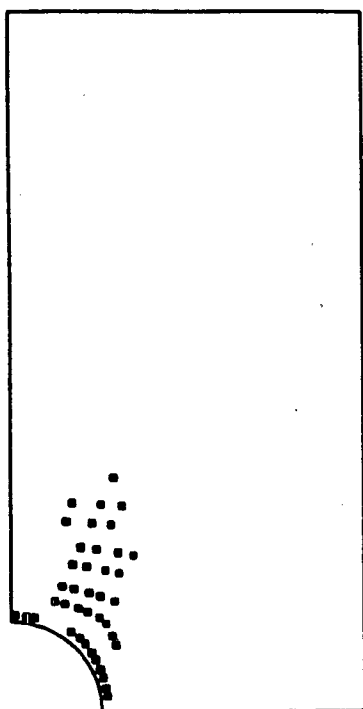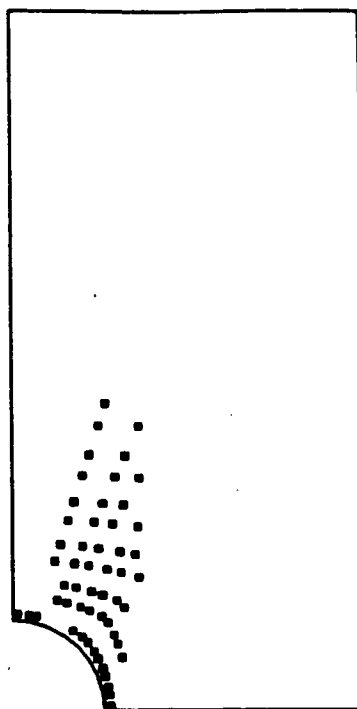
$\sigma_\infty = 25.0 \ ksi$
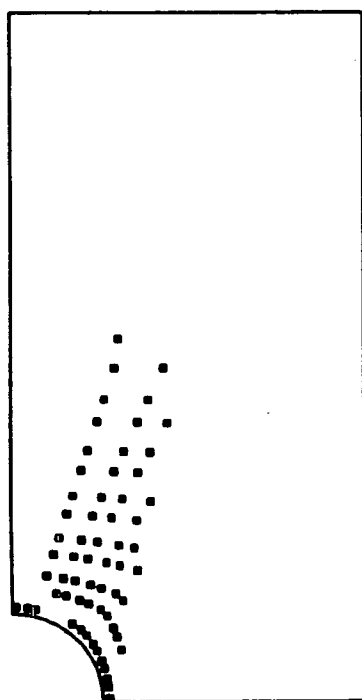
$\sigma_\infty = 30.0 \ ksi$
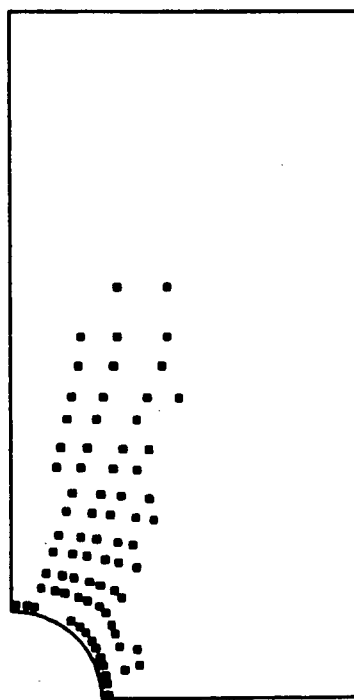
$\sigma_\infty = 35.0 \ ksi$

$\sigma_\infty = 40.0 \ ksi$

Fig. 5.44 — continued
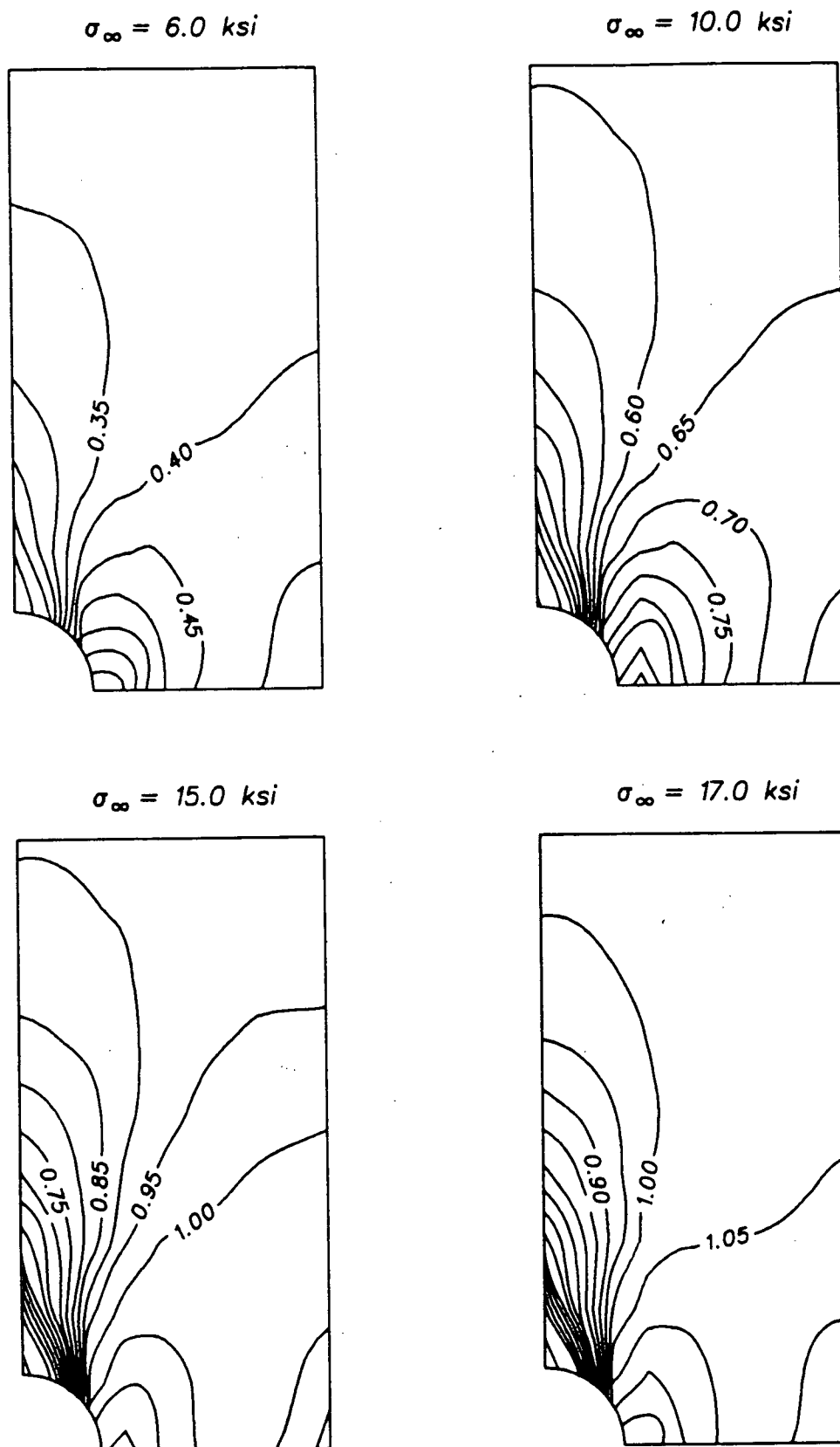
Fig. 5.45 — Nondimensional effective stress contours for the 90-deg layer of a perforated [0/90] B/Al laminate subjected to elastoplastic loading
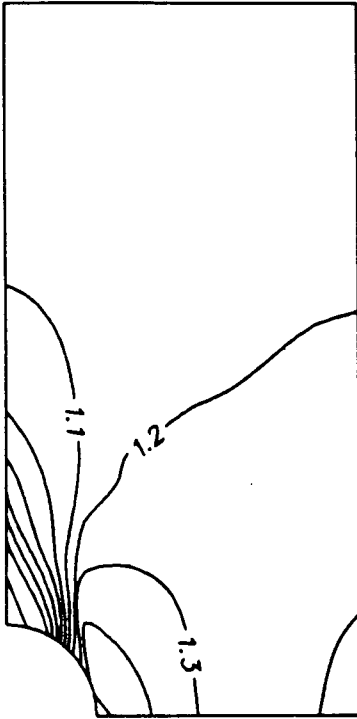
$\sigma_\infty = 25.0 \ ksi$
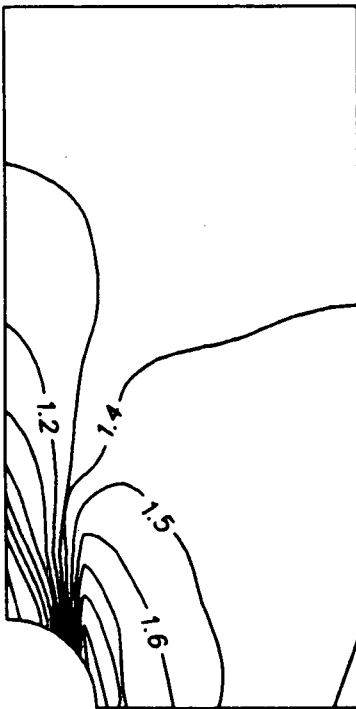
$\sigma_\infty = 30.0 \ ksi$

$\sigma_\infty = 35.0 \ ksi$

$\sigma_\infty = 40.0 \ ksi$

Fig. 5.45 — continued

$\sigma_\infty = 6.0 \ ksi$

$\sigma_\infty = 10.0 \ ksi$

$\sigma_\infty = 15.0 \ ksi$

$\sigma_\infty = 17.0 \ ksi$
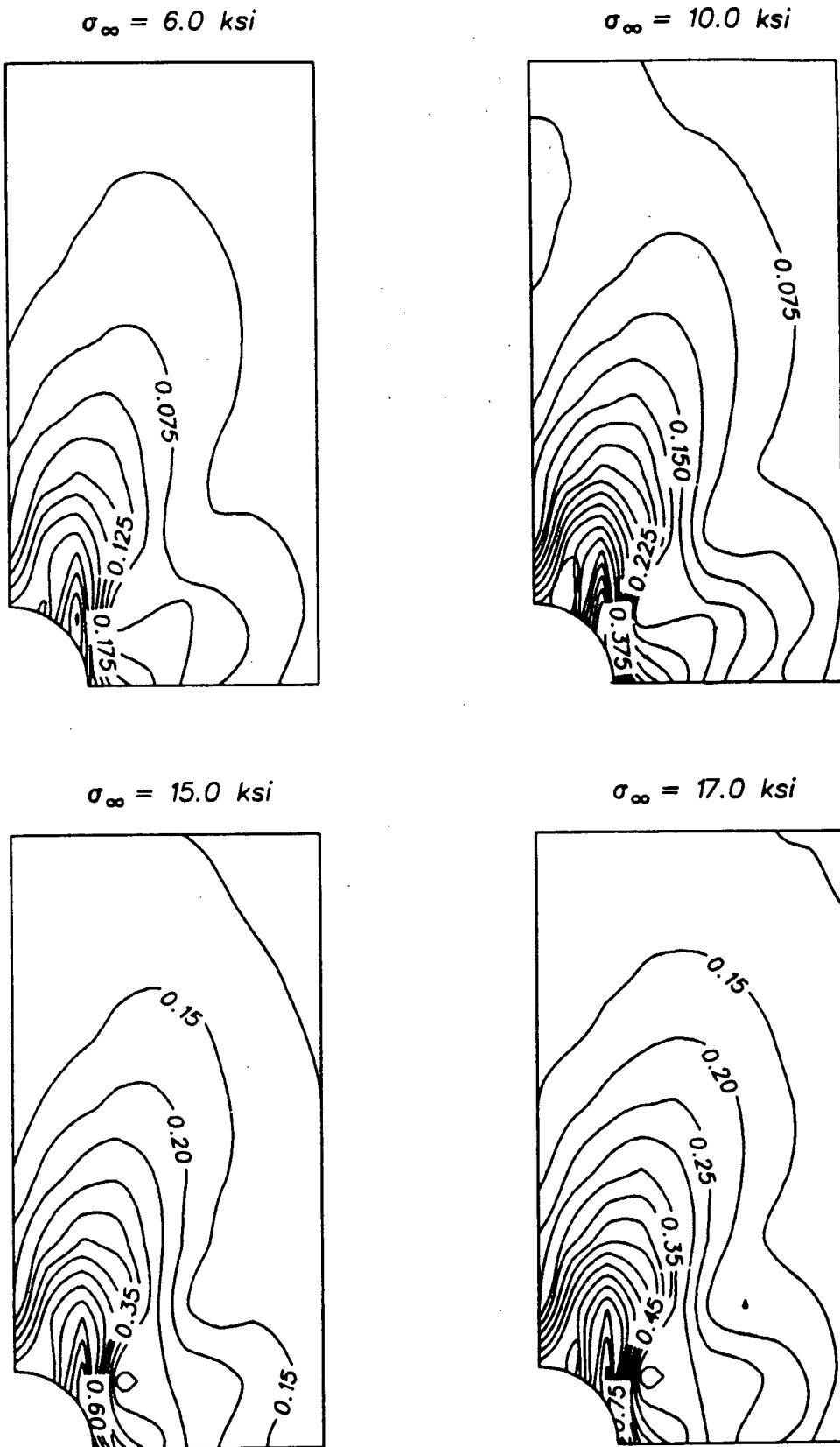
Fig. 5.46 — Nondimensional effective stress contours for the 0–deg layer of a perforated [0/90] B/Al laminate subjected to elastoplastic loading
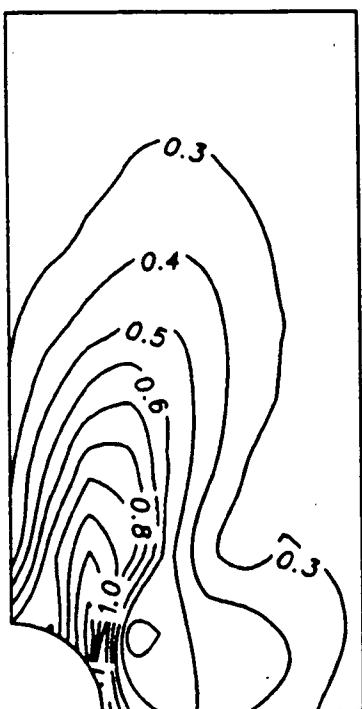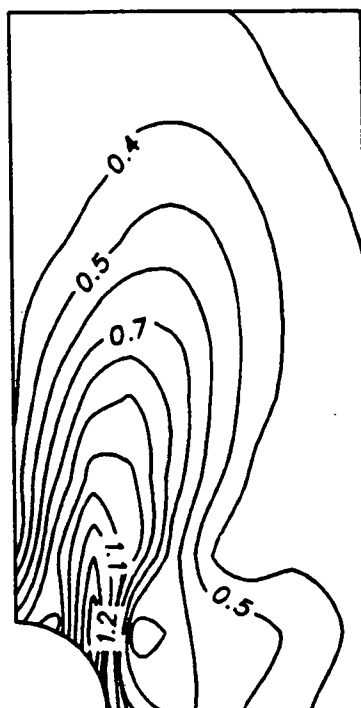
$\sigma_\infty = 25.0\ ksi$

$\sigma_\infty = 30.0\ ksi$

$\sigma_\infty = 35.0\ ksi$
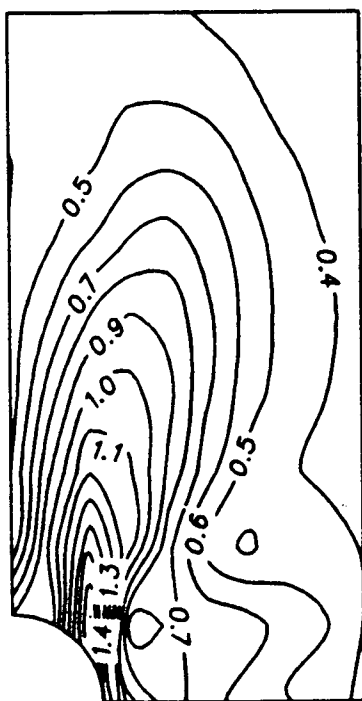
$\sigma_\infty = 40.0\ ksi$
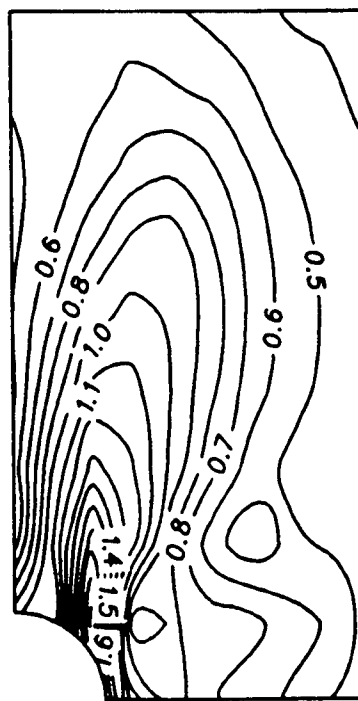
Fig. 5.46 — continued
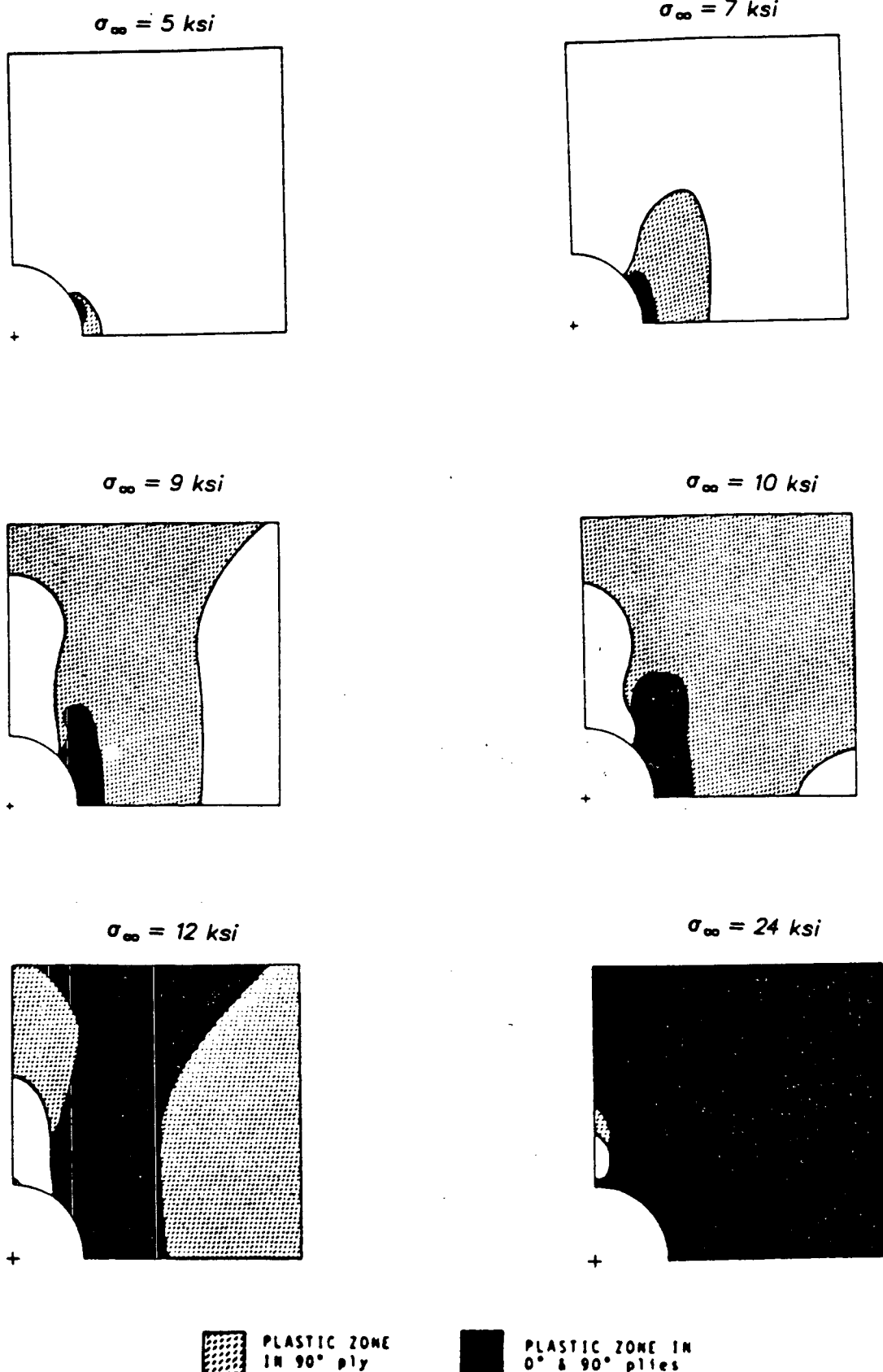
Fig. 5.47 — Development of plastic zones in a [0/90] Fp/Al laminate with a hole [Bahaei-El-Din and Dvorak, 1980]
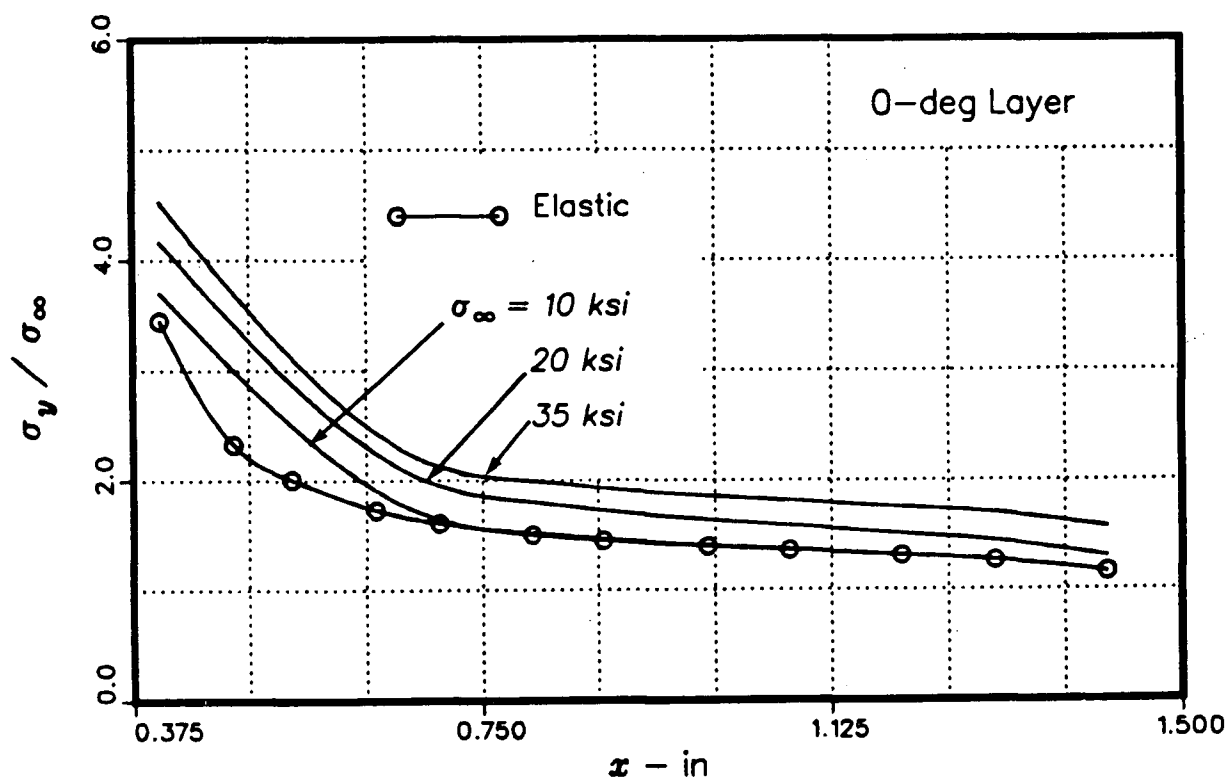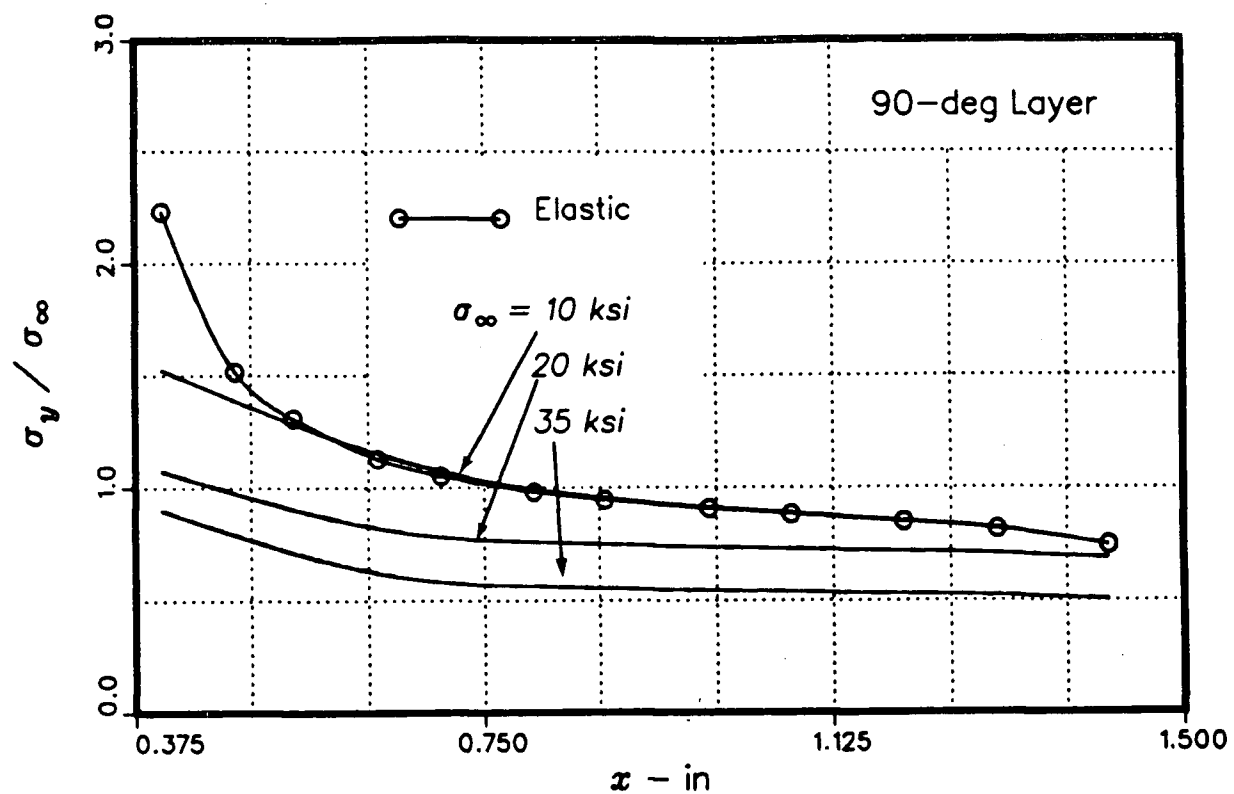
Fig. 5.48 — Longitudinal stress distribution along the net section for each
layer of a perforated [0/90] B/Al laminate
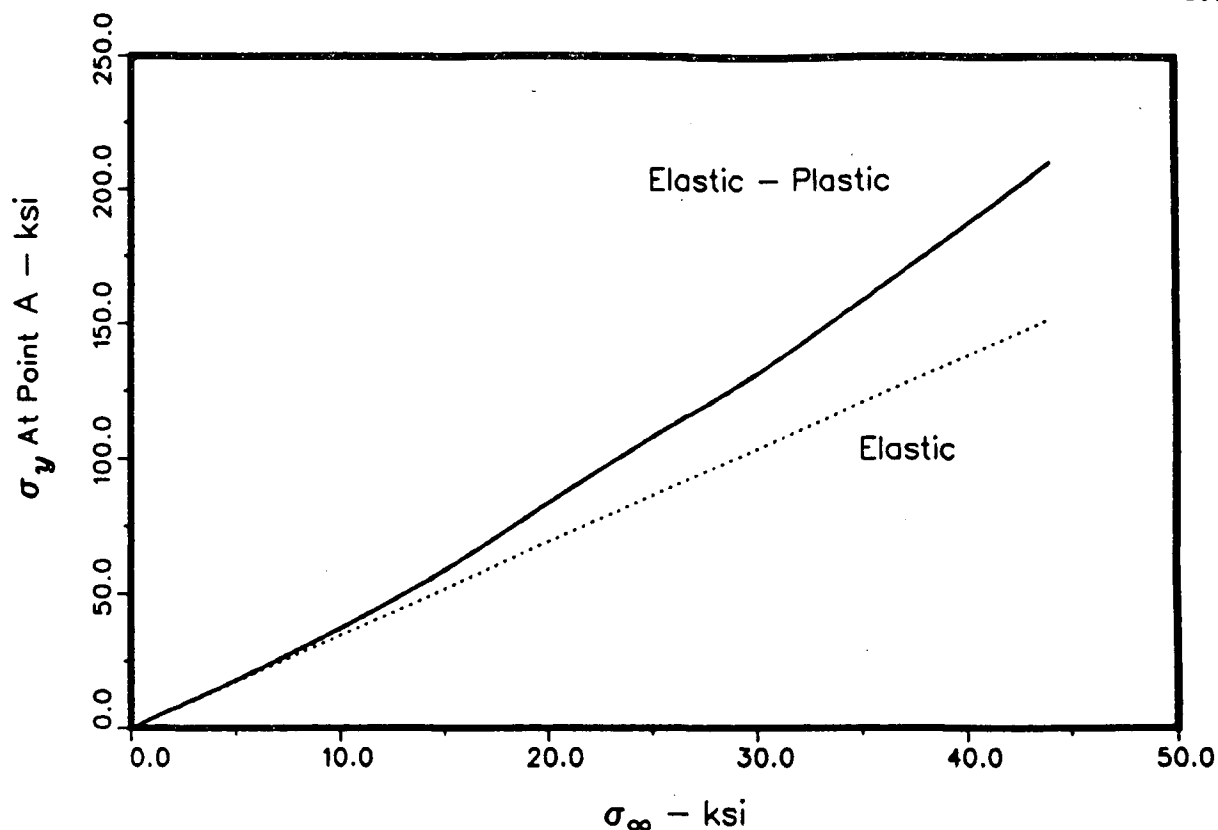
Fig. 5.49 — Longitudinal stress at point A versus the applied load for the 0 deg
layer of a perforated [0/90] B/Al laminate
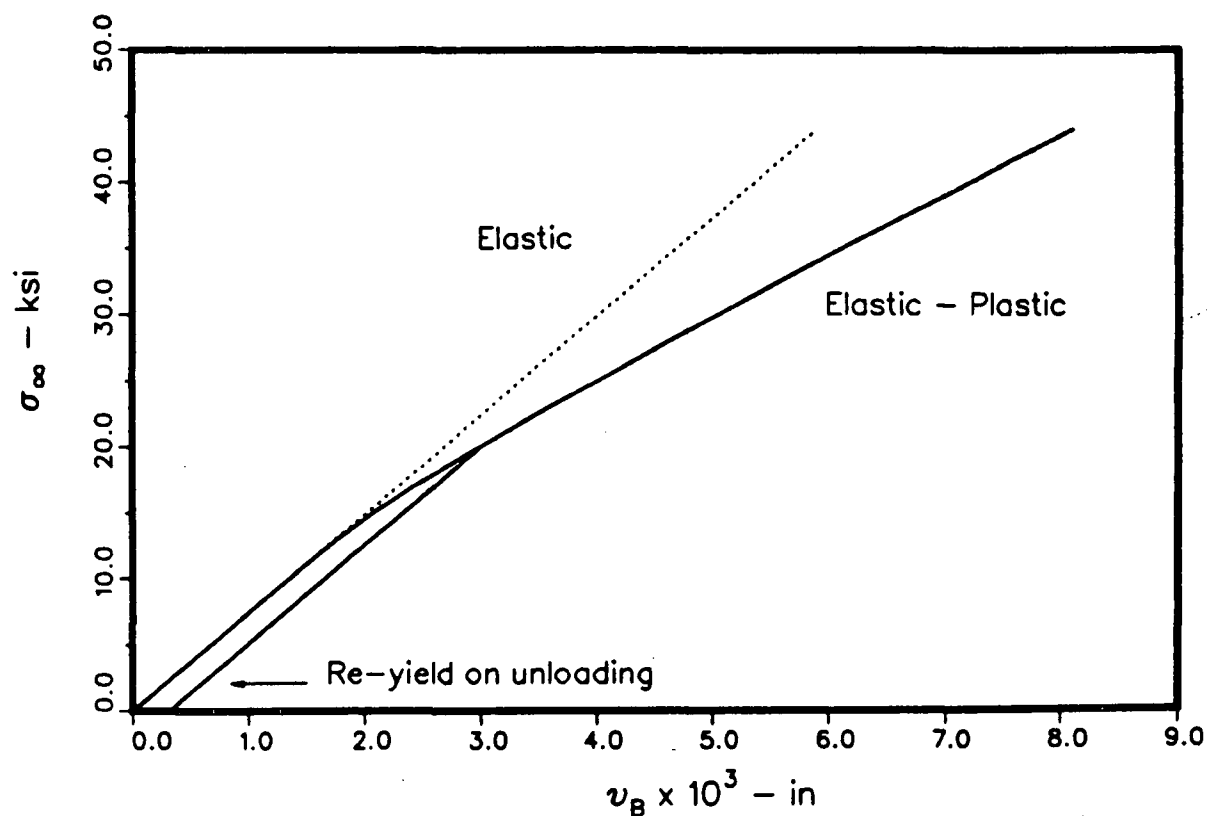
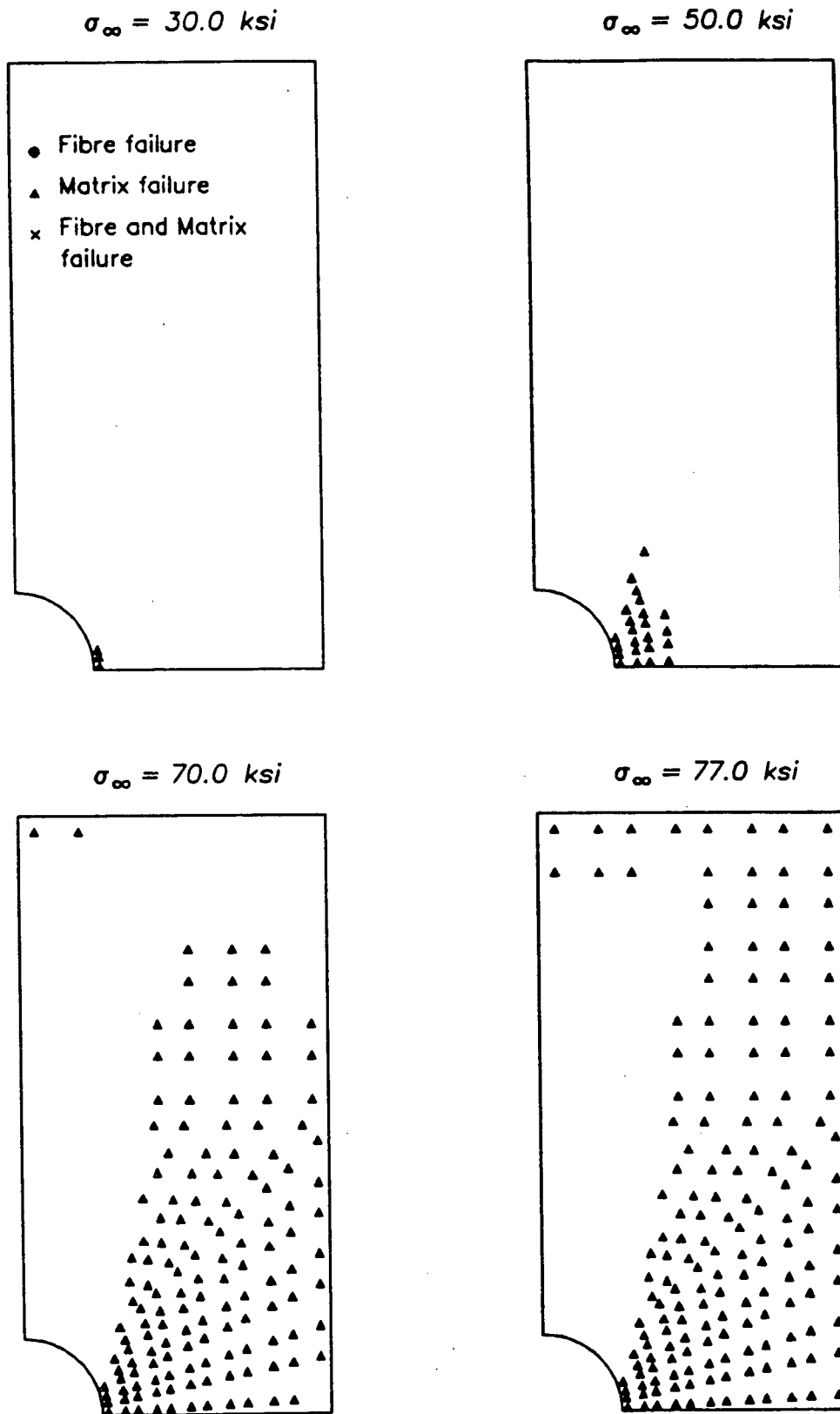Fig. 5.50 — Load versus deflection at point B for a perforated [0/90] B/Al
laminate
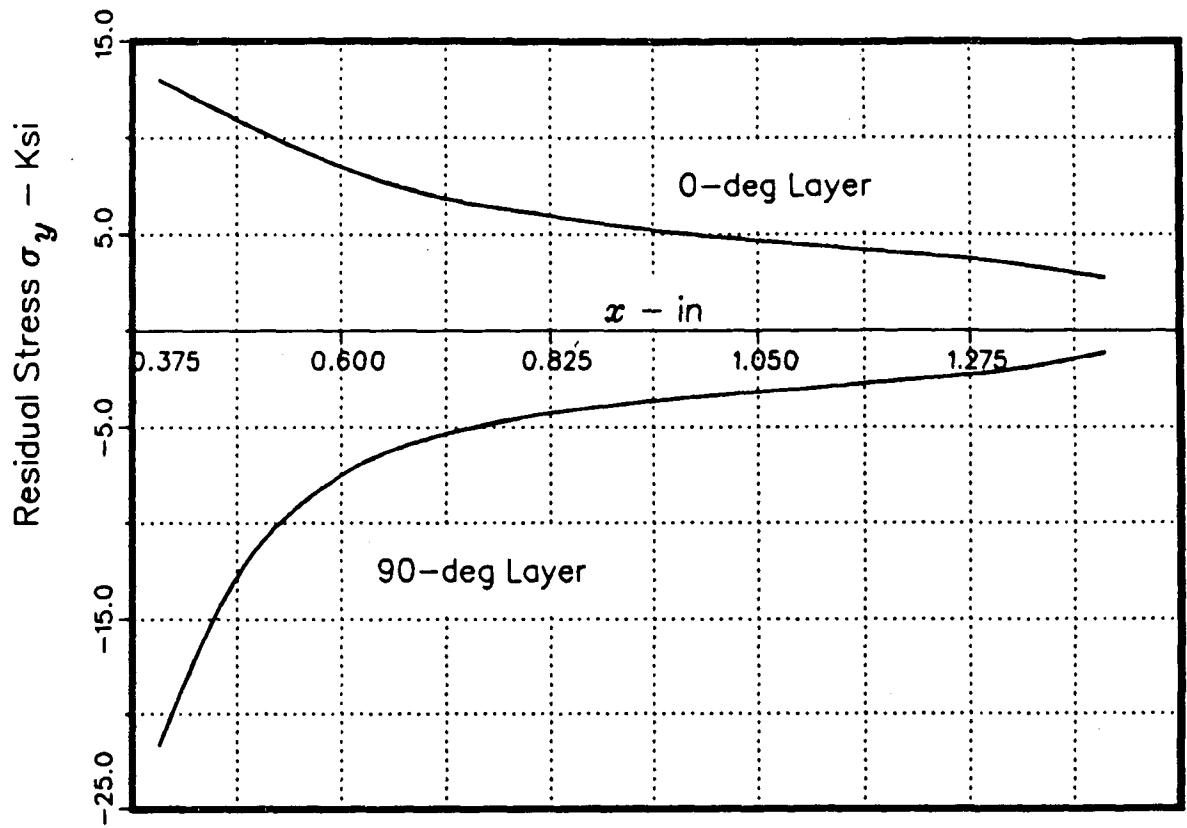
Fig. 5.51 — Longitudinal residual stress distribution along the net section for each layer of a perforated [0/90] B/Al laminate due to unloading from $\sigma_\infty = 20$ ksi

$\sigma_\infty = 4.0\ ksi$

$\sigma_\infty = 6.0\ ksi$

- • Fibre failure
- ▲ Matrix failure
- × Fibre and Matrix failure

$\sigma_\infty = 6.5\ ksi$

$\sigma_\infty = 7.0\ ksi$
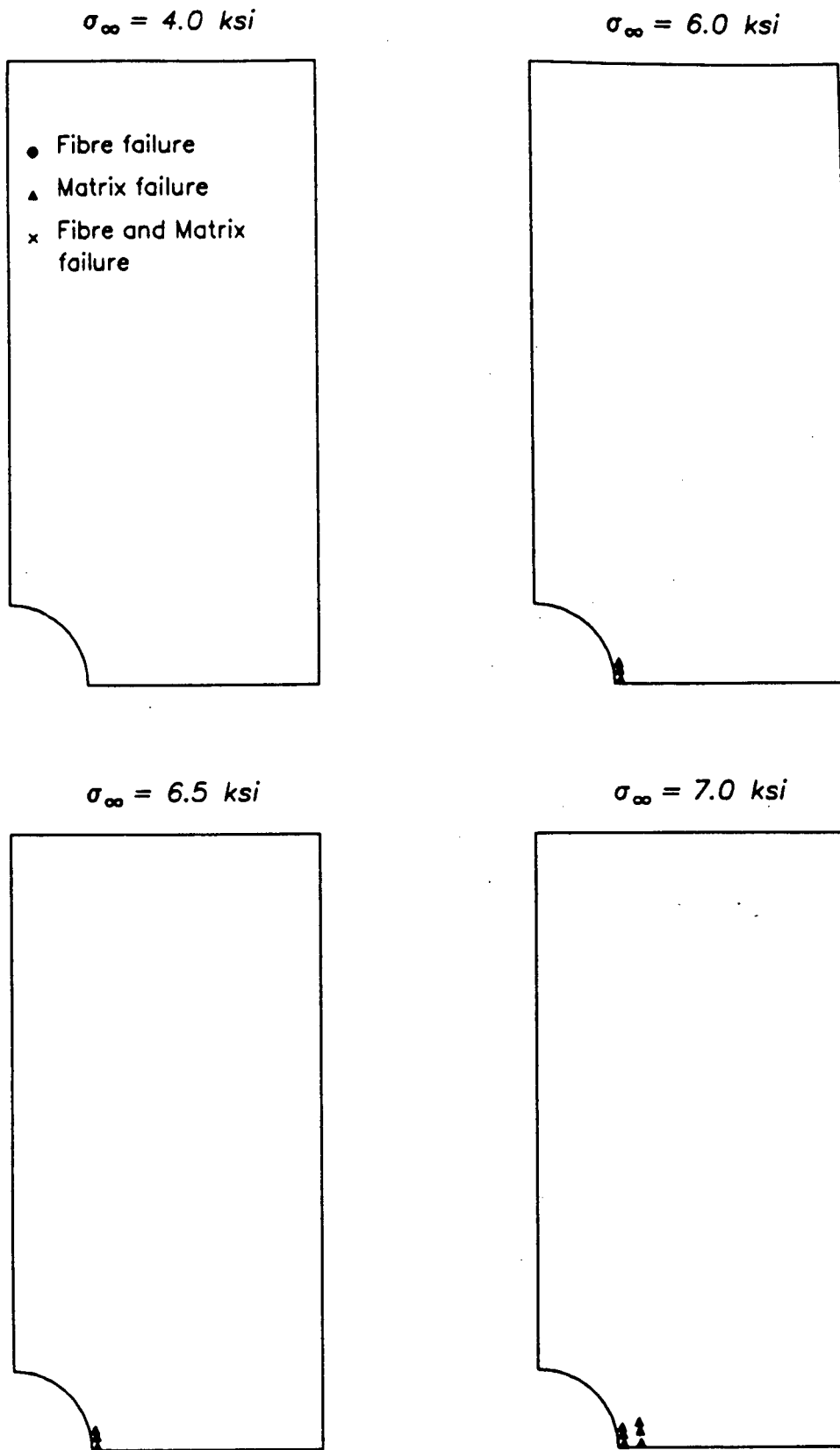
Fig. 5.52 – Predicted damage progression for a perforated 90–deg U/D B/Ep layer – Ductile Matrix

$\sigma_\infty = 55.0\ ksi$

$\sigma_\infty = 60.0\ ksi$

- Fibre failure
▲ Matrix failure
× Fibre and Matrix failure

$\sigma_\infty = 65.0\ ksi$

$\sigma_\infty = 70.0\ ksi$
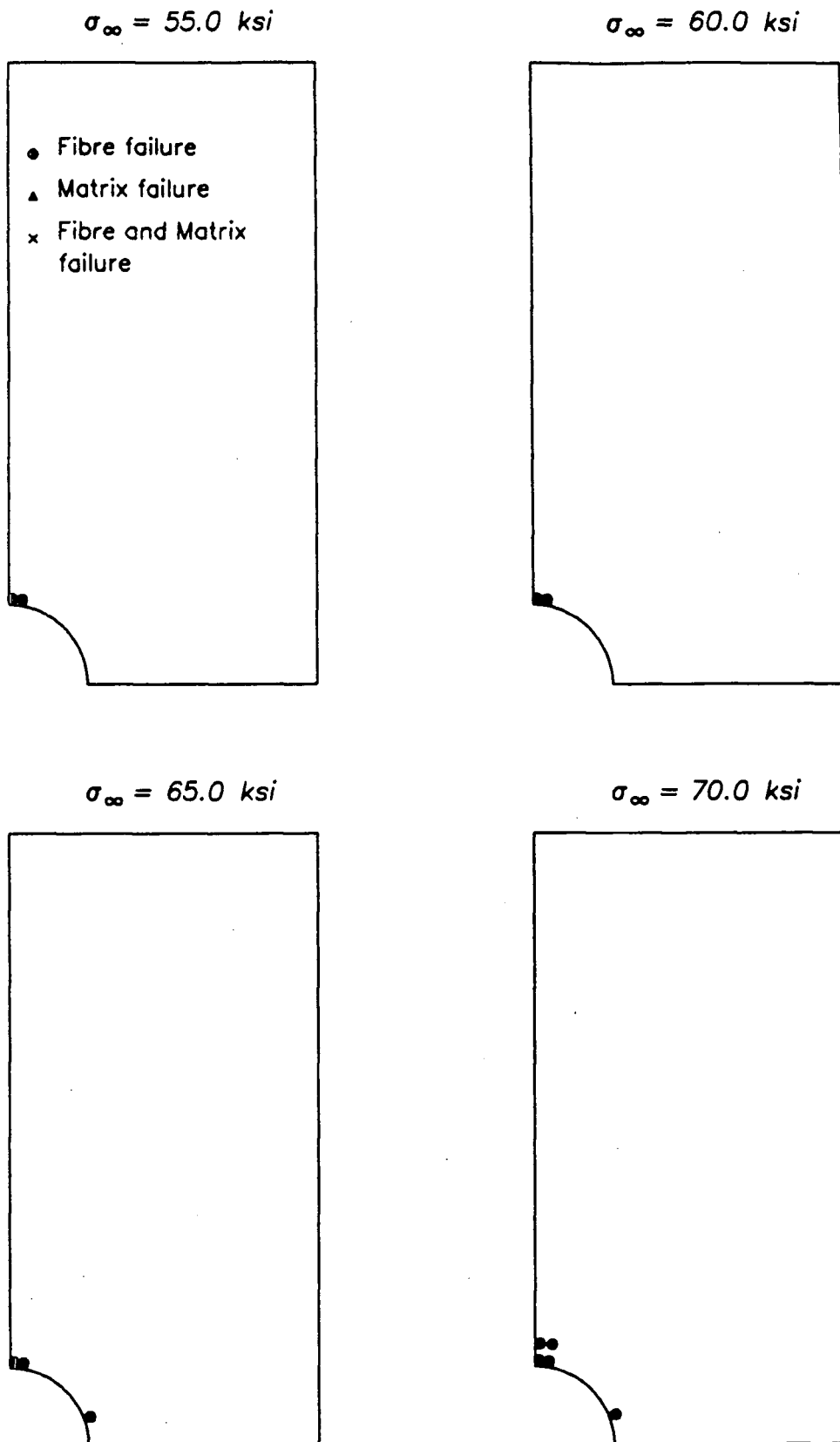
Fig. 5.53 – Predicted damage progression for a perforated 0-deg
U/D B/Ep layer – Ductile Fibre
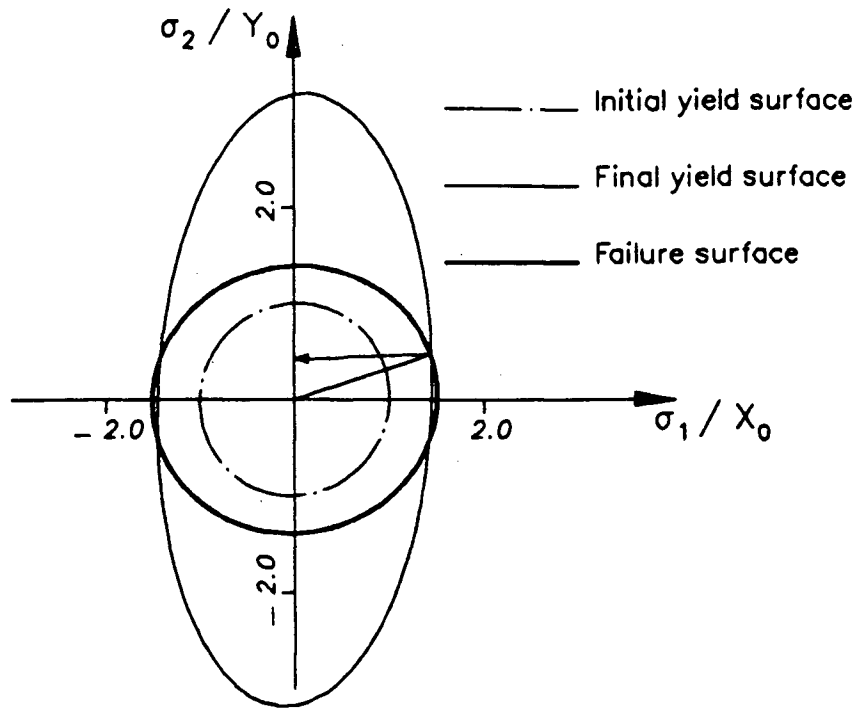
Fig. 5.54 — Stress path at point A for the 0-deg layer of
a perforated [0/90] B/Ep laminate
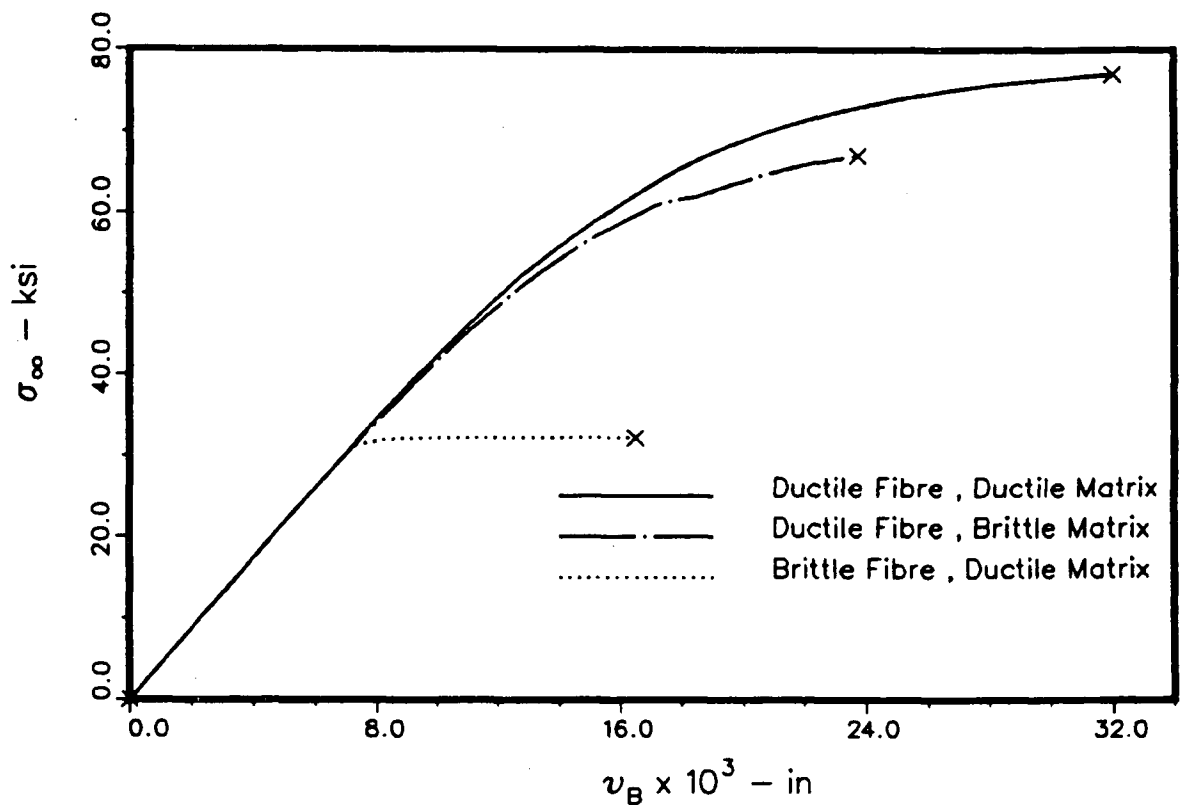
Fig. 5.55 — Load versus deflection at point B for a perforated [0/90]
B/Ep laminate

$\sigma_\infty = 30.0 \ ksi$

$\sigma_\infty = 50.0 \ ksi$

$\sigma_\infty = 70.0 \ ksi$

$\sigma_\infty = 77.0 \ ksi$

• Fibre failure

▲ Matrix failure

× Fibre and Matrix failure

Fig. 5.56 a − Predicted damage progression for the 90−deg layer of a [0/90] B/Ep laminate − Ductile Fibre and Ductile Matrix
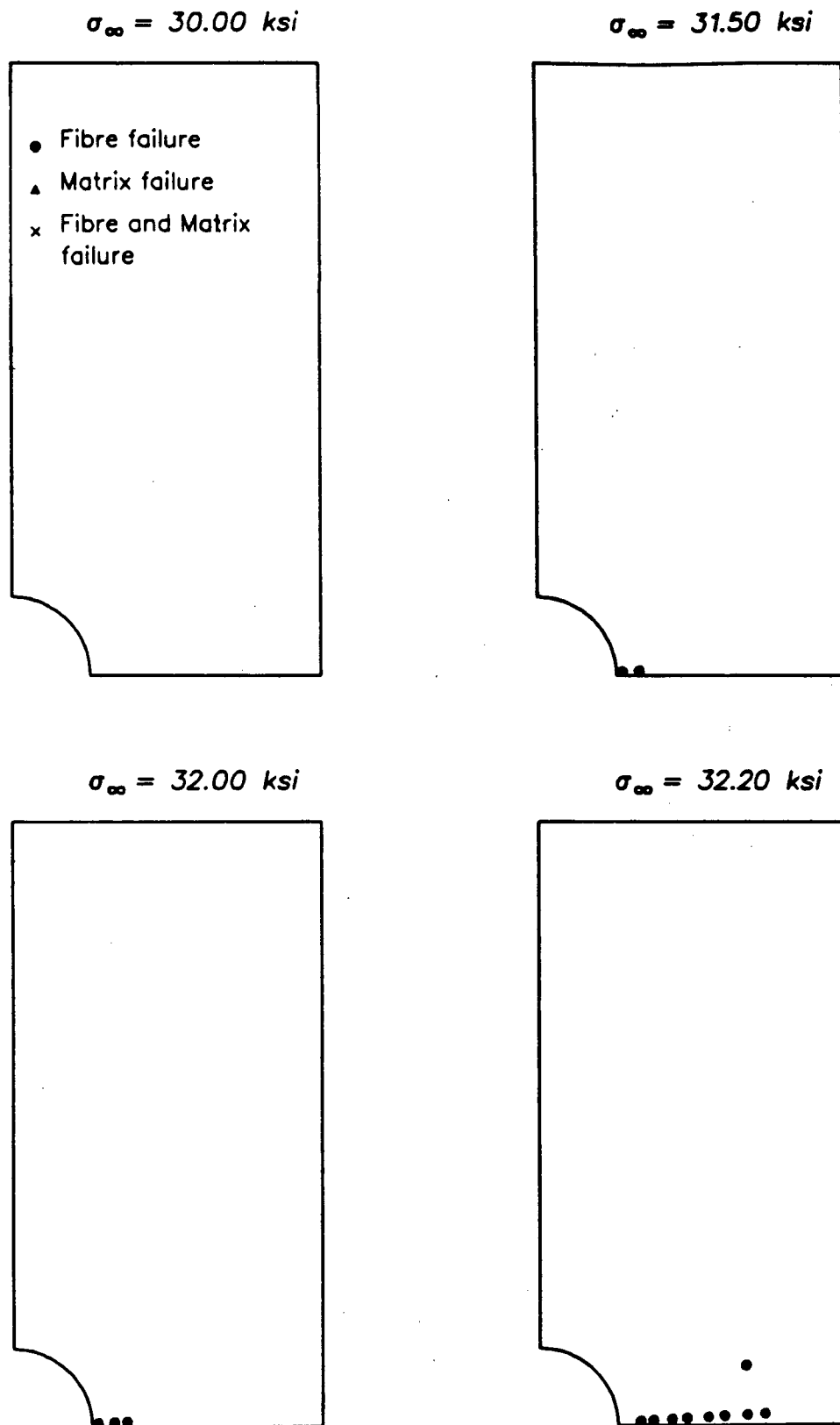
215

Fig. 5.56 b — Predicted damage progression for the 0-deg layer of a [0/90] B/Ep laminate — Ductile Fibre and Ductile Matrix

$\sigma_\infty = 30.0 \ ksi$

$\sigma_\infty = 50.0 \ ksi$

- Fibre failure
▲ Matrix failure
× Fibre and Matrix failure

$\sigma_\infty = 62.0 \ ksi$

$\sigma_\infty = 67.0 \ ksi$
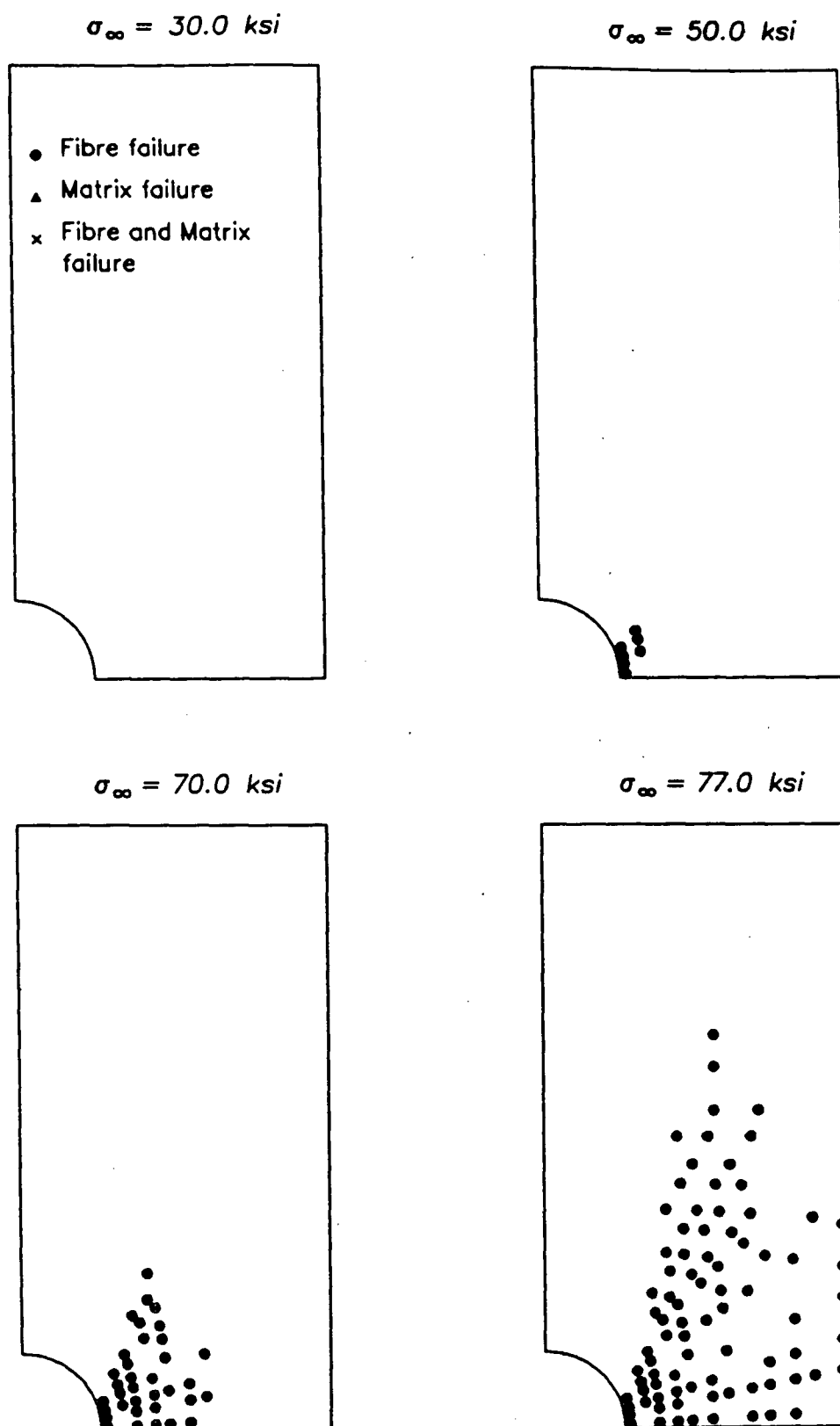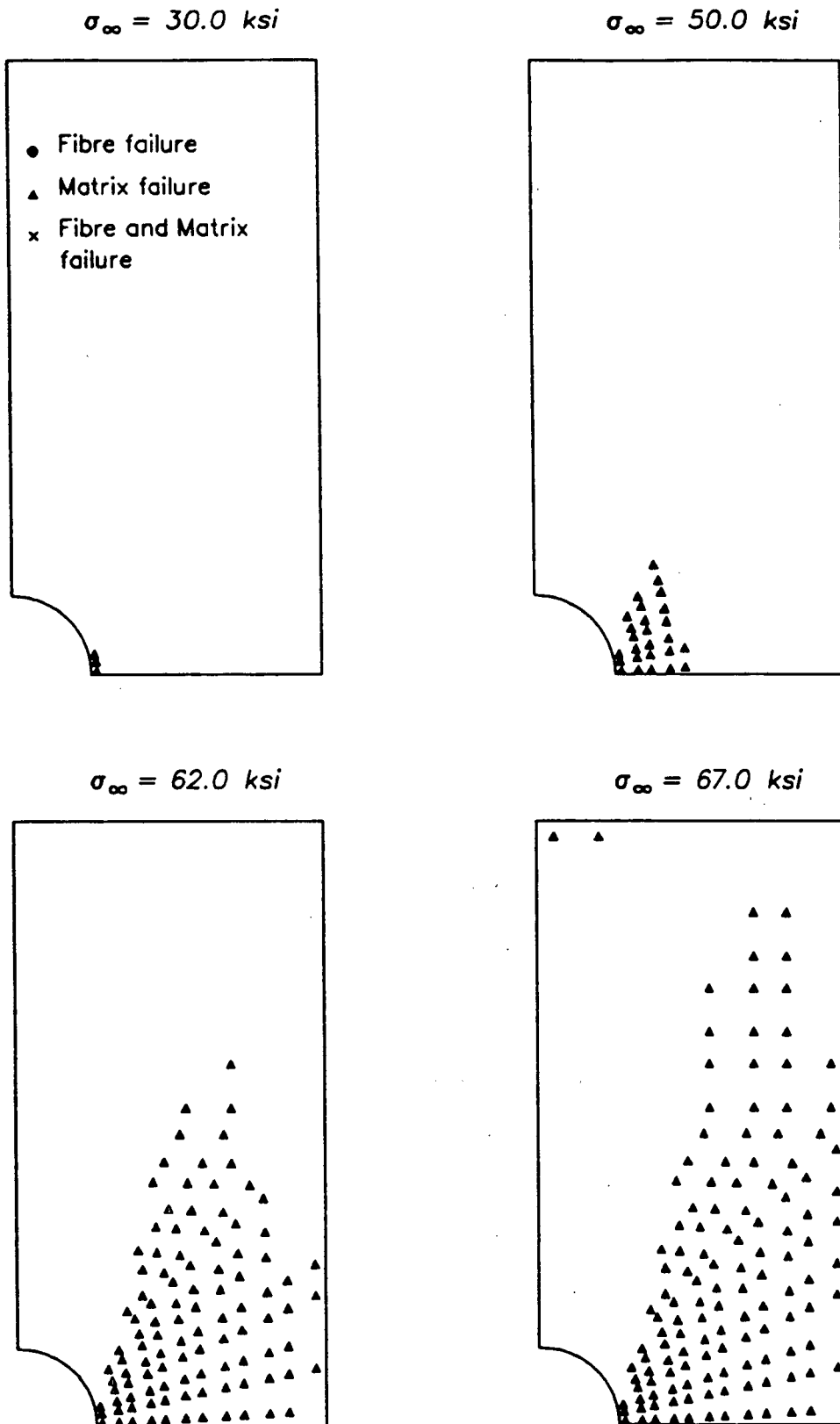
Fig. 5.57 a — Predicted damage progression for the 90—deg layer of a [0/90] B/Ep laminate — Ductile Fibre and Brittle Matrix

$\sigma_\infty = 30.0\ ksi$

$\sigma_\infty = 50.0\ ksi$

- Fibre failure
- Matrix failure
- x Fibre and Matrix failure

$\sigma_\infty = 62.0\ ksi$

$\sigma_\infty = 67.0\ ksi$
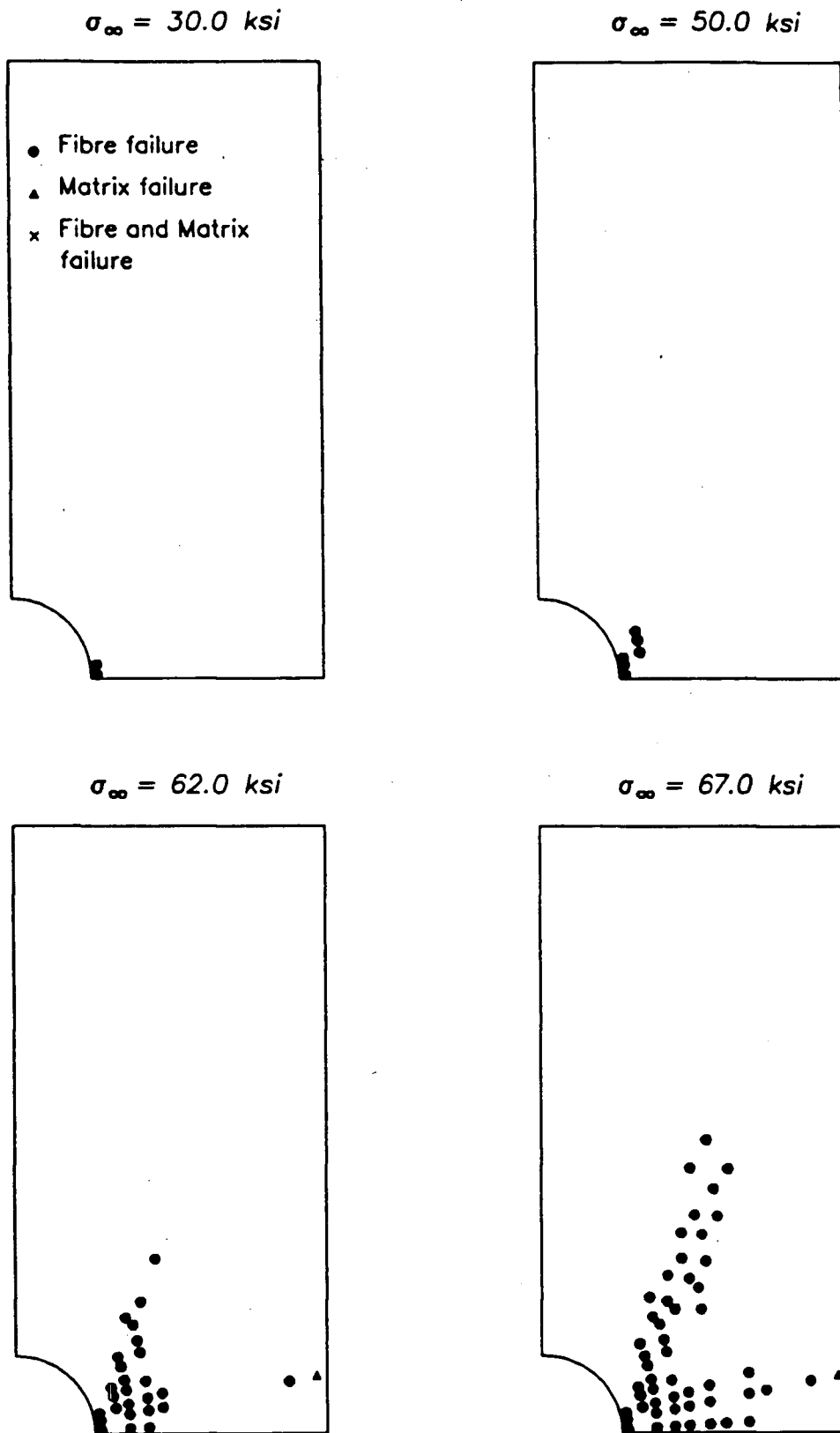
Fig. 5.57 b — Predicted damage progression for the 0−deg layer of a [0/90] B/Ep laminate — Ductile Fibre and Brittle Matrix

$\sigma_\infty = 30.00$ ksi

$\sigma_\infty = 31.50$ ksi

- Fibre failure
- ▲ Matrix failure
- × Fibre and Matrix failure

$\sigma_\infty = 32.00$ ksi

$\sigma_\infty = 32.20$ ksi
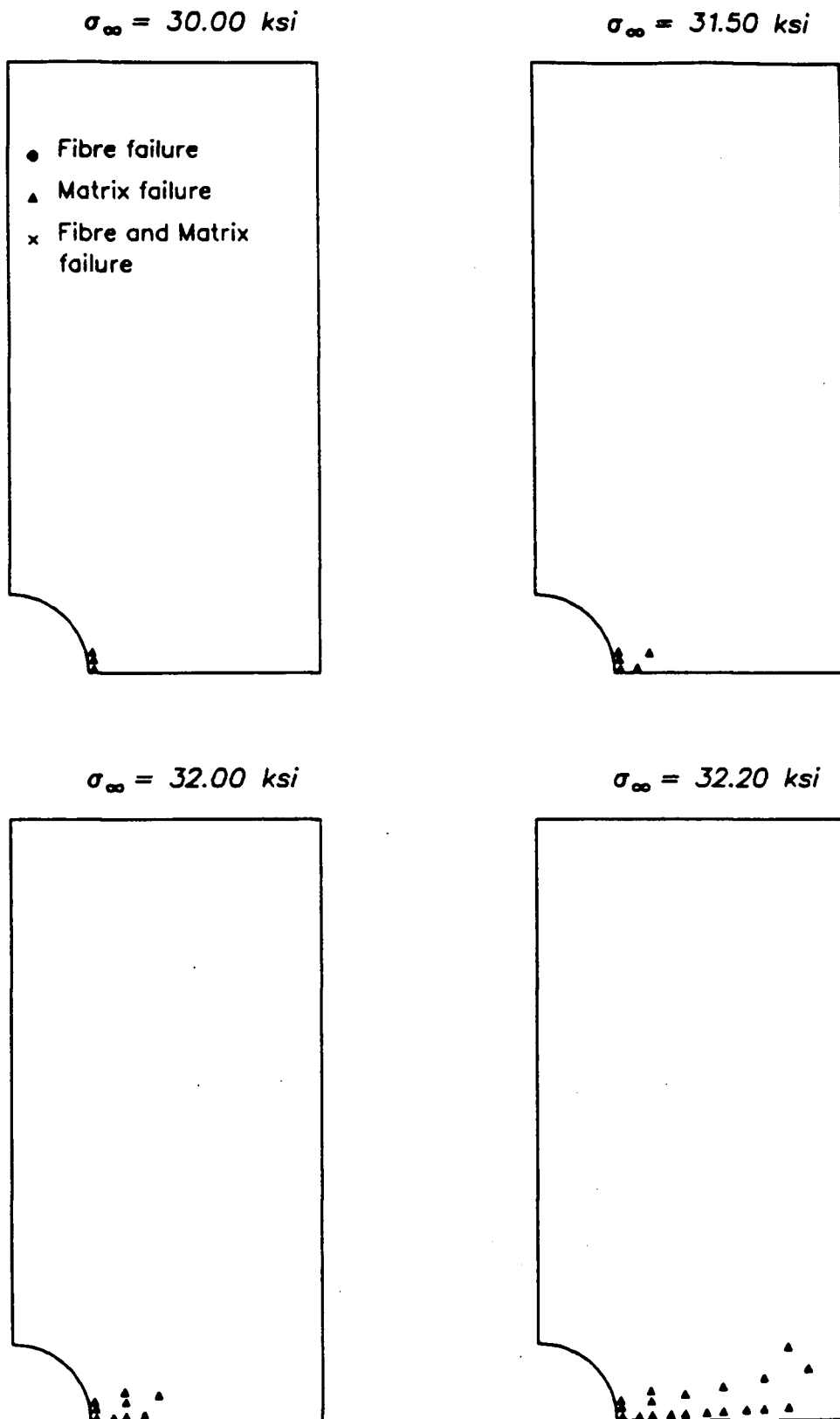
Fig. 5.58 a — Predicted damage progression for the 90-deg layer of a [0/90] B/Ep laminate — Brittle Fibre and Ductile Matrix

$\sigma_\infty = 30.00 \ ksi$

$\sigma_\infty = 31.50 \ ksi$

• Fibre failure

▲ Matrix failure

× Fibre and Matrix failure

$\sigma_\infty = 32.00 \ ksi$

$\sigma_\infty = 32.20 \ ksi$

Fig. 5.58 b — Predicted damage progression for the 0—deg layer of a [0/90] B/Ep laminate — Brittle Fibre and Ductile Matrix
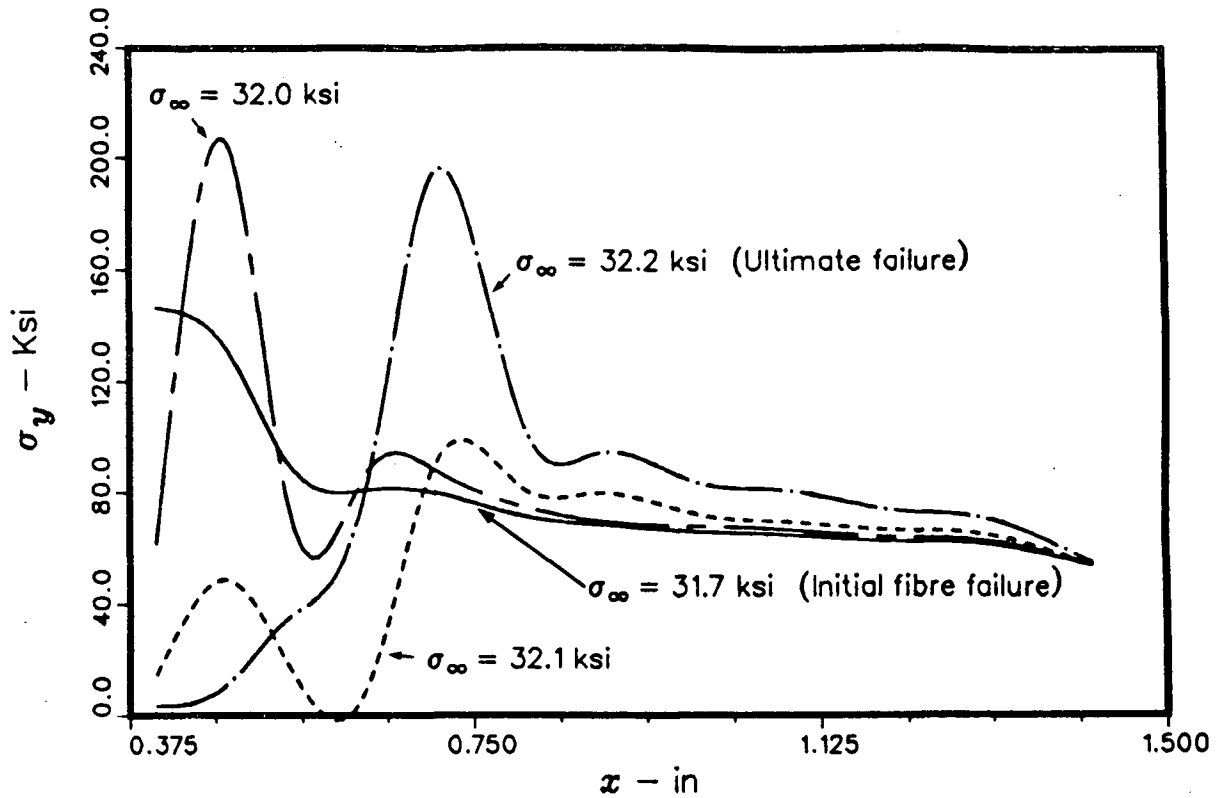
Fig. 5.59 — Change in stress distribution along the net section during the process of brittle fibre failure in the 0–deg layer of a perforated [0/90] B/Ep laminate
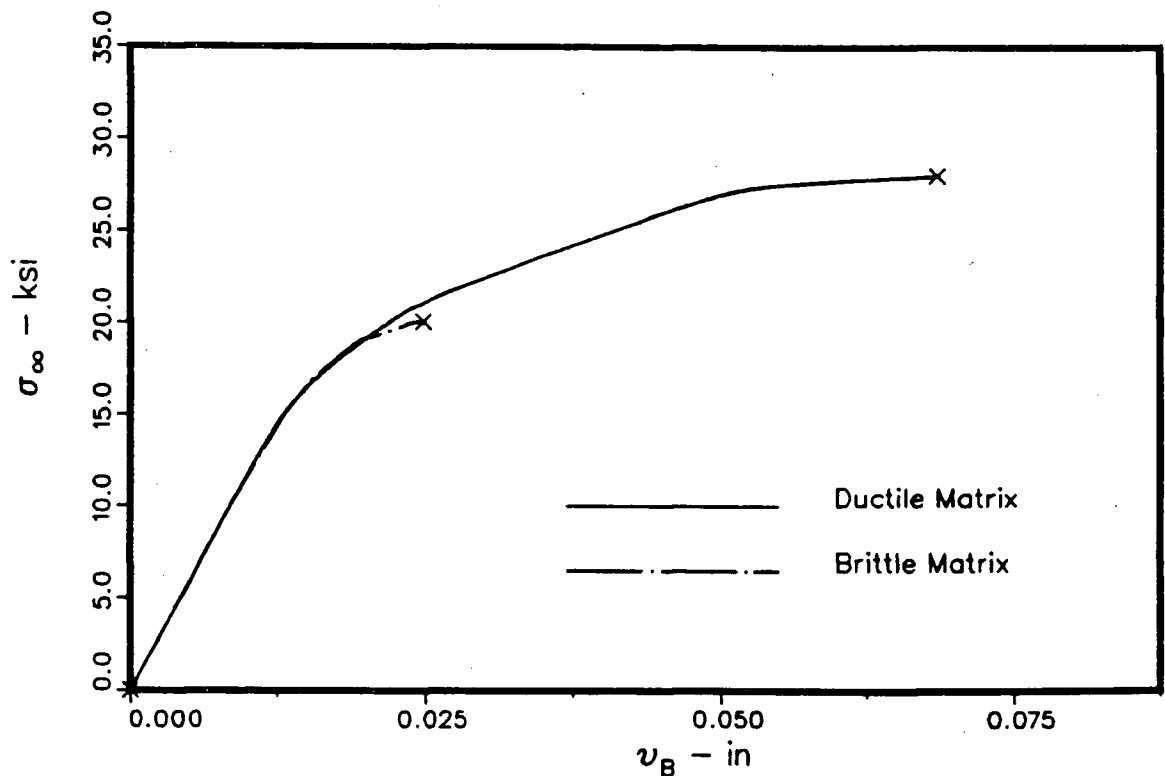
Fig. 5.60 — Load versus deflection at point B for a perforated [45/−45] B/Ep laminate

$\sigma_{\infty} = 21.0 \ ksi$

$\sigma_{\infty} = 26.0 \ ksi$

- • Fibre failure
- ▲ Matrix failure
- × Fibre and Matrix failure

$\sigma_{\infty} = 28.0 \ ksi$

$\sigma_{\infty} = 29.5 \ ksi$
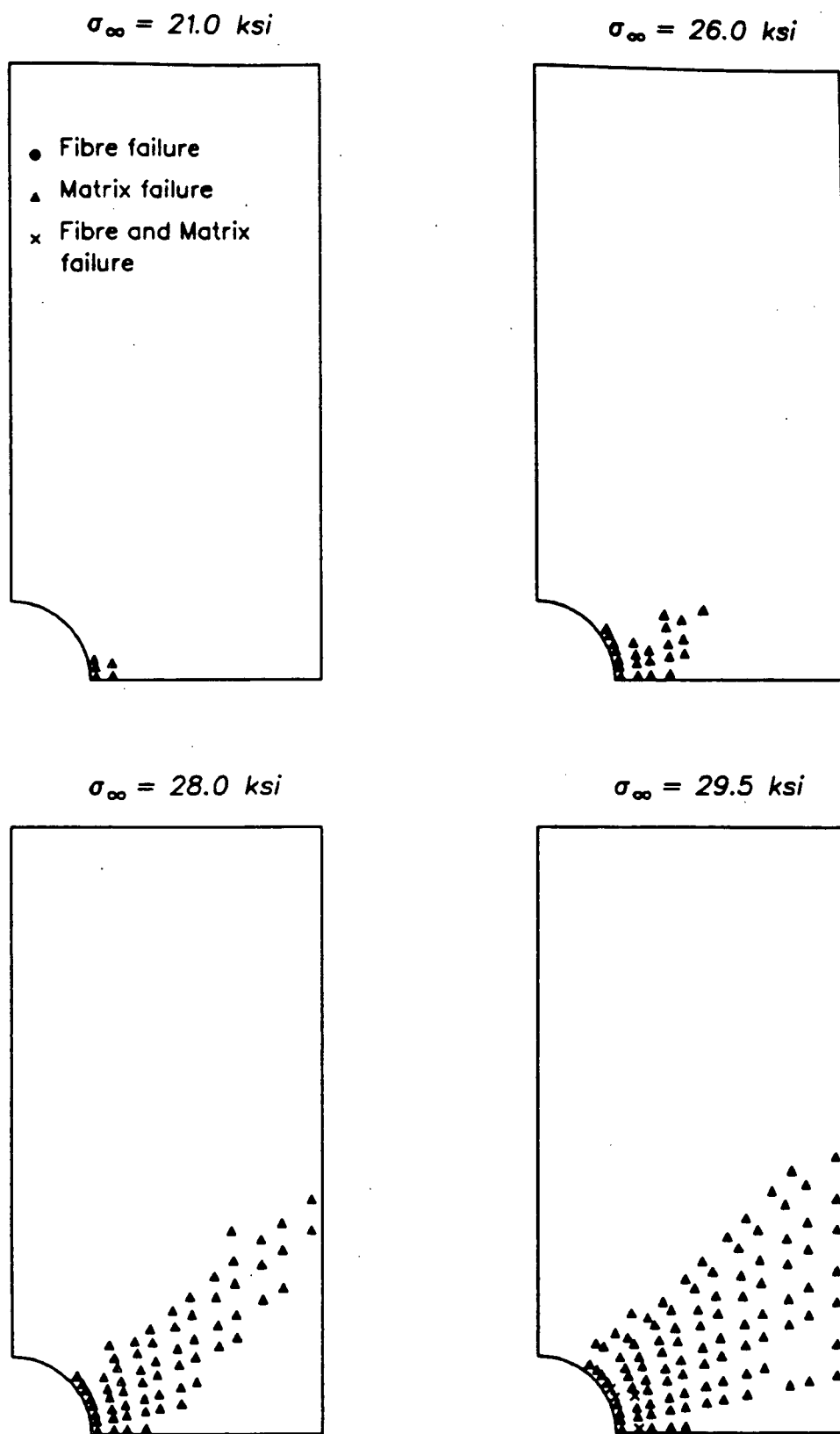
Fig. 5.61 a — Predicted damage progression for the +45-deg layer of a [45/-45] B/Ep laminate — Ductile Matrix

$\sigma_\infty = 21.0 \ ksi$

$\sigma_\infty = 26.0 \ ksi$

- Fibre failure
▲ Matrix failure
× Fibre and Matrix failure

$\sigma_\infty = 28.0 \ ksi$

$\sigma_\infty = 29.5 \ ksi$
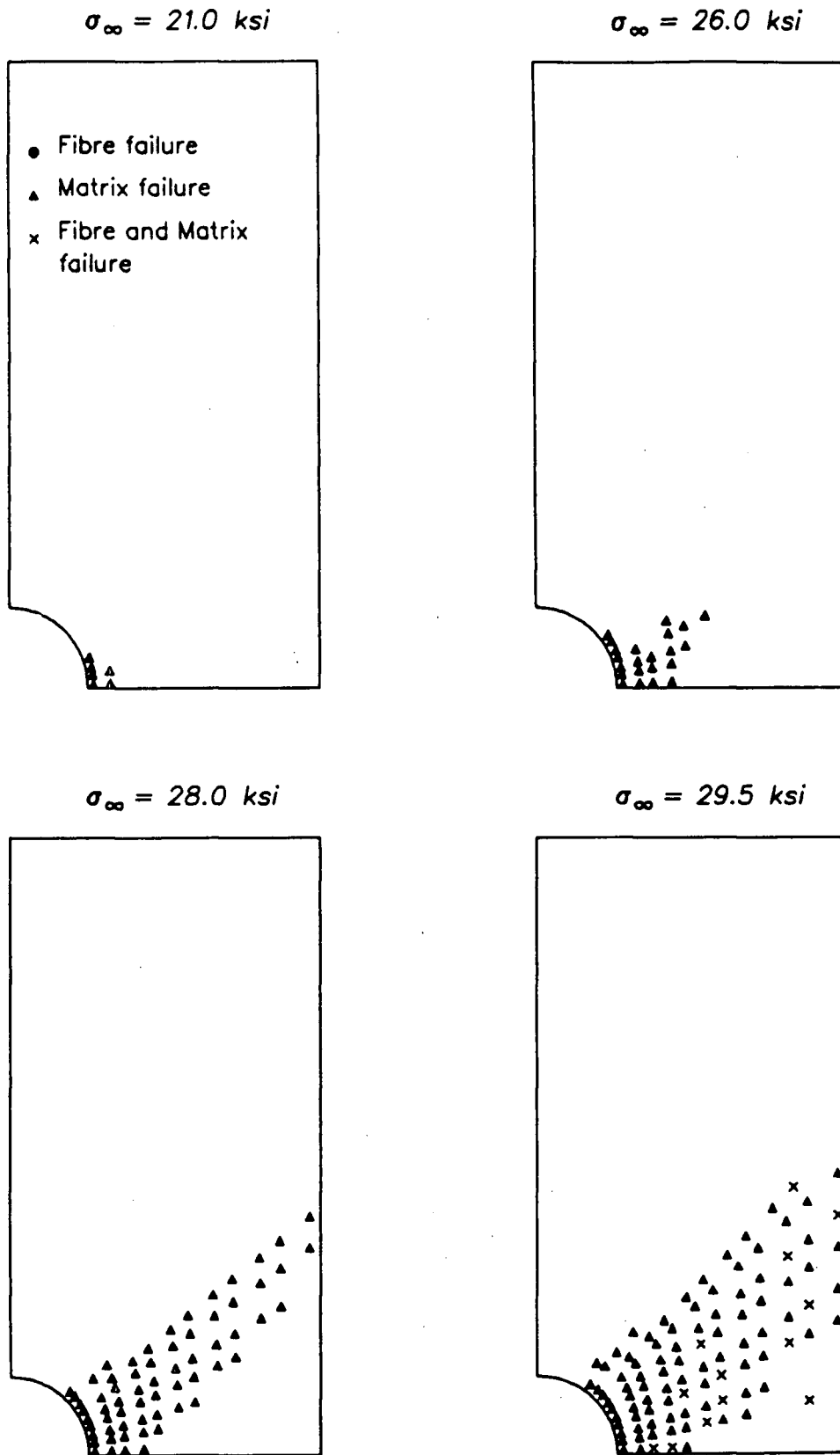
Fig. 5.61 b — Predicted damage progression for the −45−deg layer of a [45/−45] B/Ep laminate — Ductile Matrix

$\sigma_\infty = 19.6$ ksi

$\sigma_\infty = 20.1$ ksi

$\sigma_\infty = 20.4$ ksi

$\sigma_\infty = 20.8$ ksi

- Fibre failure
▲ Matrix failure
✗ Fibre and Matrix failure
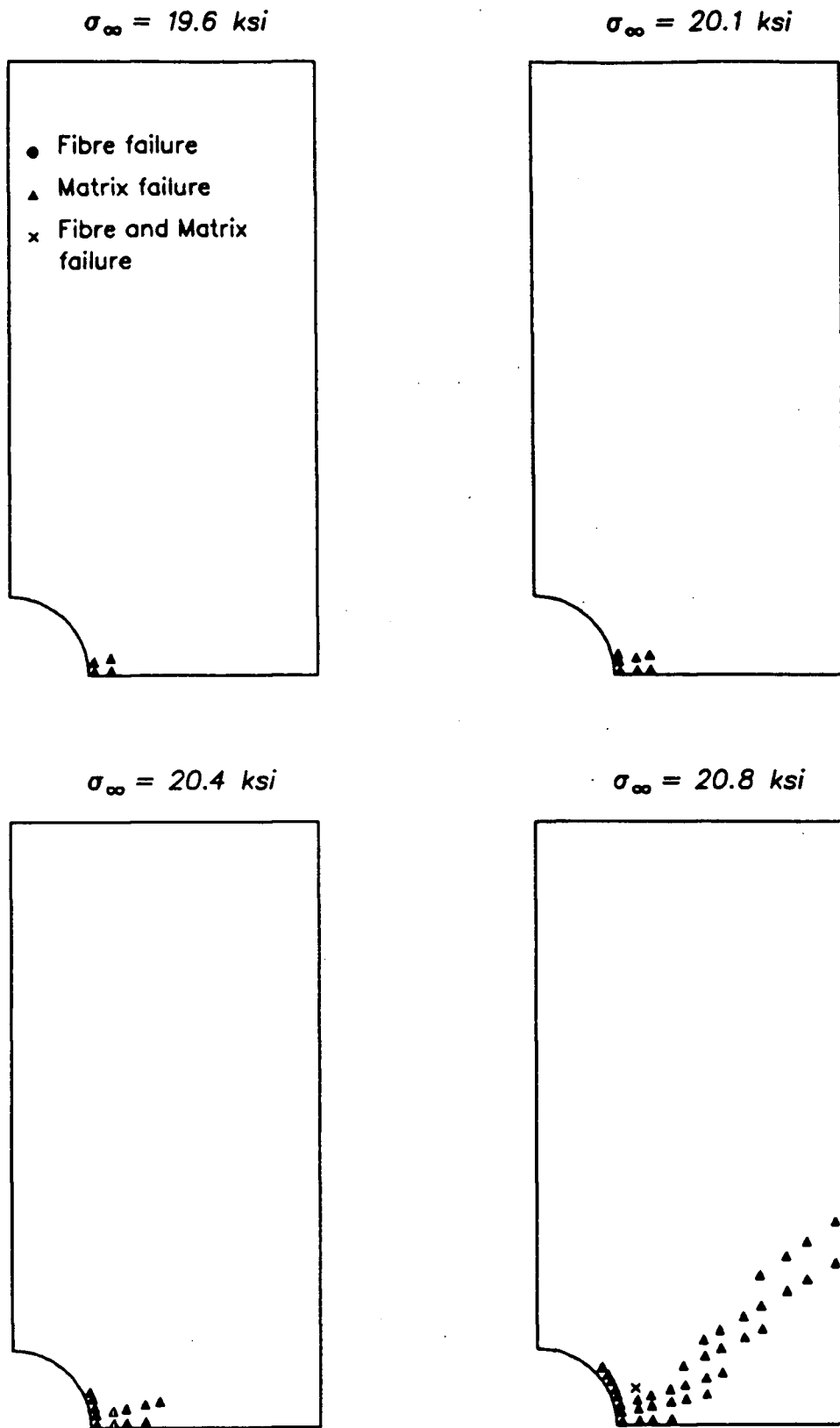
Fig. 5.62 a — Predicted damage progression for the +45–deg layer of a [45/−45] B/Ep laminate — Brittle Matrix

$\sigma_\infty = 19.6$ ksi

$\sigma_\infty = 20.1$ ksi

● Fibre failure

▲ Matrix failure

× Fibre and Matrix failure

$\sigma_\infty = 20.4$ ksi

$\sigma_\infty = 20.8$ ksi
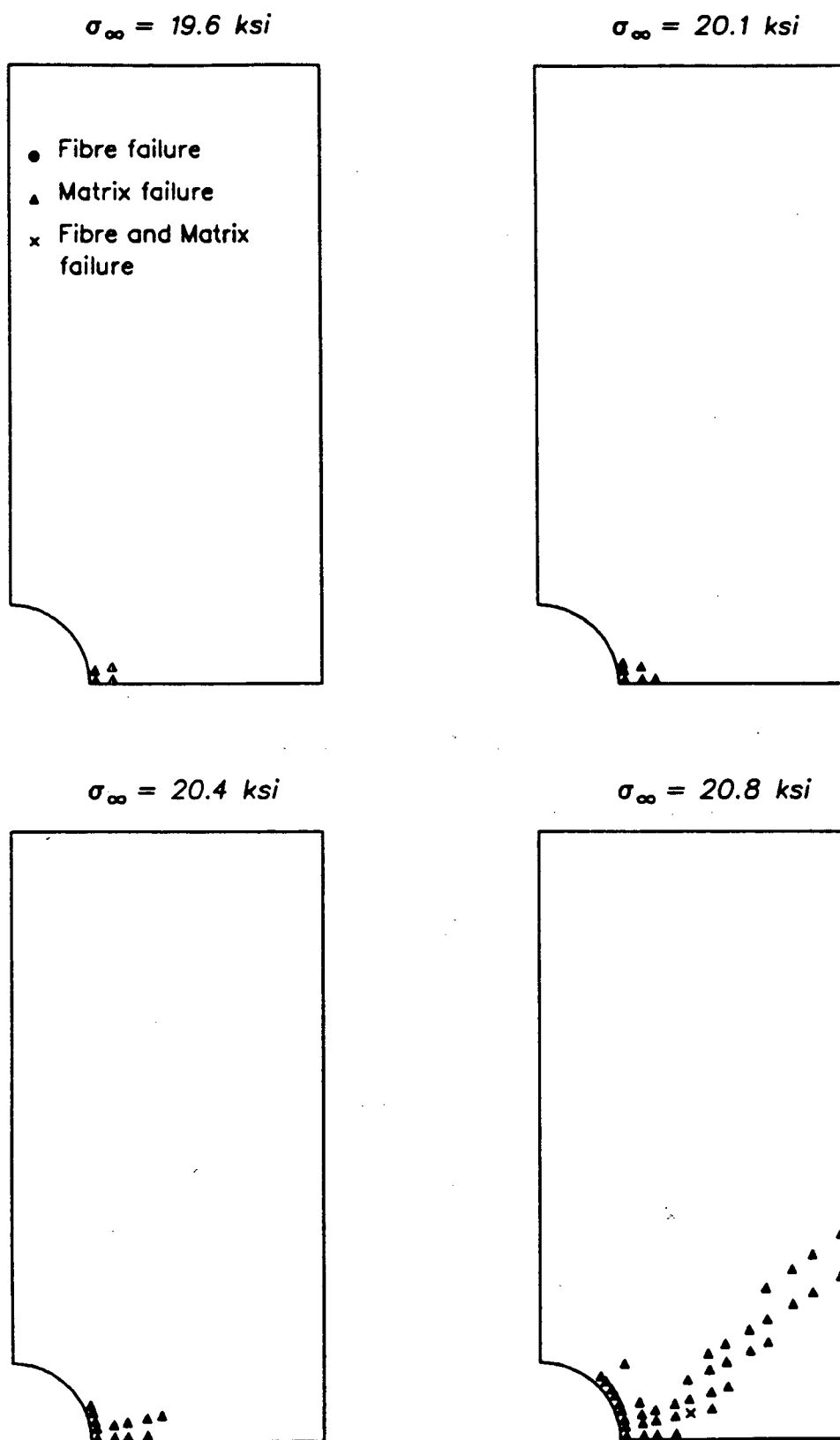
Fig. 5.62 b — Predicted damage progression for the −45−deg layer of a [45/−45] B/Ep laminate — Brittle Matrix
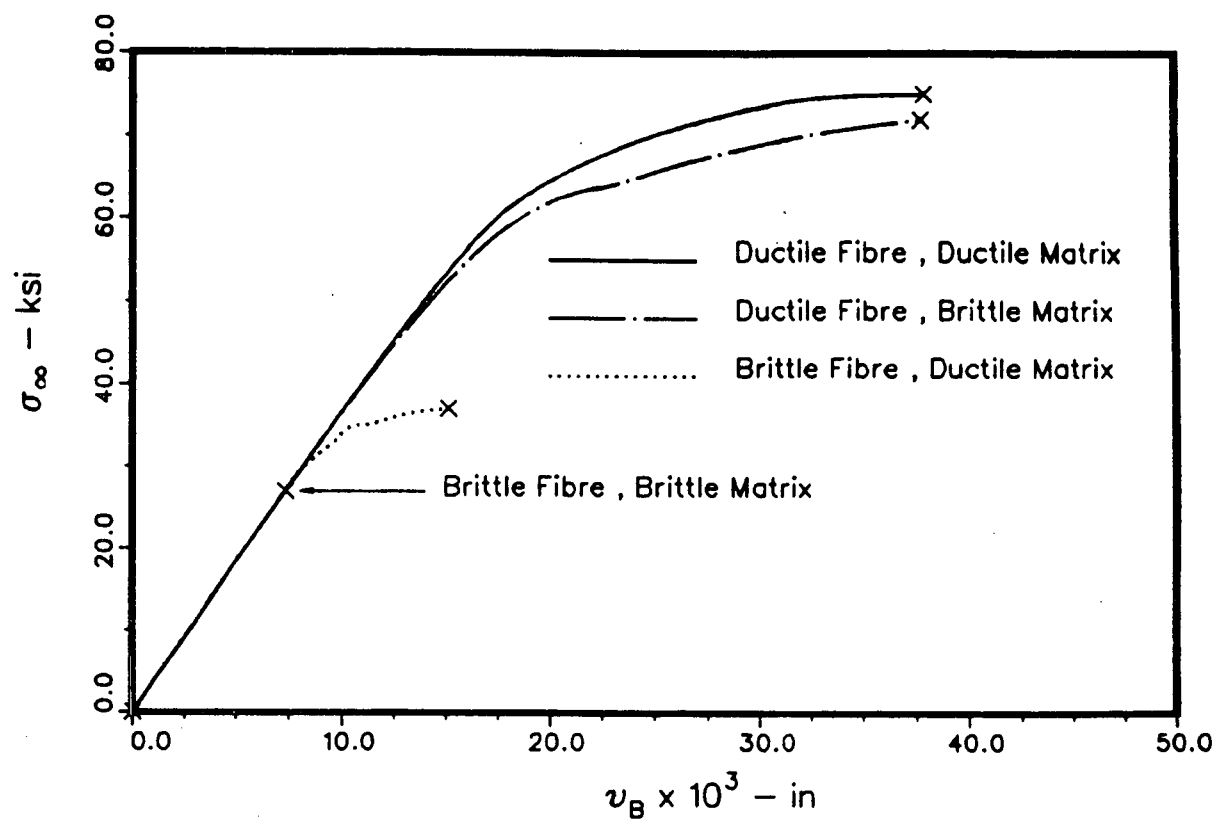
Fig. 5.63 – Load versus deflection at point B for a perforated [0/45/−45/90]
B/Ep laminate
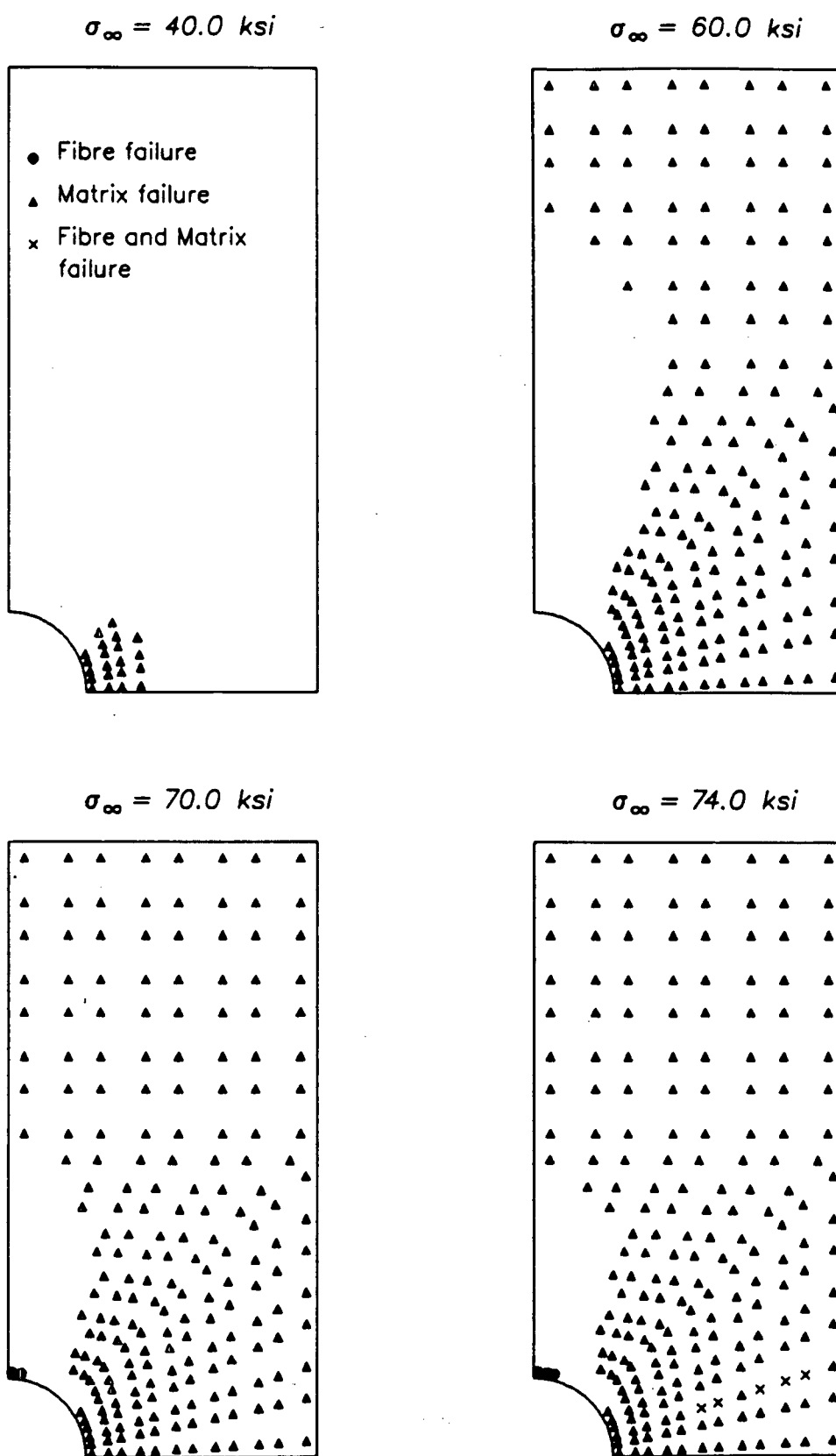
Fig. 5.64 a — Predicted damage progression for the 90-deg layer of a [0/45/−45/90] B/Ep laminate — Ductile Fibre Ductile Matrix
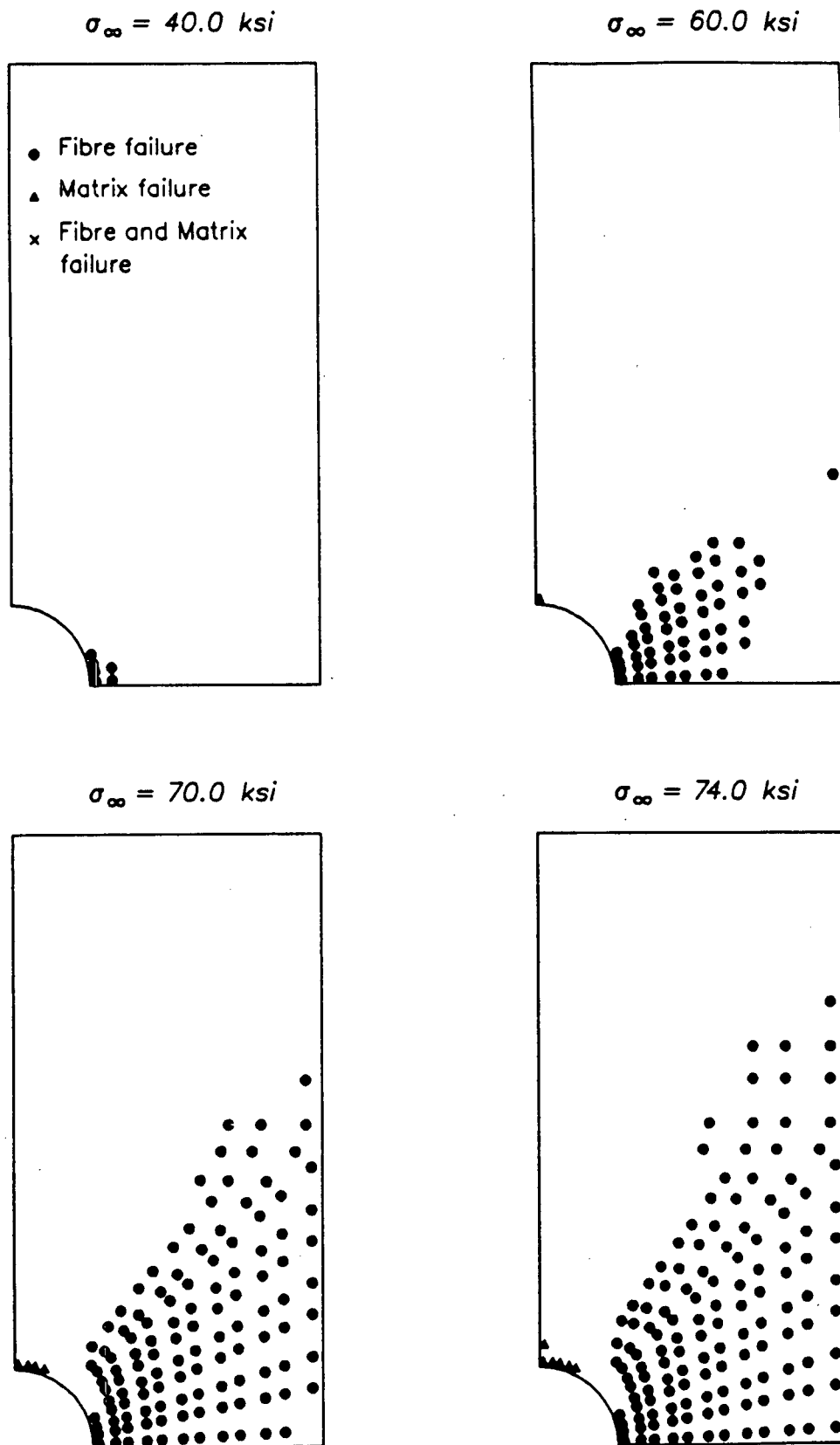
Fig. 5.64 b — Predicted damage progression for the 0-deg layer of a [0/45/−45/90] B/Ep laminate — Ductile Fibre Ductile Matrix
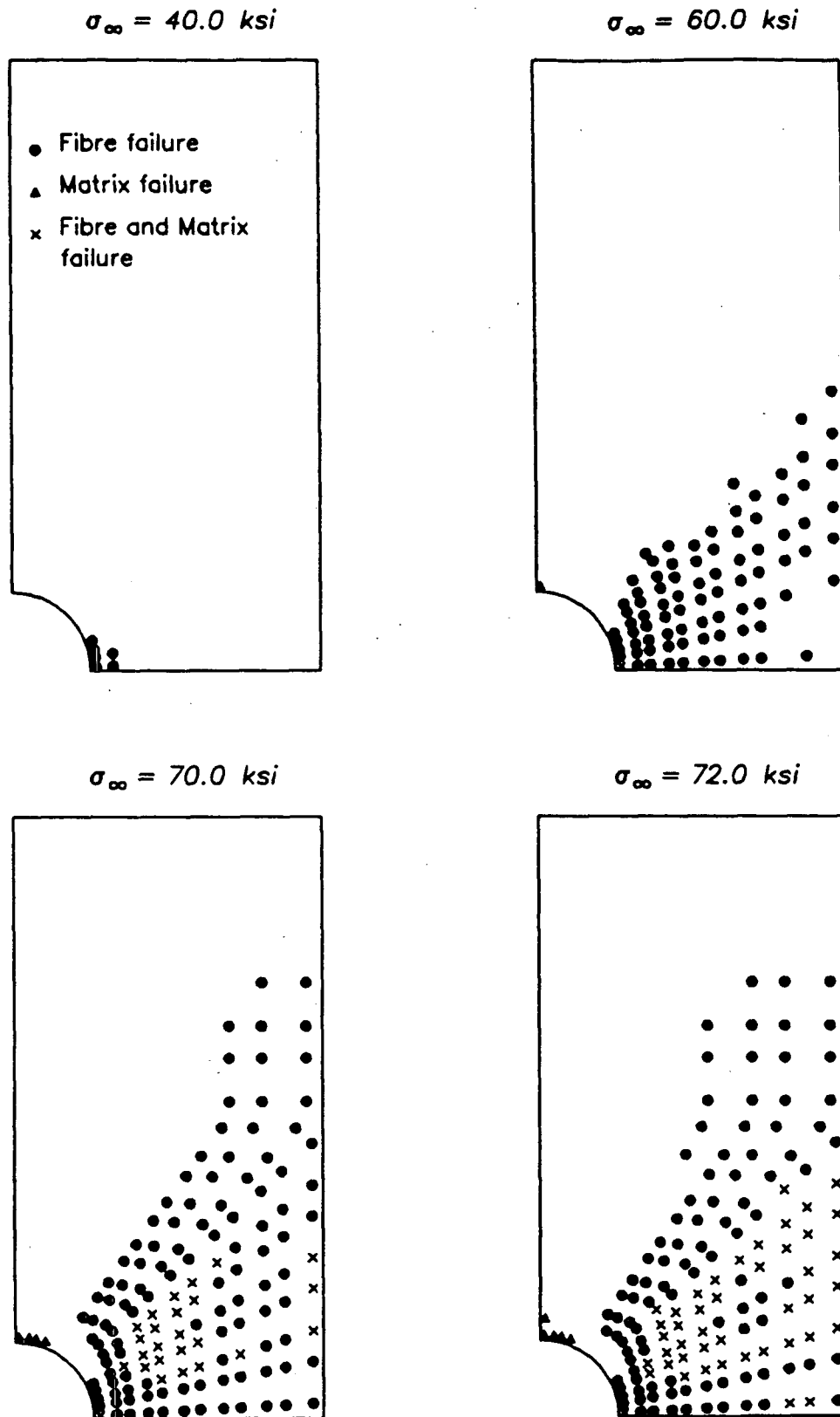
$\sigma_\infty = 40.0\ ksi$

$\sigma_\infty = 60.0\ ksi$

- Fibre failure
▲ Matrix failure
× Fibre and Matrix failure

$\sigma_\infty = 70.0\ ksi$

$\sigma_\infty = 74.0\ ksi$
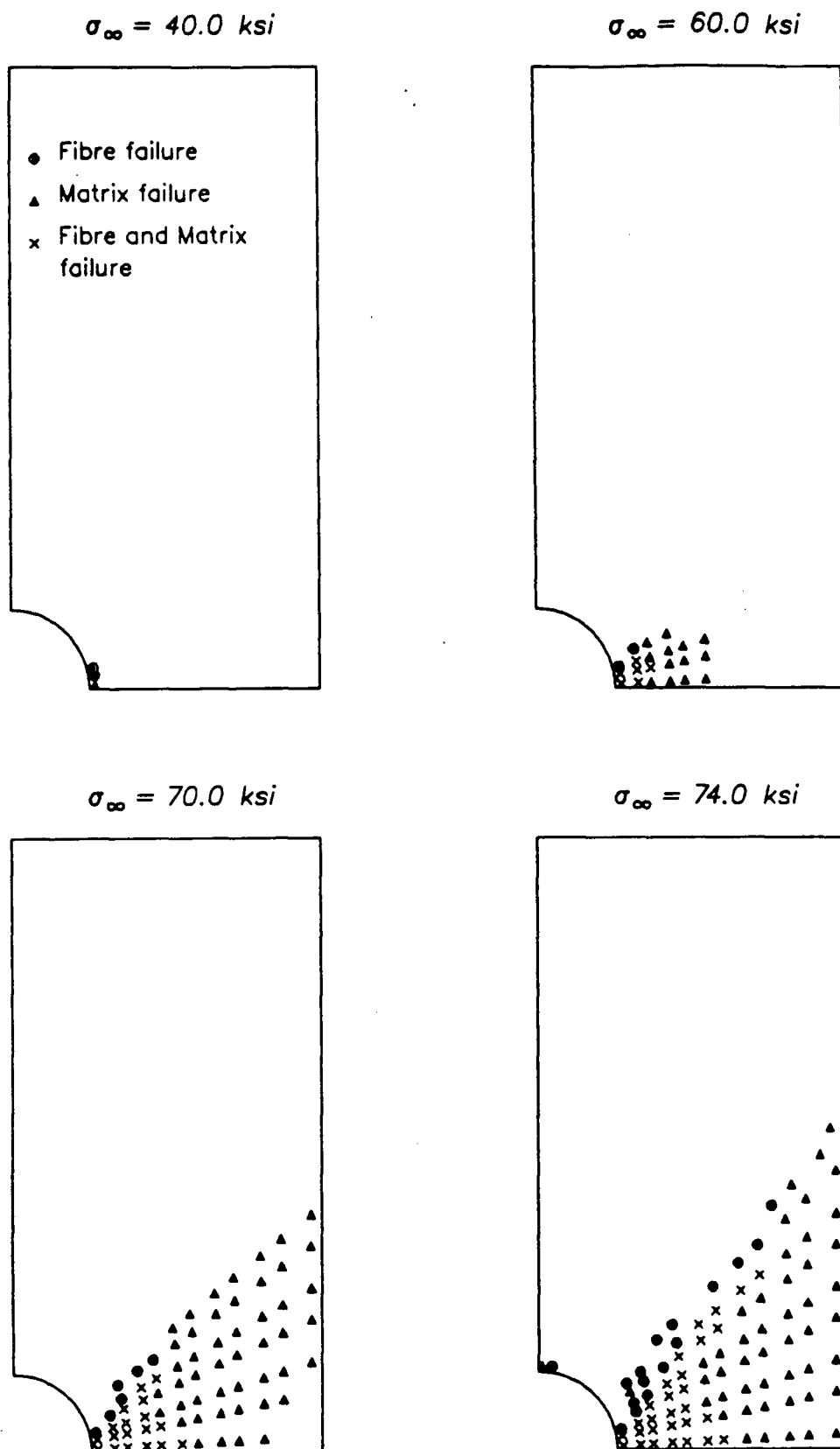
Fig. 5.64 c — Predicted damage progression for the +45-deg layer of a [0/45/-45/90] B/Ep laminate — Ductile Fibre Ductile Matrix

$\sigma_\infty = 40.0\ ksi$

$\sigma_\infty = 60.0\ ksi$

- Fibre failure
- Matrix failure
- x Fibre and Matrix failure

$\sigma_\infty = 70.0\ ksi$

$\sigma_\infty = 74.0\ ksi$
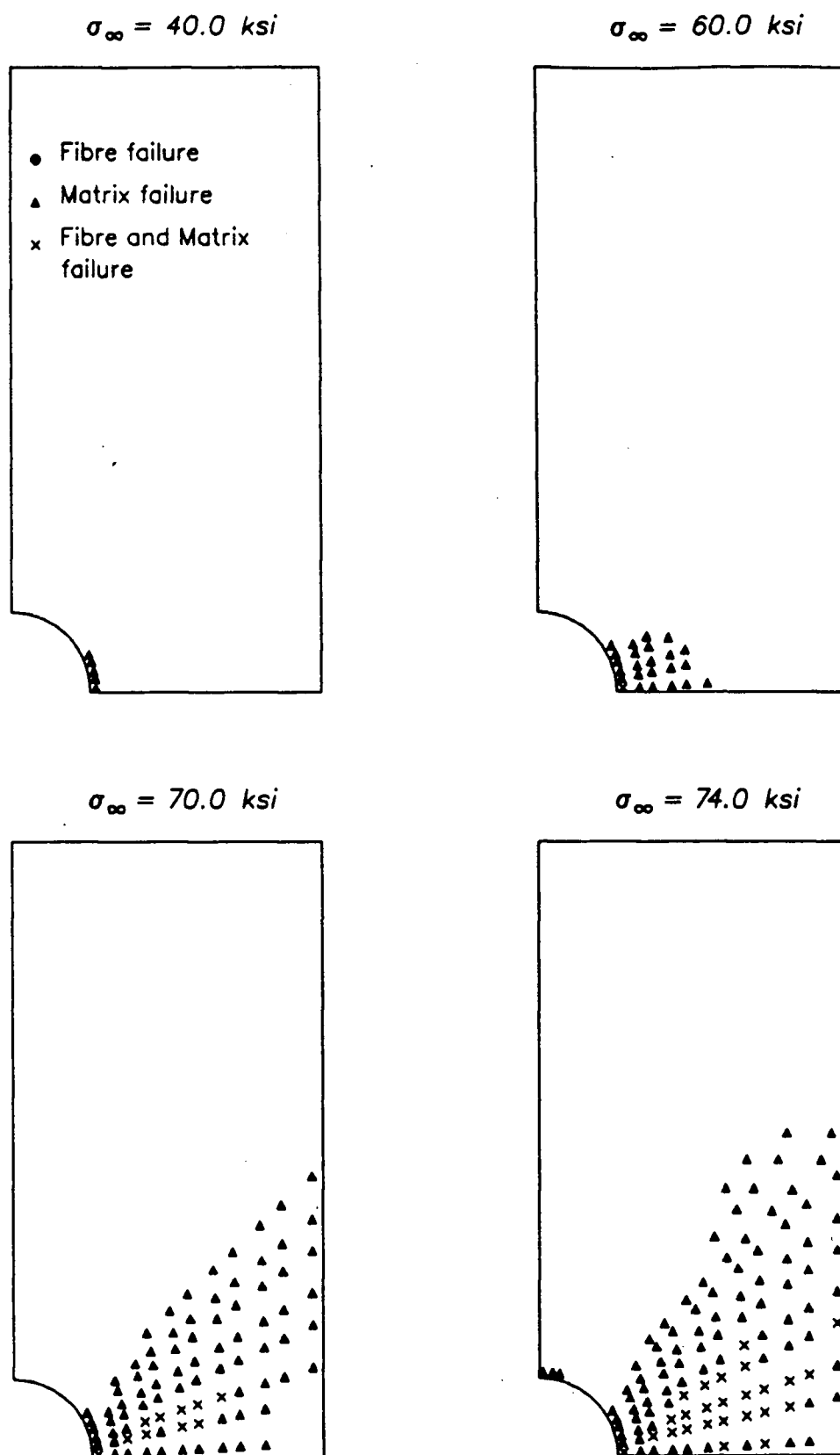
*Fig. 5.64 d — Predicted damage progression for the —45—deg layer of a [0/45/—45/90]
B/Ep laminate — Ductile Fibre Ductile Matrix*
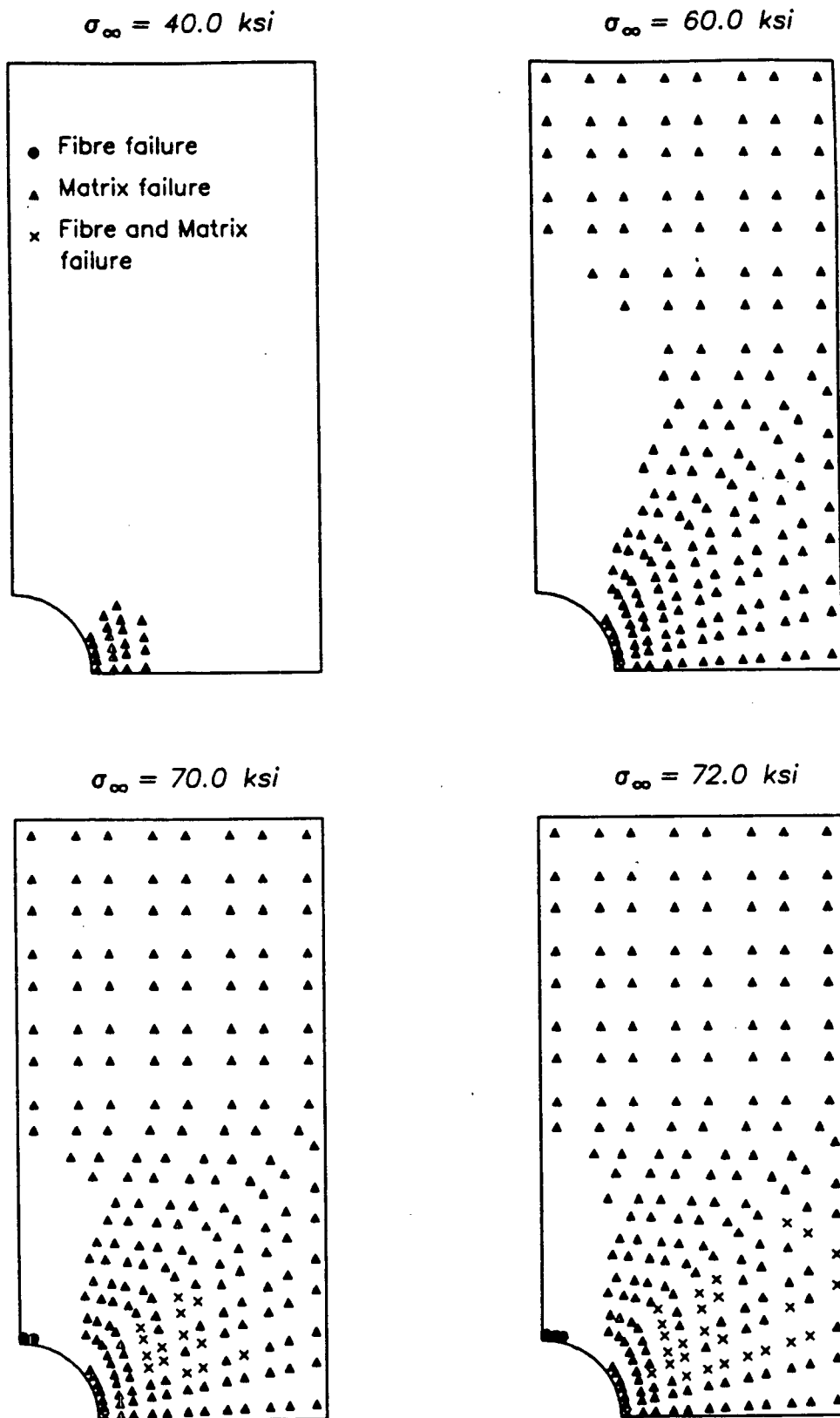
Fig. 5.65 a — Predicted damage progression for the 90-deg layer of a [0/45/-45/90] B/Ep laminate — Ductile Fibre Brittle Matrix
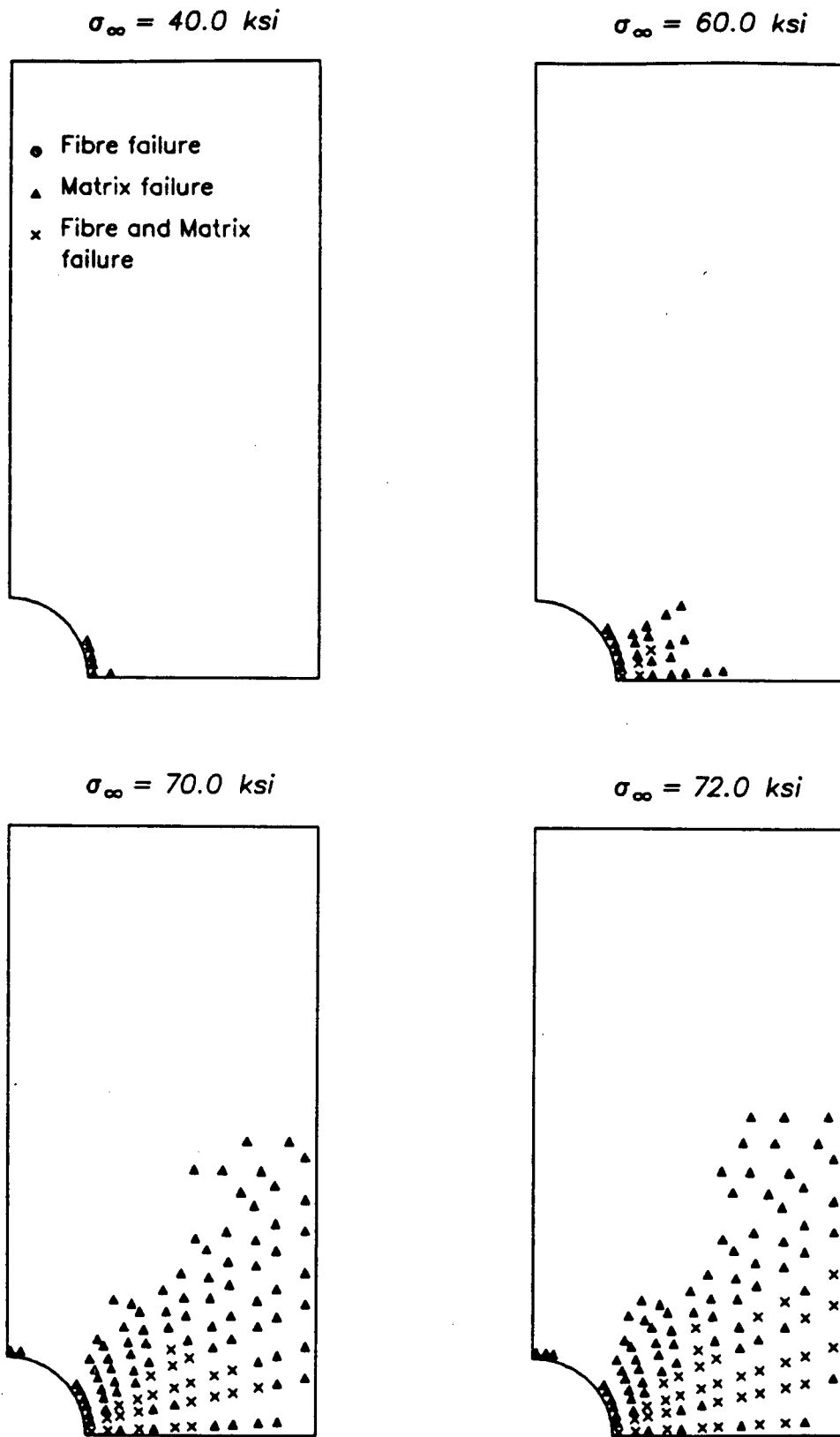
$\sigma_\infty = 40.0$ ksi

$\sigma_\infty = 60.0$ ksi

- Fibre failure
▲ Matrix failure
× Fibre and Matrix failure

$\sigma_\infty = 70.0$ ksi

$\sigma_\infty = 72.0$ ksi

Fig. 5.65 b — Predicted damage progression for the 0-deg layer of a [0/45/-45/90]
B/Ep laminate — Ductile Fibre Brittle Matrix
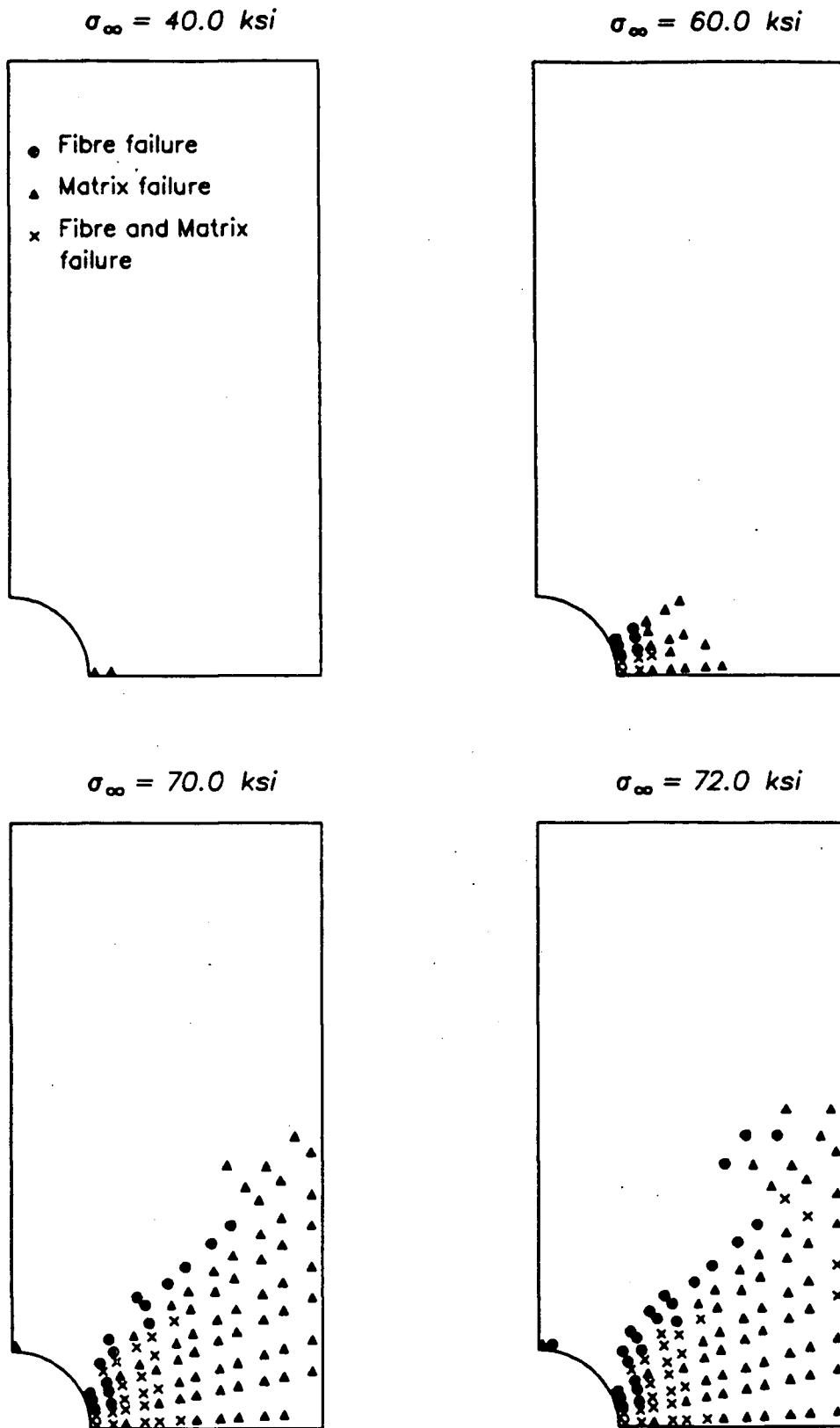
Fig. 5.65 c — Predicted damage progression for the +45-deg layer of a [0/45/-45/90] B/Ep laminate — Ductile Fibre Brittle Matrix
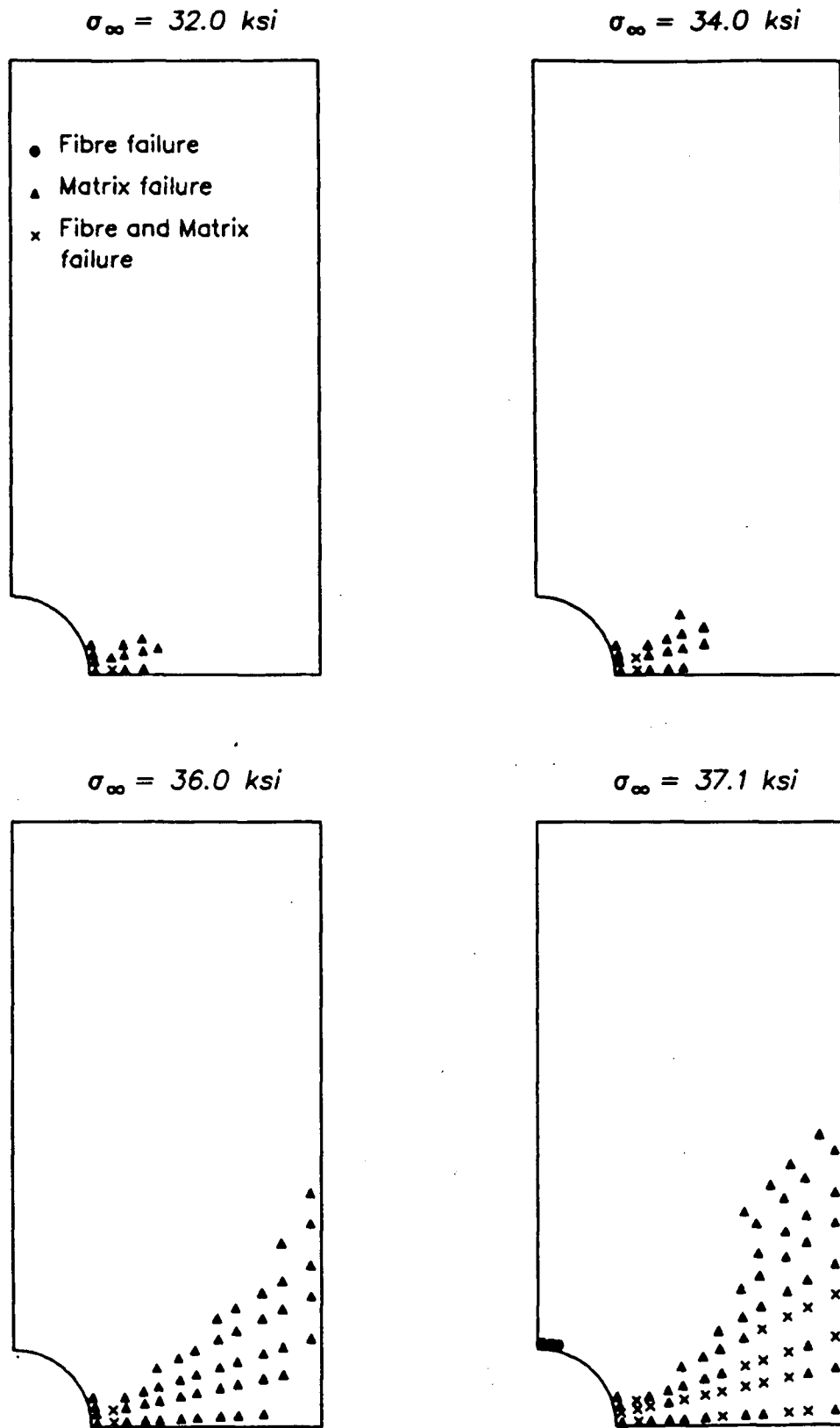
Fig. 5.65 d — Predicted damage progression for the −45−deg layer of a [0/45/−45/90] B/Ep laminate − Ductile Fibre Brittle Matrix

Fig. 5.66 a – Predicted damage progression for the 90-deg layer of a [0/45/-45/90] B/Ep laminate – Brittle Fibre Ductile Matrix
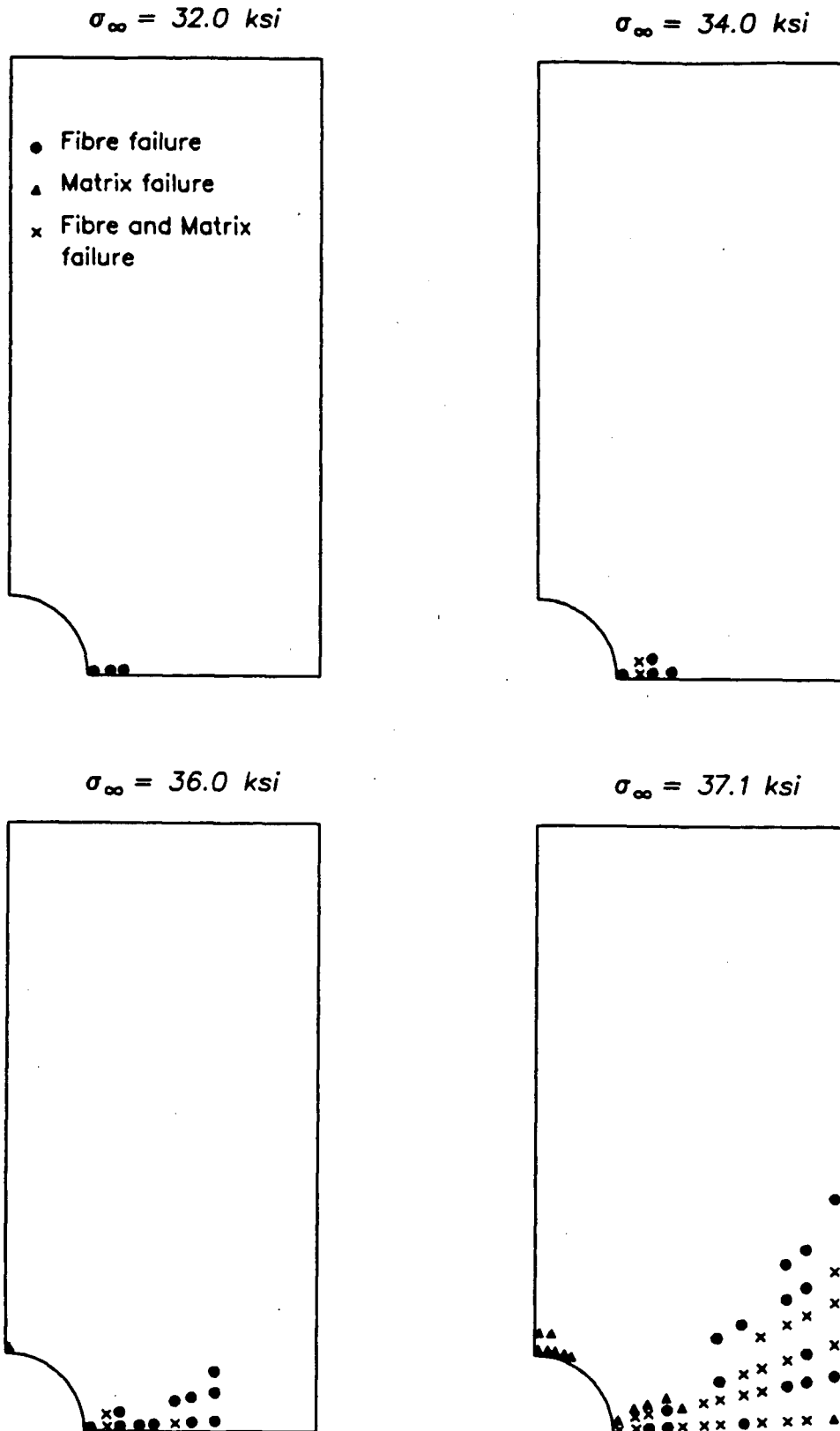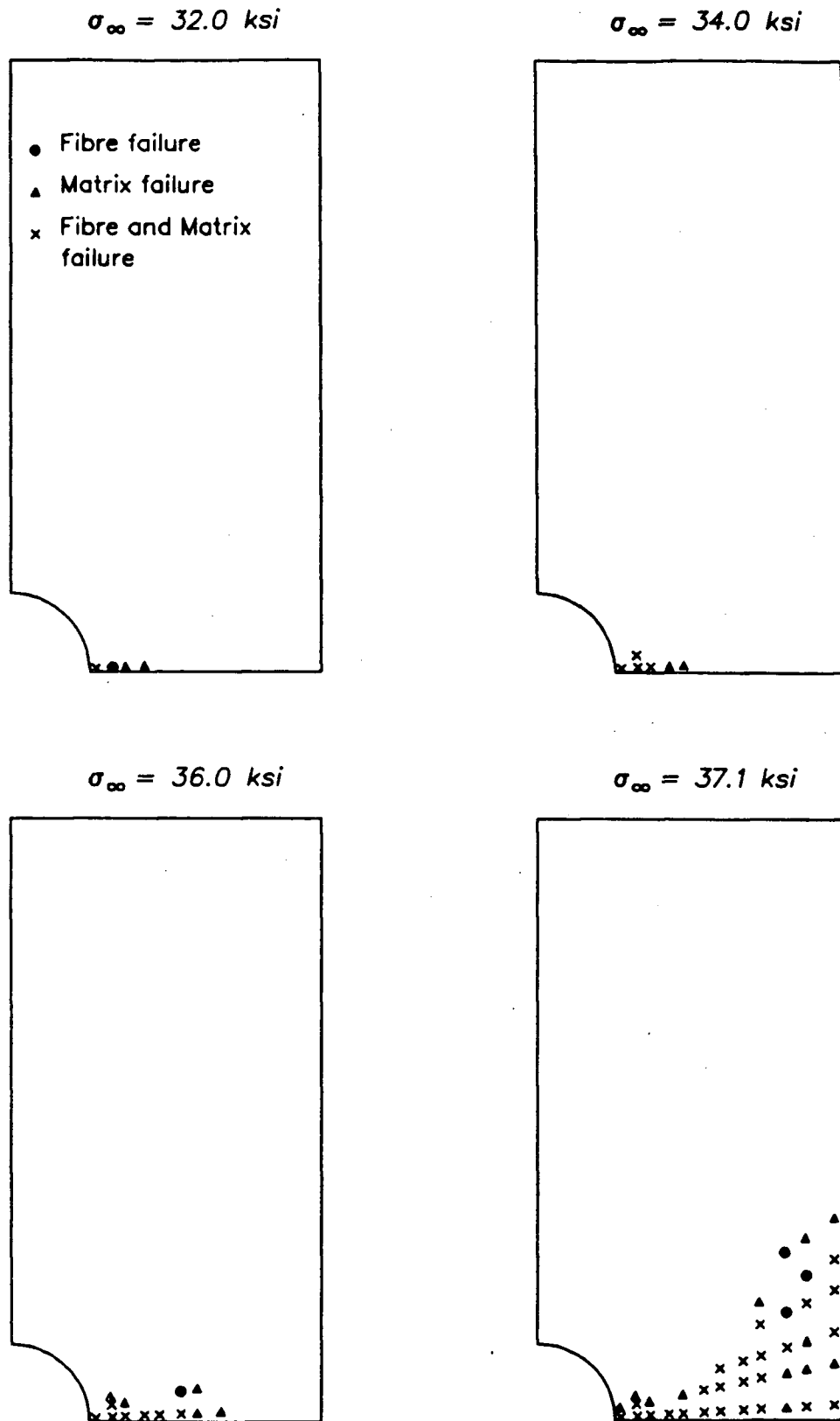
$\sigma_\infty = 32.0$ ksi

$\sigma_\infty = 34.0$ ksi

• Fibre failure
▲ Matrix failure
× Fibre and Matrix failure

$\sigma_\infty = 36.0$ ksi

$\sigma_\infty = 37.1$ ksi

Fig. 5.66 b — Predicted damage progression for the 0-deg layer of a [0/45/−45/90]
B/Ep laminate — Brittle Fibre Ductile Matrix

$\sigma_\infty = 32.0\ ksi$

$\sigma_\infty = 34.0\ ksi$

- Fibre failure
- Matrix failure
- Fibre and Matrix failure

$\sigma_\infty = 36.0\ ksi$

$\sigma_\infty = 37.1\ ksi$

Fig. 5.66 c — Predicted damage progression for the +45-deg layer of a [0/45/-45/90] B/Ep laminate — Brittle Fibre Ductile Matrix
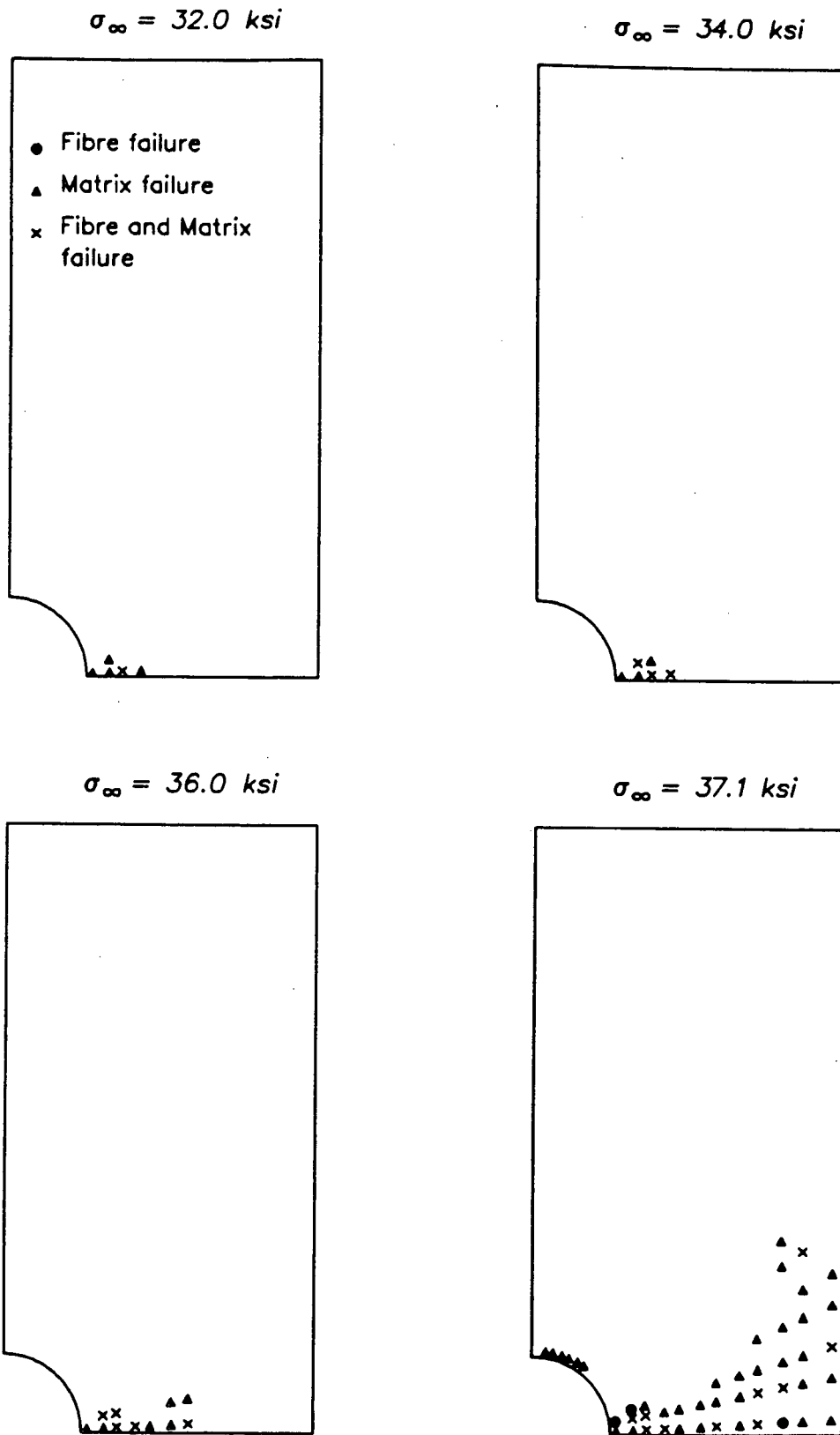
Fig. 5.66 d — Predicted damage progression for the −45−deg layer of a [0/45/−45/90]
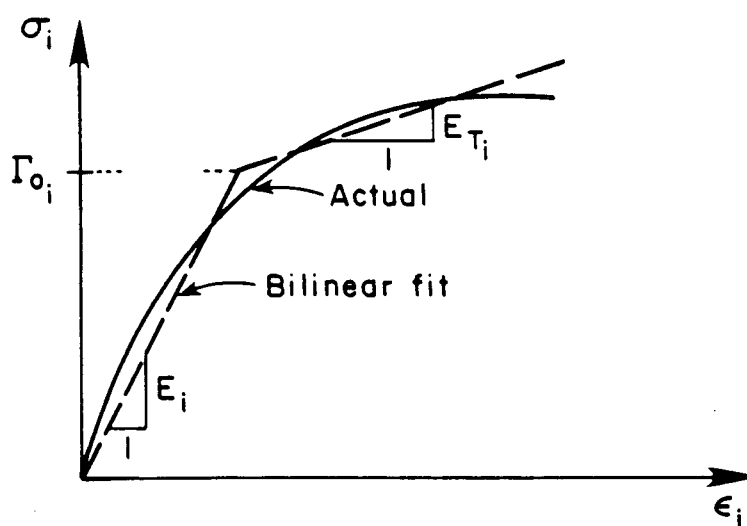B/Ep laminate − Brittle Fibre Ductile Matrix

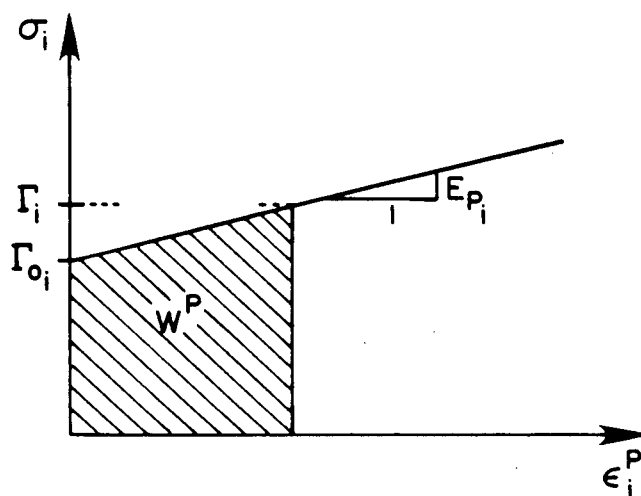*Fig. B.1 — Actual stress — strain curve and its bilinear approximation*
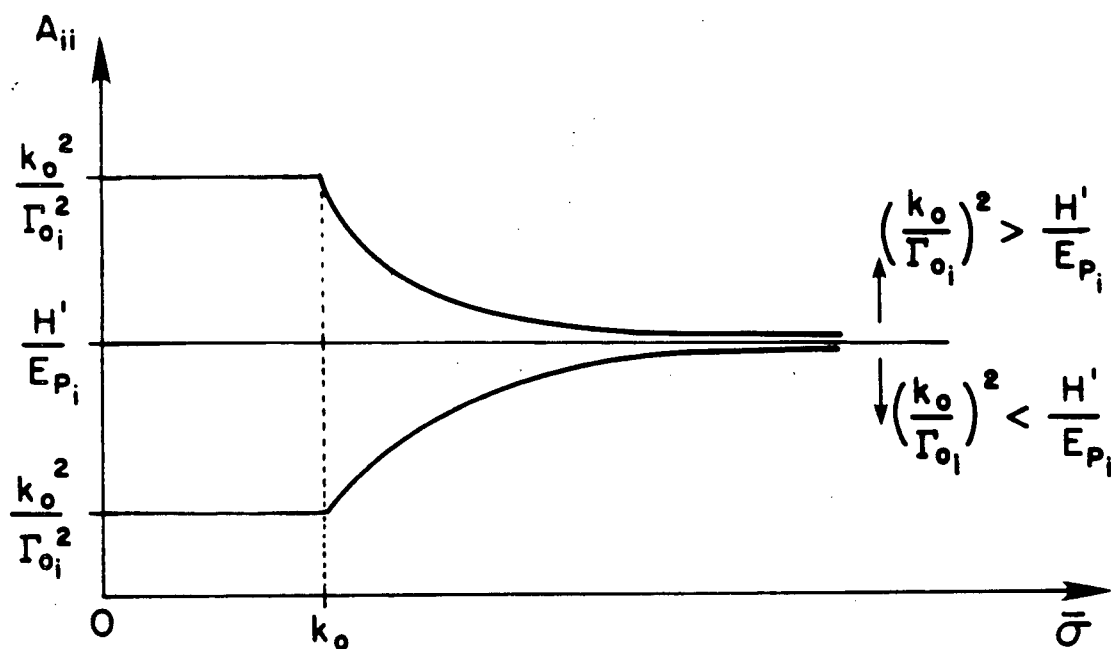

Fig. B.2 — Bilinear stress — plastic strain curve

Fig. B.3 — Variation of the principal anisotropic strength parameters with the effective stress